Investigation of Trichloroethene (TCE) Transport in Fractured Porous Media with Emphasis on Sorption onto Stylolites and Matrix Diffusion

by

Vera Waltraud Langer

A Thesis
Submitted to the Faculty of Graduate Studies
in Partial Fulfillment of the Requirements of the Degree of

Doctor of Philosophy.

Department of Civil and Geological Engineering
University of Manitoba
Winnipeg, Manitoba

THE UNIVERSITY OF MANITOBA

FACULTY OF GRADUATE STUDIES

*****

COPYRIGHT PERMISSION PAGE

INVESTIGATION OF TRICHLOROETHENE (TCE) TRANSPORT IN FRACTURED POROUS MEDIA WITH EMPHASIS ON SORPTION ONTO STYLOLITES AND MATRIX DIFFUSION

BY

VERA WALTRAUD LANGER

A Thesis/Practicum submitted to the Faculty of Graduate Studies of The University of Manitoba in partial fulfillment of the requirements of the degree of

DOCTOR OF PHILOSOPHY

Preface

This thesis consists of four independent research chapters (Chapter 2, 3, 4, and 5). Each chapter is completely self-contained with its own introduction, literature review, objectives, methodology, results, discussion and conclusions, and references. In chapter 1 the reader is first introduced to the overall problem that organic pollutants represent in our environment with an in-depth literature review. Important interactions between dissolved organic pollutants and the rock matrix in porous and fractured porous media are described before focusing on mass transport in fractured carbonates. A common feature in carbonate rock formations are **stylolites**. This research focuses on the role of stylolites in organic pollutant transport. Stylolites have never been identified as significant in previous research. The chapter concludes with a statement of the research objectives and an outline of the approaches that will be taken to study the research problem. In chapters 2, 3, and 4, the findings of experimental research on dolostone rock samples with respect to resaturation, hydraulic conductivity, total porosity, matrix diffusion, and sorption are presented. Transport parameters and rock properties are used in analytical and numerical simulations i) to predict the fate of TCE in a fractured carbonate aquifer at Smithville (Ontario) and ii) to demonstrate the impact of stylolites (Chapter 5). Chapter 6 concludes the thesis with a summary of the research results and suggestions for future research.

Abstract

It has been well documented and discussed in the literature that solute migration in a fractured, porous medium depends on matrix diffusion and sorption. Mass transport from fractures into the surrounding rock matrix has been shown to cause significant plume retardation. Parameters influencing the potential storage capacity of the porous medium are the pore volume and rock/solute interactions, which lead to temporary or permanent duration of contaminants in the matrix. Rock properties are site specific and rock/solute interactions depend largely on the chemical characteristics of the contaminant. In order to investigate mass transport in fractured porous media, researchers have employed laboratory scale and field scale experiments, as well as analytical and numerical simulations.

The present study utilized mainly laboratory scale experiments to investigate matrix diffusion and sorption parameters for TCE transport in a fractured dolostone aquifer. Semi-analytical mass transport solutions were derived and employed to evaluate the experimental data, and numerical simulations were conducted to investigate the fate of TCE in a two-dimensional domain generic to the DNAPL-spill site at Smithville (Southern Ontario). All experimental data were collected on dolostone rock samples from the Lockport Formation in Southern Ontario. First an attempt was made to re-saturate dry rock samples from drill cores, in order to produce saturated rock slices for subsequent diffusion experiments. Back-pressured triaxial cell experiments were conducted. Although full resaturation could not be achieved, valuable information on pore connectivity and

hydraulic conductivity was gathered. Analysis of the results showed that hydraulic conductivity values range from $1.2x10^{-11}$ to $9.4x10^{-12}$ [cm/s] for dense dolostone rock matrix, and from $2.2x10^{-6}$ to $9.1x10^{-6}$ cm/s for highly porous dolostone samples from the uppermost Lockport Formation. These values agree with hydraulic conductivity data found by the preliminary hydraulic testing program at the Smithville site [Lapcevic et al., 1995].

It has been well established that one of the most significant parameters influencing matrix diffusion is porosity. Its heterogeneity has received large attention in the petroleum industry but little research has been done on evaluating its impact on mass transport in dual porosity aquifers. Therefore, a vertical porosity study of the heterogeneous Lockport Formation, and subsequent mass transport simulations were undertaken. Results show that porosity in the Lockport Formation varies strongly vertically and ranges from 0.4 to 20.6 %. The rock matrix surrounding horizontal fractures shows enhanced porosity penetrating about 2 to 3 cm deep. This is thought to be the result of dissolution due to chemical disequilibrium between matrix and fracture fluids. In the Eramosa Member porosity rises near horizontal fractures up to 17 % above the background value, from 4 to 21 % total porosity. In most cases the increase ranges between 4 and 8 %. Enhanced secondary porosity in the Vinemount and Gasport Member is less dominant and values increase only by 1.7 to 3.1 % adjacent to fractures. Using hydrogeological parameters from the Lockport Formation of Southern Ontario, a short term tracer experiment and a long term contaminant spill were simulated with homogeneous and horizontally - stratified matrix

porosity. A comparison of the results indicates that the contaminant penetration depth into the matrix, and subsequently retardation and peak concentrations, depend largely on the porosity distribution. By not accounting for enhanced porosity near fractures, a significant overestimate of the bulk porosity of the medium will be obtained when fitting to field transport data. Vertical porosity profiles helped also to identify open, hydraulically active fractures.

As part of the study, batch and double reservoir diffusion cell experiments were used to investigate sorption of trichloroethene onto stylolites. Experiments were performed on thin stylolitic dolostone slices. Stylolites are common features in carbonate rock formations, and can contain high amounts of organic matter. Due to the hydrophobic character of TCE, its transport in fractured carbonate aquifers could be significantly retarded when sorbing onto stylolites. No research has ever been done evaluating the impact of stylolites on organic pollutant transport. The main objectives were to verify TCE sorption onto stylolites, and to derive sorption and diffusion parameters describing the solute/rock interaction. The test results show that stylolites from the Lockport Formation contain significant amounts of organic carbon. However, estimates from batch experiments range between 3.4 and 45.5 %, whereas carbon analyzer data on ground stylolite material range between 0.01 and 5.25 %. The discrepancy might be due to TCE sorption also onto a clay mineral phase in stylolites or due to selective sampling. In the diffusion experiment setup, TCE diffusion from a fracture into the adjacent rock matrix and the reverse process is simulated. Bromide was used as a conservative tracer for comparison. Three semi-analytical solutions for one-dimensional, reactive tracer migration

through a porous medium were derived and used to evaluate TCE time - concentration profiles. Analysis of the results showed that experimental data can best be modeled using a kinetic Langmuir sorption formulation with a maximum sorption capacity of 1.3 to 4.6 μg/g and a kinetic sorption constant of $4x10^{-7}$ to $5x10^{-7}$ l/mg s^{-1}. TCE desorption into the exit reservoir was found to be a very slow kinetic process. No retardation was observed during TCE migration through a clay and organic matter free dolostone sample. TCE seems not to interact with calcareous mineral phases and moves conservatively. Bromide diffusion curves yield geometry factors (γ) for dolostone ranging between 0.05 and 0.13.

Based on the above results, numerical simulations in a fractured porous domain were conducted. Presently, none of the public domain discrete fracture models allows for kinetic sorption within the matrix. Therefore, sorption onto stylolites was simulated with a linear sorption isotherm using the code FRACTRAN by Sudicky and McLaren (1992). Simulations resulted in mass storage calculations for matrix and stylolite layers. The calculated amounts of mass sorbed after 1000 and 10,000 days do not reach the maximum sorption capacity of stylolites in the domain. Therefore, these values are assumed to be lower estimates of the amount that would be sorbed if employing a kinetic Langmuir isotherm.

From the current study it can be concluded that TCE sorption is of importance when modeling TCE migration in fractured, stylolitic limestone aquifers where diffusion into the rock matrix takes place. Temporary TCE storage in rock matrix stylolites and

fracture wall stylolites has to be taken into consideration when evaluating actions of remediation.

Acknowledgments

Through the course of my four year Ph.D. program and research at the University of Manitoba many faculty members of the Civil and Geological Engineering Department, the Soil Science Department, the Freshwater Institute, and the Canadian Center for Inland Waters (CCIW) have supported my work, and I would like to express my sincere gratitude to these organizations. Without the financial support through the University of Manitoba Graduate Student Fellowship and funding for experimental research through the Groundwater Remediation Group at CCIW, my thesis work would not have been possible.

Special thanks go to my thesis advisor Dr. Allan Woodbury for his guidance, suggestions, and discussions to improve my work. Most of my experimental research was conducted at CCIW and I enjoyed working together with Dr. Kent Novakowski, Kelly Miller, and Lavinia Zanini. I would like to thank them for their hospitality, and extend my thanks to Dr. Kent Novakowski for his valuable critical comments, which improved my thesis immensely. The continuation of my experimental research at the University of Manitoba was made possible by Dr. Racz and Mr. Sarna from the Soil Science Department and Mike Stainton from the Freshwater Institute. I'm very grateful to them for providing me access to laboratory facilities, analytical equipment, and technical support. I would like to thank Dr. Emery Lajtai for providing me access to his computer and printing facilities, which where valuable resources in dealing with large graphic files. Special thanks go to Dr. Edward Sudicky and Robert McLaren for allowing me the use of

their computer programs FRACTRAN and CRAFLUSH to undertake contaminant transport simulations.

My deepest thanks and thoughts go to my friends, who have given me the strength and encouragement required to complete this task. During the length of my studies friendships with Pam, Marlee, Michaela, David, Greg, Maya, Edward, and Matthias were of special importance to me. I would like to thank them for their love and trust in me.

Finally, I want to thank my parents (Elfriede and Manfred Langer), my brother (Martin), my sisters (Bettina and Annette), my aunts, uncles, and cousins for their unconditional love and support. Each parcel, letter, and postcard was greatly appreciated.

Table of Contents

List of Figures

List of Tables

Chapter 1

General Introduction

1.1 Organic Pollutants in our Environment

Major air pollution and water quality problems heightened environmental awareness in Europe and North America in the 1970s. In the United States the Environmental Protection Agency (EPA) was founded (amongst other things) to protect surface and subsurface water quality. Drinking water guidelines and laws, like the Safe Drinking Water Act [SDWA, 1974], the Clean Water Act [1977], the Toxic Substances Control Act [TSCA, 1976], and the Comprehensive Environmental Response, Compensation, and Liability Act [CERCLA, 1980] were established to set standards and help limit further pollution. These standards led to many environmental-groundwater studies. The identification, characterization, computer simulation, and remediation of numerous hazardous waste sites accelerated with the establishment of the EPA Superfund. The emphasis of traditional groundwater investigations expanded greatly through the attention to organic and hazardous waste problems. Sources of organic and hazardous waste are well known and include: (a) land disposal of solid wastes, (b) disposal of liquid chemicals, (c) disposal of radioactive waste, (d) sewage disposal on land, (e) agricultural activities, (f) petroleum leakage and spills, and (g) military sites [Domenico and Schwartz, 1990; Bedient et al., 1994]. One of the most common sources of groundwater

contamination resulted from leaking underground storage tanks. These tanks frequently contained fuel oils, gasoline and other organic liquids.

Of the large group of organic pollutants, chlorinated hydrocarbons became a major concern to public health. In the middle 1970's it became increasingly apparent that highly volatile chlorinated hydrocarbons (HVCH) were found to be present in unnaturally high concentrations in the atmosphere, parts of surface- and groundwater, and plants and soils throughout the modern civilized world. HVCH are considered to be immiscible with water but can have a significant water solubility (0.15 - 8000 mg/l). A survey report from 1988 [Environmental Protection Agency, 1990] (Fig. 1.1) shows that volatile organic compounds are one of the most common pollutants in groundwater in the United States.

Nonpolar organic compounds are especially problematic to human health. Due to their high fat solubility they sorb to body fat once they are ingested by food, drinking water, or directly through the skin. Chlorinated hydrocarbons belong to this group of chemicals and include solvents, propellant gas, and pesticides. Nonpolar HVCH are used in industry as solvents to clean metal surfaces from grease, for dry cleaning in the textile industry, and in paint removal [Fricke, 1981; Kühn, 1981]. Dowty et al. [1975] detected tetrachloromethan, perchloroethen, and dichlorobenzol in surface waters (Mississippi), drinking water and in blood plasma of the local population. McConnell et al. [1975] and Bauer [1981] found HVCH in basic food groups and human tissue samples. Most HVCH are toxic and carcinogenic. Toxicity of various organic compounds varies, but most have a damaging affect on the central nervous system [Bedient et al., 1994].

For remediation purposes and for the prediction of contaminant fate, it is very important to study the transport and sorption behavior of HVCH in groundwater. To do this we need an understanding of the physical and chemical processes that control fluid flow and mass transport of organic pollutants. Pollutants belonging to the group of water-soluble organic contaminants can be transported great distances in the subsurface. Transport parameters that strongly influence the migration of dissolved contaminants are (i) advection, (ii) diffusion, (iii) dispersion, (iv) sorption, (v) decay, (vi) hydrolysis, volatilization, and biotransformation, and (vii) bimodal permeability distribution (as in fractured aquifers) [Spitz and Moreno, 1996].

A popular method to predict contaminant fate is by numerical simulation. For the modeling process to be successful we need (a) mathematical expressions that mimic geological, hydrological, and chemical processes correctly, and (b) site specific input parameters describing rock properties, fluid flow conditions, and rock/liquid phase interactions. One approach to determine hydrogeological parameters is through experimental research conducted at the laboratory scale. Through this type of experimental research a fundamental understanding of organic contaminant transport and solid/solute interactions may arise. In the following two paragraphs (1.2 and 1.3) the reader is introduced to important interactions between dissolved organic pollutants and the rock matrix in porous, and fractured media, with an introduction to the chemistry of trichloroethene (TCE) as a representative chlorinated hydrocarbon. A number of organic spills have occured above fractured rock aquifers, which contain important drinking water resources in Canada, the United States and Europe. Following an overview of recent

experimental studies on mass transport in fractured porous media and after presenting the most influential parameters (i.e. matrix diffusion, porosity), the organic spill site at Smithville, Ontario is introduced (paragraph 1.4). At this site, rock samples for experimental research were taken. The bedrock underneath Smithville is composed of a fractured dolostone sequence with numerous stylolites, which are common features in carbonate rocks. This research will focus on the role of matrix diffusion and stylolites on organic mass transport in fractured carbonates. Chapter 1 will conclude with a statement of the research objectives (paragraph 1.5) and an outline of the approaches that will be taken to achieve them (paragraph 1.6).

1.2 Basic Principles in Organic Transport

Laboratory experiments with organic pollutants make use of pollutant specific *distribution coefficients* (between gas and water phases and between solid and water phases), established *sorption isotherms*, and *retardation factors*.

1.2.1 Distribution between Gas and Water Phases

In a dual, gas-water-phase system, highly volatile chlorinated hydrocarbons (HVCH) are highly concentrated in the gas phase. Experimental researchers make practical use of this behavior through the Head-Space-Method when analyzing HVCH [Garbarini and Lion, 1985]. Henry's constant (H) describes the partitioning of a compound between gas and water phases for dilute solutions. H is concentration

dependent and is defined as the ratio between the gas phase partial pressure and its concentration in the liquid phase. As an approximation, H can be calculated from the saturation gas pressure and water solubility:

$$H_p = \frac{P^0}{S} \qquad (1.1)$$

where; H_p: Henry constant [Pa L/mole], P^0: saturation gas pressure [Pa], and S: water solubility [mole/L]. In laboratory studies pollutant concentrations are used instead of partial pressures, and therefore the non-dimensional form of Henry's constant (concentration in gas phase/ concentration in liquid phase) (Fig.1.2) is preferred:

$$H = \frac{C_G}{C_W} = \frac{P^0}{S \cdot R \cdot T} \qquad (1.2)$$

where; H: Henry constant [(μg/l) / (μg/l)], R: universal gas constant [J/(mole·K)], T: temperature [K], C_G: contaminant concentration in the gas phase [μg/l], C_W: contaminant concentration in the water phase [μg/l].

1.2.2 Distribution between Solid and Water Phases

Analogous to Henry's constant, the distribution coefficient K_d describes the partitioning of a compound between solid and water phases (see Fig. 1.2). K_d is named in

the literature as the distribution coefficient as well as partition coefficient (K_p) [Spitz and Moreno, 1995].

$$K_d = \frac{C_S}{C_W} \tag{1.3}$$

where C_S is the concentration in solid phase [µg/kg] . The concentration in the solid phase refers to dry mass of the solid phase and the concentration in the water phase refers to the volume of the liquid phase (Karickhoff, 1984). In contrast to H, the distribution coefficient K_d may depend on the equilibrium concentration. The partitioning of contaminants onto a solid phase is also known as sorption and described further in the next section.

1.2.3 Sorption

Sorption refers to the adsorption or absorption of a compound [Hasset and Banwart, 1989]. Physical, chemical and electrostatic interactions between the chemical compound, and the liquid and solid phases take place. Enthalpy related adsorption forces, involved in sorption of hydrophilic compounds (charged molecules or natural dipole), are 1) London - van der Waals, 2) hydrogen bonding, 3) dipole - dipole, and 4) dipole - induced dipole interactions [Hasset and Banwart, 1989]. Adsorption of molecules onto grain surfaces in a porous medium causes a decreasing concentration of the pollutant in the aqueous phase and a retardation of the pollutant transport compared to advection of water. If advective transport is relatively slow compared to the adsorption process, equilibrium between the concentration in the aqueous- and in the solid phase can be

assumed [Domenico and Schwartz, 1990] . The reverse process of adsorption is called desorption. Note the degree of sorption depends on:

- Concentration and characteristics of the compound,
- Composition of the solid phase,
- Composition of the aqueous phase (pH, E_H, presents of other water solutes, pressure, temperature).

Sorption of organic compounds onto organic material is discussed separately in section 1.2.3.2.

1.2.3.1 Sorption Isotherms

Adsorption kinematics depend upon the contaminant concentration in the groundwater, the rates of adsorption and the capacity the solid material has to sorb the compound in question [Fetter, 1993; Spitz and Moreno, 1995]. As mentioned, if the advective flow is relatively slow in relation to the sorption process, equilibrium between the contaminant concentrations in the water and solid phases can be assumed. Sorption processes also take place at the fracture - rock matrix interface in a dual porosity aquifer, and if the flow velocity in the fracture is relatively slow (small fracture aperture) equilibrium sorption can be assumed. In the following paragraphs equilibrium sorption isotherms and non-equilibrium (kinetic) sorption models are discussed.

Equilibrium sorption can be expressed by the relationship between the adsorbed concentration (C_s) and the concentration of the solute in the water phase (C_{eq}).

$$C_s = f(C_{eq}) \tag{1.4}$$

In the simplest case the relationship between C_s and C_{eq} is linear, meaning that the contaminant distribution between the solid- and the aqueous phases is independent of the solute concentration (Fig. 1.3).

$$C_s = K_d\, C_{eq} \tag{1.5}$$

where; C_s : concentration of contaminant sorbed to the solid surface [μg/g], C_{eq}: equilibrium concentration of contaminant in water [$\mu g/cm^3$]. The sorption of nonpolar organic compounds onto solid organic matter can be modeled in most cases with a linear sorption isotherm. The higher "nonpolar" a chlorinated hydrocarbon, the faster the partitioning process onto the solid organic matter. In water, dissolved trichloroethene (TCE), which is a representative nonpolar chlorinated hydrocarbon, reaches equilibrium with the organic material in a relatively short period of time. This has been observed in many batch experiments [Garbarini and Lion, 1985; Grathwohl, 1989; unpublished results by Mark Hilverda, 1997]. Sorption isotherms are constructed using data points from batch experiments conducted at identical temperature and pressure conditions. With some organic compounds, especially when using a large range of concentrations in batch experiments, a linear sorption isotherm cannot be justified (Ball and Roberts, 1991). In such cases, theoretical and empirical nonlinear isotherms are used to fit experimental data and model sorption. Two of the more common relationships are the

Freundlich isotherm $$C_S = K_F \cdot C_{eq}^{\frac{1}{n}} \quad (1.6)$$

and

Langmuir isotherm $$C_S = \frac{K_L \cdot C_{max} \cdot C_{eq}}{1 + K_L \cdot C_{eq}} \quad (1.7)$$

where K_F and K_L are distribution coefficients reflecting the extent of sorption, n is an empirical constant usually ranging between 0.7 and 1.2, and C_{max} is the maximum sorption capacity for the surface.

The Langmuir isotherm represents a theoretically derived sorption model. The adsorption energy for each space at the solid surface is defined to be identical; meaning no interactions between adjacent spaces take place. The maximum sorption capacity is reached when the solid surface is covered with a monomolecular layer. The Langmuir isotherm is often used when describing contaminant sorption onto coal filters during water purification [Weber and Miller, 1988]. In some cases, the empirical Freundlich isotherm (Fig. 1.4) is found to fit experimental data better than the linear Freundlich or Langmuir model. The physical and chemical reasons are not well understood and are still under investigation. For $n \neq 1$ sorption is concentration dependent, and the distribution coefficient changes as sorption of the contaminant on the solid surface (C_s) increases. To transform the Freundlich isotherm into a linear form the sorption data (C_s, C_{eq}) can be log-normalized. It is important to notice that the Freundlich isotherm also implies an infinite adsorption capacity of the solid organic phase. This is only realistic when the fraction of

organic material available for adsorption is large, and/or contaminant concentrations are low.

Several other theoretical isotherms were developed to describe nonlinear sorption processes. For completeness the BET model is briefly introduced. With the BET - isotherm (Brunauer-Emmet-Teller) Brunauer et al. [1938] derived a theoretical multi-molecular model, where several layers of sorbate might attach onto sorbent. The BET - isotherm describes sorption of gases and is S-shaped, being convex for small C_{eq} values, linear in the middle part and concave for large C_{eq} values. The reader is referred to Grathwohl [1989] for further details.

Some organic compounds (mainly polar molecules) sorb onto fracture surfaces and solid mineral phases in the rock matrix by kinetic sorption. Chemical compounds showing kinetic sorption can be linear and non-linear, depending on the enthalpy driven bounding processes (listed earlier) and the sorbing capacity of the solid phase. One possible non-equilibrium model is the **irreversible first-order kinetic sorption model** described by the equation:

$$\frac{\partial C_s}{\partial t} = k_1 C_w \qquad (1.8)$$

where k_1 is a first-order decay rate constant [Fetter, 1993]. The rate of sorption is a function of the compound concentration in the water phase. The process is irreversible; meaning no desorption takes place. A **reversible linear kinetic sorption model** (kinetic Freundlich sorption model) is used when the rate of sorption changes with the amount that

has already been sorbed onto the solid phase and the process is reversible. The model can be expressed as follows [Fetter, 1993]:

$$\frac{\partial C_s}{\partial t} = k_f C_w - k_b C_s \tag{1.9}$$

where, k_f: forward rate constant, and k_b: backward rate constant. When the system reaches equilibrium (i.e. $k_f C_w = k_b C_s$), the sorbed concentration onto the solid phase will no longer change with time. In the literature this kinetic model is also formulated in a different form [Fetter, 1993; Ibaraki and Sudicky, 1995] as:

$$\frac{\partial C_s}{\partial t} = \beta \left(K_d C_w - C_s \right) \tag{1.10}$$

where, β: kinetic rate constant. The **kinetic-Langmuir sorption model** is also called bilinear sorption model and can be written in the form:

$$\frac{\partial C_s}{\partial t} = k_f C_w (C_{\max} - C_s) - k_b C_s \tag{1.11}$$

The model implies that a limited amount of solute will be sorbed onto the solid phase. Ibaraki and Sudicky [1995] used the above kinetic Freundlich and Langmuir sorption models to simulate colloid-facilitated contaminant transport.

Some researchers have tried to relate the distribution coefficient to the specific surface area of mineral phases per unit bulk volume of porous medium [Tompson and Jackson, 1996]:

$$K_d = a_m^s k / \rho_s \qquad (1.12)$$

where, a_m^s: specific surface area of mineral (m) per unit bulk volume of porous medium [m^2/m^3], k: thermodynamic property constant [m], and ρ_s: solid density [kg/m^3]. Research in this area is not conclusive yet. Sorption studies with TCE and tetrachloroethene (PCE) in alluvial sediments suggest a linear relationship between the distribution coefficient and the specific surface area [Tompson and Jackson, 1996]. In contrast to that finding, detailed studies with the same chlorinated hydrocarbons by Grathwohl [1989] found no relationship between sorption of nonpolar compounds and mineral surface areas. He studied sorption onto sediments with different grain sizes, surface areas, and organic content. The solid phase ranged in composition from 0 to 75 % clay and from 0 to 85 % sand fraction. No relationship between distribution coefficient and specific surface area was established.

As has been discussed earlier, sorption also takes place at the fracture - rock matrix interface. Freeze and Cherry [1979] describe a separate distribution coefficient K^*_d for sorption onto fracture wall surfaces. They define K^*_d as the mass of solute adsorbed per unit area of fracture surface divided by the concentration of solute in solution. K^*_d is therefore related to K_d by specific surface area η.

$$K_d = \eta K^*_d \qquad (1.13)$$

where; K_d: distribution coefficient, K^*_d: fracture distribution coefficient [M/L^2 x L^3/M] or [L], and η: specific surface [L^2/M]. As one of the first researchers Tang et al. [1981]

implemented the above concept of sorption onto fracture wall surfaces in form of a linear sorption isotherm into his analytical solution on mass transport in a fractured porous media.

Also a number of sorption isotherms have been introduced in the above sections, but it has to be kept in mind that each of them represents a simplification of the natural physical and chemical system it tries to describe. For chlorinated hydrocarbons researchers developed a hydrophobic sorption concept, based on the octanol - water partition coefficient (K_{ow}) for each compound. This concept is introduced in the following section.

1.2.3.2 Hydrophobic Sorption of Organic Compounds

Hydrophobic compounds are chemicals that are not attracted to the water phase. In general, chemicals can be classified by their polar-ionic character:

- Ionic or charged species,
- Uncharged polar species,
- Uncharged nonpolar species (hydrophobic compounds).

The latter, nonpolar organic compounds include trichloroethene (TCE), tetrachloroethene (PCE), chlorinated benzene and components of hydrocarbon fuel. Pesticides and phenols belong to the first two groups [Bedient et al., 1994]. For nonpolar organic compounds sorption is commonly interpreted as a partitioning mechanism between soil organic matter and water phases due to the hydrophobic character of the molecules. In general, the more

hydrophobic an organic compound the greater its tendency to partition onto the solid phase. The composition of the organic matter (degree of polymerization) influences the degree of sorption as well as the hydrophobic interactions (i.e. repelling and aligning of molecules), that take place in the aqueous phase when dissolving nonpolar organic compounds. Hydrophobic sorption is entropy driven [Hassett and Banwart, 1989]. From an energy point of view it is more efficient to sorb hydrophobic compounds onto solid particles than keeping them in solution. The dissolution of nonpolar organic compounds in the aqueous phase changes the structure of water and causes a decrease in entropy [Frank & Evans, 1945]. It is generally assumed that the adsorption process is completely reversible [Karickhoff et al., 1979; Schwarzenbach & Westall, 1981; Khorsani et al., 1988]. The hydrophobic character of an organic compound can be described by its octanol - water partition coefficient (K_{ow}). The octanol-water partition coefficient describes the preference for a compound to partition into octanol over the water phase:

$$K_{ow} = \frac{C_{octanol}}{C_{water}} \tag{1.14}$$

K_{ow} has been observed to range from 10^{-3} to 10^{7}. If K_{ow} is larger than 10^{4}, the compound is referred to as being hydrophobic. Chiou et al. [1982] show that the octanol - water partition coefficient (K_{ow}) and the water solubility (S) of a compound can be expressed by the following linearized, empirical relationship:

$$\log K_{ow} = 0.73\text{-}0.747 \log S \text{ [ppm]} \tag{1.15}$$

However, the relationship has not been verified by other researchers and is not widely used in the literature. It was established by Chiou et al. [1982] using a large variety of organic compounds with a solubility range of over 4 orders of magnitude.

Sorption studies with polycyclic aromatics and chlorinated hydrocarbons allowed Karickhoff et al. [1979] to conclude that hydrophobic organic compounds sorb **exclusively** onto the organic fraction of the solid phase. They found a strong correlation between the distribution coefficient (K_d) and the organic fraction of the solid phase (f_{oc}). The following relationship was postulated; K_d increases linearly with an increase in f_{oc}:

$$K_d = K_{oc}\, f_{oc} \qquad (1.16)$$

where; K_d: distribution coefficient [L^3/M], K_{oc}: organic carbon partition coefficient [L^3/M], and f_{oc}: weight fraction of organic carbon from the solid phase. Studies with nonpolar organic compounds by Schwarzenbach and Westall [1981] (on halogenated alkenes and benzenes) and by Hassett et al. [1983] on four representative nonpolar compounds (1,3H-Dibenzocarbazole, 6-Aminochtysene, Pyrene, PCBs) have verified the above relationship. Batch and column experiments with polycyclic aromatics and chlorinated hydrocarbons resulted in linear sorption isotherms [Karickhoff et al. 1979; Schwarzenbach and Westall, 1981]. The linear correlation holds if the f_{oc} content of the sorbent is greater than 0.001 [Schwarzenbach and Westall, 1981]. However, the accurate analytical determination of organic content has been proven to be difficult. Values of f_{oc} for geological materials vary widely and are typically between 0.01 and 0.0001 (Table 1.1).

The organic carbon partition coefficient K_{oc}, can be computed from many different empirical, log-linear regression equations of the form, $\log K_{oc} = a + b \log K_{ow}$. Three of

the most commonly used relationships are derived from studies with hydrophobic nonpolar organic compounds (Domenico and Schwartz, 1990):

Equation	Chemicals	Reference
$\log K_{oc} = -0.21 + \log K_{ow}$	aromatic, polynuclear aromatic and chlorinated hydrocarbons	[Karickhoff et al., 1979]
$\log K_{oc} = 0.49 + 0.72 \log K_{ow}$	halogenated alkenes and benzenes	[Schwarzenbach & Westall, 1981]
$\log K_{oc} = 0.088 + 0.909 \log K_{ow}$	large variety of 107 organic compounds	[Hassett et al., 1983]

Organic carbon partition coefficients, $\log K_{oc}$, from the literature are tabulated for different organic pollutants and different solids (Table 1.2). In order to use any of the above K_{oc}/K_{ow} relationships for evaluation of contaminant sorption in the aquifer the following conditions have to be met [Bedient et al., 1994; Grathwohl, 1989]:

- Sorption only takes place onto organic matter in the solid phase,
- Sorption is primarily hydrophobic,
- Sorption between the organic solid phase and water follows a linear isotherm,
- K_{oc} is independent of the soil/rock type.

1.2.4 Retardation

Retardation factors are used to describe the difference in transport velocity between water and a reactive contaminant during mass transport in porous and fractured,

media. They are often incorporated into numerical models in order to simulate sorption processes. If the sorption process is considered to be at equilibrium, reversible, and independent of concentration (linear isotherm), the expression for the retardation factor can be described in the form (Freeze and Cherry, 1979):

$$R = 1 + \frac{\rho_b}{\theta} K_d \qquad (1.17)$$

where; K_d: sorption distribution coefficient [cm^3/g], ρ_b: bulk dry density [g/cm^3], R: retardation factor (linear isotherm), and θ: porosity. In general ρ_b/θ varies by less than a factor of 10, whereas K_d may vary over about 6 orders of magnitude. If the non-linear, empirical Freundlich model applies, the retardation factor can be written as:

$$R_F = 1 + \frac{\rho_b}{\theta}\left(\frac{1}{n}\right) K_F \left(C_{eq}\right)^{\frac{1}{n}-1} \qquad (1.18)$$

where; C_{eq}: equilibrium concentration of compound in the water phase [$\mu g/cm^3$], n : empirical factor, K_F: Freundlich coefficient $\left[\frac{(m^3 - water)^{\frac{1}{n}} (g - chemical)^{1-\frac{1}{n}}}{g - solid}\right]$, and R_F: Freundlich retardation factor. The Freundlich retardation factor is, in principle, a function of concentration. When n>1, as the concentration of the compound increases the retardation factor will decrease.

In the case of mass transport in a fracture the retardation factor related to sorption onto the fracture wall is described by Freeze and Cherry [1979] and by Tang et al. [1981]:

$$R_f = 1 + \frac{K_d^*}{b} \tag{1.19}$$

where; R_f: retardation factor in fracture, K_d^*: distribution coefficient in fracture [L], and b: half aperture width [L].

1.3 Physical and Chemical Properties of Trichloroethene (TCE)

Trichloroethene (also known as trichloroethylene) is a representative of the HVCH group. Due to its hydrophobic character, TCE is used mainly for cleaning metal surfaces and in paint stripping. TCE is highly toxic and probably carcinogenic. Its physical and chemical properties are summarized in Table 1.3. In this thesis, TCE is used in sorption and matrix diffusion experiments with rock samples containing various amounts of organic matter, which are described and analyzed later in Chapter 4.

In the next paragraph the high potential of TCE retardation due to sorption onto organic matter in porous, and fractured porous media, is demonstrated with two example calculations.

1.3.1 TCE Retardation in Porous, and Fractured Porous Media due to Linear, Equilibrium Sorption

Depending on the amount and type of organic matter in the rock matrix and at the fracture - rock matrix interface in dual porosity aquifers, TCE transport can be

significantly retarded due to sorption. For example, TCE with log (K_{ow}) = 2.29, a rock matrix bulk density of 2.2 g/cm^3, and a porosity of θ = 0.1, the retardation factors are calculated using different weight fractions of organic carbon, and are presented in Figure 1.5. Here, a linear, equilibrium sorption isotherm is assumed. To estimate K_{oc} from K_{ow}, the empirical equation from Karickhoff et al. [1979] is used (see section 1.2.3.2). For example, a fraction of organic carbon of 0.01 will result in a retardation factor of 42 under the above assumptions.

To demonstrate the relationship between retardation factors for modeling sorption onto fracture wall surfaces and the fraction of organic carbon, another small example is presented. Assuming a fracture half width of 0.02 cm and a specific surface area of 0.637 cm^2/g, fracture wall retardation factors with various degrees of organic carbon are calculated and shown in Figure 1.6. A fraction of organic carbon of 0.01 in the fracture wall results in a retardation factor of 12. This means that TCE would travel 12-times slower with respect to water in the fracture.

The above calculations demonstrate the importance of organic matter when simulating TCE transport in a porous, and fractured porous aquifers.

1.4 Mass Transport in Fractured Porous Media

In the last two decades, contaminant transport of organic and inorganic pollutants in fractured porous media have received greater attention mainly due to radioactive waste disposal sites located in fractured crystalline rock formations, and due to leaking

hazardous material storage tanks above fractured aquifers. An overview of recent experimental studies on mass transport in fractured porous media and influential parameters (i.e. matrix diffusion, porosity, and stylolites) is presented, before introducing the dense non-aqueous phase liquid spill site at Smithville Ontario from which all rock samples for experimental research were taken.

1.4.1 Review of Experimental Studies

Grisak and Pickens [1980a,b] performed laboratory tracer experiments in fractured till. Calculated apertures were found to be four times higher than determined from field studies. Chlorite breakthrough curves showed retardation which presumably was due to matrix diffusion and adsorption onto clay minerals. Prudic [1982] demonstrated that the fracture conductivity of clay samples depends on stress. He concluded that with depth conductivity decreases due to increasing overburden pressure. Laboratory research by Glass and Nicholl [1995] and by Tidwell et al. [1995] focused on matrix imbibition and graphical visualization of unsaturated flow through fractured tuff. Solute concentrations were visualized by x-ray examinations of the 2 cm thick rock samples. Gas tracer experiments by Rasmussen [1995] with unsaturated, fractured volcanic tuff yielded estimates for fracture hydraulic conductivity and apertures. One of the first laboratory scale tracer experiments with radioactive nuclides through a fractured granite was conducted by Vandergraaf [1995]. Migration behavior of most isotopes was complex and could not be modeled with linear, reversible sorption coefficients. Kinetic sorption, redox

conditions, and the composition of certain minerals are assumed to play an important role in radionuclide migration through fractured granite.

A number of field experiments in the 1980's and 90's, with conservative and reactive tracers, were conducted in fractured sedimentary and crystalline rocks. These tests determined fracture apertures and evaluated the effects of matrix diffusion and sorption in situ [Carlsson, 1983; Skagius and Neretnieks, 1986; Raven et al., 1988; Birgersson and Neretnieks, 1990; Rudolph et al., 1991; Birgersson et al., 1993]. McKay et al. [1993] investigated the migration of isotope (Br^-, O^{18}) and colloid-sized bacteriophage tracers through fractured clay. Due to the size difference, bacteriphages traveled two orders of magnitude faster than the conservative tracers. The smaller size of Br^- and O^{18} results in higher matrix diffusion, and consequently they were more retarded with respect to water than colloid-sized bacteriophages. Besides evaluating fracture apertures and matrix diffusion parameters, Novakowski and Lapcevic [1994] calculated tracer dispersivities from a discrete fracture experiment. They concluded that dispersivity increased asymptotically to a value of 0.3 m after 10 m travel time, and than remained relatively constant.

The major conclusion reached was that all laboratory and field scale experiments recognized the importance of matrix diffusion as a contaminant transport mechanism in fractured porous media and its significance towards contaminant retardation.

1.4.2 Matrix Diffusion

Diffusion is a kinetic spreading process due to the constant motion of particles in all directions (Brownian motion). The free-water diffusion coefficient (or Brownian diffusivity) can be described after Kessler and Hunt [1994] by:

$$D^0 = \frac{k_B T}{3\pi \mu d_p} \tag{1.20}$$

where; D^0: free-water diffusion coefficient [m^2/s], k_B: Boltzmann constant [m N/K], T: absolute temperature [K], μ: viscosity [N s/m^2], and d_p: particle (molecule) diameter [m]. Diffusion in porous media is related to the net flux of mass per unit area (J), porosity of the porous media (θ) and the concentration gradient $(\partial c / \partial x)$ according to Flick's first law:

$$J = -D^* \theta \frac{\partial c}{\partial x} \quad \text{(one - dimensional)} \tag{1.21}$$

where; J: net flux of molecules per unit area [$M/L^2/T$], $(\partial c / \partial x)$: concentration gradient [$M/L^3/L$], D^*: effective diffusion coefficient in a porous medium [L^2/T], and θ: porosity [L/L]. Fick's second law describes transient mass transport in a porous medium, with zero advective velocity:

$$\frac{\partial c}{\partial t} = \left(\frac{D^*}{R}\right) \frac{\partial^2 c}{\partial x^2} \tag{1.22}$$

where; $\partial c / \partial t$: change in concentration with time [$M/L^3/T$], and R: retardation factor (under linear, reversible, equilibrium sorption).

Shackelford [1991] refers to the combined coefficient of D^*/R as the "apparent diffusion coefficient" (D^*_A) and as the "effective diffusion coefficient of the reactive solute" (D_s).

$$D^*_A = D_s = D^*/R \tag{1.23}$$

The effective diffusion coefficient also depends on the degree of saturation in the porous medium. Diffusion values reported from saturated soils are 10 to 20 times higher then corresponding values in unsaturated soils [Shackelford, 1991]. Figure 1.7 illustrates the effect of matrix diffusion on reactive and nonreactive contaminant migration in a saturated fractured, porous medium.

Matrix diffusion is an important transport mechanism and causes significant retardation of pollutants in a fractured medium if apertures are small [Maloszewski and Zuber, 1993]. Maloszewski and Zuber [1993] demonstrated that even in short-term (24 hours) tracer experiments diffusion is not negligible. Retardation due to matrix diffusion is an important issue at potential disposal sites, even in impervious material [Mazurek et al., 1996]. Isotope disequilibria give proof of matrix diffusion into the wall rock of at least 0.08 m in Opalinus shale [Mazurek et al., 1996]. As a conclusion from a single, horizontal, discrete fracture tracer experiment, Novakowski and Lapcevic [1994] point out that the most significant physical parameter influencing matrix diffusion from the fracture into the rock matrix is porosity (see equation 1.21).

1.4.3 Porosity

As all of the experimental research in this thesis is conducted on dolostone rock samples, the short review on porosity presented herein is limited to carbonate rocks. Porosity is a fundamental rock property, and is defined as the ratio of void volume to total rock volume. It is the void space in porous media that allows for fluid-flow and contaminant transport. In a fractured porous media, like most carbonate rock formations, main fluid-flow and mass transport takes place through the fracture network. The matrix porosity of the rock mass becomes important when considering contaminant transport from the fracture into the surrounding rock matrix by diffusion. Not all the pore space is interconnected and available for contaminant transport. Note that the effective or interconnected porosity is often determined by diffusion experiments and mass balance calculations. In the literature most published porosity data from carbonate rock matrix actually represents total porosity (Table 1.4).

Heling [1968] investigated consolidated, fine-grained Upper Jurassic carbonates with 87 to 100 % carbonate fractions. Total porosity ranged from 0.3 to 8.0 % and specific surface areas ranged between 0.3 and 6 m^2/g. This research determined the interconnected pore space with radii larger 100 Å by Hg - posimetry and pore space with radii around 10 Å by benzole - vapor adsorption. The resulting porosity had a value of about 1/3 that of the total porosity (4 %). He concluded that the remaining porosity must be "dead pore" space. Selley [1988] found that in most carbonate rocks porosity and permeability do not correlate, and that the sizes and shapes of individual pores are

extremely variable. Little correlation between pore volume, pore geometry and grain size, shape and sorting exists. In compacted carbonate rocks the main contribution towards porosity comes from secondary porosity [Selley, 1988]. Leaching processes give rise to moltic and vuggy porosity (Table 1.4). It is common that secondary moltic and vuggy porosity generated by dissolution increases total porosity up to 20 % in microfacies layers with high skeleton content as in parts of the Amapá Formation in Brazil [Carozzi, 1989].

Many carbonate rock formations contain stylolites, which are pressure dissolution features. A detailed investigation of the Atokan Limestone (Middle Pensylvanian) in Texas indicate a parallel increase in secondary burial porosity with an increase in frequency and amplitude of sutured stylolites [Carozzi and Von Bergen, 1987]. The highest porosity microfacies correlates with the peak in high-amplitude sutured stylolites. From thin-section observations and porosity measurements Carozzi [1989] concludes that stylolites carried diagenetic fluids which created an adjacent secondary porosity and connected otherwise isolated pore space. Depending on subsequent cementation the stylolitic porosity can be, but is not necessarily, preserved. From the above studies by Carozzi [1989] and Carrozzi and Von Bergen [1987] it can be concluded that stylolites play an important role in mass transport in carbonate rocks due to their high porosity. In the next paragraph the reader is introduced to the origin, classification, and possible composition of stylolites.

1.4.4 Stylolites

Stylolitization of carbonate rocks takes place under pressure dissolution due to loading or tectonic related stresses. Carbonates are mobilized under high pressure, whereas relatively insoluble residual phases like silica minerals, ore minerals and organic matter become concentrated on internal discontinuity boundaries. Note that stylolite is a generic term and does not imply a specific composition.

Park and Schot [1968] report a large variety of possible stylolite materials including coal, silica, pyrite, sphalerite, molybdenite, limonite, fluorite, carbonates, phosphates, serpentine, clay and organic material. In carbonate host rock the stylolites appear as black to light gray suture lines, ranging from microns to centimeters in thickness. Stylolites are classified after a) the geometric appearance of the suture line, and b) their orientation with respect to bedding planes (Fig. 1.8 and Fig. 1.9) [Park and Schot, 1968]. Younger stylolites have lower amplitude and thinner seams compared to older stylolites. During the adolescent stages of a growing stylolite, shear stresses are generated at the tips, which cause an increase in seam thickness and suture amplitude [Rice, 1986].

The most significant characteristics of stylolites for mass transport of organic pollutants in carbonate aquifers are thought to be (i) their organic content, (ii) their large lateral extension, and (iii) their high frequency in horizontally stratified carbonates. No data concerning organic carbon content in stylolites are published in the literature.

1.4.5 Smithville Site

Smithville is a small town in southern Ontario between Hamilton and Niagara Falls (Fig. 1.10). The town sits on a plateau about 20 km west of the Niagara Escarpment. At the outskirts of the city the Twenty Mile Creek flows, which is the only large waterway running on the plateau parallel to the escarpment.

1.4.5.1 Dense Non-Aqueous Phase Liquid (DNAPL) Spill

In the 1970's PCB oils and other chlorinated organic compounds were stored at the Chemical Waste Management Ltd. facility in Smithville. Golder Associates [1995] estimated that about 30,000 liters of dense non-aqueous phase liquids (DNAPL) were released into the subsurface through leaking storage containers until 1985, when Ontario Ministry of the Environment and Energy assumed management of the site. The Canadian Center for Inland Waters (CCIW) together with the University of Waterloo, McMaster University, University of Utah, and the United States Environmental Protection Agency investigated the spill. At present, research is ongoing to evaluate the possibilities of contaminant remediation in the bedrock. A number of monitoring wells are installed at the site and CCIW drilled a number of boreholes for hydrogeological investigations (Fig. 1.11). The average composition of DNAPL samples taken from the site is represented in Table 1.6 [Golder Associates, 1995]. The source release history of the DNAPL mixture is unknown. Two separate toxic plumes were created. One dense oil phase (separated from the water phase) and one dissolved-phase plume (Fig. 1.12) can be identified. The

immiscible DNAPL is driven by gravity, and therefore moves downward through open fractures in the clay rich overburden layer onto the underlying dolostone. The bedrock with its fracture network, bedding plane partings and vuggy zones allowed for further penetration of the DNAPL into the subsurface and contact with the groundwater. The depth of DNAPL migration into the bedrock is not known but penetration through the Eramosa Member (see next section for stratigraphy) is assumed [Golder Associate, 1995].

Due to the solubility of PCBs, TCBs and TCE in water, a dissolved-phase plume migrated with the groundwater flow in the dolostone aquifer. TCE concentrations of 1000 ppb have been found in shallow containment wells at the site. Breakdown products like vinyl chloride, dichloromethane, 1,1,1-trichloroethane and dichloroethene were found in the groundwater and may indicate that in situ biodegradation is taking place. The outer limit of the TCE plume (0.5 ppb concentration) extends about 500 m southwest from the spill site and the leading edge was detected in the Vinemount Member [Golder Associate, 1995]. Sampling indicates that the dissolved-phase TCE plume reaches as deep as the Goat Island Member.

The Guidelines for Canadian Drinking Water Quality [1993] list a maximum acceptable concentration for TCE of 50 ppb (0.05 mg/l). Note the U.S. EPA Drinking Water Standard is 5 ppb (0.005 mg/l) [Spitz and Moreno, 1995]. Consequently, the above described dissolved chlorinated hydrocarbon plume in the Lockport drinking water aquifer presents a direct threat to human health.

1.4.5.2 Geological Setting at Smithville

Sedimentary rock formations of Paleozoic age make up the bedrock throughout southern Ontario and represent an important water source. At Smithville the bedrock is covered with 5 to 10 m thick, fractured sandy clay till. The underlying Middle Silurian sedimentary rocks are composed of mainly dolostone and shale, and divided into the Lockport Formation, Decew Formation, and Rochester Formation (Fig. 1.13). Information on the stratigraphic units are taken from CCIW drill logs and from Blair and McFarland [1992].

Lockport Formation

The Lockport Formation is composed of an approximately 36 m thick dolostone sequence. Lithological variations in the sequence range from clay rich, fine grained, dense dolostone to massive, calcite rich and fossiliferous beds, mimicking the different facies under which the sediment was deposited. Based on lithological observations the Lockport Formation is subdivided into the Eramosa -, Vinemount -, Goat Island -, and Gasport - Members. The Eramosa Member has a thickness of about 13 to 19 m, the Vinemount Member 7 to 8 m, the Goat Island Member 6 to 7 m, and the Gasport Member 7 to 16 m. A horizontal and vertical fracture network cuts through the dolostone and serves as the main channel for fluid flow. Secondary mineralizations of gypsum, calcite, silica and sulfites partially fill vugs and fractures.

The Upper Eramosa is composed of brownish gray, vuggy dolostone with abundant coral fossils and numerous bedding partings (bituminous and stylolitic). Only occasional vugs, coral fossils and gypsum nodules are found in the fine to medium grained, thinly to medium bedded dolostone of the Lower Eramosa Member. The medium gray, fine grained, argillaceous dolostone of the Vinemount Member contains numerous black, bituminous bedding partings and stylolites. The lower part of the Vinemount is more massive with occasional fossils. The Goat Island Member is composed of a medium brownish gray, very fine to fine grained, medium to thickly bedded dolostone with occasional stylolite partings, and chert and gypsum nodules. The change to the light creamy to bluish gray, fine to medium grained, medium to thickly bedded, crinoidal dolostone with occasional argillaceous and stylolitic partings of the Gasport Member is very distinctive.

Decew and Rochester Formation

The fine grained dolostone of the Decew Formation is only 0.5 to 1.5 m thick and not easy to identify in borehole logs, whereas the Rochester Formation , in contrast, is composed of a distinctive, dark to medium gray, fine grained calcareous shale. The shale has a thickness of about 17 m underneath Smithville [Blair and McFarland, 1992].

Mineral composition

Whole rock geochemical analyses on 27 samples [Bickerton, 1997] show that the average dolostone ranges in composition from 85 to 98 % dolomite, 2 to 16 % quartz and

0.0 to 8 % gypsum (Table 1.7). The estimated clay mineral content ranges between 0.3 and 6.7 weight % in the Lockport Formation and between 3.1 and 13.1 weight % in the Rochester Formation [Bickerton, 1997].

1.5 Research Objectives

For the organic pollutant site at Smithville (introduced in paragraph 1.5) the discussed mass transport parameters and rock properties are under investigation. As has been mentioned earlier, the fundamental understanding of contaminant migration in the subsurface, interactions with the rock matrix, and hydrogeological transport parameters are of critical importance in order to predict contaminant fate in fractured aquifers. A number of rock properties and mass transport parameters can be evaluated with tracer laboratory and field experiments. Although laboratory studies are time consuming and simplify the real physical situation due to forced boundary and source conditions, they provide valuable information and are relatively inexpensive. Effective remediation strategies based on numerical simulations are only as good as the conceptual model representing the physical reality and its input parameters. This is important to all groundwater studies, and in particular to fractured limestone aquifers as they present an important drinking water resource for large areas in Canada, the United States, and Europe.

For the DNAPL spill at Smithville it can be assumed that matrix diffusion and sorption play an important part in retarding contaminant transport. The primary aim of this

study is to investigate rock properties that are related to these transport mechanisms, and use them subsequently in analytical and numerical simulations. Laboratory experiments with TCE will be employed to study matrix diffusion through dolostone samples and sorption onto stylolites from the Lockport Formation at Smithville.

In particular, the following issues are evaluated with laboratory studies:

1. The ability to resaturate dolostone core samples and determine hydraulic conductivity;
2. The total porosity of dolostone matrix and the vertical porosity distribution in the Lockport Formation with emphasis on porosity adjacent to fractures;
3. Whether porosity data can help identifying fractures;
4. The organic carbon content of stylolites, and whether stylolites adsorb significant amounts of TCE;
5. Sorption parameters describing the interaction between dissolved TCE and stylolites;
6. The dolostone matrix tortuosity factor for dissolved contaminants.

Analytical solutions in Laplace space are derived to simulate non-linear sorption behavior, and numerical inversion is used to calculate solute concentrations. Selected parameters from the laboratory experiments are further investigated by conducting numerical simulations with the finite element code FRACTRAN [Sudicky and McLaren, 1992].

In particular the following will be evaluated:

1. The impact of heterogeneous, vertical porosity on mass transport;
2. Whether TCE adsorption and desorption onto stylolites can be simulated with a linear or non-linear sorption isotherm and whether the process is kinetic;
3. The significance of stylolites on TCE migration in the Lockport Formation.

1.6 Scope of Research

In order to achieve the objectives of this work the following methods are employed and approaches are taken:

- Resaturation and hydraulic conductivity experiments on thin dolostone core slices (originally saturated and unsaturated samples) from the Smithville site will be conducted in a triaxial cell with a back-pressure reservoir.
- Sections of the saturated drill core 65 will be cut into thin (0.5 to 1.0 cm) slices and their total porosity will be determined using the volumetric water content.
- TCE batch experiments with stylolitic dolostone and 'pure' dolostone samples will be conducted to evaluate possible sorption and organic carbon content.
- A double reservoir diffusion cell will be designed to investigate TCE diffusion through thin stylolitic dolostone samples. In a double reservoir diffusion cell adsorption and desorption behavior can be studied simultaneously.

- Analytical solutions in Laplace space will be derived to simulate one-dimensional mass transport in the diffusion cell. Three sorption models will be considered; a) linear, reversible equilibrium sorption, b) irreversible, kinetic sorption, c) non-linear, irreversible, kinetic sorption model.
- Bromide will be used as a conservative tracer in the diffusion cell experiments. This will allow the estimation of the matrix tortuosity factor and subsequently the TCE effective diffusion coefficient.
- The analytical solution for two-dimensional mass transport in a single fracture environment by Tang et al. [1981] will be modified to simulate a homogeneous stylolitic dolostone matrix with non-linear, irreversible, kinetic sorption.
- A numerical discrete fracture model will be used to simulate TCE transport in a randomly fractured porous media with discrete stylolite layers. The individual stylolite layers will be modeled with a linear, reversible sorption isotherm. Mass balance calculations will reveal the significance of matrix diffusion and sorption onto stylolites.

References

Ball, W. P., and P. V., Roberts, Long-term sorption of halogenated organic chemicals by aquifer material. 1. Equilibrium, Environ. Sci. Technol., 25(7), 1223-1236, 1991.

Bauer, U., Belastung des Menschen durch Schadstoffe in der Umwelt - Untersuchungen über leichtflüchtige organische Halogenverbindungen in Wasser, Luft, Lebensmittel und im menschlichen Gewebe. Zbl. Bakt. Hyg., 1. Abt. Orig., 174, 1981.

Bedient, P. B., H. S. Rifai, and C. J. Newell, Ground Water Contamination. Prentice Hall PTR, Englewood Cliffs, New Jersey, 1994.

Bickerton, G.S., Chemical and mineralogical composition of the Lockport and Rochester formations, Smithville, Ontario. NWRI Contribution No. 97-130, 1997.

Birgersson, L., and I. Neretnieks, Diffusion in the matrix of granitic rock: Field tests in the Stripa mine, Water Resour. Res., 26(11), 2833-2842, 1990.

Birgersson, L., L. Moreno, I. Neretnieks, H. Widén, and T. Ågren, A tracer migration experiment in a small fracture zone in granite, Water Resour. Res., 29(12), 3867-3878, 1993.

Blair, R., and S. McFarland, Regional correlation of the Middle and Lower Niagara Escarpment Area. Proceedings of the 1992 Conference of the Canadian National Chapter, International Association of Hydrogeologists, Hamilton Ontario, 659-696, 1992.

Brunauer, S., P. H. Emmet, E. Teller, Adsorption of gases in multimolecular layers. J. Amer. Chem. Soc., 60(2), 309-319, Washington, 1938.

Carlsson, A., and T. Olsson, Stress and water flow relation in fractured rock, Bulletin Eng. Geol., 26-27, 371-375, 1983.

Carozzi. A. V., Carbonate rock depositional models: A microfacies approach, Prentice Hall, New Jersey, 1989.

Carrozi, A.V. and D. Von Bergen, Stylolitic porosity in carbonates: a critical factor for deep hydrocarbon production, J. Petrol. Geol., 10, 263-282, 1987.

CERCLA (Comprehensive Environmental Response, Compensation, and Liability Act), 1980.

Chiou, C.T., D.W. Schmedding, and M. Manes, Partitioning of organic compounds in octanol-water-systems, Envirom. Sci. Technol., 16 (1), 4-10, Washington D.C., 1982.

Clean Water Act, 1977.

Dilling, W.L., N.B. Tefertiller, and G.J. Kallos, Evaporation rates and reaktivities of methylene chloride, chloroform, 1,1,1-trichloroethane, trichloroethylene, tetrachloroethylene and other chlorinated compounds. Environ. Sci. Technol., 9 (9), 833-838, Washington, 1975.

Domenico, P. A. and F. W. Schwartz, Physical and Chemical Hydrogeology. John Wiley & Sons, New York, 1990.

Dowty, B., D. Carlisle, and J.L. Laseter, Halogenated hydrocarbons in New Orleans drinking water and blood plasma. Science, 187 (2), 75-77, Washington, 1975.

Fetter, C. W., Contaminant Hydrogeology, Macmillan Publishing Company, New York, 1993.

Frank, H., and M. Evans, Free volume and entropy in condensed system. III. Mixed liquids. J. Chem. Phys., 13, 507-532, Lancaster, New York, 1945.

Freeze, R. A., and J. A. Cherry, Groundwater. Prentice Hall, Englewood Cliffs, New Jersey, 1979.

Fricke, H, Grundwasserverunreinigungen durch Herstellung und Anwendung von chlorierten Lösungsmittel aus Sicht der Industrie. DVGW-Schriftenreihe, 29, 119-132, Frankfurt (ZfGW-Verlag GmbH), 1981.

Garbarini, D. R., and L. W. Lion, Evaluation of sorptive partitioning of nonionic pollutants in closed systems by headspace analysis. Environ. Sci. Technol., 19, 1122-1128, 1985.

Giger, W., R.P. Schwarzenbach, E. Hoehn, K. Schellenberg, J.K. Schneider, H.R. Wasmer, J. Westall, and J. Zobrist, Das Verhalten organischer Wasserinhaltsstoffe bei der Grundwasserbildung und im Grundwasser. Gas - Wasser - Abwasser, 63, (9), 517-531, Zürich, 1983.

Glass, R. J., and M. J. Nicholl, Quantitative visualization of entrapped phase dissolution within a horizontal flowing fracture, Geophys. Res. Letters, 22(11), 1413-1416, 1995.

Golder Associates Ltd. "Hydrogeologic Data Compilation and Assessment CWML Site Smithville, Ontario." Smithville Phase IV Bedrock Remediation Program. Project No.94-106. May 1995.

Grathwohl, P., "Verteilung unpolarer organischer Verbindungen in der wasserungesättigten Bodenzone am Beispiel leichtflüchtiger aliphatischer Chlorkohlenwasserstoffe (Modellversuche)." Tübinger Geowissenschaftliche Arbeiten (PH.D. theses publications), Reihe C, 1, 1989.

Grisak, G. E., and J. F. Pickens, Solue transport through fractured media, 1. The effect of matrix diffusion, Water Resour. Res., 16 (4), 719-730, 1980a.

Grisak, G. E., J. F. Pickens, and J. A. Cherry, Solute transport through fractured media, 2, Column study of fractured till, Water Resour. Res., 16(4), 731-739, 1980b.

Hansch, L., and A. Leo, Substitute constants for correlation analysis in chemistry and biology. Amsterdam (Elsevier), 1979.

Hassett, J. J., W. L. Banwart, and R. A. Griffin, Correlation of compound properties with sorption characteristics of nonpolar compounds by soils and sediments: concepts and limitations. in: Environment and solid wastes, ed., C. W. Francis and S. I. Auerbach, Butterworths, Boston, 1983.

Hassett, J.J., and W.L. Banwart, The sorption of nonpolar organics by soils and sediments. Soil Science Society of America (SSSA) special publication, 22, 31-44, 1989.

Heling, D., Microporosity of carbonate rocks, in: Recent Developments in Carbonate Sedimentology in Central Europe, ed. G. Müller and G. M. Friedman, Springer Verlag, New York, 1968.

Ibaraki, M., and E. A. Sudicky, Colloid-facilitated contaminant transport in discretely fractured porous media, 1. Numerical formulation and sensitivity analysis. Water Resour. Res., 31(12), 2945-2960, 1995.

Karickhoff, S.W., D.S. Brown, and T.A. Scott, Sorption of hydrophobic pollutants on natural sediments. Water Research, 13 (3), 241-248, Oxford (Pergamon Press), 1979.

Karickhoff, S.W., Organic pollutant sorption in aquatic system. Journal of Hydraulic Engineering, 10 (6), 707-735, New York, 1984.

Kessler, J. H., and J. R. Hunt, Dissolved and colloidal contaminant transport in a partially clogged fracture, Water Resour. Res., 30(4), 1195-1206, 1994.

Khorsani, R., R. Wienberg, and U. Förstner, Verfestigung, Stabilisierung und Einbindung organischer Schadstoffe aus Deponien unter besonderer Berücksichtigung anorganischer und organischer Füllstoffe und Bindemittel. Altlastensanierung '88, Proc. 2nd International TNO/BMFT Congress (11-15 April 1988; Hamburg), 987-996, Dordrecht, Boston, Lancaster (Kluwer Academic Press), 1988.

Kirk, R.E., and D.F. Othmer, Encyclopedia of chemical technology. 1318 p., New York, 1985.

Kühn, W., Organische Chlorverbindungen in der Umwelt und im Grundwasser. DVGW-Schriftenreihe Wasser, 29, 7-23, Frankfurt (ZfGW-Verlag GmbH), 1981.

Mackay, D.M., and W.-Y. Shiu, A critical review of Henry's law constants of environmental interest. J. Phys. Chem. Ref. Data, 10 (4), 1175-1202, 1981.

Maloszewski, P., and A. Zuber, Tracer experiments in fractured rocks: Matrix diffusion and the validity of models, Water Resour. Res., 29(8), 2723-2735, 1993.

Mazurek, M., W.R. Alexander, and A.B. MacKenzie, Contaminant retardation in fractured shales: matrix diffusion and redox front entrapment, J. of Contam. Hydrology, 21, 71-84, 1996.

McKay, L. D., R. W. Gillham, and J. A. Cherry, Field experiments in fractured clay till, 2, Solute and colloid transport, Water Resour. Res., 29(12), 3879-3890, 1993.

McConnell, G., D.M. Ferguson, and C.R. Pearson, Chlorierte Kohlenwasserstoffe in der Umwelt. Endeaver, 34, 13-18, Oxford (Pergamon Press), 1975.

Novakowski, K. S., and P. A. Lapcevic, Field measurement of radial solute transport in fractured rock, Water Resour. Res., 30(1), 37-44, 1994.

Park, W., and E.H. Schot, "Stylolitization in Carbonate Rocks", in: Recent Developments in Carbonate Sedimentology in Central Europe, eds. German Muller and Gerald M. Friedman, New York (Springer-Verlag New York Inc.), 66-74, 1968.

Prudic, D.E., Hydraulic conductivity of a fine-grained till, Cattaraugus County, New York, Ground Water, 20(2), 194-204, 1982.

Rasmussen, T. C., Laboratory characterization of fluid flow parameters in porous rock containing a discrete fracture, Geophys. Res. Letters, 22(11), 1401-1404, 1995.

Raven, K. G., K. S. Novakowski, and P. A. Lapcevic, Interpretation of field tracer tests of a single fracture using a transient solute storage model, Water Resour. Res., 24(12), 2019-2032, 1988.

RCRA (Resource Conservation and Recovery Act), 40 C. F. R. Parts 260-271, 1976.

Rice, M.C., "Stylalitization Mechanisms, Permeability Barriers and Pressure Solution Generated Cements: Examples from the Lockport Formation (Middle Silurian) of Dundas, Ontario and Nisku Formation (Upper Devonian) of Central Alberta." Unpublished MSc theses, McMaster University, 1986.

Rudolph, D. L., J. A. Cherry, and R. N. Farvolden, Groundwater flow and solute transport in fractured lacustrine clay near Mexico City, Water Resour. Res., 27(9), 2187-2201, 1991.

Schlichting, E., and H.-P. Blume, Bodenkundliches Praktikum. Hamburg (P. Parey-Verlag), 1966.

Schwarzenbach, R.P., and J. Westall, Transport of nonpolar organic compounds from surface water to groundwater. Laboratory sorption studies. Environ. Sci. Technol., 15 (11), 1360-1367, Washington, 1981.

SDWA (Safe Drinking Water Act), 1974.

Selley, R. C., Applied Sedimentology, Academic Press, London, 1988.

Shackelford, C.D., Laboratory diffusion testing for waste disposal - A review. J. of Contam. Hydrology, 7, 177-217, 1991.

Skagius, K., and I. Neretnieks, Porosities and diffusities of some nonsorbing species in crystalline rocks, Water Resour. Res., 22(3), 389-398, 1986.

Spitz, K.-H., and J. Moreno, A Practical Guide to Groundwater and Solute Transport Modelling. New York (Wiley-Interscience Publication), 1996.

Sudicky, E.A., and R.G. MaLaren, The Laplace transform Galerkin technique for large scale simulation of mass transport in discretely fractured porous formations. Water Resour. Res., 28 (2), 499-514, 1992.

Tang, D.H., E.O. Frind, and E.A. Sudicky, Contaminant transport in fractured porous media: Analytical solution for a single fracture. Water Resour. Res., 17 (3), 555-564, 1981.

Tidwell, V. C., R. J. Glass, and W. Peplinski, Laboratory investigation of matrix imbibition from a flowing fracture, Geophys. Res. Letters, 22(11), 1405-14-8, 1995.

Tompson, A. F. B., and K. J. Jackson, Reactive transport in heterogeneous systems: An overview, in: Reactive Transport in Porous Media, ed. P. C. Lichter, C. I. Steefel, and E.H. Oelkers, Mineralogical Society of America, Reviews in Mineralogy, v. 34, 269-310, 1996.

TSCA (Toxic Substances Control Act), 1976.

U.S. Environmental Protection Agency, National water quality inventory. 1988 Report to Congress, EPA-440-4-90-003, 187 p., 1990.

Vandergraaf, T. T., Radionuclide migration experiments under laboratory conditions, Geophys. Res. Letters, 22(11), 1409-1412, 1995.

Verschueren, K., Handbook of environmental data on organic chemicals. Second Edition. 1310 p., New York (Van Nostrand Reinhold Company Inc.), 1983.

Weber, W. J. Jr., and C.T. Miller, Modeling the sorption of hydrophobic contaminants by aquifer materials. 1. Rates and equilibria, Water Research, 22(4), 457-464, 1988.

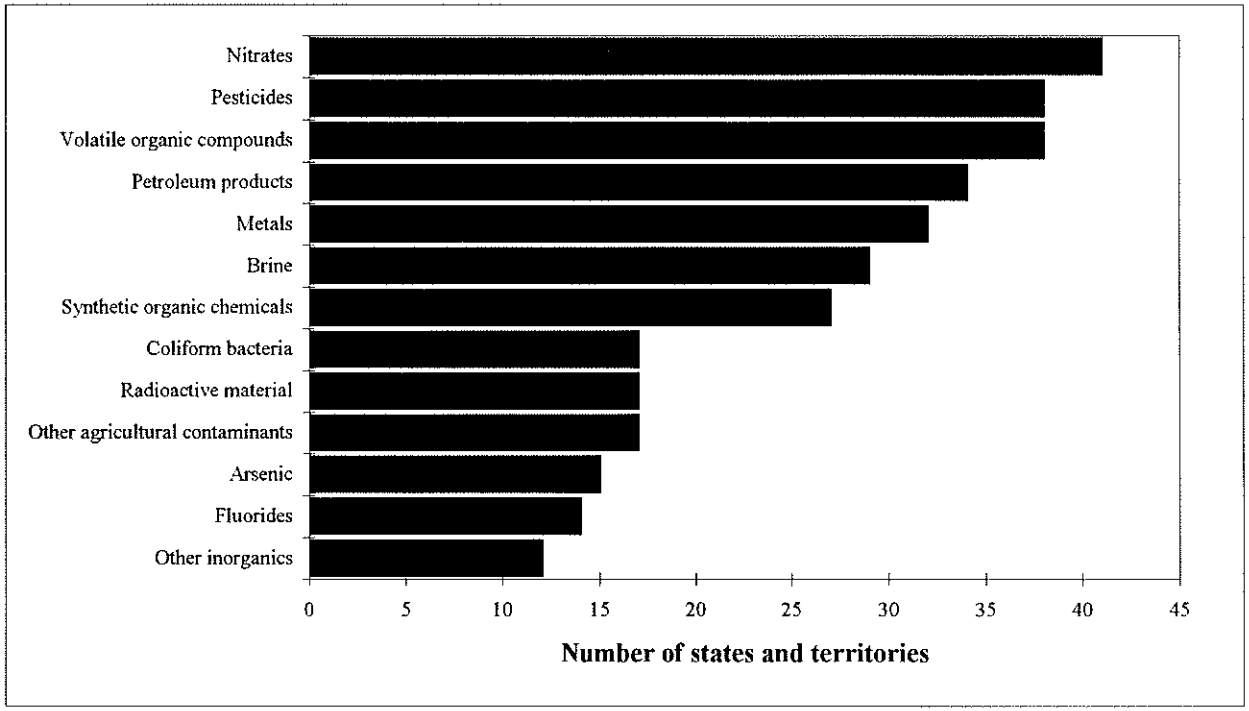

Figure 1.1: Frequency of various contaminants considered by state and territories of the United States to be major threats to ground water quality (National Water Quality Inventory, 1988 Report to Congress, Environmental Protection Agency, 1990).

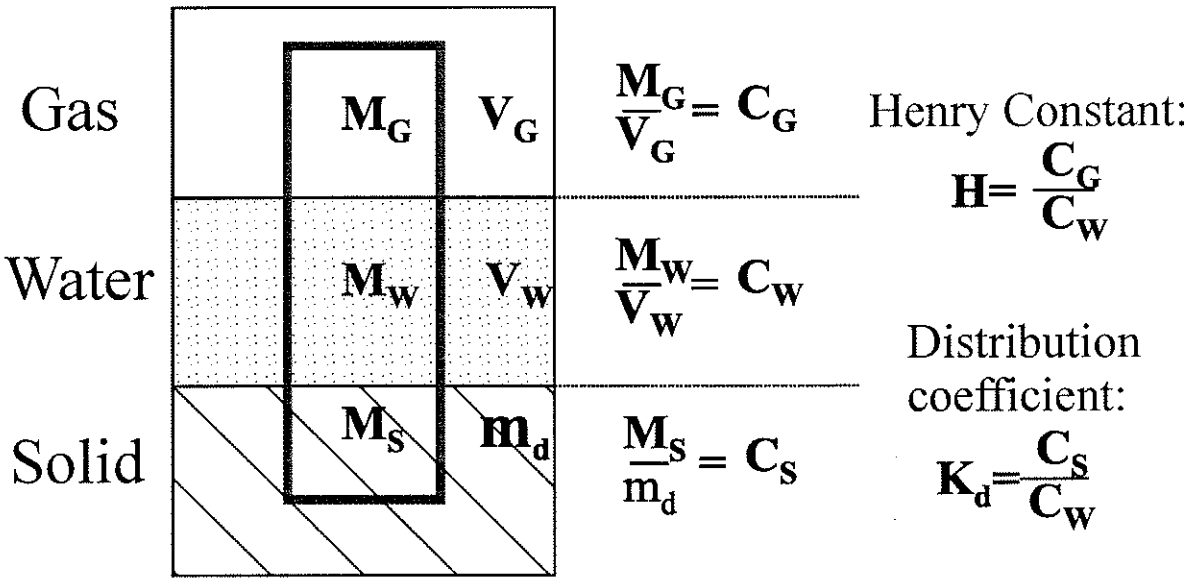

V_G, V_W	: volume of gas - and water - phase [l]
m_d	: dry mass of solids [kg]
M_G, M_W, M_S	: mass of contaminant in the three phases; gas, water, solids [µg]
C_G, C_W, C_S	: contaminant concentration in the three phases; gas, water [µg/l] solids [µg/kg]
H	: Henry constant
K_d	: distribution coefficient solid/water [l/kg or cm^3/g]

Figure 1.2: Gas-water phases and water-solid phases distribution coefficients.

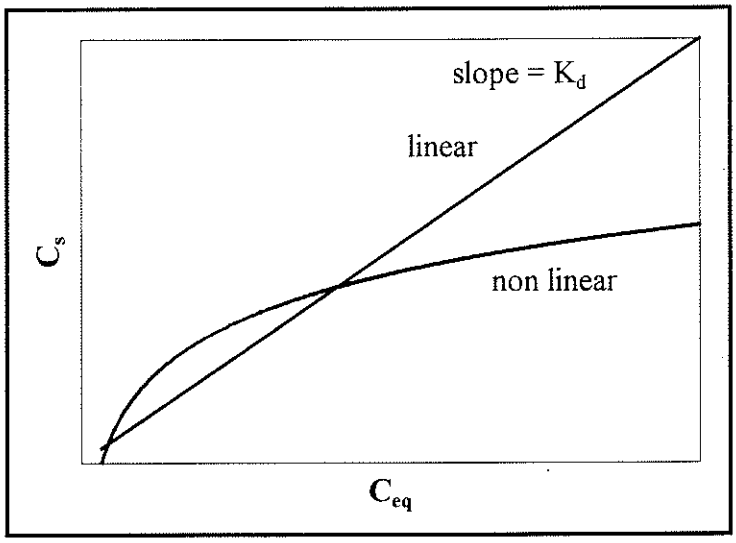

Figure 1.3 General form of linear and non linear sorption isotherm.

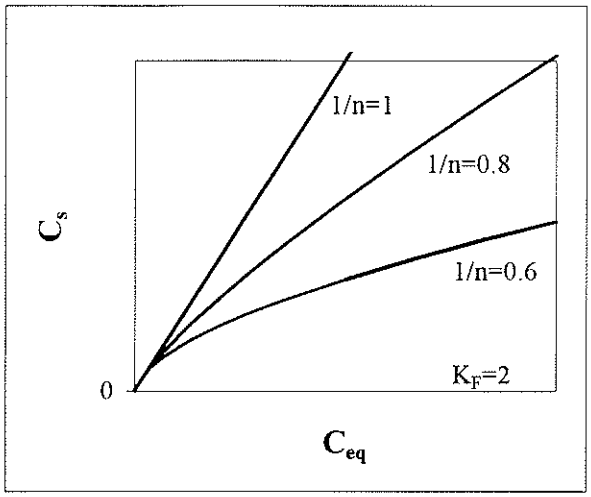

$C_S=K_F*C_{eq}^{1/n}$

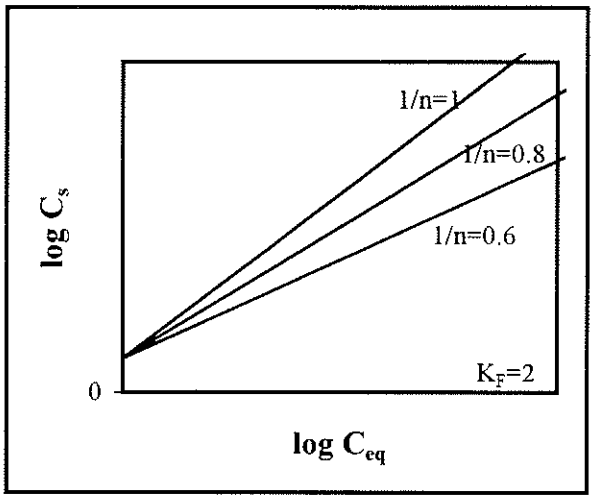

$\log C_S=1/n*\log C_{eq}+\log K_F$

Figure 1.4 Empirical Freundlich sorption isotherm in power-law and log-normatized forms.

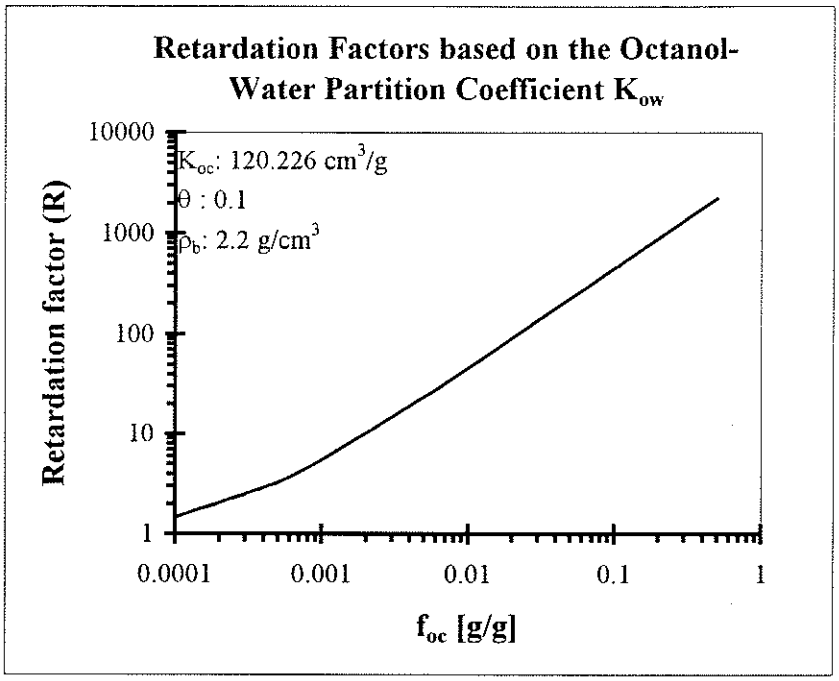

Figure 1.5: Retardation factors versus fraction of organic carbon content in the porous media.

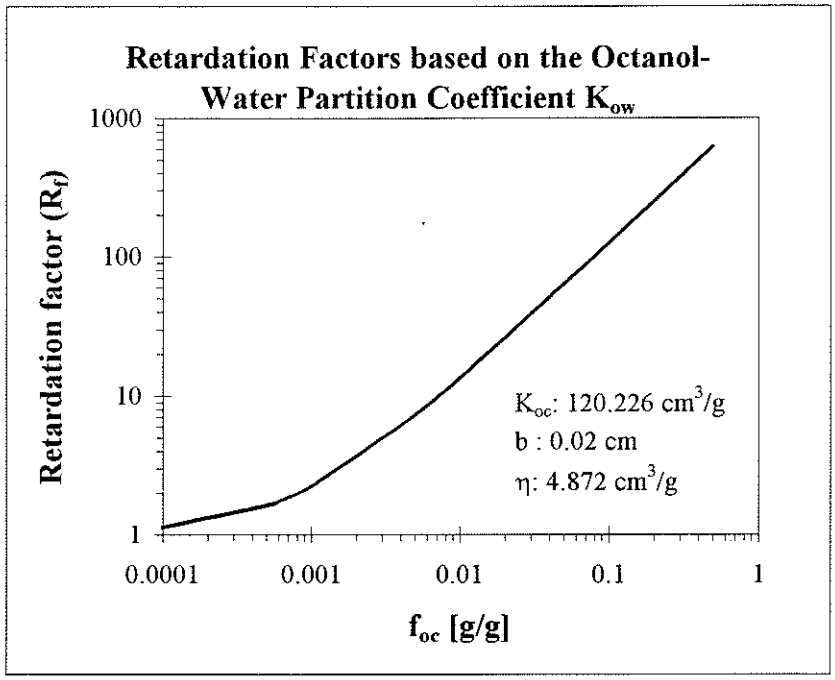

Figure 1.6 Retardation factors versus fraction of organic carbon content along the fracture wall.

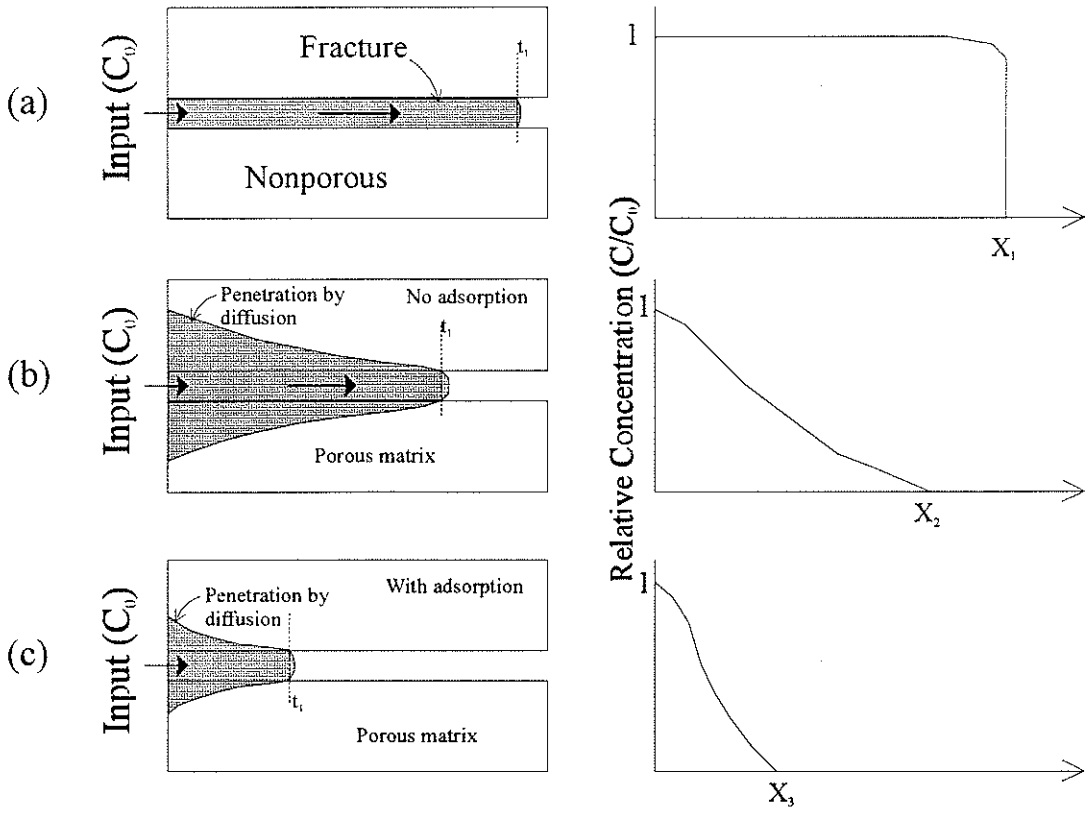

Figure 1.7: Effect of matrix diffusion on contaminant migration in a fractured, porous medium; a) without diffusion, b) with matrix diffusion, c) with matrix diffusion and adsorption; relative concentrations in the fracture are shown at t=1 (after Freeze and Cherry, 1979).

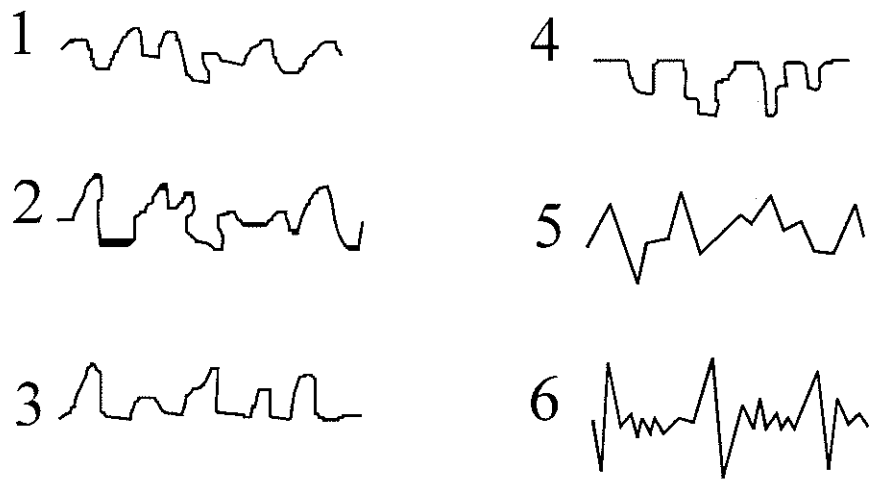

Figure 1.8: Classification of stylolites with respect to suture geometry:
1. Simple wave length; 2. Suture like; 3. Up-peak;
4. Down-peak; 5. Sharp-peak; 6. Seismogram type
(after Park and Schot, 1968).

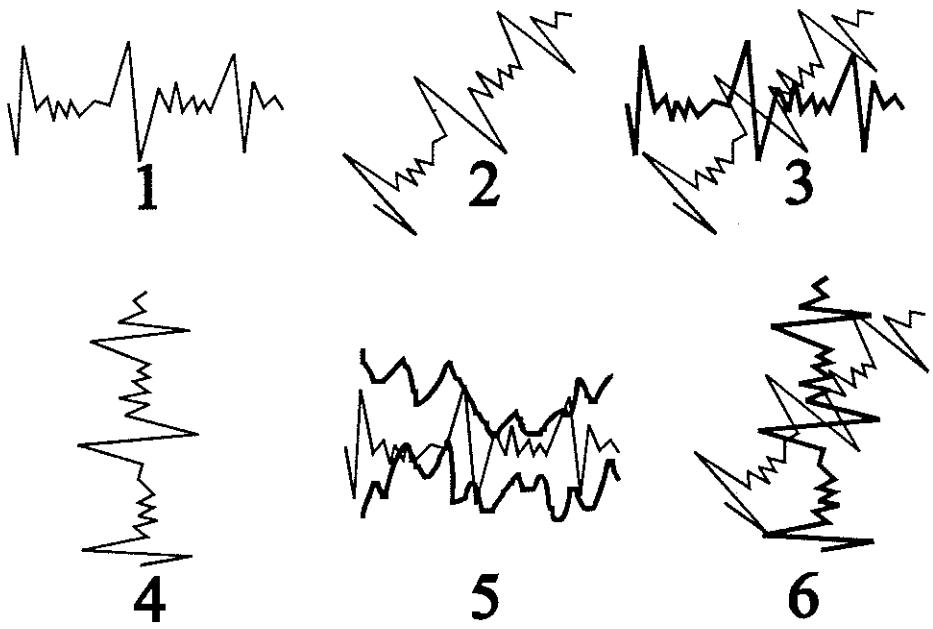

Figure 1.9: Classification of stylolites with respect to bedding planes:
1. Horizontal, 2. Inclined; 3. Horizontal-Inclined;
4. Vertical; 5. Interconnected Network; 6. Vertical-Inclined
(after Park and Schot, 1968).

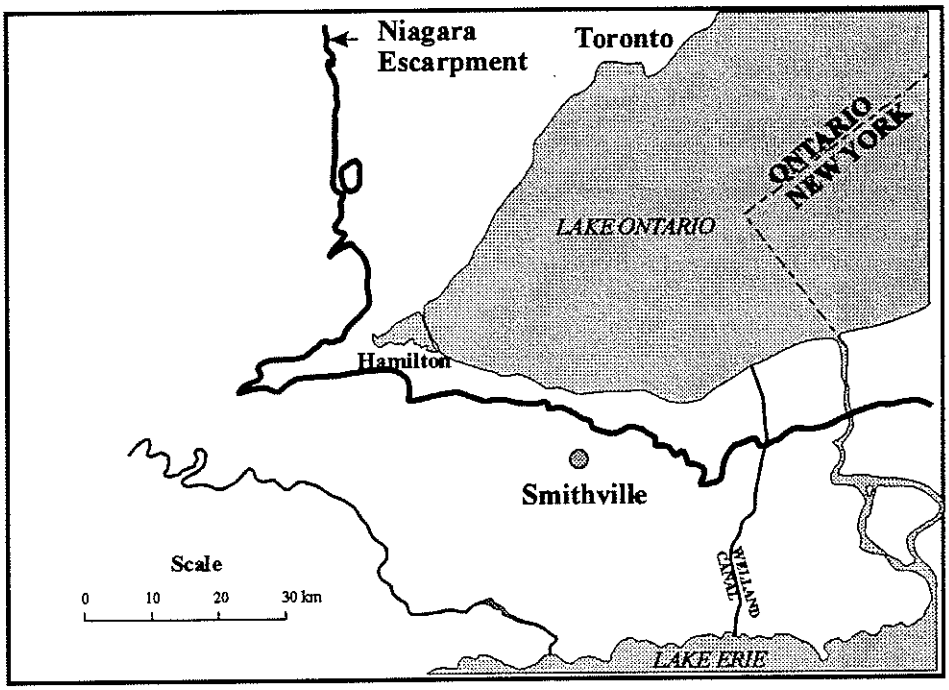

Figure 1.10: Location of Smithville in Southern Ontario
(source: Canadian Center for Inland Waters, 1997).

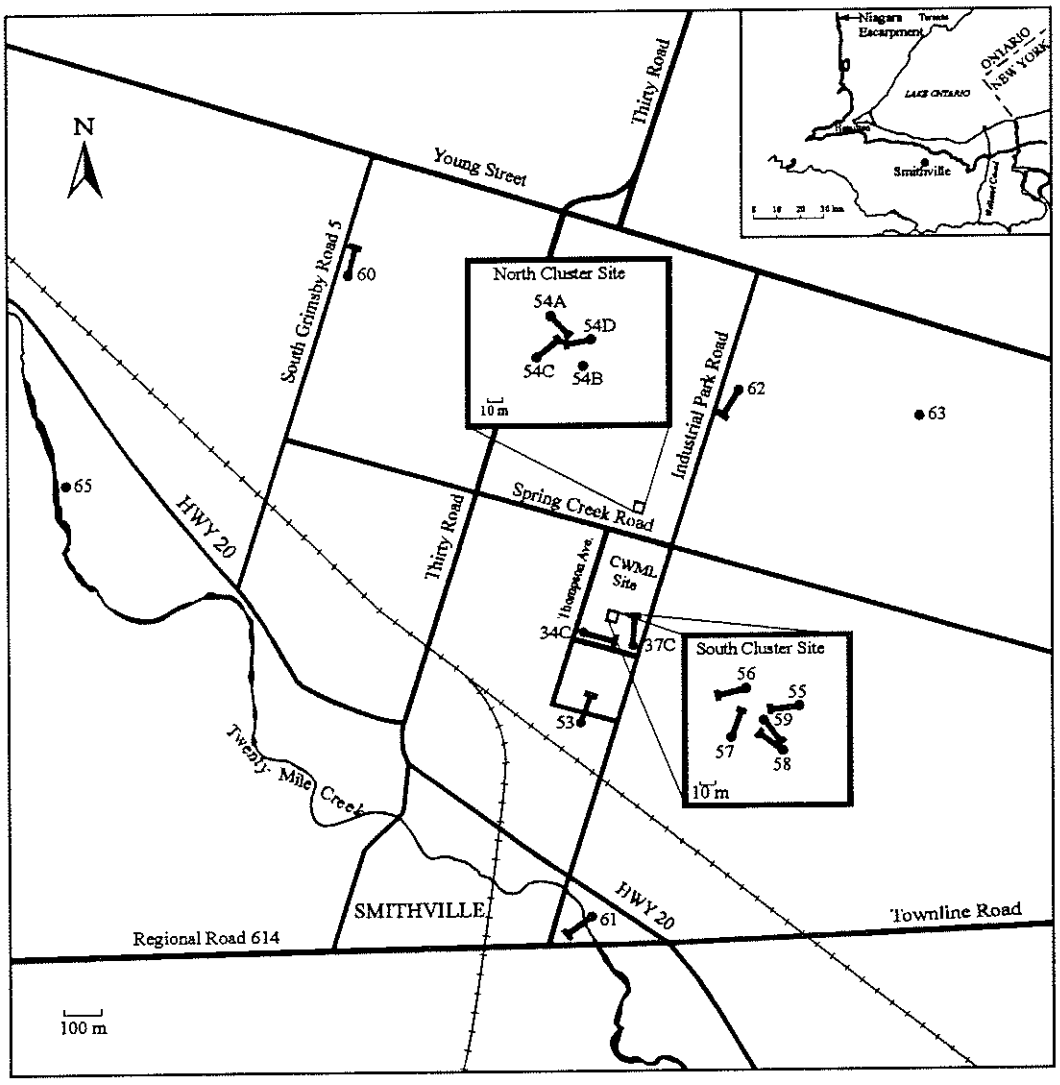

Figure 1.11: Site of DNAPL spill with test hole locations
(Source: Canadian Center for Inland Waters, 1997).

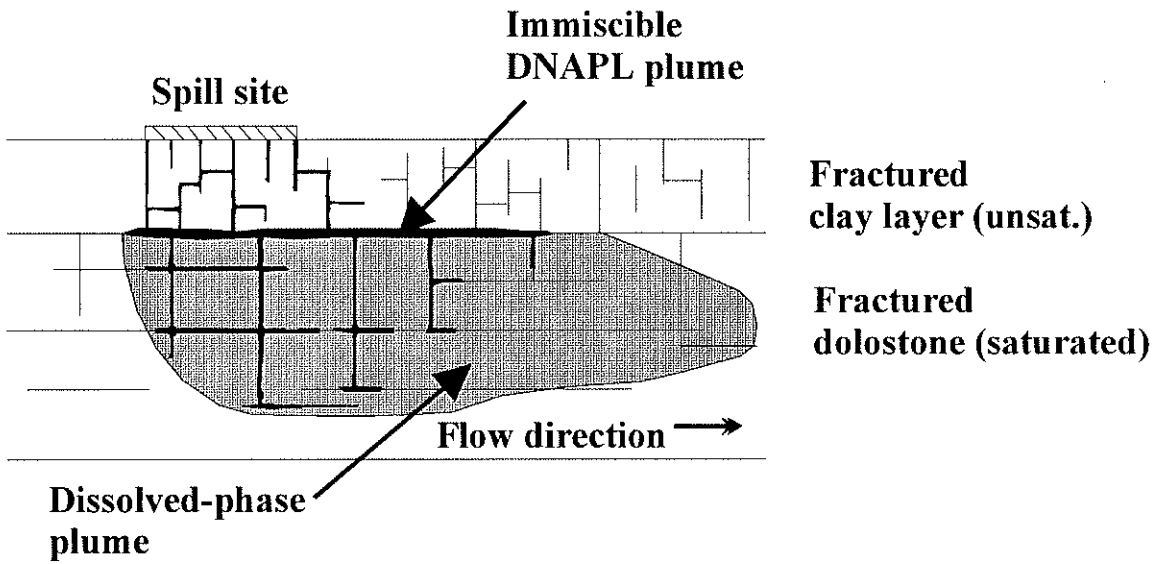

Figure 1.12: Schematic picture showing the different migrations of immiscible DNAPL plume and dissolved-phase plume.

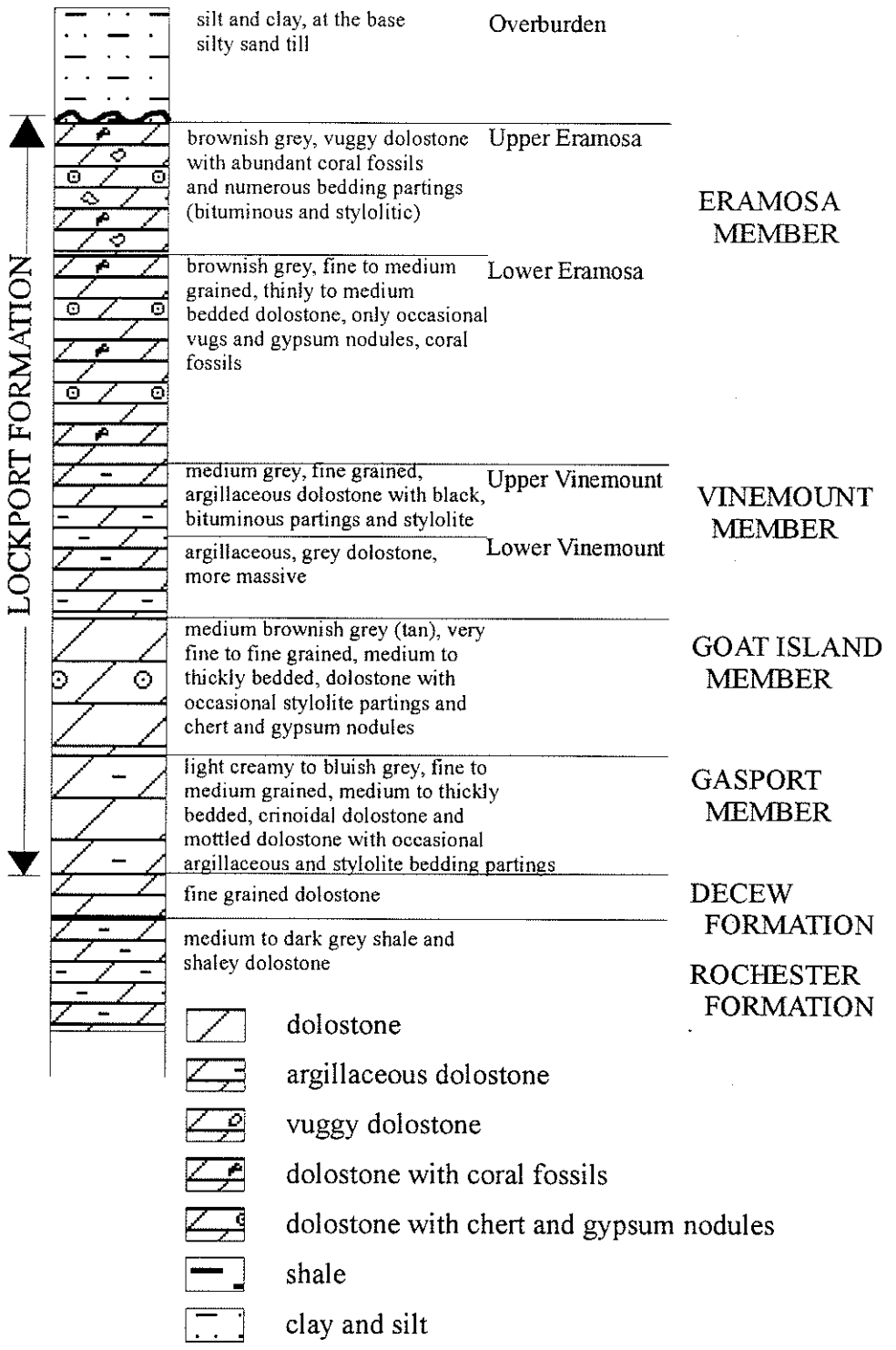

Figure 1.13: Stratigraphic column at Smithville, Southern Ontario (modified after Blair and McFarland, 1992).

Table 1.1
Organic Carbon Content (f_{oc}) of Sediments
(modified after Spitz and Moreno, 1996)

Material	f_{oc}	Reference
medium sand, glacio-fluvial (North Bay)	0.00017	Gillham et al. (1987)
fine- to medium-grained sand, glacio-fluvial (Woolwich)	0.00023	"
fine sand, glacio-fluvial (Chalk River)	0.00026	"
fine to medium sand, glacio-fluvial (Borden)	0.00028	"
fine to medium sand, fluvio-glacial (Ottawa-Gloucester)	0.00060	"
medium sand, glacio-fluvial (Cambridge)	0.00065	"
fine-grained sand, glacio-lacustrine	0.00102	"
silt, lacustrine (Wildwood)	0.00108	"
sand, gravel (Glatt Valley)	0.0004 to 0.0073	Schwarzenbach & Westall (1981)
sand, gravel (Aare Valley)	0.0023	"
sediment from a eutrophic lake	0.019 to 0.058	"
oilschist, Eocene (Messel,Germany)	0.2675	Grathwohl (1989)
Impressamergel[1], Jurassic (SW Germany)	0.00561	"
Opalinus clay, Jurassic (SW Germany)	0.01497	"
Posidonian schist, Jurassic (SW Germany)	0.11085	"
Knollenmergel[1], Triassic (SW Germany)	0.00048	"
Schilfsandstone, Triassic (SW Germany)	0.0077	"
Wellendolomite. Triassic (SW Germany)	0.00076	"

[1]: calcareous clay and clayey limestone

Table 1.2
Physical and Chemical Properties of TCE

molecular weight	131.5 [g/mole]	Verschueren, 1984
density	1.465 [g/cm^3]	Kirk & Othmer, 1985
boiling point	86.7 [°C]	Verschueren, 1984
water solubility at 20°C	1100 [mg/l]	Verschueren, 1984
saturation pressure at 20°C	7.72 [kPa]	McConnell et al., 1975
	9.86 [kPa]	Dilling et al., 1975
	8.00 [kPa]	Mackay & Shiu, 1981
Henry constant at 20°C	0.36 [-]	McConnell et al., 1975
	0.48 [-]	Dilling et al., 1975
	0.37 [-]	Mackay & Shiu, 1981
partition coefficient log K_{ow}	2.29	Giger et al., 1983
	2.29	Hansch & Leo, 1979

Table 1.3
Experimental and Calculated log K_{oc} Values

Material	TCA	TCE	PCE	Reference
sand		2.69	2.43	Sontheimer et al.,1983
peatty silt	1.92		2.29 to 2.56	"
peat	1.66	1.77	2.28	"
fossil wood	1.85	1.97	2.26	"
brown coal			2.87 to 3.26	"
sediments			2.32	Giger et al., 1983
soils[1]	2.26	2.03	2.56	Chiou et al., 1981
humid acid		1.79		Peterson et al., 1988
K_{ow}[2]	2.08	1.97	2.39	Sontheimer et al., 1983
K_{ow}[2]	2.29	2.15	2.57	Giger et al., 1983

[1]: calculated from K_{om}; K_{om} is the sorption coefficient related to organic material instead of organic carbon bounded in the soil (K_{oc}= 1.724 *x* K_{om}; Lyman, 1982)
[2]: calculated from K_{ow}

Table 1.4
Total Porosity in Carbonates
(modified after Spitz and Moreno, 1996)

Rock type	Porosity [%]	Reference
dolomite	5 to 15	Cross et al., 1985
dolomite	3.4	Halevy and Nir, 1962
dolomite, fractured	18	Bentley and Walter, 1983
dolomite, fractured	12	Grove and Beetem, 1971
dolomite, fractured	2.4	Kreft et al., 1974
dolomite, fractured	7 to 11	Walter, 1983
dolomite and limestone fractured	6 to 60	Claasen and Cordes, 1975
limestone	0.3 to 8	Heling, 1968
Atokan limestone	2 to 8	Carozzi and Von Bergen,1987
Amapá Formation, dolomite	2 to 20	Carozzi, 1989

Table 1.5
Classification of Porosity Types (Selley, 1988)

	Type	**Origin**
I. Primary or depositional	a) Intergranular	Sedimentation
	b) Intragranular	"
II. Secondary or post-depositional	c) Intercrystalline	Cementation
	d) Fenestral	"
	e) Moltic	Solution
	f) Vuggy	"
	g) Fracture	Tectonic movement compaction or de-hydration

Table 1.6
Average DNAPL Composition at Smithville [Golder Associates, 1995]

PCBs	40.0 %
Trichlorobenzenes (TCB)	10.0 %
Tetrachlorobenzenes	0.8 %
Trichloroethene (TCE)	2.0 %
Petroleum Hydrocarbons (C16 to C32)[1]	4 .0 %
High molecular weight polar material (>C32)	20.0 %
Total:	76.8 %

[1] : (C16: hydrocarbon molecule with 16 carbon atoms in its structure)

Table 1.7
Mineral Composition from XRF Analyses (after Bickerton, 1997)

Stratigraphic unit	Estimated clay mineral content [wt%]	Mineral composition [%]			
		dolomite	quartz	gypsum	calcite
Eramosa	0.3-0.9	93.7-97.6	2.4-2.9	-	0.0-3.8
Upper Vinemount	2.0-6.7	91.1-96.9	3.1-6.0	0.0-3.4	-
Lower Vinemount	1.2-3.0	87.6-96.3	2.8-8.7	0.0-7.7	-
Goat Island	0.3-3.5	91.7-96.7	2.0-6.3	0.0-6.3	-
Gasport	0.9-6.0	84.5-97.6	2.1-15.5	0.0-6.5	-
Decew Fm.	0.9	91.8	2.1	6.2	-
Rochester Fm.	3.1-13.1	73.3-93.0	6.2-12.5	-	-

Chapter 2

Resaturation and Hydraulic Conductivity of Rock Samples from the Lockport Formation at Smithville, Southern Ontario

2.1 Introduction

As discussed in the introductory chapter, matrix diffusion is an important transport mechanism in fractured aquifers. In this thesis the focus of the investigation is the determination of transport parameters and rock matrix properties from the dense non-aqueous phase spill (DNAPL) site at Smithville. These parameters are critical for a mass transport assessment. One approach to measure transport parameters is through diffusion experiments. Laboratory scale diffusion and sorption experiments require *saturated* rock samples. For example, in the fall 1995 drilling campaign, at Smithville, only a small number of drill core samples were preserved under saturated conditions. To conduct further laboratory experiments on saturated dolostone samples an attempt was made to resaturate thin, dry rock slices from the vertical bore core 54B. The storage conditions (dry or in water basins) of further drill cores for the early summer 1997 drilling campaign also depended on the outcome of these resaturation experiments.

Two of the most common methods to resaturate rock samples are 1) back-pressure saturation, and 2) specimen soaking under a partial vacuum. These methods are described in the ASTM Standard D5084-90 [1990] and also by Lowe and Johnson [1960]. Back-pressure saturation of specimens in a triaxial cell also allows for the measurement of

hydraulic conductivity. Monitoring the hydraulic conductivity during resaturation gives additional valuable information on matrix permeability, compressibility of the rock, and interconnectivity of pores used for fluid flow in relation to total porosity. It is common in dual porosity or discrete fracture simulations to assume that fluid flow in the matrix is very slow or non existent, and mass transport occurs exclusively by diffusion. This assumption might not be valid in many carbonate aquifers and in particular in parts of the Upper Lockport Formation.

Hydraulic conductivity tests on rock samples in a triaxial cell have an advantage over slug and pump test evaluations in boreholes. Hydraulic conductivity values from triaxial cell experiments are only valid for the matrix, whereas slug and pump tests are evaluated for intervals between packers that might contain fractures. It is difficult, and may even be impossible to distinguish between the hydraulic conductivity of the matrix and that of the fractures.

The objectives of this phase of the research are to attempt resaturation of dry dolostone rock samples from the Lockport Formation and to determine the matrix hydraulic conductivity of saturated rock samples. To meet these goals a triaxial cell with a deaired water containing back pressure tank is set up for thin, 45 mm diameter rock samples (Fig. 2.1). The experiments are conducted under different back-pressures and total running times. Repetitions and resaturation of originally saturated rock samples are used for verification. The amount of resaturation is evaluated through the volumetric water content, which is determined based on weight difference between oven-dried (105° C) and saturated samples. Seven saturated and unsaturated rock samples are chosen for

the experiments, and these come from different depths and members of the Lockport Formation.

As has been mentioned earlier in this thesis, the Lockport Formation is an approximately 36 m thick dolostone sequence. Lithological variations in the sequence range from clay rich, fine grained, dense dolostone, to massive, calcite rich and fossiliferous beds, reflecting the different facies under which the sediment was deposited. Based on lithological observations, the Lockport Formation is subdivided into the Eramosa, Vinemount, Goat Island, and Gasport members [Blair and McFarland, 1992]. A horizontal and vertical fracture network cuts through the dolostone and serves as the main channels for fluid flow. Secondary mineralizations of gypsum, calcite, silica and sulfites fill vugs and fractures partially

2.2 Rock Sample Description

Five saturated rock samples from borehole core 54B are dried in the oven to determine their original porosity. Samples SMV-14-2 and SMV-14-1 are fine grained, clay rich, dense and from a depth between 17.78 m to 17.96 m below surface, which is part of the Eramosa Member. Their porosity is 3.57 % and 3.60 %, respectively. SMV-18-1 is light gray in color, fossiliferous, calcite rich, and is located from 40.07 m to 40.23 m depth below surface (Gasport Member). It has a porosity of 7.74 %. Sample SMV-19-1 is from the dark gray, clay rich Rockport Formation, which underlies the Lockport Formation and has a porosity of 5.01 %.

The sample SMV-14-3, from the same depth as SMV-14-2 and SMV-14-1, is used to measure the hydraulic conductivity of a saturated rock. The results are then compared with hydraulic conductivity measurements during the resaturation process from samples SMV-14-2 and SMV-14-1.

Hydraulic conductivity measurements are conducted on two unsaturated rock samples from vertical borehole 65. The samples from the Eramosa Member are chosen because of their visibly high porosity. Sample 65E2-18 from 5.24 m depth has a porosity of 16.70 % and is adjacent to a major fracture; sample 65E1-3 from 3.91 m depth has visible large pores of 0.5 to 3.0 mm and a porosity of 7.54 %.

2.3 Experimental Setup

The triaxial apparatus confines a 0.6 to 1.2 cm thick rock disk in a rubber tube inside the pressure cell. A porous plate with a steel cap on top (which closes the pressure cell) is placed above and below the sample. A narrow hollow opening in the middle of the steel caps allows pressurization of the sample from a water reservoir, which itself is pressurized by nitrogen gas. The confining pressure from sides, top, and bottom is applied through hydraulic fluid by an oil hand pump (Fig. 2.1). Through monitoring the pressure gage on the nitrogen cylinder a constant hydraulic gradient can be applied to the rock sample. Keeping the confining pressure at least 207 kPa (30 psi) above the hydraulic back pressure prevents any water leakage along the rubber-rock contact in the cell. At the beginning of each run the confining pressure is set equal to the back pressure to bleed air

out of the tubing and the triaxial cell. During the experiments the confining pressure, as well as the back-pressure, are kept at a constant value. Runs are conducted with confining pressures in the range between 689.5 kPa (100 psi) and 3723.3 kPa (540 psi) and with back pressures between 69 kPa (10 psi) and 1034.3 kPa (150 psi).

2.4 Results and Data Analyses

2.4.1 Resaturation

The results are presented in Figure 2.2, Figure 2.3 and Table 2.1. Increasing the back pressure from 689.5 kPa (100 psi) to 1034.25 kPa (150 psi) and increasing the total time of fluid flow to 90 hours forced a higher resaturation in sample SMV-14-1 from 72.2 % to 84.2 %. This was the highest resaturation value reached in all runs. According to ASTM standard D 5084-90, a back-pressure of 1034.25 kPa (150 psi) should be enough to reach 97 % resaturation. However, this could not be confirmed.

An increase in the confining pressure from 2758 kPa to 3723.3 kPa may be the reason for a lower hydraulic conductivity of $9.3x10^{-12}$ cm/s in the second run compared to $7.8x10^{-11}$ cm/s. The total porosity decreases with increasing confining pressure, and therefore, a complete resaturation can never be reached at such high confining pressures. As the confining pressure increases, cracks and pores close. In two sample runs with confining pressures up to 2758 kPa (400 psi) crack initiation is observed. Crack initiation occurred before K_{min} is reached, this is also well documented in other experiments [Singh, 1997]. In sandstone samples Singh [1997] found that the permeability was reduced by up

to 34 % when increasing the confining pressure from 1.1 to 6.85 MPa. It is important to notice that the decrease in total porosity due to compression is not necessarily equivalent to an equal loss in interconnected pores. Therefore, it is not possible to determine the amount of compression from the hydraulic conductivity curve during the experiment.

After three short runs (each below 2 minutes) with low back pressures of 68.95 kPa (10 psi) and 137.9 kPa (20 psi), sample SMV-18-1 reached 81.9 % resaturation. This clearly demonstrates that the pores are highly interconnected and not many dead end pores exist in this sample. The porosity is visible in the fossiliferous rock sample and is most likely a secondary feature due to dissolution of calcareous skeletons. Running times and back-pressures had to be kept as low as 2 minutes and 68.95 kPa (10 psi), respectively, because of a high matrix hydraulic conductivity of $5.7x10^{-6}$ cm/s and the limited volume of the water reservoir.

An attempt to resaturate sample SMV-19-1 from the Rochester Formation is terminated after 20 hours. At a confining pressure of 2758 kPa (400 psi) and a back-pressure of 1034.25 kPa (150 psi) no flow could be measured. Therefore, the hydraulic conductivity must be below $1.6x10^{-12}$ cm/s. This corresponds with the clay rich appearance of the rock sample.

2.4.2 Hydraulic Conductivity

The volumetric water content in sample SMV-14-3 was determined after the hydraulic conductivity experiments were completed. The experimental results are very similar to the values obtained during resaturation of sample SMV-14-1. This can only be explained by assuming that the missing 27.8 to 15.8 % of saturation in sample SMV-14-1 represents for a large part dead pore space, and does not contribute towards permeability.

The hydraulic conductivity for the saturated matrix of the Eramosa Member at 17.78 m depth with a porosity of 3.34 % is in the range from $1.2x10^{-11}$ cm/s to $9.4x10^{-12}$ cm/s. The Rochester Formation, in contrast to the Eramosa Member, can be assumed to be an aquitard because of its clay rich composition. The hydraulic conductivity of the rock matrix was not measurable; however, it must be below the test limit of $1.6x10^{-12}$ cm/s for a two hour testing period. The fossiliferous, porous sample SMV-18-1 is not representative for the rock matrix of the whole Gasport Formation. Its hydraulic conductivity ranges from $1.7x10^{-6}$ cm/s to $5.7x10^{-6}$ cm/s and likely represents a rock matrix close to an open fracture.

From borehole 65, two samples are examined in the triaxial cell. Samples 65E2-18 and 65E1-3 were chosen for their visibly high porosity of 16.70 % and 7.54 %, respectively. Both samples are from the upper part of the Eramosa Formation and their porosity seems to be enhanced due to dissolution. The hydraulic conductivity of the porous rock matrix, determined with confining pressures of 689.5 kPa (100 psi) to 2758

kPa (400 psi) and back-pressures of 68.95 kPa (10 psi) and 137.9 kPa (20 psi), is $2.2x10^{-6}$ cm/s to $9.1x10^{-6}$ cm/s. These porous zones are adjacent to open fractures.

2.5 Conclusions

Despite the fact that only a limited number of rock matrix samples were analyzed, valuable information on resaturation, hydraulic conductivity, and pore connectivity was gathered. The following conclusions are made:

- The highest resaturation value of 84.2% is reached with a back-pressure of 1034.25 kPa after 90 hours.
- A complete resaturation in the dolostone rock samples could not be achieved, even with high confining pressures.
- The fact that similar hydraulic conductivity values for the saturated sample SMV-14-3 and the resaturated sample SMV-14-1 (72.2 to 84.2 %) were achieved, leads to the conclusion that the remaining, originally-water filled porosity does not contribute significantly towards hydraulic conductivity. It is assumed that 15.8 to 27.8 % of the total pore space are dead end pores.
- The experimentally determined hydraulic conductivity values range from $1.2x10^{-11}$ to $9.4x10^{-12}$ [cm/s] for dense dolostone rock matrix, and from $2.2x10^{-6}$ to $9.1x10^{-6}$ cm/s for highly porous dolostone samples from the upper Eramosa Formation. The hydraulic conductivity values did not only depend on total porosity, but also on pore

inter-connectivity. These values agree with hydraulic conductivity data found by the preliminary hydraulic testing program at the site [Lapcevic et al., 1995].

- High confining pressures caused volume reduction of the sample and resulted in a decrease in hydraulic conductivity. This is due to a decrease in total porosity and pore connectivity. The amount of volume reduction depends on the rock matrix composition.
- Volume reduction has no effect on highly porous samples during very short run times.

References

Blair, R., and S. McFarland, Regional correlation of the Middle and Lower Niagara Escarpment Area. Proceedings of the 1992 Conference of the Canadian National Chapter, International Association of Hydrogeologists, Hamilton Ontario, 659-696, 1992.

Lapcevic, P., K. Novakowski, G. Bickerton, and J. Voralek, Preliminary results of the fall 1995 drilling and hydraulic testing program at the Smithville Phase IV bedrock remediation site, NWRI Contribution, No. 96-50, 1996.

Lowe, J., and T. C. Johnson, Use of back pressure to increase degree of saturation of triaxial test specimens, Proceedings, ASCE Research Conference on Shear Strength of Cohesive Soils, Boulder, CO, 1960.

Singh, A. B., Study of rock fracture by permeability method, J. of Geotech. and Geoenviromental Eng., 7, 601-608, 1997.

ASTM Standard D 5084-90, Standard test method of measurement of hydraulic conductivity of saturated porous materials using a flexible wall permeameter, ASTM, 151-158, 1990.

Table 2.1

Summary of Results from Triaxial Cell Experiments for Resaturation and Hydraulic Conductivity

(a) resaturation of unsaturated rock samples

BH	Sample #	Formation	Depth [m]	Porosity [%]	Back pressure [KPa]	Conf. pressure [KPa]	Δl [cm]	Total time [hr]	K [cm/s]	Resaturation [%]
54B	SMV-14-2	Eramosa	17.78-17.96	3.57	948.06	2758.0	0.85	18.77	1.70E-10	71.0
54B	SMV-14-1	"	"	3.6	689.50	2758.0	0.85	24.41	7.80E-11	72.2
54B	SMV-14-1	"	"	3.6	1034.25	3723.3	0.85	90	9.30E-12	84.2
54B	SMV-19-1	Rochester	46.63-46.96	5.01	1034.25	2758.0	1.18	20 total time [sec]	<1.60E-12	no flow!!
54B	SMV-18-1	Gasport	40.07-40.23	7.74	68.95	2758.0	1.22	120	5.70E-06	
54B	SMV-18-1	"	"	7.74	68.95	1379.0	1.22	120	5.70E-06	
54B	SMV-18-1	"	"	7.74	137.90	3309.6	1.22	50	1.70E-06	81.9

(b) measurment of K on saturated samples

BH	Sample #	Formation	Depth [m]	Porosity* [%]	Back pressure [KPa]	Conf. pressure [KPa]	Δl [cm]	Total time [hr]	K [cm/s]
54B	SMV-14-3	Eramosa	17.78-17.96	3.34	1034.25	2758.0	0.88	140.02	1.20E-11
54B	SMV-14-3	"	"	3.34	1034.25	1379.0	0.88	not completed	
54B	SMV-14-3	"	"	3.34	1034.25	1379.0	0.88	160.65	9.40E-12

* : porosity was determined at the end of all runs

(c) measurment of K on unsaturated samples

BH	Sample #	Formation	Depth [m]	Porosity [%]	Back pressure [KPa]	Conf. pressure [KPa]	Δl [cm]	Total time [sec]	K [cm/s]
65	65E2-18	Eramosa	5.24	16.7	137.90	689.5	0.63	90	2.20E-06
65	65E2-18	"	"	16.7	68.95	2758.0	0.63	52	7.70E-06
65	65E1-3	"	3.91	7.54	68.95	1379.0	0.82	60	7.60E-06
65	65E1-3	"	"	7.54	68.95	2758.0	0.82	50	9.10E-06

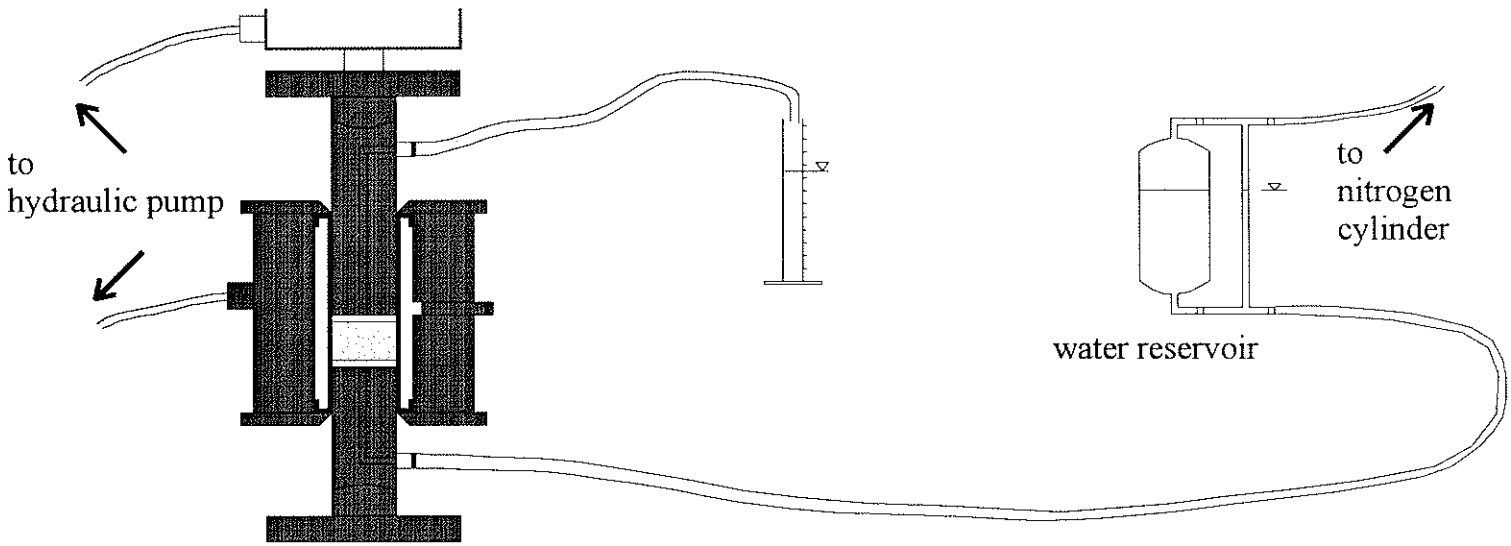

Figure 2.1: Experimental setup with triaxial press and back pressured water reservoir.

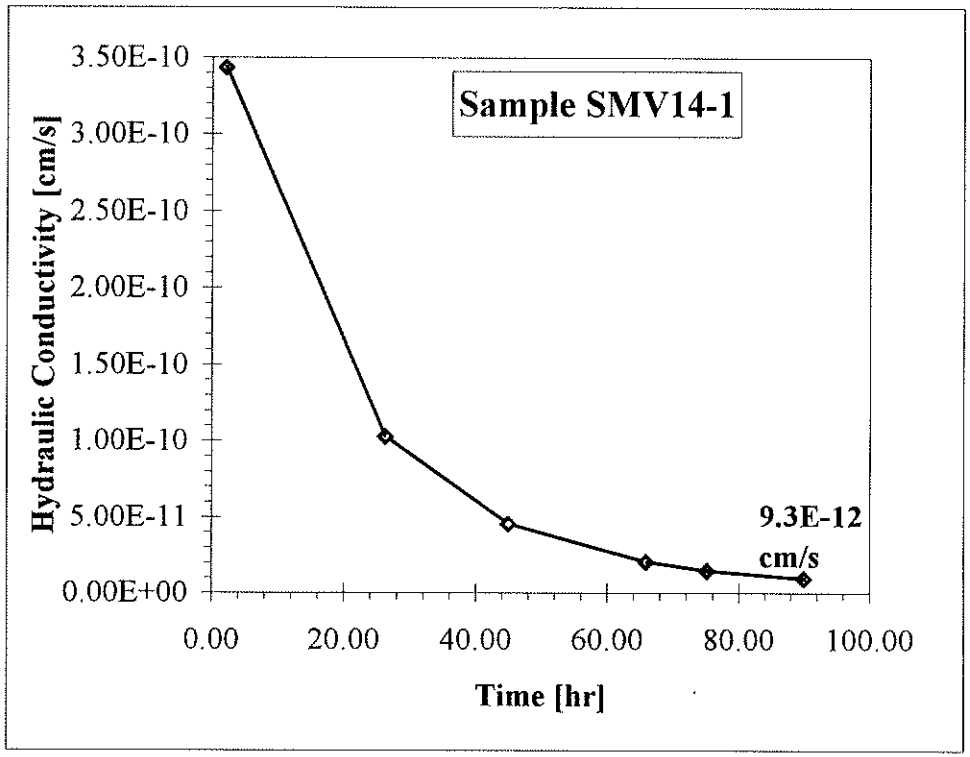

Figure 2.2 Hydraulic conductivity as a function of time during the resaturation process with a confining pressure of 3723.3 kPa.

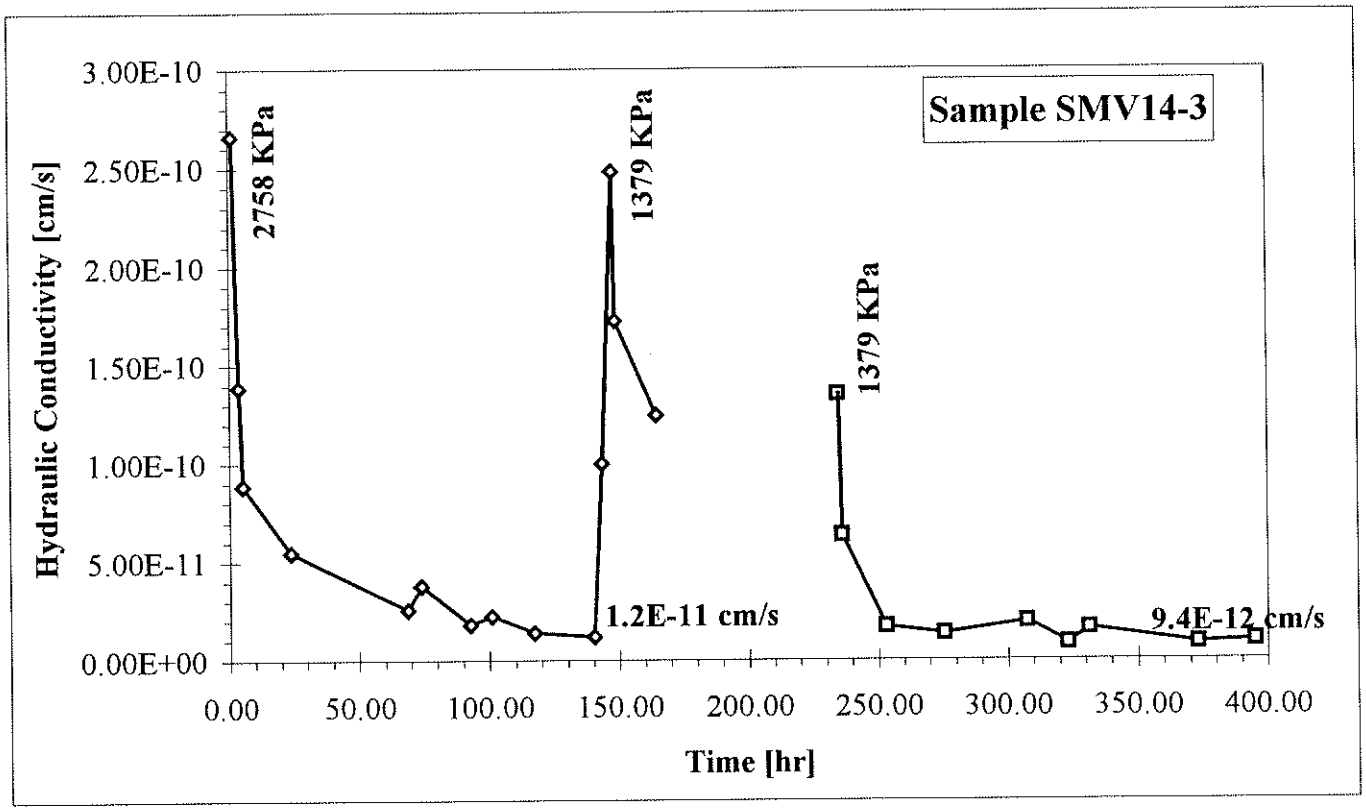

Figure 2.3: Hydraulic conductivity as a function of time during two resaturation experiments. The first run was conducted under 2758 kPa, the second run under 1379 kPa confining pressure.

Chapter 3

Heterogeneity of Matrix Porosity in Horizontally-Stratified Dolostone and Its Implication on Mass Transport

3.1 Introduction

In a dual porosity aquifer contaminant transport occurs in fractures as well as through the porous rock matrix. The dominant spreading process in the fractures is through advection and dispersion, whereas matrix diffusion dominates contaminant migration in the surrounding porous media. Matrix diffusion from the fracture into the surrounding rock matrix increases and causes significant retardation of pollutants if fracture apertures are small [Maloszewski and Zuber, 1993; Novakowski and Lapcevic, 1994; McKay et al., 1993]. Maloszewski and Zuber [1993] demonstrated that even in short-term (24 hr) tracer tests, conducted by Skagius and Neretnieks [1986] and Birgersson and Neretnieks [1990], in granites, matrix diffusion is significant. Retardation due to matrix diffusion is therefore also an important issue at potential nuclear waste sites in fractured crystalline rocks. Even in impervious material (Opalinus shale) isotope disequilibria give proof of diffusion into the matrix of at least 8 cm [Mazurek et al., 1996]. One conclusion reached from a single, horizontal, discrete fracture tracer experiment in Ordovician shale was that the single most significant physical parameter influencing peak contaminant concentrations is matrix porosity [Novakowski and Lapcevic, 1994]. The

amount of contaminant mass that can be stored in the rock matrix of a dual porosity aquifer depends on the pore volume of the rock matrix and on its sorption capacity when dealing with reactive substances. The larger the porosity the faster contaminants can diffuse into the rock matrix. Also, more mass can be temporary stored in the rock matrix, if the pore system is well connected.

In general, tracer and pump test data are used to deduce transport parameters in geological formations. Tsang [1995] demonstrates that the interpretation of pump test data leads to non-unique solutions. One large uncertainty in the conceptual models is associated with the spatial heterogeneity of matrix diffusion. Small scale matrix heterogeneity is of special importance to flow and transport processes through unsaturated, fractured rock, like at Yucca Mountain, Nevada [Tidwell et al., 1995; Glass et al., 1995]. The influence of fracture coatings or skins, which diminish the exchange of fluids between fracture and matrix, has been recently studied by Chekuri et al. [1994] and by Robinson et al. [1998].

Porosity is a fundamental hydraulic parameter and is defined as the ratio of void volume to total rock volume. This void space generally allows for fluid flow and mass transport. However, not all pore space is interconnected and available for transport, although most experimentally determined and published porosity data from carbonate rocks represent total porosity. In compacted carbonate rocks (such as the Lockport Formation), the main component of total porosity comes from secondary porosity. Leaching processes give rise to moltic and vuggy porosity. It is common that secondary moltic and vuggy porosity generated by dissolution increases total porosity up to 20 % in

microfacies layers with high skeleton content [Carozzi, 1989]. A detailed investigation of the Atokan Limestone (Middle Pennsylvanian) in Texas indicates a parallel increase in secondary burial porosity with an increase in frequency and amplitude of sutured stylolites [Carozzi and Von Bergen, 1987]. The microfacies with the highest porosity correlates with the peak in high amplitude sutured stylolites. From thin-section observations and porosity measurements, Carozzi [1989] concluded that stylolites carried diagenetic fluids, which created an adjacent secondary porosity and connected otherwise isolated pore space. Horizontal, unloading fractures are frequently found in direct association with stylolites.

Giles and De Boer [1989] described the creation of enhanced secondary porosity due to dissolution of carbonate cement as a result of cooling waters. Secondary porosity is often associated with post-depositional leaching of detrital particles such as feldspar, fossil debris and intergranular cements and may not always increase the total porosity [Giles and de Boer, 1989]. More intense zones of leaching in carbonates are often associated with high permeability zones like fractures and layers with fossil shells. Infiltrating rainwater from the surface can cause enhanced porosity adjacent to hydraulic fractures (due to dissolution of calcite or dolomite cement). Such leaching processes are observed to reach down to 500 m depth [Giles and de Boer, 1990]. Thus, heterogeneous porosity adjacent to fractures has potentially significant impact on contaminant migration. A detailed vertical porosity study can also help in identifying open, hydraulically active fractures.

With depth and aging, water in the fractures is more likely to become chemically equilibrated with the rock matrix, especially when fluid flow is negligible, and dissolution

of the pore space adjacent to deep fractures is less dominant or absent. Therefore, it is expected that porosity variations decrease with depth.

This study on matrix porosity in the Lockport Formation has three objectives: (1) to determine vertical profiles of porosity from dolostone core samples obtained from the Lockport Formation underlying Smithville (southern Ontario) and to statistically evaluate the data, (2) to determine matrix porosity in the vicinity of horizontal fractures and identify enhanced secondary porosity in the rock matrix, if present, and (3) to study the implication of spatial heterogeneous matrix porosity on mass transport. To conduct the study, sections of the saturated core obtained from a vertical borehole, are cut into thin (0.5 to 1.0 cm) slices for porosity measurements. Detailed sampling adjacent to potential fractures is carried out to help identify small scale variations related to horizontal fractures and stylolites in the dolostone formation. Statistical evaluation of the mean porosity of the four lithologically distinct rock members of the Lockport Formation is also conducted to identify multimodal distributions and to estimate enhanced secondary porosity.

To study the implications of spatial heterogeneity of porosity, two different mass transport scenarios are simulated. The first scenario is that of a short term, conservative field tracer experiment conducted in a horizontal fracture using a pulse source. In the second case, spreading behavior of a plume generated by a continuous source through a horizontal fracture is simulated. As will be shown, failure to property account for matrix diffusion can result in underestimating the contaminant mass present at a site and in predicting incorrect contaminant peak concentrations at specific locations and times.

3.2 Geological Setting and Stratigraphy of the Lockport Formation

Sedimentary rock formations of Paleozoic age make up the bedrock throughout southern Ontario and represent an important source of water. At Smithville, the bedrock is covered with a 5 to 10 m thick, fractured sandy clay till. The underlying Middle Silurian sedimentary rocks are composed of mainly dolostone and shale, and divided into the Lockport Formation, Decew Formation, and Rochester Formation (Fig. 3.1). The following summary of the stratigraphic units is derived from drill logs, which are from several boreholes drilled in the vicinity of Smithville, and from Blair and McFarland [1992].

The Lockport Formation is composed of an approximately 36 m thick dolostone sequence. Lithological variations in the sequence range from clay rich, fine grained, dense dolostone to massive, calcite rich and fossiliferous beds, representing the different facies under which the sediment was deposited. Based on lithological observations the Lockport Formation is subdivided into the Eramosa, Vinemount, Goat Island, and Gasport Members. The Eramosa Member (the uppermost member) has a thickness of about 13 to 19 m, the Vinemount Member 7 to 8 m, the Goat Island Member 6 to 7 m, and the Gasport Member 7 to 16 m. A horizontal and vertical fracture network pervades the dolostone and serves as the main channels for fluid flow. Secondary mineralizations of gypsum, calcite, silica and sulfites partially fill vugs and fractures.

The Upper Eramosa is composed of brownish gray, vuggy dolostone with abundant coral fossils and numerous bedding partings (bituminous and stylolitic). Only occasional vugs, coral fossils and gypsum nodules are found in the fine to medium grained, thinly to medium bedded dolostone of the Lower Eramosa Member. The medium gray, fine grained, argillaceous dolostone of the Vinemount Member contains numerous black, bituminous bedding partings and stylolites. The lower part of the Vinemount is more massive with occasional fossils. The Goat Island Member is composed of a medium brownish gray, very fine to fine grained, medium to thickly bedded dolostone with occasional stylolite partings, and chert and gypsum nodules. Very distinctive is the contact with the light creamy to bluish gray, fine to medium grained, medium to thickly bedded, crinoidal dolostone with occasional argillaceous and stylolitic partings of the Gasport Member. The fine grained dolostone of the Decew Formation is only 0.5 to 1.5 m thick and not easy to identify in bore logs, whereas the Rochester Formation , in contrast, is composed of a distinctive, dark to medium gray, fine grained calcareous shale. The shale has a thickness of about 17 m underneath Smithville [Blair and McFarland, 1992]. For further details the reader is referred to Blair and McFarland [1992].

3.2.1 Mineral Composition

Whole-rock geochemical analyses on 27 samples [Bickerton, 1997] show that the average dolostone ranges in composition from 85 to 98 % dolomite, 2 to 16 % quartz and 0 to 8 % gypsum (Table 3.1). The estimated clay mineral content ranges between 0.3 and

6.7 weight % in the Lockport Formation and between 3.1 and 13.1 weight % in the Rochester Formation.

3.3 Experimental Method

Rock samples for porosity measurements are taken from saturated drill core (#65) at Smithville, Ontario. All samples come from the Lockport Formation. In order to obtain porosity distribution profiles, several representative, 20 to 100 cm long core sections are sampled and cut into thin, 0.5 to 1.0 cm thick slices. Because of difficulties encountered in resaturating the core, the samples are maintained in a saturated state. Porosity is measured on the basis of weight difference between oven-dried and saturated samples. Heating is conducted at 105° C for 20 hours. A total of 546 samples are analyzed. Diameter, thickness and weight of the discs are recorded in advance. The volume of irregular slabs adjacent to potential horizontal fractures is determined by submerging the rock under water and measuring the amount of displacement. Although the Lockport Formation is uniformly dolostone in lithology, some variations in bedding and character are observed with depth.

3.4 Statistical Analyses

Quantifying the porosity in the dolostone matrix is of importance when trying to determine the amount of contaminant that can be temporary stored in the rock formation through matrix diffusion. In the following, porosity profiles taken from each stratigraphic

unit of the Lockport Formation are described. The porosity data are further analyzed using frequency histograms and descriptive statistics. The results are summarized in Figure 3.4 and Table 3.2.

3.4.1 Upper Eramosa Member

Numerous vugs and fractures, which cause mechanical breaks of the drill core, characterize the upper zone from 3.5 to approximately 7.0 m depth below surface. Porosity profiles from 3.88 to 4.20 m and from 5.12 to 5.34 m show large variations, which suggest dissolution processes from the infiltrating surface waters (Fig. 3.2 and 3.3). The sampled sections contained no visible large vugs or cavities. Adjacent to a hydraulically active fracture, porosity increased up to 20.6 % (Fig. 3.3). This fracture was observed in the core during the sampling and cutting process. An enhanced porosity effect is visible up to 3 cm into the rock matrix. Small 2 to 5 cm long vertical cracks, which open up towards horizontal fractures, contribute to increased porosity values. Thin zones with fossil skeletons create high porosity adjacent to openings. From the upper zone, 66 porosity values are obtained, ranging from 0.43 to 20.63 % (Fig. 3.4). The histogram shows a bimodal distribution with peaks at 2 % and 12 %. The central tendency of the porosity data can be described by an arithmetic mean of 8.29 %. The variation of the data is expressed as a large sample standard deviation (s) of 4.95 (Table 3.3).

3.4.2 Lower Eramosa Member

Porosity data from 7.4 to 18 m depth below surface show less variation than the uppermost part of the Eramosa Member (Fig. 5). At 16.36 m depth a major horizontal fracture is easily identified by an increase in porosity from 2.0 to 9.8 %. Visual control during sampling confirms the presence of a fracture. The lower contact is found to be missing due to dill core loss. At 15.92 m and at 16.02 m horizontal fractures are assumed from the porosity profiles, but could not be identified during sampling without doubt. Due to the drilling process, mechanical breaks, which may represent major openings, are often characterized by core loss. In this sample section numerous open, as well as galena-filled vertical cracks/fractures leading from stylolite breaks into the rock matrix are observed (7.43m, 7.54m, 8.48m, 10.77m, 15.92 m). Most likely these breaks (no loss of core is observed) represent very thin, but hydraulically active fractures.

Over 90 % of the porosity values fall in the range between 2 and 7 % (Fig. 3.4). The arithmetic mean from 129 analyses is 4.4 %, and variation in the data is small compared to the upper zone with a standard deviation of 1.55 (Table 3.3). Note, that none of the samples obtained from the Eramosa Member contain visible gypsum. This is of importance because gypsum contains water in its structure, which would be partially lost during the drying process. Therefore, the weight loss would not be entirely due to the water in the pore space, and subsequently contribute towards the calculated total porosity. The impact on the total porosity is estimated to be less than 1 %.

3.4.3 Vinemount Member

The sampled section between 20.9 m and 25.0 m is dark gray, dense and clay rich dolostone from the Vinemount Member. Small portions are fossiliferous. The relatively homogeneous lithology correlates with a small range in porosity from 3.95 % to 8.81 % (Fig. 3.4). High porosity values of 7.0 %, 7.9 % and 8.8 % at 22.16 m, 22.28 m and 22.35 m depth respectively, are enhanced porosity values adjacent to open, hydraulically active fractures (Fig. 3.6). For example, at 22.35 m the porosity towards the fracture increases from 4.68 % to 8.81 % over a distance of 4.5 cm; at 22.28 m the porosity increases from 5.73 % to 7.92% over a distance of 2.9 cm. Two high values of 8.2 % at 21.97 m depth below surface are due to small amounts of gypsum in the rock matrix. None of the other samples contain visible gypsum. In some cases fossiliferous layers seem to have a slightly higher porosity than their surroundings. Only a few open, vertical cracks are found in the sampled sections compared to the Eramosa Member. The arithmetic mean from 107 analyzed samples is 5.7 % and the standard deviation of the data is small with 1.00 (Table 3.3). The frequency distribution has a positive skewness of 0.63. This indicates that the porosity distribution is different from a Normal or Gaussian distibution.

3.4.4 Goat Island Member

A homogeneous section from 29.0 m to 29.7 m depth with only one mechanical break is examined. Compared to the Vinemount Member, samples taken from Goat Island have higher carbonate concentrations, are harder, and are very light in color and compact.

Although these samples do not contain any visible gypsum, it cannot be ruled out that the mineral is finely distributed within the matrix. The contribution towards porosity is expected to be negligible. No vertical cracks are observed, which might enhance porosity values. They can also indicate the presence of horizontal fractures. From the porosity data, the mechanical break at 29.5 m cannot be identified as an open, hydraulically active fracture (Fig. 3.7). The arithmetic mean from 93 samples is high at 9.81 % and the standard deviation of the data is low at 1.05 (Table 3.3). The frequency distribution appears to be bimodal due to few porosity data around 10.5 % (Fig. 3.4).

3.4.5 Gasport Member

The sections analyzed for porosity are between 33.1 m and 38.2 m depth. The fossiliferous part between 33.1 m and 33.4 m shows no visible dissolution features on skeletons and the section has no enhanced porosity compared to the rest of the Gasport Member (Fig. 3.8). Numerous argillaceous bands pervade the dolostone and contribute to larger variation in the porosity data, which range from 3.6 % to 10.4 %. At two locations, 36.74 m and 37.28 m depth, open, hydraulically active fractures are assumed from the porosity profile (Fig. 3.9), but could not be identified during the sampling process without doubt. At 37.28 m the porosity increases from 7.1 % to 10.0 % over a distance of 4.1 cm towards the fracture. Vertical cracks are not observed. The arithmetic mean of 151 samples is 7.15 % and the standard deviation is 1.30 (Table 3.3). Over 90 % of the data

fall in a range between 5 % and 9.5 % (Fig. 3.4). The frequency distribution has a slight positive skewness with 0.03.

3.5 Implications for Mass Transport

The inspection of vertical porosity profiles identified open, hydraulically active fractures through the observation of core breaks and enhanced porosity values in the Eramosa, Vinemount, and Gasport Members. It is assumed that the first few centimeters (1.5 to 5 cm) into the rock matrix, in the direction perpendicular to a fracture, are often altered by dissolution due to chemical disequilibrium with the fracture fluid. A number of fractures show enhanced porosity penetrating approximately 2 to 3 cm into the neighboring rock matrix (Fig. 3.10 and 3.11). The highest increase in secondary porosity can be observed in the Eramosa Member. Here porosity rises near horizontal fractures by up to 17 % above the background value, i.e. from 4 to 21 % total porosity. In most cases, the increase ranges from 4 to 8 %. Enhanced secondary porosity in the Vinemount and Gasport Member is less prevalent and values increase only by 1.7 to 3.1 % adjacent to fractures (Fig. 3.11). These vertical porosity variations near fractures are of potential significance for mass transport. Porosity profiles are also a useful tool to distinguish fractures from mechanical breaks induced by the drilling process.

The significance of matrix porosity and enhanced secondary porosity adjacent to horizontal fractures on mass transport is evaluated using the finite-element transport model FRACTRAN [Sudicky, 1989; Sudicky and McLaren, 1992]. To demonstrate the

impact of diffusion from a single fracture into the surrounding rock matrix on contaminant peak concentrations, tracer breakthrough curves in a postulated dual porosity system are simulated (Fig. 3.12). In order to evaluate only the effect due to matrix diffusion and not advection, the hydraulic conductivity in the porous medium is purposely set low. An arbitrary flow velocity in the horizontal fracture of 4.0 m/d is chosen. All input parameters for the rock matrix and fracture are given in Table 3.4.

To explore the influence of variation in matrix porosity, three vertical porosity profiles are compared to an average matrix porosity case. Enhanced porosity is assumed to penetrate 2.5 cm into the surrounding porous medium. Five layers, each 0.5 cm thick, are used to simulate the gradation in porosity, the outermost linked to a 97.5 cm thick uniform matrix zone. The three profiles have the following porosity values:

	Zone 1	Zone 2	Zone 3	Zone 4	Zone 5	Zone 6
Profile A	8.0 %	7.5 %	7.0 %	6.5 %	6.0 %	5.65 %
Profile B	12.0 %	10.0 %	6.5 %	6.0 %	5.8 %	5.62 %
Profile C	15.0 %	10.0 %	8.0 %	6.5 %	6.0 %	5.59 %

The weighted average of each porosity profile is 5.68 %, which is equal to the average porosity in the Eramosa Member at Smithville. As expected, breakthrough curves with porosity profiles A, B, and C are retarded in the longitudinal direction, compared to an average matrix porosity profile (Figures 13 and 14). Note that there is an increase in peak concentrations between profile A and B, and between B and C. The reason for this is the

lower background porosity in each case, which results in a shallower matrix penetration of the contaminant plume and higher peak concentrations despite the higher porosity adjacent to the fracture. By not accounting for enhanced porosity near the fracture, a significant overestimate of the bulk porosity of the medium or the fracture aperture will be obtained when calibrating actual, field transport data.

Enhanced secondary porosity may also affect long-term contaminant transport in a dual porosity aquifer. Two porosity profiles D and E (Figures 15 and 16) are assumed, one representative for the Eramosa Member with an average porosity of 5.68 %, and the other a special case taken from the upper Eramosa Member with an average porosity of 8.29 %. In one simulation, a contaminant plume migrates through a horizontal fracture (fed by a continuous source) and is observed after 1000 days. The first five porosity layers are each 1.0 cm thick. Penetration distance ($d_{0.01}$) into the rock matrix and travel distance along the horizontal fracture are defined by a concentration value equal to 1 % C/C_0. As in the short term tracer simulation, the contaminant plume is retarded when accounting for enhanced secondary porosity adjacent to the fracture (Fig. 17). Contaminant concentrations in the fracture with porosity profile E are higher compared to an average porosity profile up to 62 m downstream, at which point the concentrations in the average porosity profile become higher. This is due to the heterogeneity in profile E, where porosity does not continuously decrease away from the fracture. The penetration distance in the fracture reduces from 196 m to 120 m and in the matrix from 47.5 cm to 45.0 cm, when comparing the average porosity case (5.68 %) to porosity profile D (Table 3.5). The

same trends are observed for porosity profile E compared to the average porosity case (8.29 %). The simulations shown in Fig. 17 were conducted with v_f=4.0 m/d.

Using a low fracture flow velocity (v_f=0.1 m/d), the travel distance in the fracture reduces to 3.6 m and 3.4 m, and penetration into the matrix is reduced to 22.5 cm and to 18.0 cm (at x = 2.0 m) for profile D and E, respectively (Table 3.5). Through further simulations it was found that a higher fracture flow velocity results in a larger amount of retardation in the models with a decreasing porosity gradient away from the fracture. This is due to the larger horizontal plume extension along the fracture, and subsequently larger amount of pore space available for matrix diffusion. When reducing the fracture aperture by half, the penetration distance for the low velocity case with porosity profile D is about the same (3.6 m) as for the average matrix porosity profile (5.68 %). However, the matrix penetration distance is considerably reduced from 22.5 cm to 15 cm at x= 2m. This is of special importance when evaluating contaminant sorption in the matrix and when estimating the amount of contaminant present in the porous media. In all simulated cases the total amount of mass stored in the porous medium after 1000 days was over 98 % of the mass input.

3.6 Conclusions

Experimental data obtained from the Lockport Dolostone in southern Ontario show that secondary porosity contributes significantly towards the total porosity of the Lockport Formation. Thin bands of biomolitic porosity with 10 to 20 % pore space could

be identified in the uppermost Member. Vertical porosity profiles obtained from core slices also helped to identify open fractures. Layers of enhanced porosity values penetrating 2 to 3 cm into the rock matrix are observed. The rock matrix adjacent to fractures is assumed to be altered by dissolution due to chemical disequilibrium with fracture fluids. A number of horizontal fractures in the dolostone show enhanced porosity in the surrounding rock matrix. Using drill core observations together with porosity analyses, it can be concluded that some of the breaks along stylolites are thin open, hydraulically active fractures. This finding is in agreement with Carozzi [1989], who suggested that stylolites are preferred pathways for fluid transport in carbonates, which create adjacent secondary porosity.

Vertical porosity variations are found to range from 0.43 to 20.63 % in the Lockport Formation. Bimodal porosity distributions in the Upper Eramosa and Goat Island Member support the finding of enhanced secondary porosity. This study has shown that porosity variations near the fracture have significant impact on mass transport in a dual porosity aquifer like the Lockport Formation. During a simulated long term contaminant spill, over 98 % of the total mass is stored in the porous medium due to matrix diffusion. Enhanced secondary matrix porosity results in additional contaminant retardation and lower peak concentrations downstream. The penetration depth into the matrix depends largely on the vertical porosity distribution adjacent to the fracture and on the fracture fluid flow velocity. Complex porosity profiles result in changes in the fracture peak concentrations depending on the penetration depth reached in the matrix. Neglecting vertical porosity variations will result in incorrect predictions of plume migration, peak concentrations, and contaminant penetration depth into the rock matrix.

References

Bickerton, G.S., Chemical and mineralogical composition of the Lockport and Rochester formations, Smithville, Ontario. NWRI Contribution No. 97-130, 1997.

Birgersson, L., and I. Neretnieks, Diffusion in the matrix of granitic rock: Field tests in the Stripa mine, Water Resour. Res., 26(11), 2833-2842, 1990.

Blair, R., and S. McFarland, Regional correlation of the Middle and Lower Niagara Escarpment Area. Proceedings of the 1992 Conference of the Canadian National Chapter, International Association of Hydrogeologists, Hamilton Ontario, 659-696, 1992.

Carozzi. A. V., Carbonate rock depositional models: A microfacies approach, Prentice Hall, New Jersey, 1989.

Carozzi, A.V. and D. Von Bergen, Stylolitic porosity in carbonates: a critical factor for deep hydrocarbon production, J. Petrol. Geol., 10, 263-282, 1987.

Glass, R. J., M. J. Nicholl, and V. C. Tidwell, Challenging models for flow in unsaturated, fractured rock through exploration of small scale processes, Geophysical Research Letters, v.22, no.11, 1457-1460, 1995.

Giles, M. R. and R. B. de Boer, Secondary porosity: creation of enhanced porosities in the subsurface from the dissolution of carbonate cements as a result of cooling formation waters, Marine and Petroleum Geology, v.6, 261-269, 1989.

Giles, M. R. and R. B. de Boer, Origin and significance of redistributional secondary porosity, Marine and Petroleum Geology, v.7, 378-397, 1990.

Maloszewski, P., and A. Zuber, Tracer experiments in fractured rocks: Matrix diffusion and the validity of models, Water Resour. Res., 29(8), 2723-2735, 1993.

Mazurek, M., W.R. Alexander, and A.B. MacKenzie, Contaminant retardation in fractured shales: matrix diffusion and redox front entrapment, J. of Contam. Hydrology, 21, 71-84, 1996.

McKay, L. D., R. W. Gillham, and J. A. Cherry, Field experiments in fractured clay till, 2, Solute and colloid transport, Water Resour. Res., 29(12), 3879-3890, 1993b.

Novakowski, K. S., and P. A. Lapcevic, Field measurement of radial solute transport in fractured rock, Water Resour. Res., 30(1), 37-44, 1994.

Radcliffe, A.J., "Analysis of Stylolitization and Fracturing in Rock Core from the Smithville Phase IV Site." Unpublished thesis, University of Waterloo, 1995.

Robinson, N. I., J. M. Sharp, and I. Kreisel, Contaminant transport in sets of parallel finite fractures with fracture skins, J. Contam. Hydrology, 31, 83-109, 1998.

Sudicky, E. A., The Laplace transform Galerkin technique: A time-continuous finite element theory and application to mass transport in groundwater, Water Resour. Res., 25(8), 1833-1846, 1989.

Sudicky, E. A., and R. G. McLaren, The Laplace transform Galerkin technique for large-scale emulation of a mass transport in discretely fractured porous formations, Water Resour. Res., 38, 499-514, 1992.

Skagius, K., and I. Neretnieks, Porosities and diffusities of some nonsorbing species in crystalline rocks, Water Resour. Res., 22(3), 389-398, 1986.

Tidwell, V. C., and R. J. Glass, Laboratory investigation of matrix imbibition from a flowing fracture, Geophysical Research Letters, v.22, no.11, 1405-1408, 1995.

Tsang, Y. W., Study of alternative tracer tests in characterizing transport in fractured rocks, Geophysical Research Letters, v.22, no.11, 1421-1424, 1995.

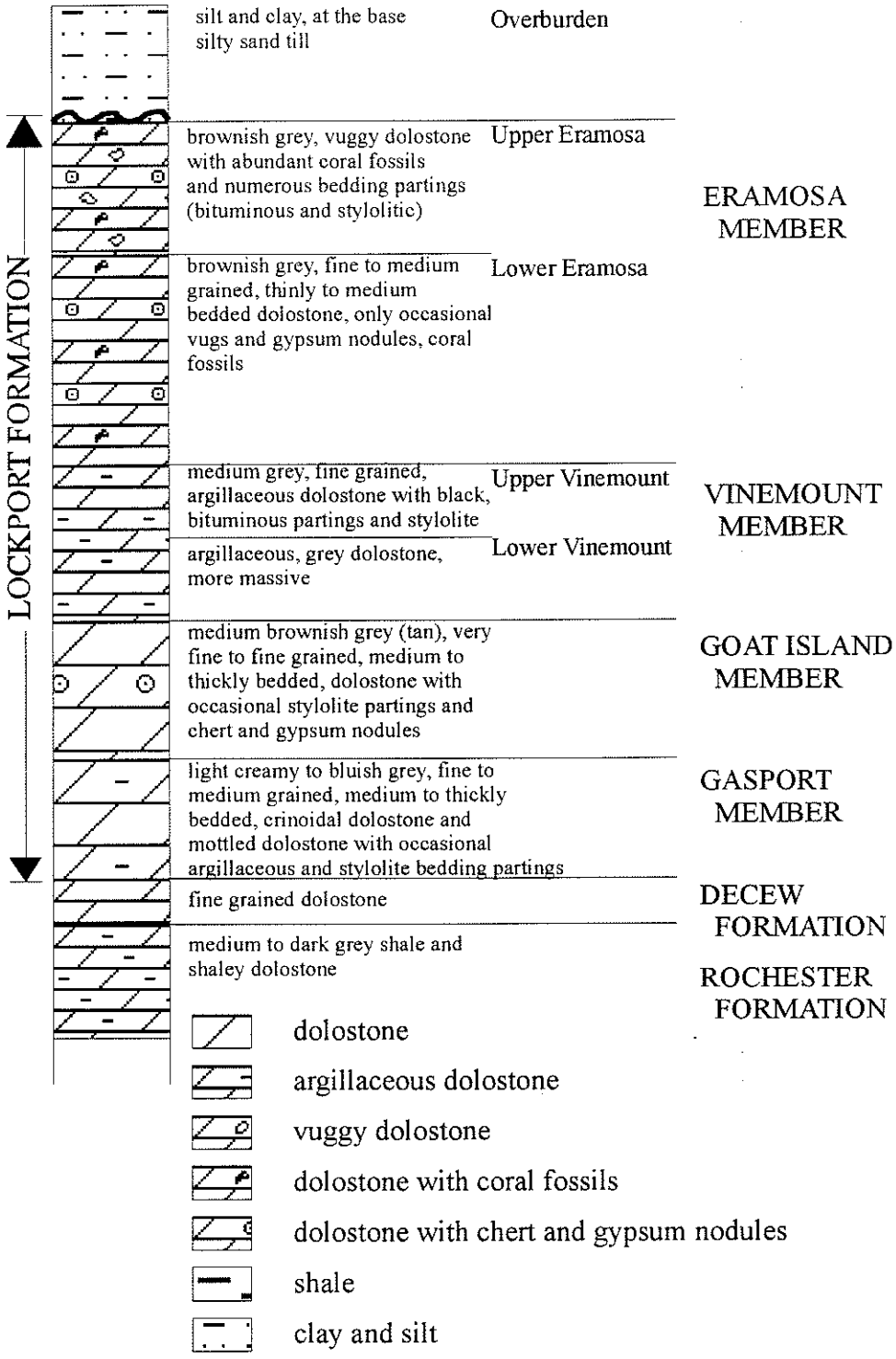

Figure 3.1: Stratigraphic column at Smithville, Southern Ontario (modified after Blair and McFarland, 1992).

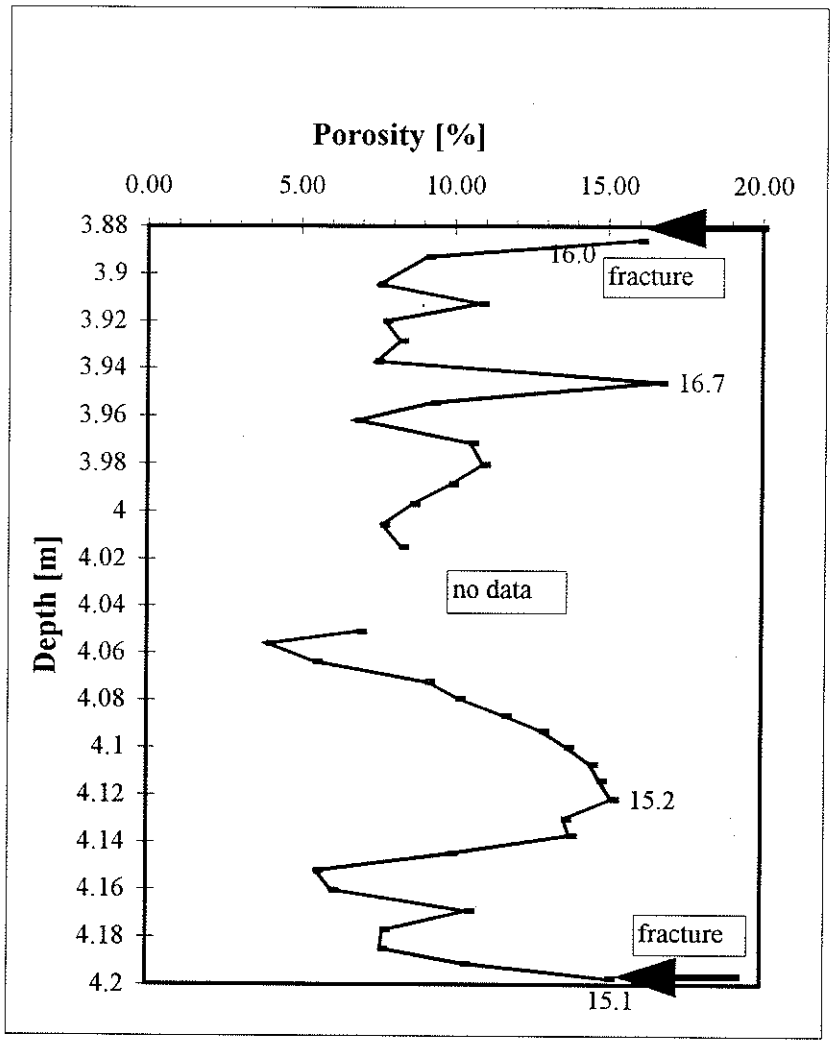

Figure 3.2: Porosity profile from 3.88 m to 4.2 m, Upper Eramosa Member.

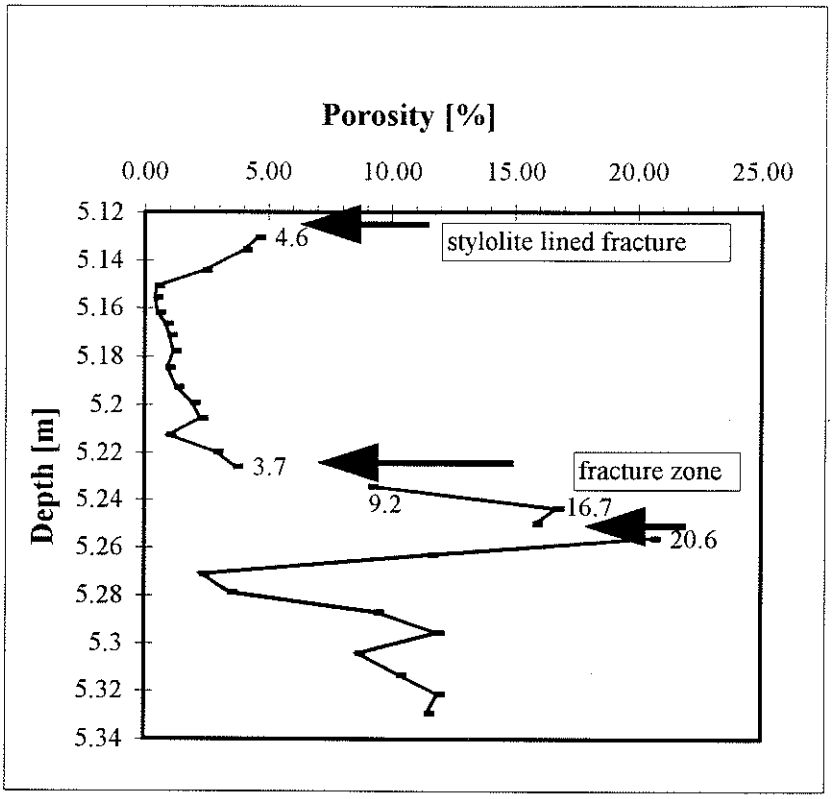

Figure 3.3: Porosity profile from 5.12 m to 5.22 m, Upper Eramosa Member.

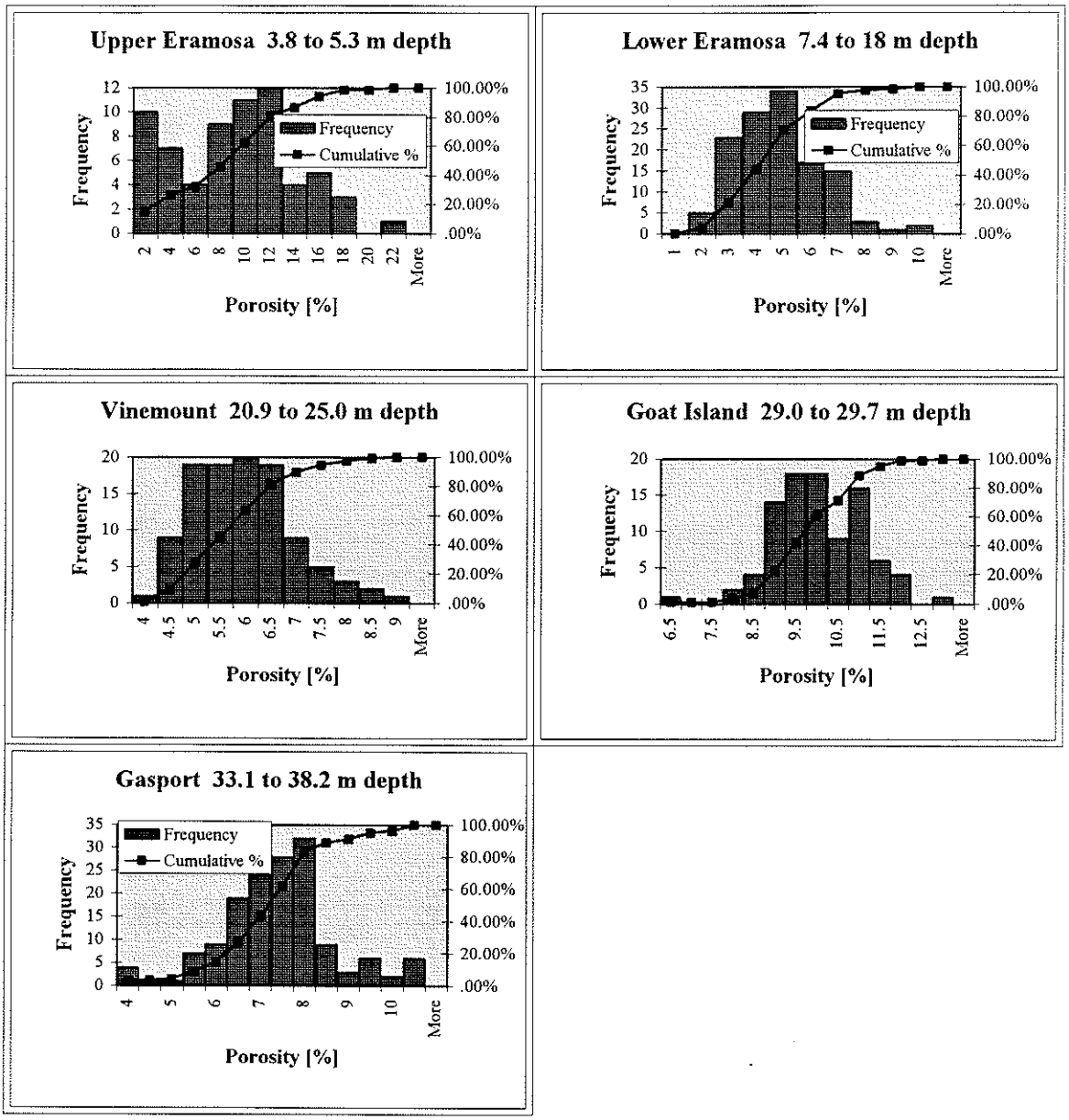

Figure 3.4: Frequency distribution of porosity data.

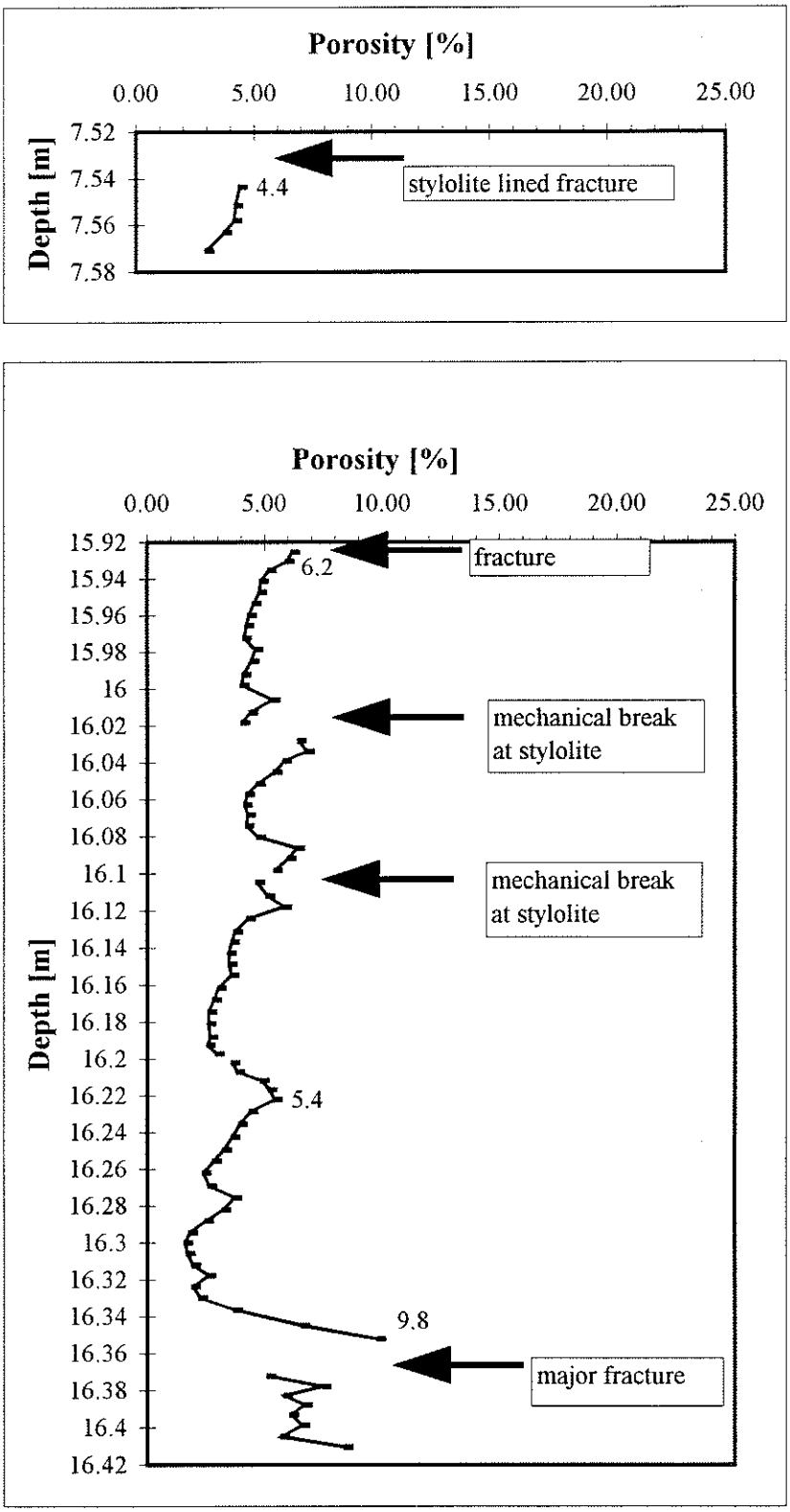

Figure 3.5: Porosity profiles from parts of the Lower Eramosa Member.

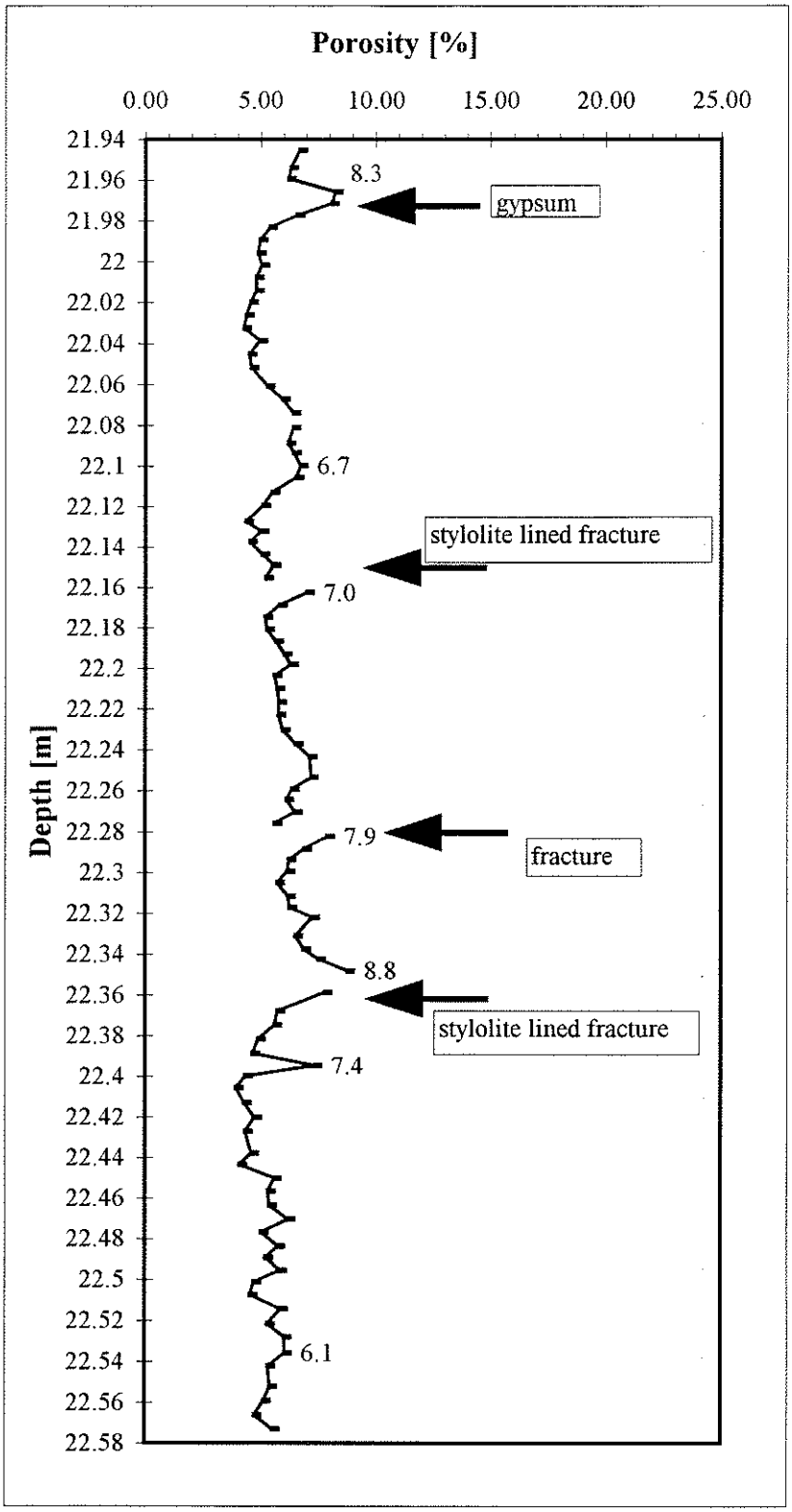

Figure 3.6: Porosity profile from part of the Vinemount Member.

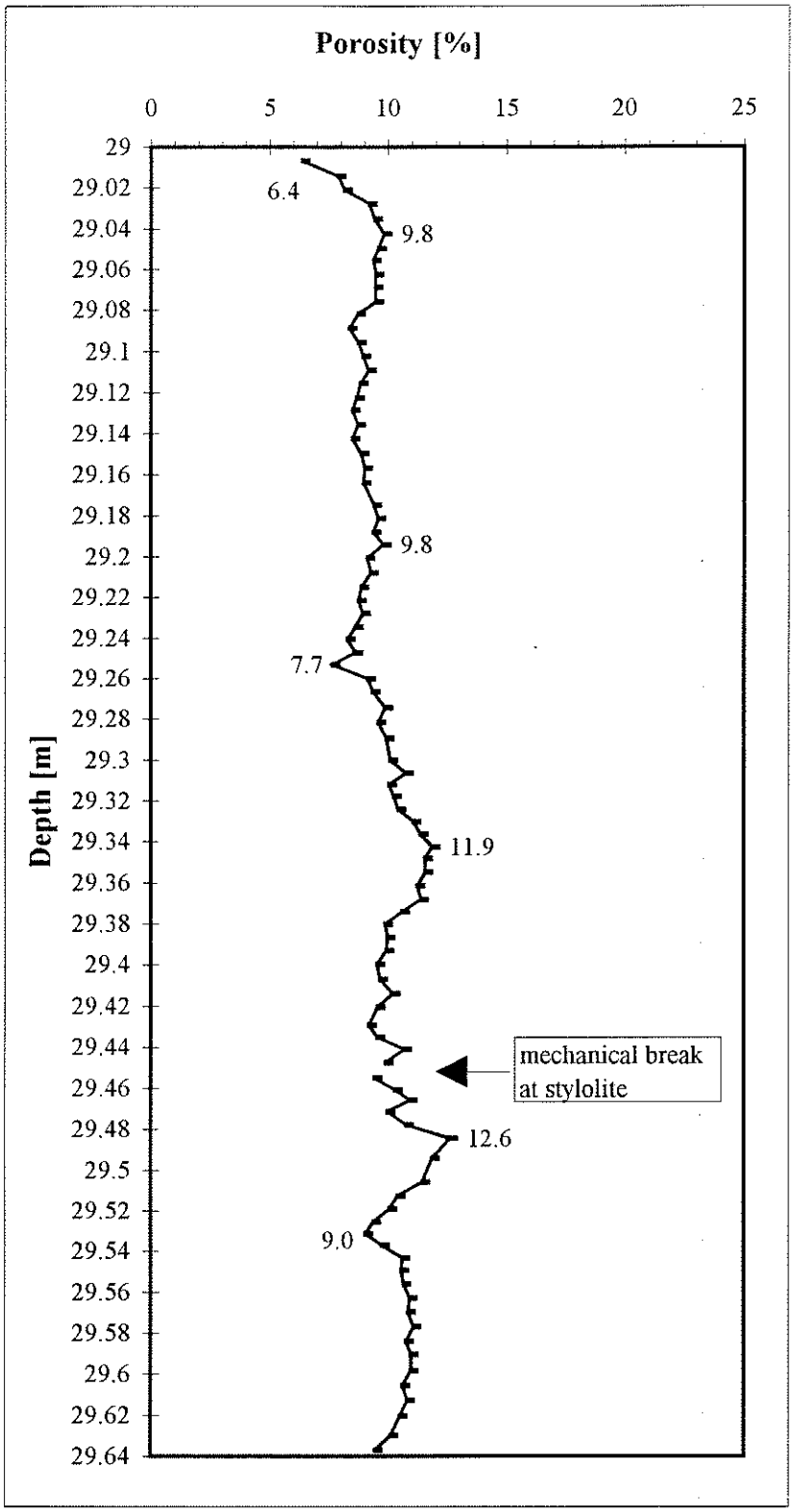

Figure 3.7: Porosity profile from part of the Goat Island Member.

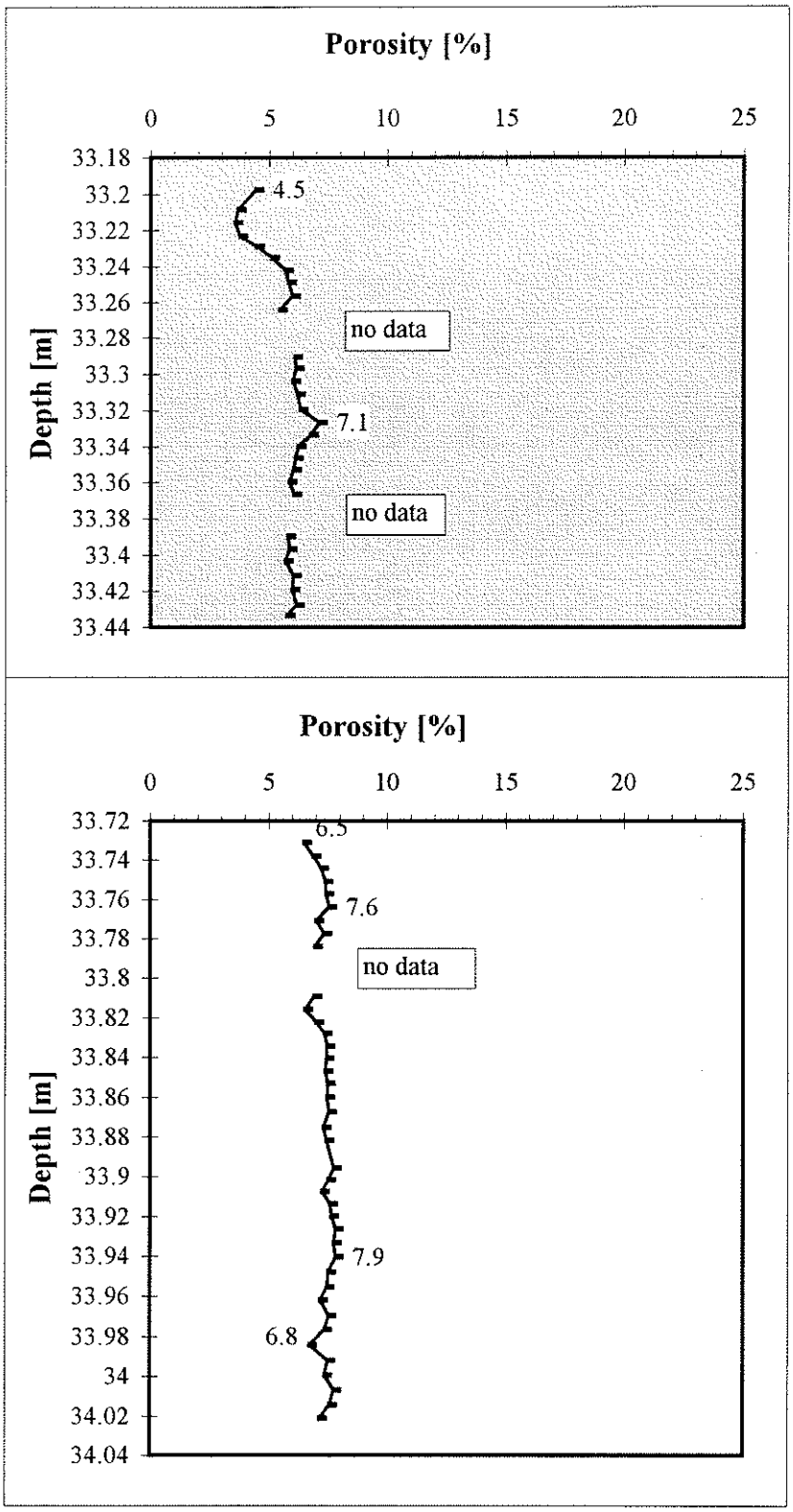

Figure 3.8: Porosity profiles from homogeneous parts of the Gasport Member.

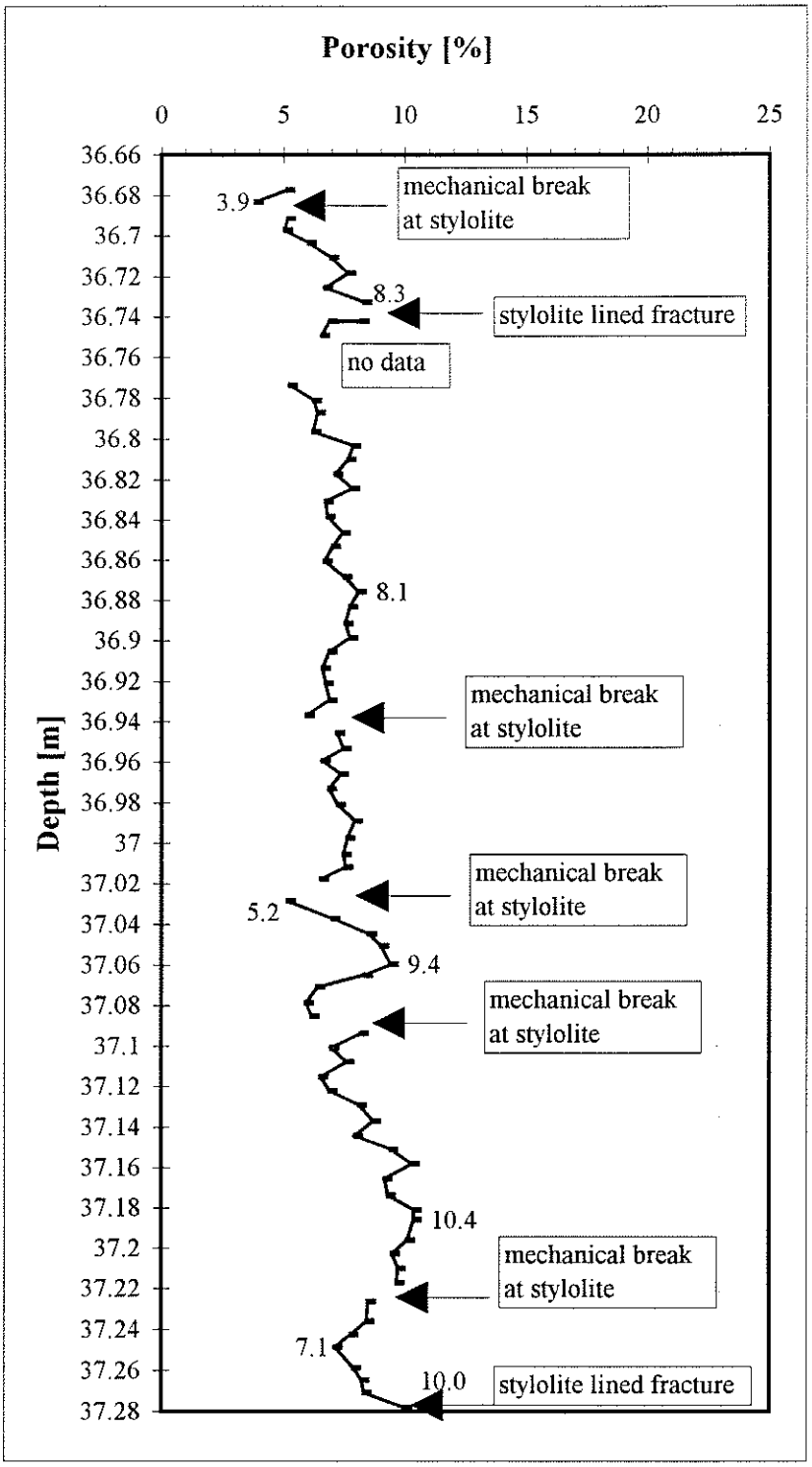

Figure 3.9: Porosity profile from fractured, stylolitic part of the Gasport Member.

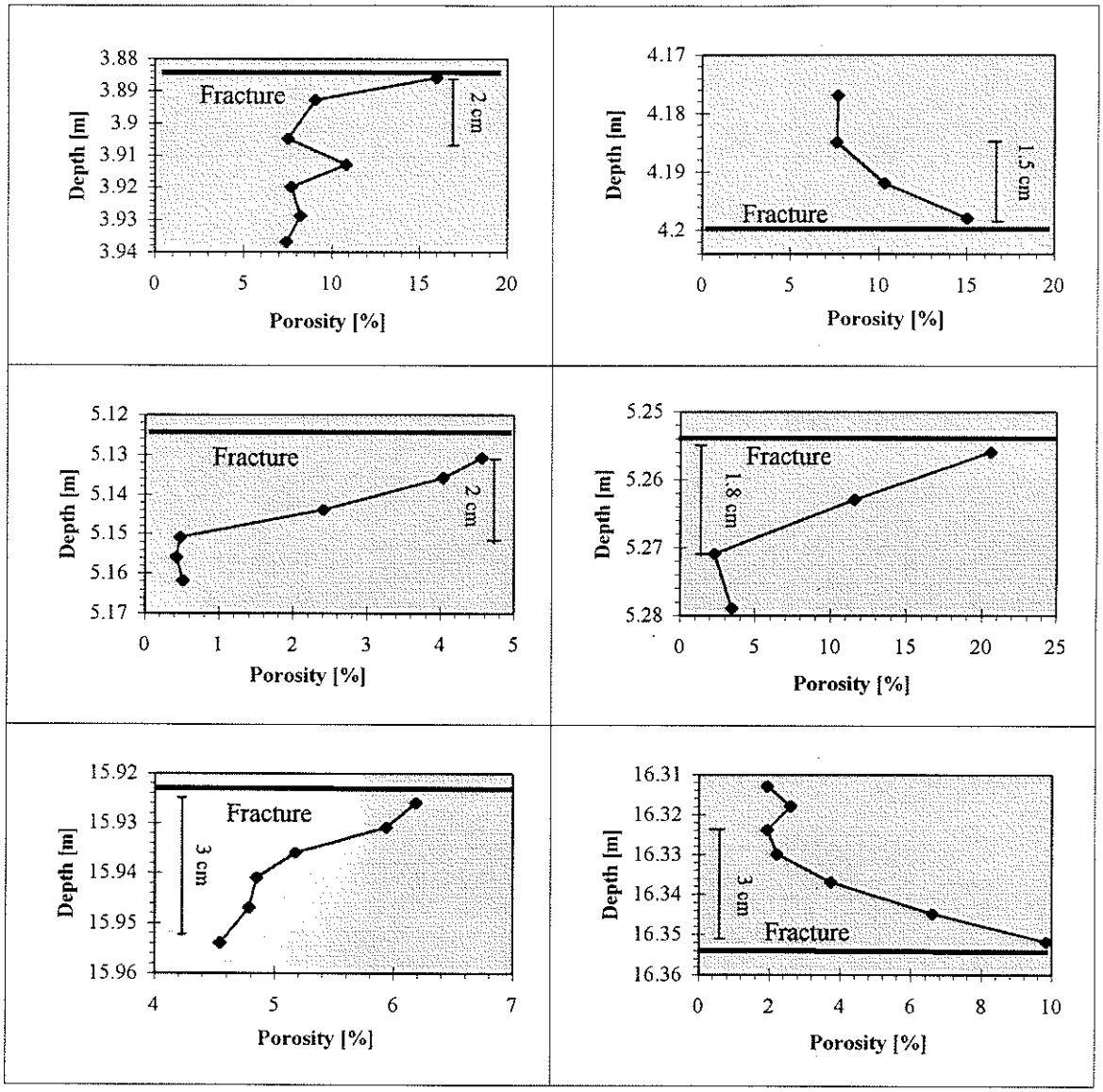

Figure 3.10: Enhanced porosity adjacent to horizontal fractures in the Eramosa Member.

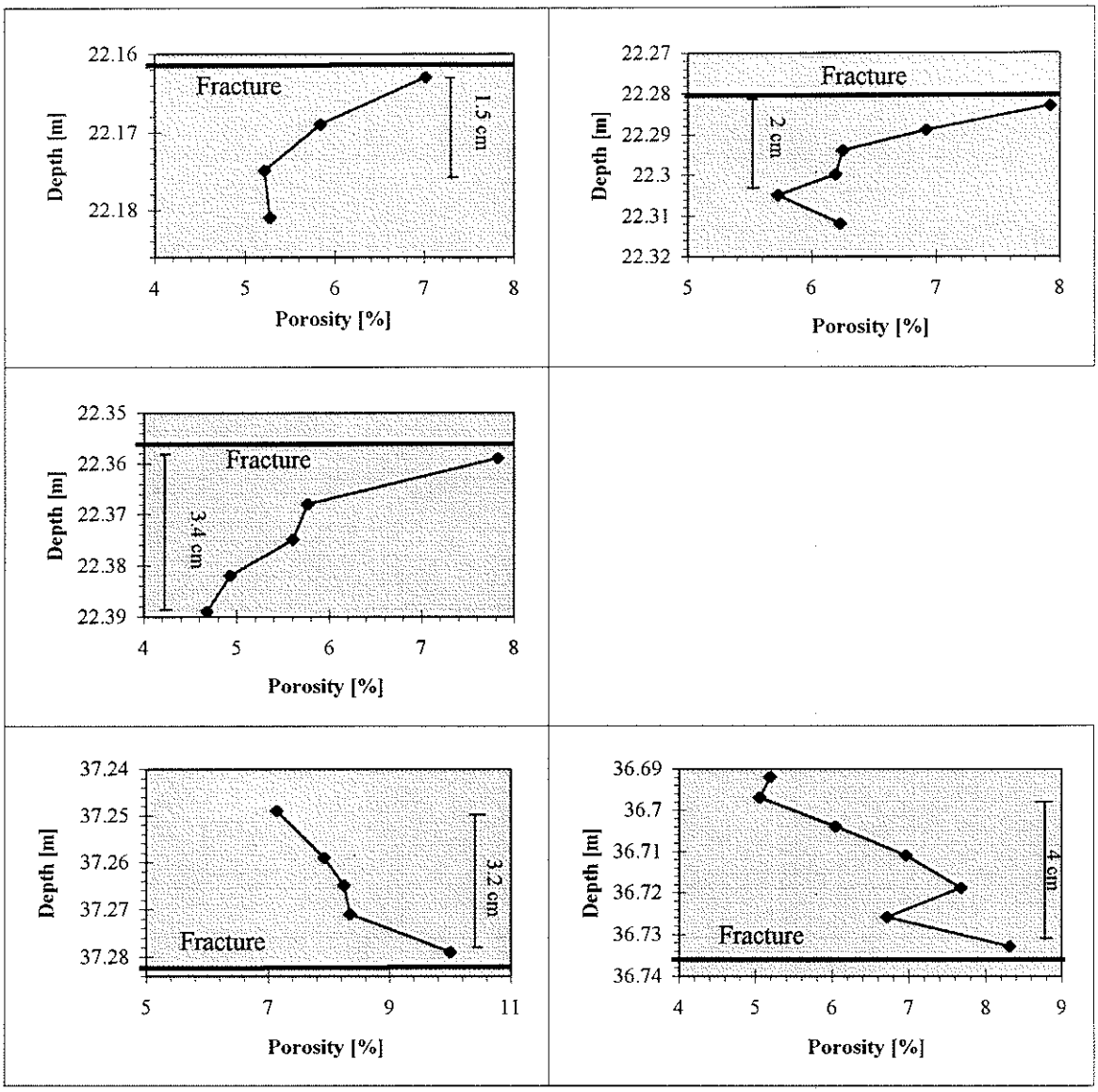

Figure 3.11: Enhanced porosity in the Vinemount and Gasport Member.

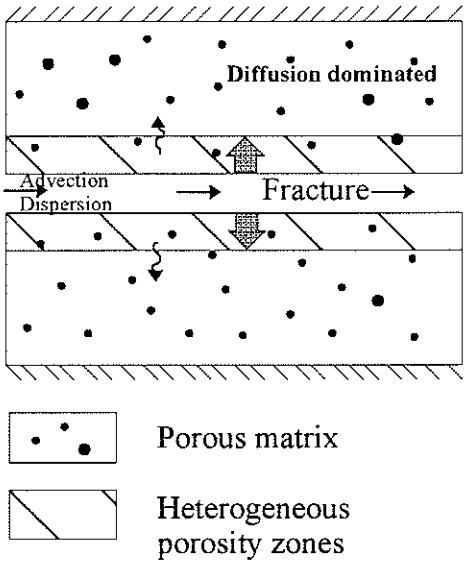

Figure 3.12: Schematic picture of mass transport model through a fractured porous medium with heterogeneous porosity zones perpendicular to the fracture.

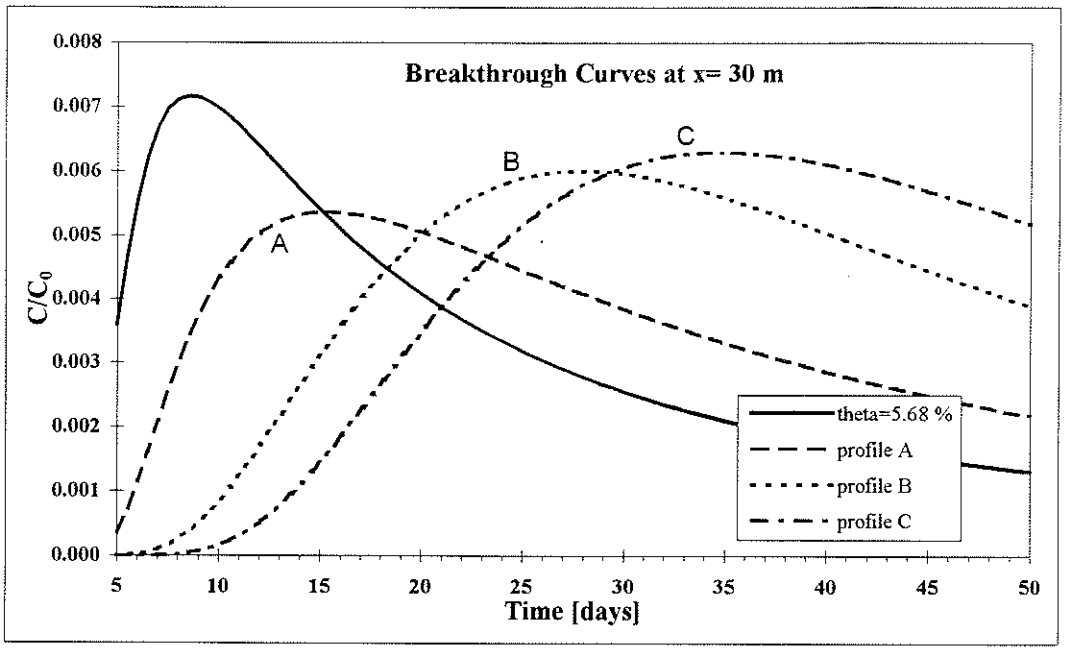

Figure 3.13: Computed breakthrough curves for different vertical matrix porosity profiles, where theta represents a homogeneous average porosity, and profiles A, B, and C heterogeneous matrix porosity profiles.

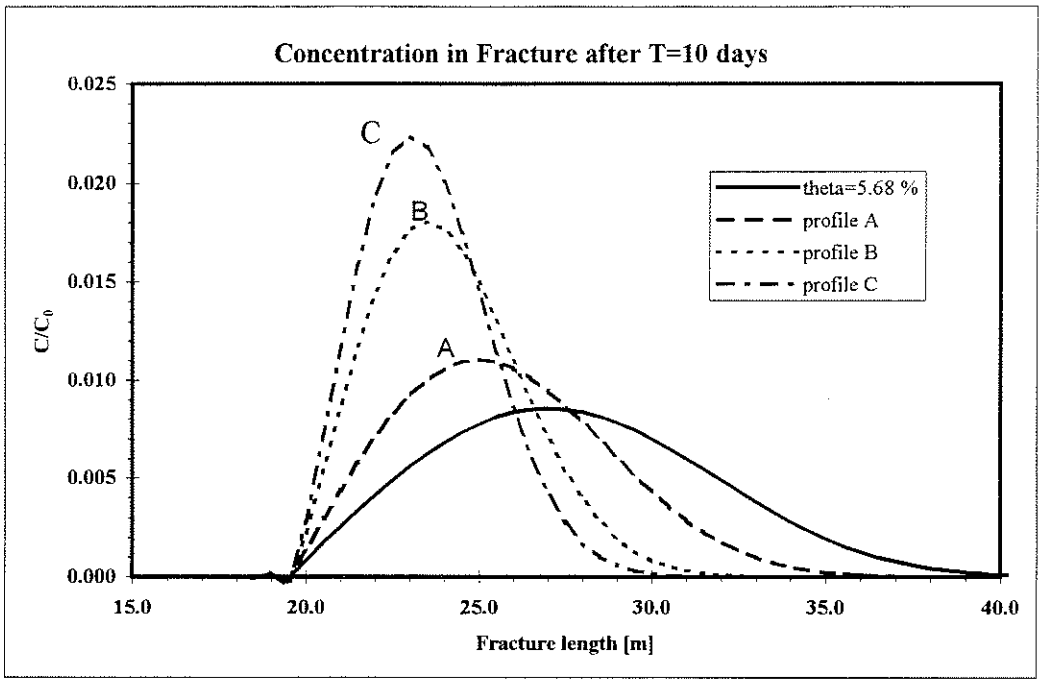

Figure 3.14: Computed plume spreading along the fracture for different vertical matrix porosity profiles, after 10 days, where theta represents a homogeneous average porosity, and profiles A, B, and C are heterogeneous matrix porosity profiles.

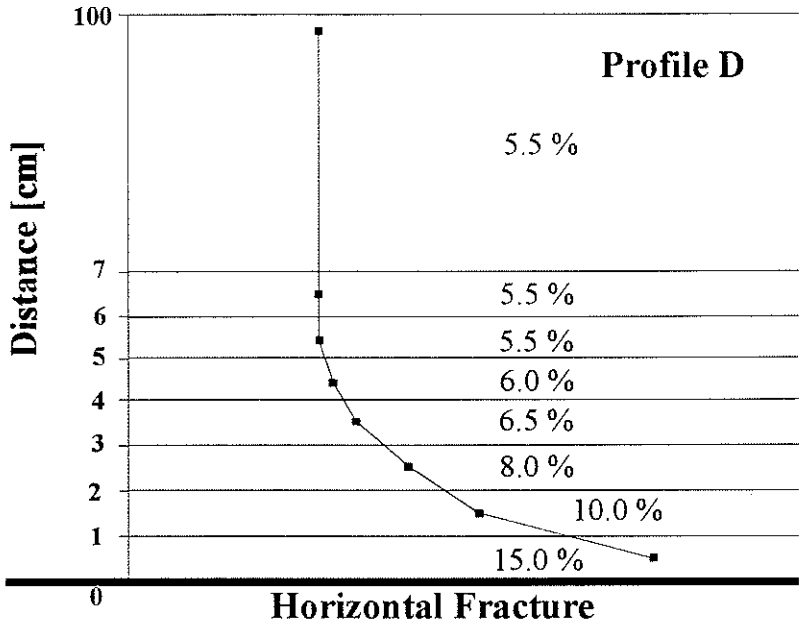

Figure 3.15: Schematic, six zone porosity profile perpendicular to the fracture with an average of 5.68 %, representative for the Eramosa Member.

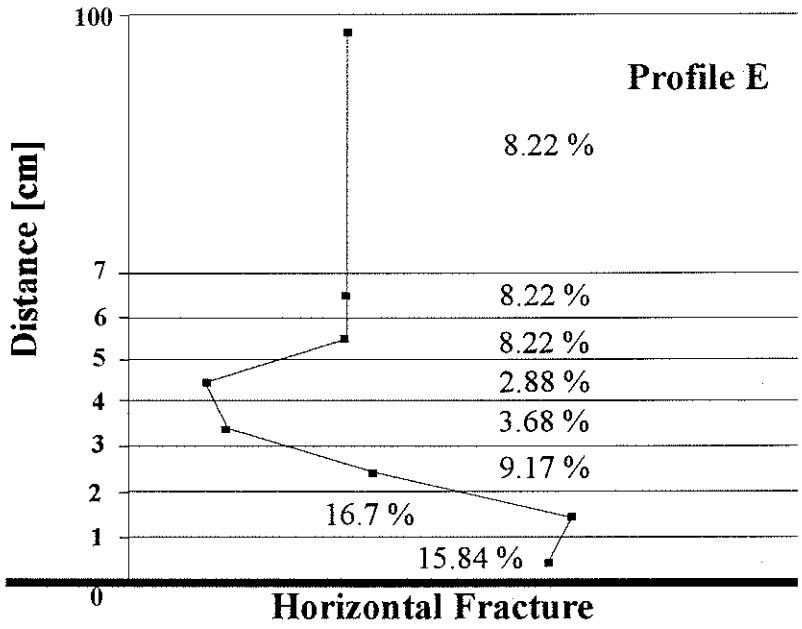

Figure 3.16: Schematic, six zone porosity profile with an average porosity of 8.29 %. This special case is taken from the upper Eramosa Member.

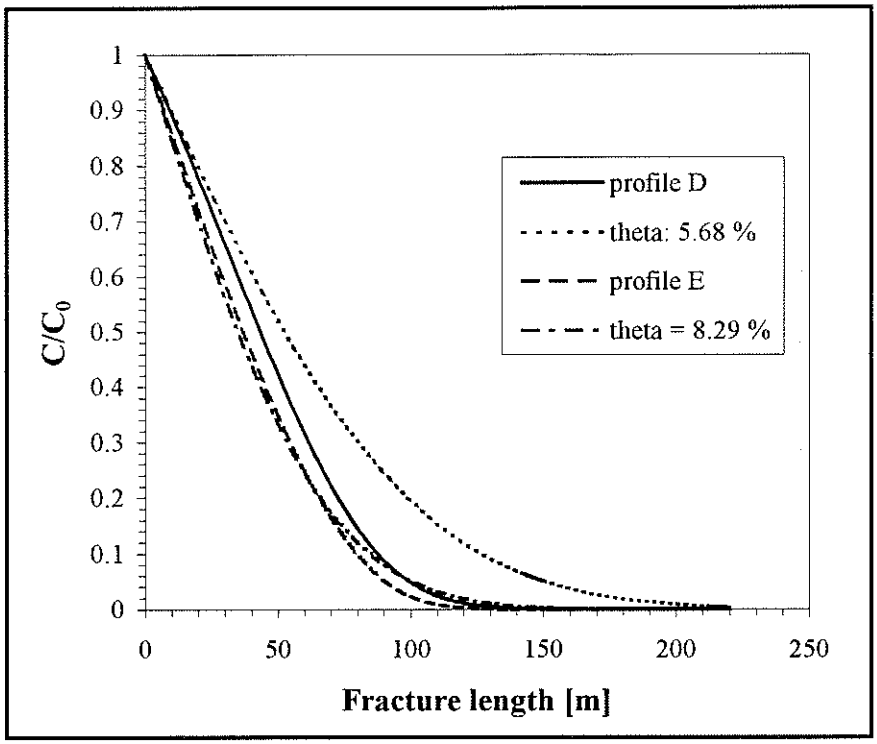

Figure 3.17: Computed contaminant concentrations along the fracture for different porosity profiles after 1000 days. Fracture fluid flow velocity is 4.0 m/d. Theta: 5.68 % and theta: 8.29 represent homogeneous average matrix porosity, and profiles D and E are heterogeneous.

Table 3.1
Mineral Composition of Dolostone Samples Near Smithville (after Bickerton, 1997)

Stratigraphic unit	Estimated clay mineral content [wt%]	Mineral composition [%]			
		dolomite	**quartz**	**gypsum**	**calcite**
Eramosa	0.3-0.9	93.7-97.6	2.4-2.9	-	0.0-3.8
Upper Vinemount	2.0-6.7	91.1-96.9	3.1-6.0	0.0-3.4	-
Lower Vinemount	1.2-3.0	87.6-96.3	2.8-8.7	0.0-7.7	-
Goat Island	0.3-3.5	91.7-96.7	2.0-6.3	0.0-6.3	-
Gasport	0.9-6.0	84.5-97.6	2.1-15.5	0.0-6.5	-
Decew Fm.	0.9	91.8	2.1	6.2	-
Rochester Fm.	3.1-13.1	73.3-93.0	6.2-12.5	-	-

Table 3.2
Summary of Porosity Analyses

Unit	N[1]	Porosity [%]	Porosity [%]	Vertical cracks	Enhanced porosity near fractures	Visible gypsum
		mean	min-max			
Upper Eramosa	66	8.29	0.43-20.63	numerous	yes (most dominant)	none
Lower Eramosa	129	4.4	1.60-9.85	numerous	yes	none
Vinemount	107	5.7	3.95-8.81	some	yes	some
Goat Island	93	9.81	6.39-12.62	none	none observed (further study req.)	none
Gasport	151	7.15	3.59-10.38	none	yes (less dominant)	none

[1]: Number of samples analyzed.

Table 3.3
Descriptive Statistics of Porosity Data (%)

	Upper Eramosa	Lower Eramosa	Vinemount	Goat Island	Gasport
Count	66	129	107	93	151
Mean	8.29	4.38	5.70	9.81	7.15
Standard Error	0.61	0.41	0.10	0.11	0.11
Median	8.65	4.18	5.63	9.67	7.23
Standard Deviation	4.95	1.55	1.00	1.05	1.30
Sample Variance	24.52	2.40	0.99	1.10	1.68
Kurtosis	-0.68	1.12	0.29	0.47	0.85
Skewness	0.09	0.84	0.63	-0.04	0.03
Range	20.31	8.24	4.86	6.24	6.79

Table 3.4
Input Parameters for Mass Transport Simulations

Porous Media:		
K_x:	$8.64x10^{-6}$ [m/d]	hydraulic conductivity in x-direction
K_y:	$8.64x10^{-6}$ [m/d]	hydraulic conductivity in z-direction
α_L:	0.0 [m]	longitudinal dispersivity
α_T:	0.0 [m]	transverse dispersivity
R:	1.0	retardation factor
D*:	$17.37x10^{-6}$ [m^2/d]	effective diffusion coefficient
ρ_b:	2650 [kg/m^3]	bulk density
Horizontal Fracture:		
α_L:	0.1 [m]	longitudinal dispersivity
R:	1.0	fracture wall retardation factor
2b:	$2.0x10^{-4}$ [m]	fracture aperture
Constants:		
D_0:	$17.37x10^{-5}$ [m^2/d]	free-water diffusion coefficient
ρ_f:	1000 [kg/m^3]	fluid density
μ:	86.4 [kg / (m*d)]	fluid viscosity
g:	$0.7322x10^{11}$ [m/d^2]	gravity constant
λ:	0.0 [d^{-1}]	decay rate

Table 3.5
Contaminant Penetration Distances after 1000 Days

Fracture Flow Velocity v_f [m/d]	Porosity θ [%]	Time [d]	$d_{0.01}$ in Fracture [m]	$d_{0.01}$ into Matrix [cm]
				at x = 4.0 m
4.0	5.68	1000	196	45.0
4.0	profile D	1000	120	47.7
4.0	8.29	1000	131	45.0
4.0	profile E	1000	108	45.0
				at x = 2.0 m
0.1	5.68	1000	5.3	30.0
0.1	profile D	1000	3.6	22.5
0.1	8.29	1000	3.8	22.5
0.1	profile E	1000	3.4	18.0

Chapter 4

Sorption of Trichloroethene Onto Stylolites

4.1 Introduction

Trichloroethene (TCE) is a non-polar organic compound belonging to the group of highly volatile chlorinated hydrocarbons (HVCH). In the middle 1970's it became increasingly apparent that chlorinated hydrocarbons were present at numerous locations in Europe and North America in unnaturally high concentrations in the atmosphere, parts of surface- and groundwater, and in plants and soils [Drowty et al., 1975; McConnell et al., 1975; Bauer, 1981]. Even at low concentrations TCE is a serious risk to human health and is probably carcinogenic [Agency for Toxic Substances and Disease Registry, 1993; U.S. Environmental Protection Agency, 1994]. HVCH's are often considered to be immiscible with water but nevertheless have significant water solubility (0.15 to 8000 mg/l). The U.S. EPA Drinking Water Standard for TCE is 5ppb (0.005 mg/l) [Spitz and Moreno, 1995]. Note its water solubility is 1100 mg/l at 25°C [Verschueren, 1984], which is much higher than the aforementioned water standard. Therefore, small amounts of organic fuel leaking into our drinking water supply can represents a serious health risk and pollute a large water volume.

In some carbonate aquifers around the world groundwater has become contaminated by volatile organic compounds, through industrial activity or waste disposal. In these rocks, the transport of the contaminant to local water supplies or surface waters

occurs primarily through a network of bedding plane and vertical fractures. Interactions between contaminants and the solid rock mass must be considered in order to assess the risk for spills and plume migration, and in evaluating remediation plans. For example, the processes of sorption and matrix diffusion can result in significant retardation of organic pollutants in fractured rock formations [Freeze and Cherry, 1979; McKay et al., 1993; Novakowski and Lapcevic, 1994]. In water, dissolved non-polar organic compounds, like the common groundwater contaminant TCE, will adsorb to the surface of organic particles present in the geological material during transport. Adsorption kinematics depend on the contaminant concentration in the groundwater, the rates of adsorption and the capacity of the solid to sorb the compound [Fetter, 1993; Spitz and Moreno, 1995].

Stylolites are common pressure dissolution features, which occur in carbonate formations that underwent compression due to sedimentation or tectonic events. Organic particles and other residual phases become concentrated in these thin (0.1 to 5 mm), serrated dark layers during their evolution. Because stylolites are often associated with the presence of fractures, TCE sorption onto the organic fraction of stylolites may provide for a significant retardation mechanism. No studies to date have recognized the importance of stylolites on the geochemical transport of volatile, chlorinated hydrocarbons such as TCE. The impact of stylolitization on hydrogeological issues, like contaminant transport, is unknown but is potentially significant. Stylolite distribution, frequency, composition and relationship to bedding plane fracturing are of interest when modeling rock matrix sorption of organic solutes. Because sorption of hydrophobic contaminants onto organic

matter is thought to be reversible, stylolites might act as contaminant sinks during adsorption and as contaminant sources during desorption.

In studies of TCE transport in porous media, batch- and diffusion experiments are often conducted to determine distribution coefficients (K_d). To study sorption in fractured media, estimates of the fracture wall distribution coefficient (K^*_d), specific surface area (η), and the organic fraction of the matrix are also required. In addition, the geometric factor of the rock matrix related to tortuosity (γ), the TCE effective diffusion coefficient (D), and kinetic diffusion parameters describing adsorption and desorption behavior are determined. Diffusion experiments have also been used to determine the effective diffusion coefficient, retardation factor, and effective porosity for tracers [Shackelford, 1991; Bickerton, 1993; Novakowski and van der Kamp, 1996]. The effective porosity is defined as the porosity through which flow occurs. Pores that are not interconnected and dead-end pores are not considered part of the effective porosity [Fetter, 1993]. In most diffusion experiments the effective porosity for a certain tracer is unknown and practitioners commonly use total porosity, when evaluating the effective diffusion coefficient analytically. However, the effective diffusion coefficient depends on the tortuosity of the porous media and its free water molecular diffusion coefficient (D_0). Diffusion through a porous media is somewhat slower than in pure water because molecules must follow a longer pathway. If D_0 is known for a particular tracer, the geometric factor for the porous

media can be calculated. For geological materials γ ranges commonly from 0.5 to 0.01 [Freeze and Cherry, 1979].

One-dimensional molecular diffusion transport of a dissolved, conservative tracer through a saturated porous medium is described by Fick's second law:

$$\frac{\partial C}{\partial t} = D\frac{\partial^2 C}{\partial x^2} \tag{4.1}$$

where C is the dissolved tracer concentration in the porous medium. A concentration gradient is the only driving force. A number of different diffusion cell designs and analytical evaluation of concentration-time-plots are described in the literature. Shackelford [1991] summarizes steady state and transient, column, half-cell, and reservoir (single and double) methods and describes analytical solutions for most. Novakowski and van der Kamp [1996] developed a radial diffusion method to minimize gas losses when using volatile, organic substances as a tracer and to maximize the volume of the porous media in relation to the liquid reservoir volume. Therefore, in a radial diffusion cell equilibrium is reached faster than in other diffusion cells. In addition, the method provides information about the effective rock sample porosity.

TCE batch experiments are used to measure the amount of sorption from the aqueous phase onto the solid phase. Measuring the TCE concentration in the water phase at equilibrium and calculating the mass sorbed to the solid phase at equilibrium allows one to determine the distribution coefficient K_d and any other pertinent empirical constants. To

detect if the relationship between the adsorbed concentration (C_s) and the concentration of the solute in the water phase (C_{eq}) is linear, (i.e. $C_s=K_d*C_{eq}$), batch tests with different initial concentrations but equal rock sample mass (same amount of organic matter) should be conducted. However, this was not possible to achieve with natural stylolitic dolostone samples, because stylolites vary in thickness, amplitude and amount of organic carbon content. The amount of organic material in the whole rock samples and in the stylolite layers can be estimated from the TCE distribution coefficient and TCE organic carbon partition coefficient. The organic carbon partition coefficient K_{oc} is computed from an empirical, log-linear regression equation established by Karickhoff et al. [1979] using different chlorinated hydrocarbons and knowing the octanol-water partition coefficient for TCE [log K_{ow} = 2.29; Giger et al, 1983].

$$\log K_{oc} = -0.21 + \log K_{ow} \qquad (4.2)$$

where K_{oc} is the organic carbon partition coefficient [L^3/M], and K_{ow} is the octanol - water partition coefficient [L^3/M]. The weight fraction of organic carbon from the solid phase (f_{oc}) is estimated after

$$K_d = K_{oc} f_{oc} \qquad (4.3)$$

where K_d is the sorption distribution coefficient [L^3/M]. Note also that the fracture wall distribution coefficient (K^*_d) is related to the matrix sorption distribution coefficient (K_d) by the specific surface area (η) of a fracture [Freeze and Cherry, 1979].

$$K^*_d = K_d / \eta \qquad (4.4)$$

The purpose of this paper is to investigate possible TCE sorption onto stylolites and determine TCE sorption and diffusion parameters that describe the interactions. To study the influence of stylolites on the amount of TCE, batch and diffusion experiments are conducted. The diffusion experiments are conducted in horizontal, double - reservoir diffusion cells, which allow the simultaneous observation of adsorption and desorption behavior of reactive compounds. In a horizontal diffusion cell the tracer is forced to migrate orthogonally through the linear stylolite layers. Analytical solutions for three different sorption models are derived in Laplace space and inverted using a numerical inversion algorithm. The models differ in their finite or infinite sorption capacity and kinetic sorption behavior. Each model is tested to explain and fit the experimental data. The geometric factor γ for the rock matrix is determined using time - concentration profiles of the conservative tracer bromide. All rock samples were obtained from the Lockport Formation, which is a fractured dolostone aquifer with numerous, parallel - bedding stylolites at Smithville (Ontario).

4.2 Stylolites in the Lockport Formation

Stylolites are commonly found in carbonate rocks. The term 'stylolite' is generic and does not imply a specific composition. Stylolitization takes place under pressure dissolution due to loading or tectonically related stresses. Carbonates are mobilized under

high pressure, whereas relatively insoluble residual phases like silica minerals, ore minerals and organic matter are concentrated on internal discontinuities. Stylolites are classified following the geometric appearance of the line of discontinuity and their orientation [Park and Schot, 1968]. In the Lockport Formation, stylolites have a suture-like geometry with a large range in amplitude (0.1 to 10 mm). The orientation of stylolites to bedding planes is dominantly horizontal, with occasional stylolites inclined or in interconnected network form. In the Lincoln quarry near Smithville, it can be observed that individual stylolites extend laterally to over 100 m.

Drill core observations associate two types of fractures with stylolitization; horizontal unloading fractures and vertical cracks. Nelson [1985] explains vertical cracks as extension fractures resulting from paleo-stresses associated with stylolitization. Vertical cracks are found most predominantly in the upper 25 m of the dolostone aquifer at Smithville. Horizontal unloading fractures are perpendicular to the maximum paleo-stresses and can be grouped into 1) coring induced mechanical breaks and 2) open bedding plane fractures. Unloading induced fracturing occurs in association with stylolites having low amplitude, leaving the stylolite horizontally divided into two parts. Statistical evaluations from drill cores obtained at the Smithville site verify a correlation between highly fractured zones and zones with numerous stylolites [Radcliff, 1995]. The highest stylolite density of 2.9 stylolites per meter, is found in the upper portion of the Lockport Formation (Fig. 4.1).

The organic content of stylolites and of the 'pure' rock matrix from the Lockport Formation was determined with a carbon analyzer on crushed and powdered material (Table 4.1 and 4.2). The organic carbon fraction in stylolites is between 0.01 and 5.26 % and in the rock matrix between 0.0 and 0.29 % [unpublished data; Hilverda and Langer, 1997; personal communication].

4.3 TCE Sorption Studies

4.3.1 Sampling Procedure

To conduct the batch and diffusion experiments, samples of stylolitic material were required. These were obtained from the vertical drill core 65, which was taken from the Lockport Formation in the vicinity of Smithville. Its stylolite distribution is shown in Figure 4.1. For batch experiments, eleven stylolitic and eleven control dolostone samples without large, visible stylolites were cut from the drill core. The complete drill core was stored in water basins to ensure saturation of the rock matrix at all times. The stylolitic dolostone samples were cut adjacent to potential bedding plane fractures so that one side exposed a stylolitic, dark gray to black surface. The control samples were cut next to the stylolitic dolostone samples. This procedure assures that control samples are from the same depth and similar in chemical composition. It is desirable that the control samples should contain no organic carbon, but some of the controls also showed dark lines and spots indicating possible organic matter (organic matter is also finely distributed throughout the rock matrix and therefore not visible). The volume of each sample was

measured beforehand, whereas the dry solid mass and porosity are calculated from weight loss by heating the samples in the oven at 105°C after TCE equilibrium concentrations were determined. For the diffusion experiments six thin (0.8 to 1.0 cm), water saturated dolostone rock samples were cut parallel to the bedding. One sample contains no stylolite or other visible organic matter and is very light colored, whereas the other samples contain one or more stylolites. The stylolites embrace a large variety of amplitude (0 to 5 mm) and thickness (0.5 to 3 mm) (Fig. 4.2). The total porosity of the rock samples ranges from 2 to 8 %. Samples are taken from different depth covering the upper 19 m of the Lockport Formation.

4.3.2 Batch Experiments

The batch experiments are performed in special 50 ml glass vials capped with a Teflon® coated silicon septum. The glass vials and caps are EPA certified for experimental use with volatile, organic compounds. The rock samples are put into the wide mouth glass vials and covered with 25 ml de-ionized H_2O. A 500 ppb initial TCE solution is obtained by spiking the 25 ml H_2O with 10 µl TCE stock solution (1250 g/l) in methanol. After spiking, the glass vials are turned over to prevent any gas leakage through the caps. TCE concentrations in the solution are monitored using the Head Space Method [Garbarini and Lion, 1985], where 50 µl gas is extracted with a gas tight syringe from the head space and analyzed using a Photovac® 10s Plus gas chromatograph. All TCE concentrations are

calibrated using three blanks. The samples are monitored over 19 days to assure equilibrium is reached.

4.3.3 Diffusion Experiments

The double reservoir diffusion cell is constructed of stainless steel and Teflon® to assure no sorption of dissolved organic tracers onto the apparatus itself. Two stainless steel tubes are separated by the rock sample and are cone shaped towards the ends to prevent air entrapment during filling with deaired, deionized water (Fig. 4.3). This design leaves only a small opening at either end, which are closed off by a Swagelog® fitting with a Teflon® coated silicon septa in the cap. Through the septa both reservoirs can be sampled with a syringe without opening the ends. Stainless steel tubes and rock sample are hold in place by a Teflon® coat, which closes tight around both reservoirs. This is accomplished by heating the Teflon® liner, which causes it to shrink. Six double reservoir diffusion cells and one blank single reservoir cell are built. The blank is capped at one side with a stainless steel plate. The source reservoir in all cells has a volume of 20 ml. The exit reservoir is built with a volume of 20 ml for two cells and 209 ml for 4 cells. Having a 10-fold larger exit reservoir than source reservoir accelerates the drop in tracer concentration in the source reservoir, but on the other hand significantly prolongs equilibrium times and causes analytical problems due to very low tracer concentrations in the exit reservoir.

Bromide (Br^-) is chosen as a conservative tracer because it does not naturally occur in the dolostone aquifer and therefore the background concentration in the saturated rock sample can be assumed to be zero. Bromide is thought to be non-reactive with calcareous minerals like calcite and dolomite as well as with organic matter [Smart and Laidlaw, 1977]. The free-water diffusion coefficient (D_0) for a diluted potassium bromide electrolyte at 25 °C is $20.1x10^{-10}$ m^2/s [Stokes, 1950]. Although D_0 is a function of concentration, the experimental method is utilized over a sufficiently small concentration range so that D_0 can be considered constant.

TCE, in contrast, is a volatile organic compound with a water solubility of 1100 mg/l at 25°C. It reacts quickly with organic matter in the dolostone samples by adsorption, as shown in the batch experiments. The TCE free-water diffusion coefficient is initially thought to be lower than bromide due to its larger molecule size, but is found to be similar. The TCE molecule is elliptical in shape with the smaller diameter about equal in size as bromide and with the long diameter about twice its size.

The source reservoirs of all double diffusion cells are filled with a 309 ppm Br^- solution. After the source reservoirs are closed off, 20 µl liquid are extracted with a syringe through the septa and all diffusion cells are than spiked with 2x10 µl TCE stock solution. The stock solution is composed of 1000 mg/l TCE in methanol. This procedure results in an initial TCE concentration of 1000 ppb in all source reservoirs. The exit reservoirs remain filled with deionized water.

Over a period of 6 to 7 months 150 µl liquid samples are taken out of the source reservoirs with a gas tight syringe and analyzed for Br^- and TCE. The extracted volume is directly replaced with the some amount of deionized water. The liquid samples are injected in special, gas tight, 300 µl glass vials with a Teflon® coated silicon septa in its cap. After equilibration of liquid and gas phase, 50 µl gas phase from the glass vial is sampled and analyzed for TCE with a gas chromatograph (head space analysis). In the first three sample rounds a Photovac® is used, in later rounds a 5890A Hewlett Packard gas chromatograph with a sensitivity below 1 ppb is used. For each sample round three TCE standards are prepared and analyzed for calibration.

After TCE analyses, 100 µl liquid from the glass vial are diluted with 4 ml deionized water for Br^- analyses with an ion chromatograph. Standards of 3, 5, and 10 ppm are used for calibration.

4.4 Analytical Models for Diffusion Cell Experiments

To classify TCE sorption behavior onto stylolites, analytical solutions for three different one-dimensional sorption models are derived in Laplace space (see Appendix). Solutions are obtained using an inversion algorithm by De Hoog et al. [1982]. Computed time - concentration profiles obtained from the analytical solutions are used to evaluate contaminant concentrations measured in source and exit reservoirs of the diffusion cells. Optimal sorption parameters are determined by calibration of the experimental and computed data. The percent error is defined as

$$\% \; error = \sqrt{\frac{\sum_{1}^{N}\left(C_{comp.} - C_{\exp.}\right)^2}{\sum_{1}^{N}\left(C_{\exp.}\right)^2}} \; x\, 100. \qquad (4.5)$$

In a horizontal diffusion cell, advective flow and longitudinal dispersivity are zero. Therefore, a concentration gradient is the only driving force, and is given by Fick's law for a conservative tracer. Adding a sorption term the governing equation becomes:

$$\frac{\partial \, \mathrm{C}}{\partial \, \mathrm{t}} = D\frac{\partial^2 C}{\partial \, \mathrm{x}^2} - \frac{\rho_b}{\theta}\frac{\partial C^*}{\partial t} \quad 0 \le \mathrm{x} \ge \mathrm{L} \qquad (4.6)$$

where

$$D = D_0 \gamma \qquad (4.7)$$

with D: effective diffusion coefficient, D_0: free-water diffusion coefficient, γ: geometric factor related to tortuosity, C: solute concentration in the pore fluid [M/L^3], C^*: solute sorbed onto rock mass [M/M], θ: porosity [L^3/L^3], ρ_b: rock bulk density [M/L^3], and $\frac{\partial \, \mathrm{C}}{\partial \, \mathrm{t}}$: change in concentration with time [$M/L^3/T$]. Note that the x direction extends from 0 to L where L is the rock sample thickness. For many dilute organic contaminants, the sorption process onto organic matter in the porous rock sample is thought to be linear and reversible [Karickoff et al., 1979]. Assuming instantaneous equilibrium, the linear Freundich sorption isotherm can be applied with $C^* = CK_d$ where K_d is the organic

contaminant distribution coefficient. Transport equations (4.8) and (4.9) are derived [Fetter, 1993], (see also Table 4.3; models I and II):

$$\frac{\partial C}{\partial t} = D\frac{\partial^2 C}{\partial x^2} - \frac{\rho_b}{\theta}\frac{\partial\left(K_d C\right)}{\partial t} \tag{4.8}$$

$$\text{or } \frac{\partial C}{\partial t} = \frac{D}{R}\ \frac{\partial^2 C}{\partial x^2} = D_A \frac{\partial^2 C}{\partial x^2} \tag{4.9}$$

$$\text{with } R = 1 + \frac{\rho_b}{\theta} K_d$$

Non-equilibrium or kinetic sorption describes the interaction of the organic solute with the rock matrix where adsorption and desorption processes have different rates. Irreversible and reversible, linear, first-order kinetic sorption [Fetter, 1993] is modeled using

$$\frac{\partial\, C^*}{\partial\, t} = k_2 C \ - \ k_3 C^* \tag{4.10}$$

(sorption) (desorption)

where k_2 and k_3 are rate constants (model III). The governing transport equation is:

$$\frac{\partial\ C}{\partial\ t} = D\frac{\partial^{\ 2} C}{\partial\ x^2} - \frac{\rho_b}{\theta}\left(k_2 C - k_3 C^*\right) \tag{4.11}$$

Contaminant sorption might also be limited by the capacity of the organic material to adsorb. This non-linear behavior can be modeled with the Langmuir sorption isotherm (model IV). The kinetic version is given by

$$\frac{\partial\, C^*}{\partial\, t} = k_4 C\left(C_{\max} - C^*\right) \ - \ k_5 C^* \tag{4.12}$$

where k_4 and k_5 are rate constants and C_{max} is the maximum sorption capacity [Fetter, 1993]. Assuming that the desorption rate is near zero ($k_5 \rightarrow 0$), contaminant transport is formulated through equation (4.13).

$$\frac{\partial C}{\partial t} = D\frac{\partial^2 C}{\partial x^2} - \frac{\rho_b}{\theta} k_4 C\left(C_{max} - C^*\right) \tag{4.13}$$

To solve equations 4.9, 4.11 and 4.13 for contaminant migration in a horizontal diffusion cell the Laplace transform is applied. The nonlinear Langmuir sorption case is approximated with a linear approach. It is assumed that C* is constant over small time increments. Due to this assumption the reactive mass transport problem becomes linear. After obtaining a solution in Laplace space a semi-analytical approach is used to solve for C in the source or exit reservoir [Bickerton, 1993]. A detailed outlines the procedure of how to obtain a solution of the second order, linear differential equation in Laplace space can be found at Bickerton [1993]. A discrete time stepping scheme is used to incorporate non-linear sorption behavior, and the aqueous tracer concentration at each location (x), and the amount sorbed (C*) at each location is updated after each time step (see Appendix). The semi-analytical approached used in this study is verified with a numerical formulation derived by Fabritz [1995]. The finite difference program BUGS simulates mass transport with kinetic reactions in saturated porous media.

4.4.1 Model Verification

For comparison, mass transport of TCE through a porous rock slice of 0.81 cm thickness is simulated using the above outlined semi-analytical approach for diffusive transport with kinetic Langmuir sorption (model IV) and a numerical formulation [Fabritz, 1995]. The following input parameters are used: A porosity of 5.1 %, a density of $2.5x10^{6}$ mg/l, an effective diffusion coefficient of $9.05x10^{-11}$ m^2/s, a maximum sorption capacity of $3.18x10^{-6}$ mg/mg, a kinetic rate constant of $5x10^{7}$ l/mg *s, and an initial tracer concentration of 1 mg/l at x=0. Time-concentration data are calculated after two time periods, 10 and 100 days (Fig. 4.4). Discrepancies between the calculated concentration data (C/C_0) at x = 0.0, 0.001, 0.002, 0.003, 0.004, 0.005, 0.006, and 0.008 m are below $1x10^{-4}$. It can be concluded that the semi-analytical approach simulates the diffusive mass transport problem accurately.

4.5 Results and Interpretations

4.5.1 Batch Experiment Data Analyses and Results

TCE loss due to gas leakage and/or degradation is eliminated from the results by calibration with control samples containing the same initial TCE concentration but no rock material. Due to the differences in organic content and rock mass in the samples, TCE concentrations drop at different time rates. Sample 65E-ST3-20 shows the highest sorption capacity for TCE (Fig. 4.5). The largest amount of sorption takes place in the first two days. The concentration decreases to 0.26 C/C_0, whereas in the following 17

days the concentration decline slows down and reaches equilibrium at 0.11 C/C_0. In all other samples most of the sorption is completed after about eight days and fifty percent of the total amount of sorption takes place in the first five days. The result from a batch experiment on ground, pure stylolitic matter is used for comparison [unpublished data; Hilverda, 1997; personal communication]. The pure, ground stylolite material sorbed 75% of the starting 500 ppb (0.25 C/C_0) in less than a day (20 hours). The five cm^3 (11 g) pure, grounded stylolite material interacted much faster with TCE than most stylolitic dolostone samples. This behavior is expected because the ground material exposes a larger surface area to the dissolved TCE. In the rock sample batch experiments an initial mass of 12.5 μg TCE is injected. The stylolite mass is calculated to range from 1.7 to 5.2 g, and the TCE mass sorbed lays between 2.8 and 11.3 μg. The pure, ground stylolite sample had a mass of 11 g. The initial TCE mass injected was 17.5 μg, and the TCE mass sorbed was 14.6 μg.

The TCE distribution coefficient for each sample is calculated using the ratio C_{eq}/C_s and assuming a linear, equilibrium sorption isotherm. The fraction of organic carbon (f_{oc}) is estimated using the relationship $K_d=K_{oc}\cdot f_{oc}$, where K_{oc} is 120.226 [cm^3/g] for TCE. As a result, K_d ranges from 0.6 to 7.8 cm^3/g (average 2.6) in the stylolitic dolostone samples and between 0.4 and 2.0 cm^3/g (average 0.9) in the dolostone control samples (Table 4.4). The data indicate clearly that the stylolitic rock matrix contains organic matter of significant amount which contributes to TCE sorption. The fraction of organic carbon for all 22 rock samples ranges between 0.0032 and 0.066. The thickness of the stylolite

layers ranges between 0.5 to 1.5 mm. Assuming a density of 2.2 g/cm^3, the stylolite mass is calculated for each sample. The stylolite mass from the 11 samples ranges between 1.7 and 5.2 g. Taking the fraction of organic carbon from the dolostone control sample as background value, the f_{oc} for the stylolite mass part is calculated (Table 4.4).

The average f_{oc} for the stylolite layers is 0.1875 (with an average K_d of 22.54 cm^3/g) compared to a f_{oc} of 0.15 (with K_d of 17.61 cm^3/g) found for the pure, ground stylolite sample in trial test-1. A wide range in K_d for the different stylolite layers is expected due to the large variation in their composition. The dolostone matrix without stylolites has an average amount of 0.8 % (f_{oc}=0.008) organic carbon.

The fracture wall distribution coefficient is calculated for each stylolite surface by knowing the concentration of TCE in solution and the mass of TCE adsorbed per unit area of fracture surface.

$$K_d^* = \frac{\text{mass of solute adsorbed per unit area of fracture surface } [M / L^2]}{\text{concentration of solute in solution } [M / L^3]}$$

Therefore, knowing K^*_d and K_d, the specific surface area η for TCE sorption is evaluated using equation (4.4) and ranges between 1.9 and 8.2 cm^2/g. The average specific surface area for TCE sorption onto the stylolite fracture wall layer is 4.872 cm^2/g.

4.5.2 Estimation of Retardation Factors

Assuming linear - reversible equilibrium sorption, retardation factors (R) are estimated to range between 100 and 1000 for stylolite layers and between 10 and 50 for the rock matrix based on the range of TCE distribution coefficients and log K_{ow}=2.29 (Fig. 4.6). From 546 core sample measurements the average total porosity of the rock matrix in the Lockport Formation is 6.81 %, and the bulk density is 2.51 g/cm^3. Estimation of the stylolitic fracture wall retardation factor of 30 to 400 is based on the range of TCE specific surface area data and an assumed fracture half aperture width (b) of 0.02 cm.

$$R_f = 1 + \frac{K_d^*}{b} \qquad (4.14)$$

4.5.3 Diffusion Experiment Data Analyses and Results

All analytical concentrations are calibrated with concentrations from a blank diffusion cell containing no rock sample but the same solute initial source reservoir concentrations. In this way, TCE loss due to volatilization and degradation is accounted for. Decreases in solute concentration with time are strictly due to diffusion and sorption.

A semi-analytical solution is used to evaluate the effective diffusion coefficient of conservative tracers in double reservoir diffusion cells [Bickerton, 1993]. Knowing the initial tracer concentrations in the source reservoir, porous medium and exit reservoir, and an estimate of the porosity and diffusion coefficient, concentration-time data for the solute in source- and exit reservoir are calculated. Porosity values for the rock samples are determined after the experiments are finished. Curve fitting by calibration between

analytical- and experimental data determines the effective or apparent diffusion coefficient for the specific tracer. Knowing the free-water diffusion coefficient for bromide and the sample porosity, the Br^- time - concentration profiles are used to evaluate the rock sample's tortuosity related geometry factor γ (model I; Table 4.3). The effective diffusion coefficient for Br^- ranges from $0.9x10^{-10}$ m^2/s to $2.6x10^{-10}$ m^2/s (Table 4.5). This yields geometry factors between 0.045 and 0.13 for Br^- migration through dolostone. It is assumed that the geometry factors for Br^- and TCE are the same. The amount of TCE retardation due to adsorption is evaluated by comparing the conservative tracer behavior with TCE.

First, all time-concentration profiles from source and exit reservoirs are analyzed assuming reversible, linear, equilibrium sorption (model II) for TCE sorption onto stylolites in the porous medium. Bromide and TCE concentrations in the source and exit reservoir of control sample 65E-ST18-1 are best modeled with an effective diffusion coefficient of $2.61x10^{-10}$ m^2/s. TCE concentrations in the exit reservoir show no sign of retardation (Fig. 4.7). This suggests that the free-water diffusion coefficient for TCE is very similar to the one for bromide and no adsorption or reaction took place in the porous medium. In all other five diffusion cells (with stylolite samples) the TCE time-concentration curves from source reservoirs are below their respective Br^- profiles. The apparent diffusion coefficient for TCE lies between $5.0x10^{-10}$ and $12.1x10^{-10}$ m^2/s (Fig. 4.7). Retardation factors can then be separated from the apparent diffusion coefficient by assuming D_{TCE} equals D_{Br^-}. This results in unacceptable retardation factors between 0.2

and 0.4 (Table 4.5), which would be even lower when assuming a free-water diffusion coefficient for TCE that is smaller than the one for Br^-. Therefore, model II is not physically meaningful and must be rejected. However, the low TCE time-concentration curves from exit reservoirs can be evaluated with model II, and result in retardation factors of 110 to 160. It is apparent that concentration profiles from the source and exit reservoirs cannot be modeled together when assuming reversible, linear, equilibrium sorption for TCE. TCE strongly adsorbs onto stylolites in the porous medium, but during the observed time period (6 month) does not desorb.

A kinetic, irreversible sorption model (model III) is much more appropriate to describe the observed behavior. This model leads to attenuation of the solute in the stylolite layers. In the given time frame the TCE desorption rate is zero, suggesting $k_3 \rightarrow 0$. The forward, first order kinetic constant k_2, lies between 3.15 and 9.46 cm/g yr^{-1} (Fig. 4.8). The steep drop in TCE concentration during the first 30 days suggests that the adsorption process is non-linear (meaning concentration dependent). In the two smaller diffusion cells (samples 65E-ST1-17 and 65E-ST27-4) TCE concentrations in the source reservoirs seem to have reached equilibrium, which cannot be explained with a linear, irreversible sorption model. In fact, a non-linear, kinetic Langmuir type (model IV) adsorption model with a zero desorption rate provides an even better correlation between experimental and analytical data for source and exit reservoirs. The percent error decreases to about 16 to 26 % using a linear, irreversible sorption model (model III), and to about 6 to 15 % using a kinetic Langmuir sorption model (model IV) (Table 4.6). How low TCE concentrations drop in the source reservoir depends on the rock sample sorption

capacity. Because the organic content in all samples is assumed to be different, it is not surprising to observe a range of sorption capacities (Fig. 4.9). Sample 65E-ST11-3 with the highest, visible organic content has also the highest TCE sorption capacity with 4.6 μg/g and sample 65E-ST1-17 with the thinnest stylolite layer has the lowest capacity with 1.3 μg/g. A forward kinetic rate constant (k_4) ranging between $4x10^{-7}$ and $5x10^{-7}$ l/mg s^{-1} and a backward kinetic rate constant (k_5) near zero fits the observed concentration profiles in source and exit reservoirs best.

4.6 Discussion and Conclusions

Using a semi-analytical solution for conservative tracers and knowing that the free-water diffusion coefficient for bromide in dilute systems is $20.1x10^{-10}$ m^2/s, the tortuosity related geometry factor γ for dolostone matrix samples ranges between 0.045 and 0.13. This is in good agreement with published data for geological materials [Freeze and Cherry, 1979]. Bromide, as a conservative tracer, is used for comparison with TCE. Time - concentration profiles from both tracers show that when migrating through a clay and organic-matter free dolostone sample (65E-ST18-1) TCE moves conservatively. Therefore, it can be concluded that no interactions between TCE and calcareous mineral phases take place. Benker et al. [1997] showed in a TCE - bromide tracer field experiment, which was conducted in a sand aquifer with less than 1 % silt and clay and virtually no organic matter present, that TCE moves conservatively. TCE, as a non-polar organic compound, does not sorb onto quartz mineral surfaces. Note that the organic

carbon fraction determined by carbon analyzer in stylolites is between 0.01 and 5.26 % and in the rock matrix between 0.0 and 0.29 %. Estimates of the organic carbon content in stylolites from batch adsorption experiments yields values between 3.4 % and 45.5 %. The organic carbon in the rock matrix is estimated to be 1.67 %. This discrepancy might be explained by TCE adsorption not only onto organic matter but also onto clay minerals in stylolites and rock matrix in batch experiments or simply by selective sampling. The small number of samples for carbon analyses might not represent the large compositional range of stylolites.

Batch experiments and diffusion studies in this research have also clearly demonstrated the capability of stylolites to adsorb significant amounts of TCE out of an aqueous solution. In the experimental time frame of 6 months no significant amount of TCE desorption was measurable. Only 1.7 % TCE from the initial mass injected into the source reservoir was detected in the exit reservoir. This supports experimental results from Culver et al. [1997] that showed only 5% of the initial sorbed mass from batch experiments had been desorbed after 600 h. A slow desorption behavior might also depend on long term TCE exposure [Grathwohl and Reinhard, 1993; Cluver et al., 1997]. With large advective flows (24000 times the void volume), 72 % of the initial soil TCE was removed in desorption column experiments from soils with 0.13 % organic carbon [Pavlostathis and Jaglal, 1991]. It seems that advective flow has a large influence on the time dependent desorption behavior of TCE.

The difficulty of finding an appropriate distribution coefficient for TCE due to time dependent changes in mass transfer has to be pointed out. TCE distribution coefficients for stylolites from our adsorption batch experiments are found to range from 4.1 to 54.7 cm^3/g ,which correlates with published data [Pavlostathis and Jaglal, 1991; Zytner, 1992, Culver et al., 1997]. Unusually low (1 cm^3/g) TCE distribution coefficients for fine to medium grained soil are reported from Picatinny Arsenal (New Jersey) with 1.04 % organic material [Sahoo and Smith, 1997]. Retardation factors for stylolite layers estimated from TCE distribution coefficients range between 100 and 1000. Comparison between bromide and TCE concentration profiles in diffusion cell exit reservoirs yields retardation factors of 110 to 160 assuming linear, reversible equilibrium sorption.

TCE specific surface areas are estimated from batch experiment results on stylolitic dolostone samples. The values range from 1.9 to 8.2 cm^2/g, which seems unusually high when compared to specific surface areas of peat moss (0.4 m^2/g) and GAC (1300 m^2/g), a commercial product with 74.1 % organic carbon.

Zytner [1992] was able to model TCE adsorption and desorption onto different organic soils with an organic carbon content ranging from 1.0 % to 49.4 % using a non-linear, reversible Freundlich isotherm. TCE time - concentration profiles from our diffusion study does not support that finding. An interesting conclusion from Zytner's [1992] batch experiments was that not only the adsorption potential increases with increasing organic carbon content, but also the soils retention capability. Due to unknown organic carbon content in the stylolite samples used in the diffusion cells this potential could not be evaluated. The non-linear, kinetic Langmuir sorption model (model IV)

provides significantly improved fits of experimental TCE data with computed concentrations when compared to the reversible, linear equilibrium sorption model (model II) and the irreversible, kinetic sorption model (model III). There appears to be a maximum sorption capacity of organic contaminant onto stylolites. The rate of mass transfer decreases as more solute adsorbs onto organic surfaces and time - concentration profiles flatten out. In other words, the TCE distribution coefficient is not constant. Stylolitic rock samples, containing different amounts of organic material, showed a maximum TCE sorption capacity of 1.3 to 4.6 μg/g. The time dependent adsorption behavior is also seen in the batch experiment profiles. Depending on the stylolite rock sample (its organic carbon content), equilibration times ranged between 8 and 17 days.

The importance of stylolites on TCE transport through dolostone aquifers is apparent. An average of 55 horizontal stylolite layers with an average thickness of 0.5 mm per stylolite in the upper Lockport Formation (Eramosa Member) can adsorb 78.7 to 278.3 g TCE per square meter surface area. A dissolved TCE plume that extends over 5000 m^2 could lead to TCE attenuation in stylolites of 393.25 to 1391.5 kg (270 to 955 l pure TCE) assuming that all stylolites are reached by the TCE plume and the maximum possible amount of TCE is adsorbed. Any bedrock remediation plan should take into account that TCE desorption from stylolites back into the pore volume of rock matrix and into fractures is a very slow kinetic process. Instead of trying to retrieve dissolved TCE by pumping, other remediation schemes, such as biodegradation may be more practical or achieve better results. Of course, the investigation of various options is outside the scope of this research. Incorporating the determined physical and hydrogeological parameters

into a larger scale model and a stylolite sensitivity analyses is the next step in the ongoing research project.

Appendix

Application of Laplace transform

The Laplace transform of f(C) is defined as

$$\bar{c}(x,p) = \int_0^\infty \exp(-pt)\ C(x,t)\ \mathrm{dt} \tag{4.15}$$

with

p: Laplace variable

$\bar{c}$: solution of C in Laplace space

Equation (4.9), (4.11), and (4.13) transforms to

$$p\bar{c}(x,p) - c(x,0) = \frac{D}{R}\frac{d^2\bar{c}}{dx^2} \tag{4.16}$$

$$p\bar{c}(x,p) - c(x,0) = D\frac{d^2\bar{c}}{dx^2} - \frac{\rho_b}{\theta}k_2\bar{c} + \frac{\rho_b}{\theta}k_3\frac{C^*}{p} \tag{4.17}$$

and $$pc(x,p) - c(x,0) = D\frac{d^2c}{dx^2} - \frac{\rho_b}{\theta}k_4 c(C_{\max} - C^*) \text{ respectively.} \tag{4.18}$$

In the transformations above the sorbed-phase concentration C* is treated to be time-invariant. The nonlinear Langmuir sorption case is approximated with a linear approach. Using the following initial and boundary conditions the particular solution of the Laplace transform equations (4.16), (4.17) and (4.18) are found:

initial conditions: $C(x,0) = 0$ $0 \le x \le L$ in the porous medium

$C_s(0) = C_0$ in the source reservoir

$C_e(0) = 0$ in the exit reservoir

boundary conditions: $C_s(t) = C(0,t)$

$C_e(t) = C(L,t)$

The solution in Laplace space of (4.16), (4.17) and (4.18) are formulated (following the procedure by Bickerton, 1993) as:

$$\bar{c}(x,p) = \frac{C_0\left(p - \xi_e\sqrt{Rp}\right)\exp\left(\sqrt{Rp}\left(\frac{x}{\sqrt{D}} - \lambda\right)\right)}{\Delta} - \frac{C_0\left(p + \xi_e\sqrt{Rp}\right)\exp\left(\sqrt{Rp}\left(\lambda - \frac{x}{\sqrt{D}}\right)\right)}{\Delta} \tag{4.19}$$

with

$$\Delta = \left(p - \xi_s\sqrt{Rp}\right)\left(p - \xi_e\sqrt{Rp}\right)\exp\left(-\lambda\sqrt{Rp}\right) - \left(p + \xi_s\sqrt{Rp}\right)\left(p + \xi_e\sqrt{Rp}\right)\exp\left(\lambda\sqrt{Rp}\right)$$

and

$$\bar{c}(x,p) = \frac{\left[\left(C_0 - \frac{\sigma C^*}{(p+\tau)}\right)\exp\left(-\sqrt{(p+\tau)}\lambda\right)\left(p-\xi_e\sqrt{(p+\tau)}\right)-\left(p+\xi_e\sqrt{(p+\tau)}\right)\left(\frac{\sigma C^*}{(p+\tau)}\right)\right]}{\Delta} *$$

$$\exp\left(\sqrt{\frac{(p+\tau)}{D}}x\right)$$

$$+ \frac{\left[-\left(C_0 - \frac{\sigma C^*}{(p+\tau)}\right)\exp\left(\sqrt{(p+\tau)}\lambda\right)\left(p+\xi_e\sqrt{(p+\tau)}\right)+\left(p-\xi_e\sqrt{(p+\tau)}\right)\left(\frac{\sigma C^*}{(p+\tau)}\right)\right]}{\Delta} *$$

$$\exp\left(-\sqrt{\frac{(p+\tau)}{D}}x\right) + \left(\frac{\sigma C^*}{p(p+\tau)}\right) \qquad (4.20)$$

with

$$\xi_s = \frac{A\sqrt{D}\theta}{V_s}$$

$$\xi_e = \frac{A\sqrt{D}\theta}{V_e}$$

$$\lambda = \frac{L}{\sqrt{D}}$$

$$\tau = \frac{\rho_b}{\theta}k_2$$

$$\sigma = \frac{\rho_b}{\theta}k_3$$

$$\Delta = \left(p-\xi_s\sqrt{p+\tau}\right)\left(p-\xi_e\sqrt{p+\tau}\right)\exp\left(-\lambda\sqrt{p+\tau}\right)$$
$$-\left(p+\xi_s\sqrt{p+\tau}\right)\left(p+\xi_e\sqrt{p+\tau}\right)\exp\left(\lambda\sqrt{p+\tau}\right)$$

and

$$\bar{c}(x,p) = \frac{C_0\left(p - \xi_e\sqrt{p+\tau(C_{\max}-C^*)}\right)\ \exp\left(\sqrt{p+\tau(C_{\max}-C^*)}\left(\frac{x}{\sqrt{D}}-\lambda\right)\right)}{\Delta} - \frac{C_0\left(p + \xi_e\sqrt{p+\tau(C_{\max}-C^*)}\right)\ \exp\left(\sqrt{p+\tau(C_{\max}-C^*)}\left(\lambda-\frac{x}{\sqrt{D}}\right)\right)}{\Delta} \quad (4.21)$$

with

$$\Delta = \left(p - \xi_s\sqrt{p+\tau(C_{\max}-C^*)}\right)\left(p - \xi_e\sqrt{p+\tau(C_{\max}-C^*)}\right)\exp\left(-\lambda\sqrt{p+\tau(C_{\max}-C^*)}\right)$$
$$-\left(p + \xi_s\sqrt{p+\tau(C_{\max}-C^*)}\right)\left(p + \xi_e\sqrt{p+\tau(C_{\max}-C^*)}\right)\exp\left(\lambda\sqrt{p+\tau(C_{\max}-C^*)}\right)$$

where A is the rock sample surface, C_s and C_e are the concentration in the source and exit reservoir, respectively, and V_s and V_e are the volume of the source and exit reservoir, respectively. The solution in real space was obtained using a numerical inversion algorithm [De Hoog et al., 1982]. The sorbed concentration (C^*) and the initial concentration was updated after each time step at each location. The discrete time stepping scheme is computed as follow:

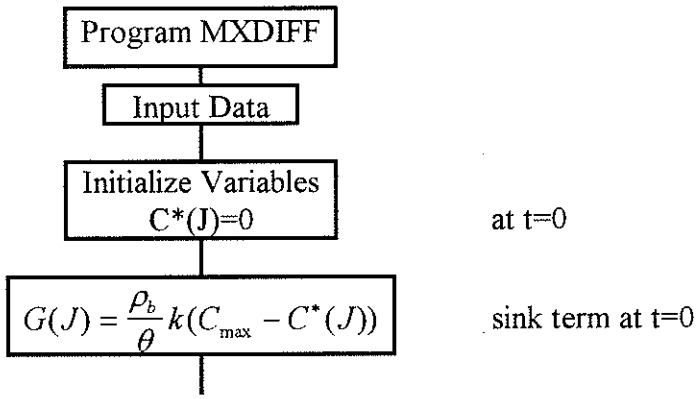

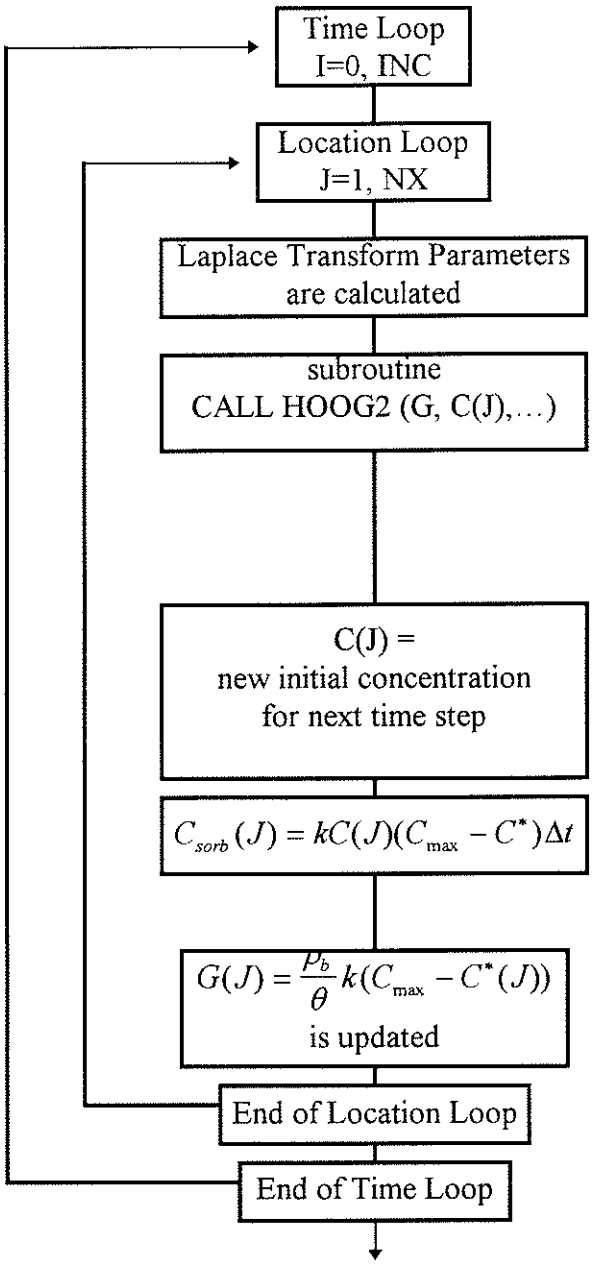

in the subroutine $\bar{c}(x,p)$ is defined and an inversion algorithm is used to solve for C in real space (De Hoog et al., 1982)

the amount sorbed at each location for Δt

for t=n+1

References

Agency for toxic substances and disease regustry (ATSDR). Toxicological profile for Trichloroethylene. U.S. Public Health Service, U.S. Department of Health and Human Services, Atlanta, GA. 1993.

Bauer, U., Belastung des Menschen durch Schadstoffe in der Umwelt - Untersuchungen über leichtflüchtige organische Halogenverbindungen in Wasser, Luft, Lebensmittel und im menschlichen Gewebe. Zbl. Bakt. Hyg., 1. Abt. Orig., 174, 1981.

Benker, E., Davis, G. B., and A. D. Barry, Factors controlling the distribution and transport of trichloroethene in a sandy aquifer - hydrogeology and results of an in situ transport experiment. J. Hydrogeology, 202 (1-4), 315-340, 1997.

Bickerton, G.S., "A Semi-Analytical Model for Solute Diffusion Trough Rock Samples of Finite Thickness." Unpublished B.S. theses, University of Waterloo, Ontario, Canada, 1993.

Culver, T. B., Hallisey, S. P., Sahoo, D., Deitsch, J. J., and J. A. Smith, Modeling the desorption of organic contaminants from long-term contaminated soil using destributed mass transport rates. Environmental Science and Technology, 31 (6), 1581-1587, 1997.

De Hoog, F.R., J.H. Knight, and A.N. Stokes, An improved method for numerical inversion of Laplace trancforms, SIAM. Journal on Scientific and Statistical Computing, 3 (3), 357-366, 1982.

Dowty, B., D. Carlisle, and J.L. Laseter, Halogenated hydrocarbons in New Orleans drinking water and blood plasma. Science, 187 (2), 75-77, Washington, 1975.

Fabritz, J. E. , "A Two Dimensional Numerical Model for Simulating the Movement and Biodegradation of Contaminants in a Saturated Aquifer." Unpublished M.Sc. thesis, University of Washington, 1995.

Fetter, C. W., Contaminant Hydrogeology, Macmillan Publishing Company, New York, 1993.

Freeze, R. A., and J. A. Cherry, Groundwater. Prentice Hall, Englewood Cliffs, New Jersey, 1979.

Garbarini, D. R., and L. W. Lion, Evaluation of sorptive partitioning of nonionic pollutants in closed systems by headspace analysis. Environ. Sci. Technol., 19, 1122-1128, 1985.

Giger, W., R.P. Schwarzenbach, E. Hoehn, K. Schellenberg, J.K. Schneider, H.R. Wasmer, J. Westall, and J. Zobrist, Das Verhalten organischer Wasserinhaltsstoffe bei der Grundwasserbildung und im Grundwasser. Gas - Wasser - Abwasser, 63, (9), 517-531, Zürich, 1983.

Grathwohl, P., and M. Reinhard, Desorption of trichloroethylene in aquifer material. Rate limitation at the grain scale. Environmental Science and Technology, 36(1), 89-108, 1993.

Karickhoff, S.W., D.S. Brown, and T.A. Scott, Sorption of hydrophobic pollutants on natural sediments. Water Research, 13 (3), 241-248, Oxford (Pergamon Press), 1979.

Maloszewski, P., and A. Zuber, Tracer experiments in fractured rocks: Matrix diffusion and the validity of models, Water Resour. Res., 29(8), 2723-2735, 1993.

McConnell, G., D.M. Ferguson, and C.R. Pearson, Chlorierte Kohlenwasserstoffe in der Umwelt. Endeaver, 34, 13-18, Oxford (Pergamon Press), 1975.

McKay, L. D., J. A. Cherry, and R. W. Gillham, Field experiments in fractured clay till, 1, Hydraulic conductivity and fracture aperture, Water Resour. Res., 29(4), 1149-1162, 1993a.

McKay, L. D., R. W. Gillham, and J. A. Cherry, Field experiments in fractured clay till, 2, Solute and colloid transport, Water Resour. Res., 29(12), 3879-3890, 1993b.

Nelson, R.A., Geological Analysis of Naturally Fractured Reservoirs. Ed. George V. Chillingar, Houston, Texas (Gulf Publishing Company), Vol. 1, 1985.

Novakowski, K. S., and P. A. Lapcevic, Field measurement of radial solute transport in fractured rock, Water Resour. Res., 30(1), 37-44, 1994.

Novakowski, K.S., and G. van der Kamp, The radial diffusion method: 2. A semianalytical model for the determination of effective diffusion coefficients, porosity, and adsorption, Water Res. Research, 32 (6), 1823-1830, 1996.

Park, W., and E.H. Schot, "Stylolitization in Carbonate Rocks", in: Recent Developments in Carbonate Sedimentology in Central Europe, eds. German Muller and Gerald M. Friedman, New York (Springer-Verlag New York Inc.), 66-74, 1968.

Pavlostathis, S. G., and K. Jaglal, Desorption behavior of trichloroethylene in contaminated soil. Environmental Science and Technology, 25 (2), 274-279, 1991.

Radcliffe, A.J., "Analysis of Stylolitization and Fracturing in Rock Core from the Smithville Phase IV Site." Unpublished thesis, University of Waterloo, 1995.

Shackelford, C.D., Laboratory diffusion testing for waste disposal - A review. J. of Contam. Hydrology, 7, 177-217, 1991.

Smart, P.L. and I.M.S. Laidlaw, An evaluation of some fluorescent dyes for water tracing, Water Resources Research, 13(1), 15-33, 1977.

Spitz, K.-H., and J. Moreno, A Practical Guide to Groundwater and Solute Transport Modelling. New York (Wiley-Interscience Publication), 1996.

Stokes, R. H., The diffusion coefficients of eight uni- univalent electrolytes in aqueous solution. Am. Chem. Soc. J., 72, 2243-2247, 1950.

U.S. Environmental Protection Agency. Technical background document to support rulemaking pursuant to the clean air act—section 122(g). Ranking of pollutants with respect to hazard to human health. EPA-450/3-92-010. Emissions Standard Devision, Office of Air Quality Planning and Standards, Research Triangle Park, NC. 1994.

Verschueren, K., Handbook of environmental data on organic chemicals. Second Edition. 1310 p., New York (Van Nostrand Reinhold Company Inc.), 1983.

Zytner, R. G., Adsorption-desorption of trichloroethylene in granular media. Water, Air, and Soil Pollution, 65 (3-4), 245-255, 1992.

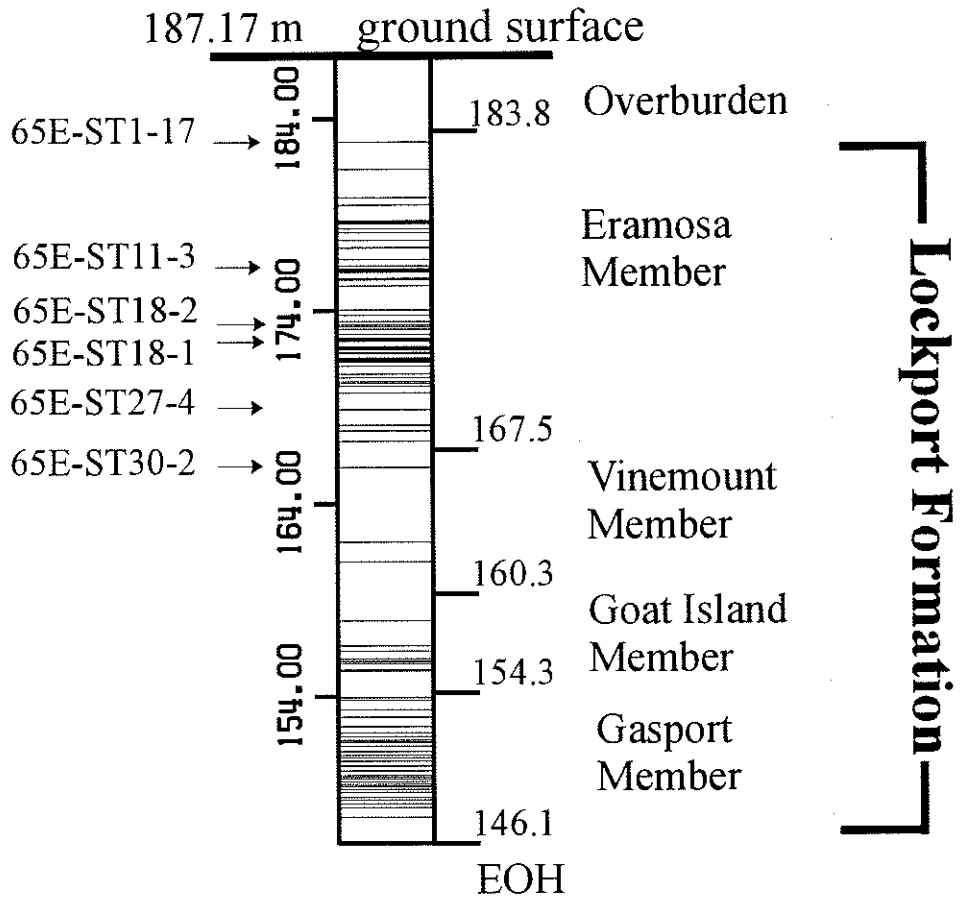

Figure 4.1: Stylolite distribution in the Lockport Formation from borehole 65 near Smithville. Sample numbers at the left hand side refer to diffusion cell experiments (see Fig. 4.6, 4.7, and 4.8).

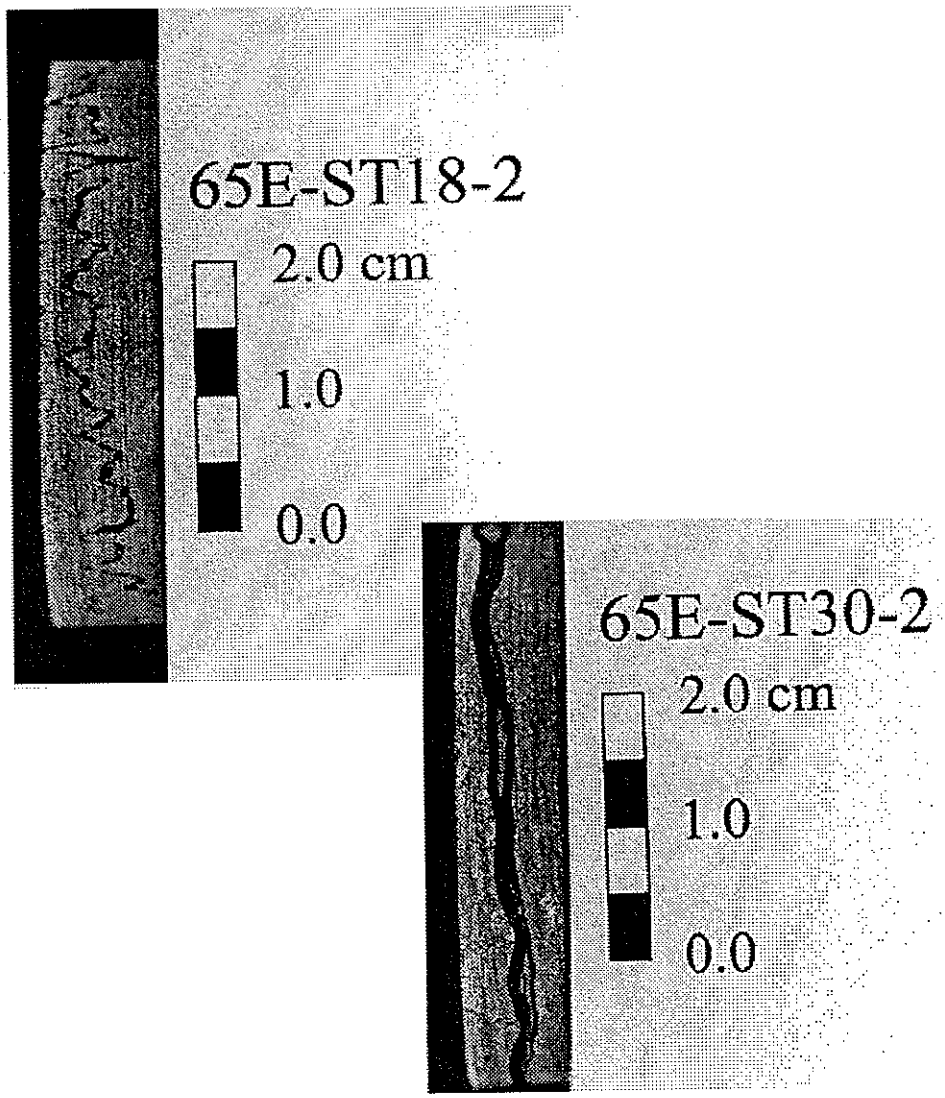

Figure 4.2: Stylolitic dolostone slices for diffusion experiments.

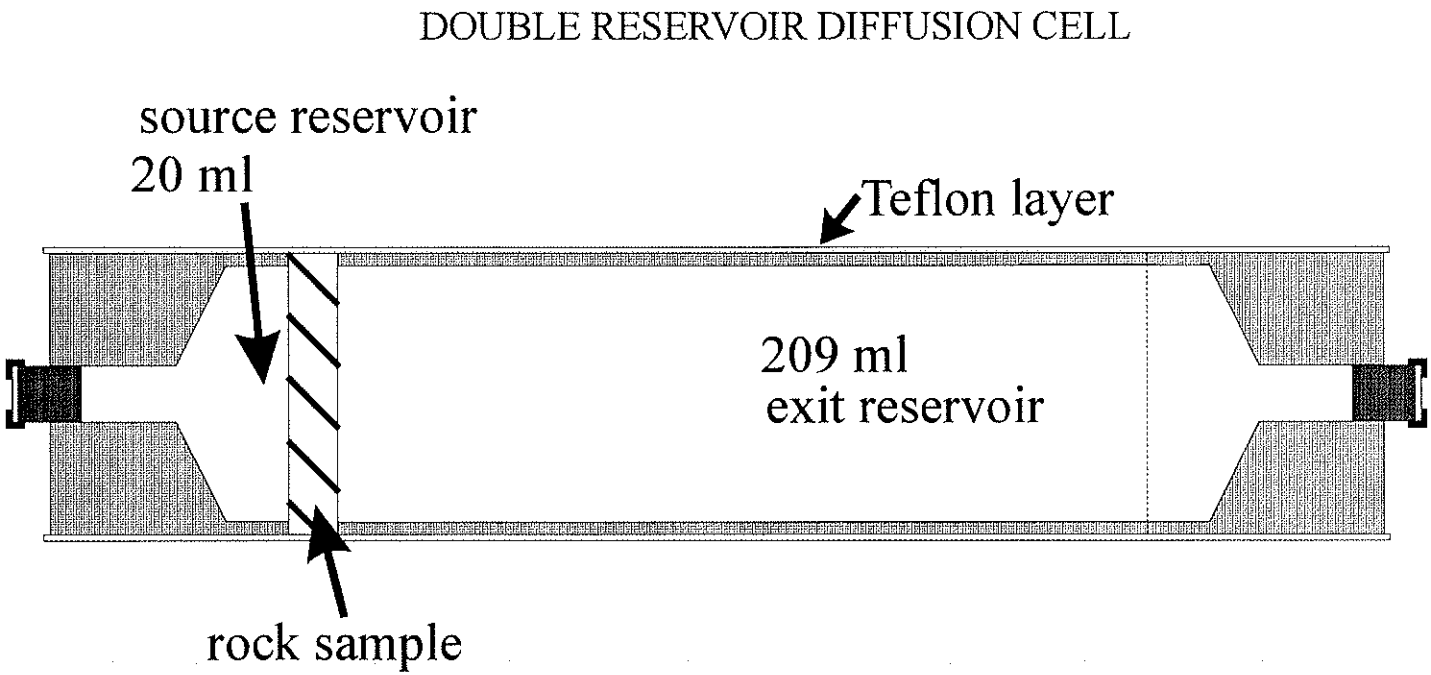

Figure 4.3: Design of double reservoir diffusion cell.

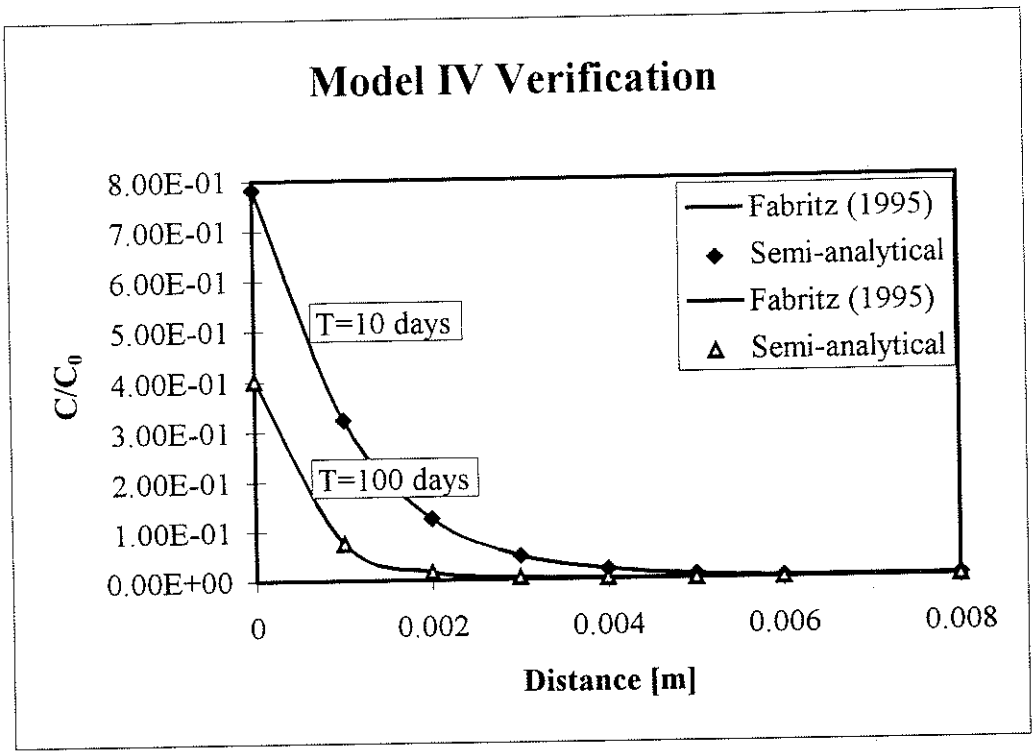

Figure 4.4 Simulation of TCE mass transport through a thin rock slice using a semi-analytical and numerical method for comparison.
Model IV incorporates a kinetic Langmuir sorption expression.

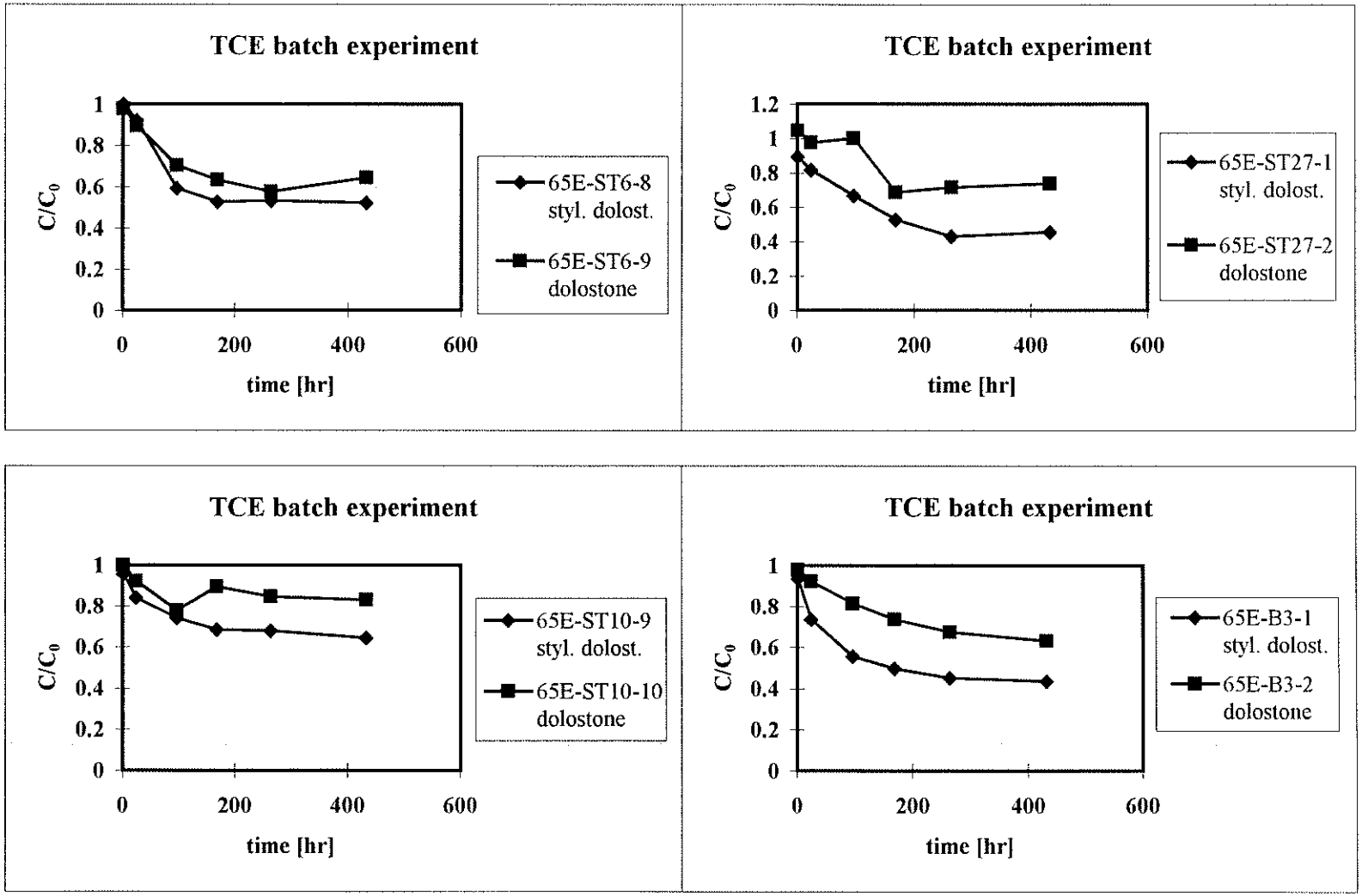

Figure 4.5: Batch experiment TCE time - concentration profiles for stylolitic dolostone and dolostone rock matrix.

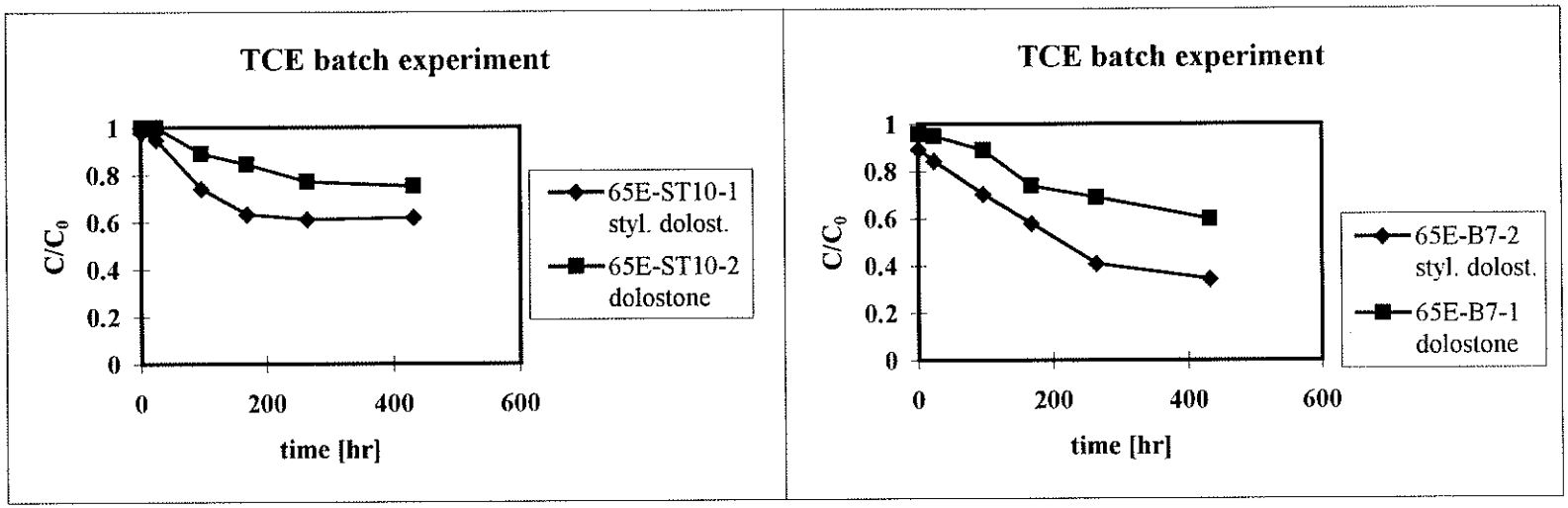

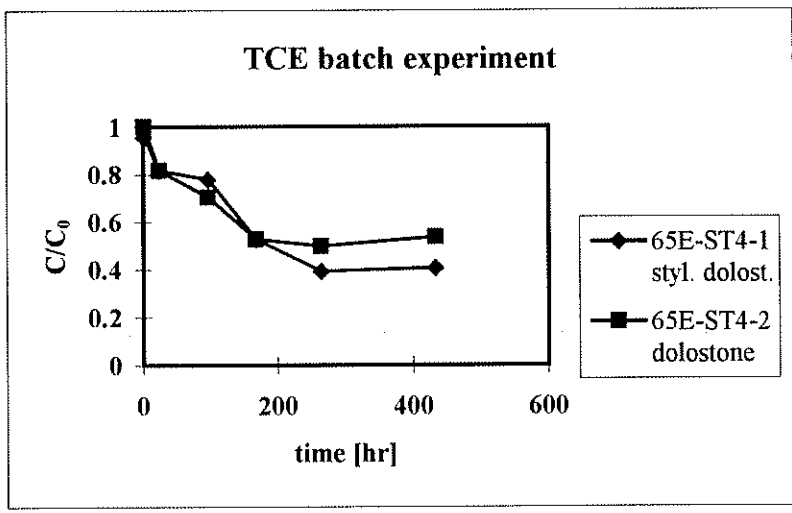

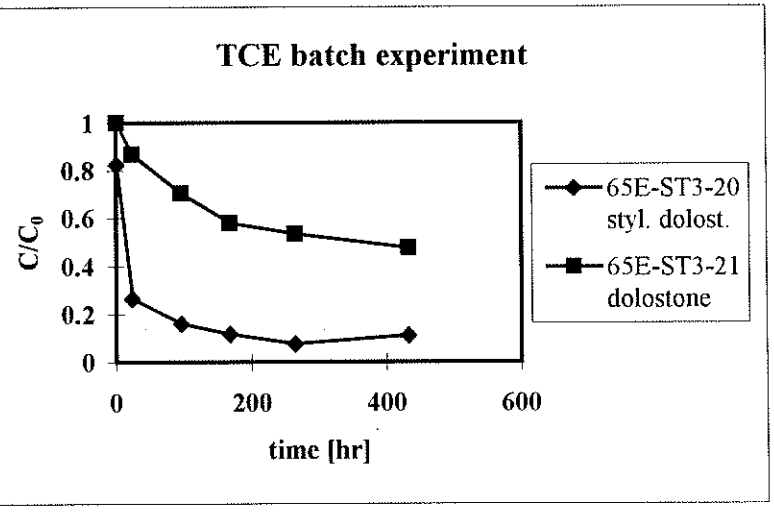

Figure 4.5, continued

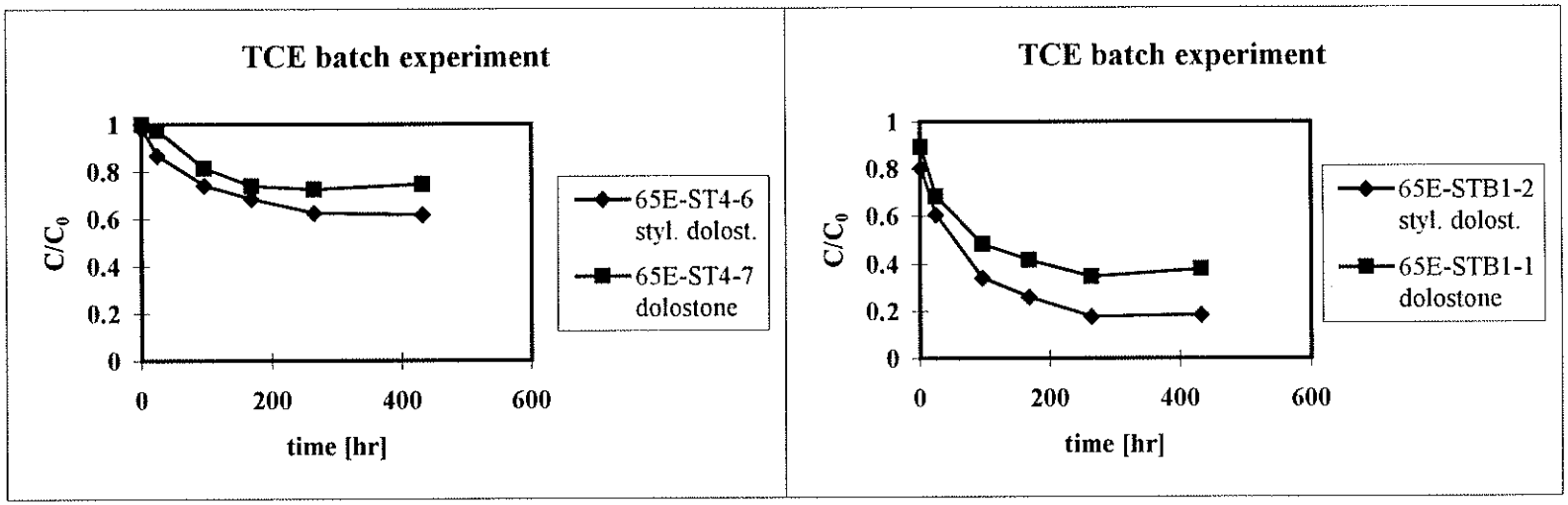

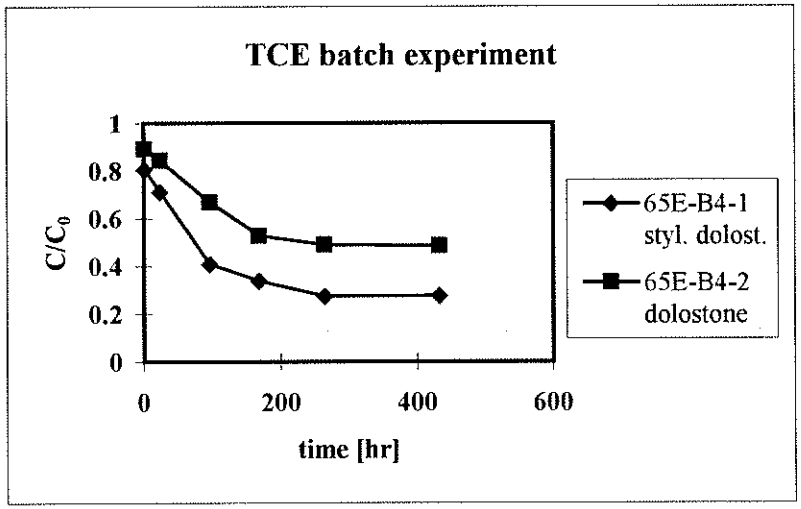

Figure 4.5, continued

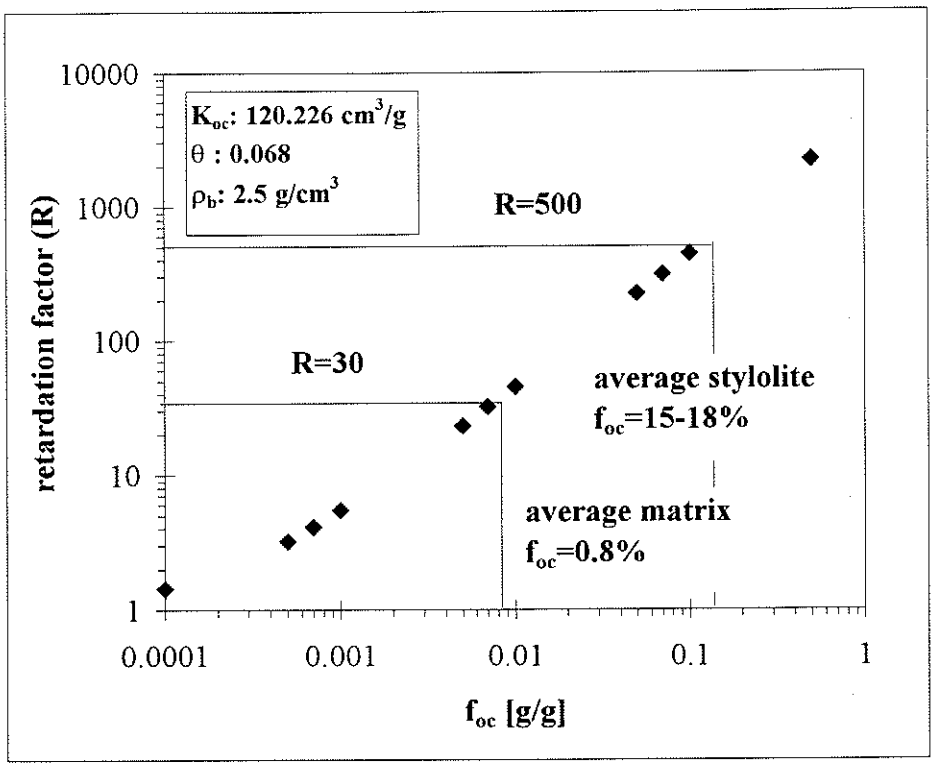

Figure 4.6 Assuming linear, reversable equilibrium sorption, retardation factors for dolostone rock matrix and stylolite layers are estimated on the bases of the TCE octanol - water partition coefficient.

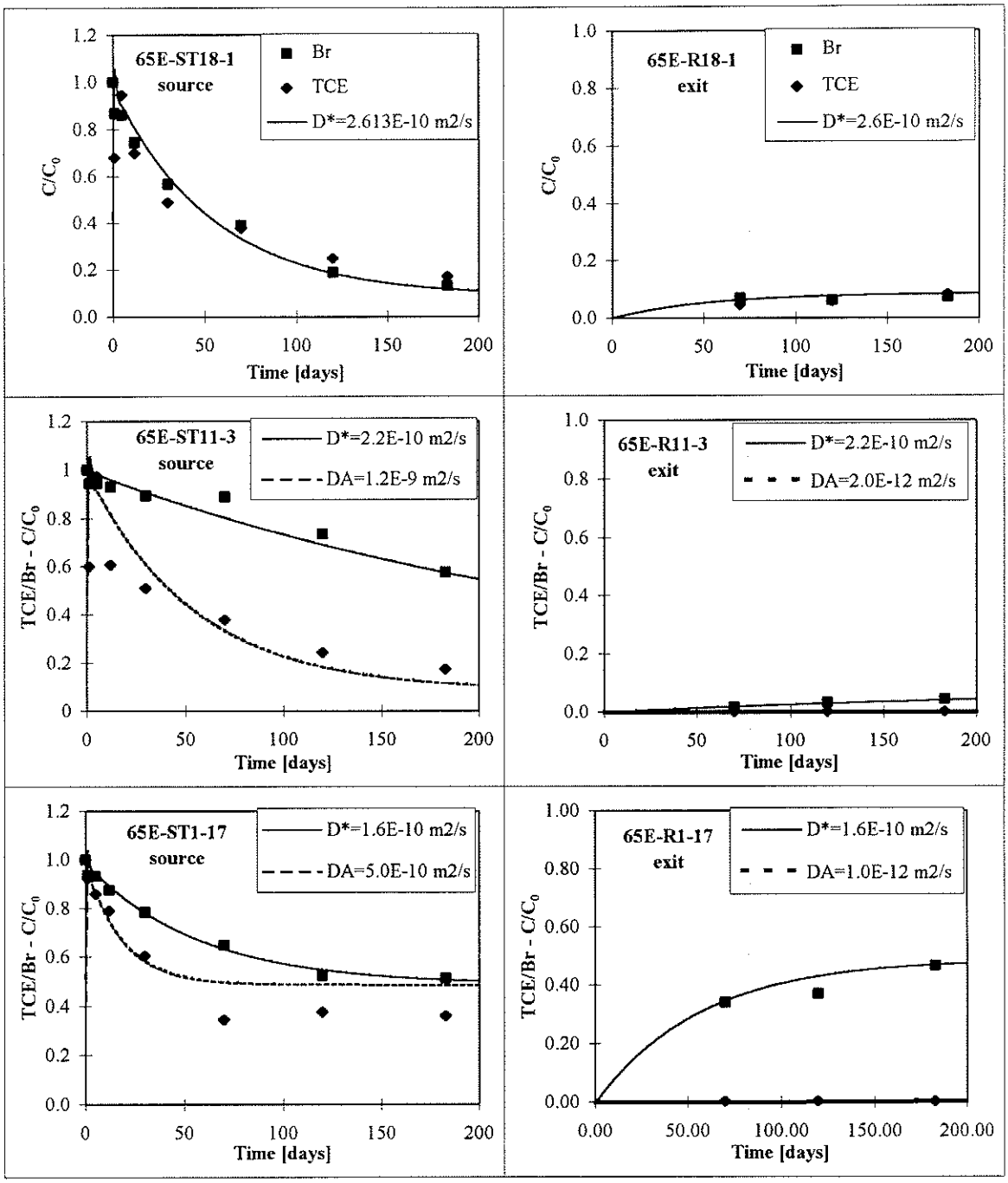

Figure 4.7: TCE and bromide time - concentration profiles from source and exit reservoirs.
Assuming reversible sorption (model II), the apparent diffusion coefficient is evaluated.

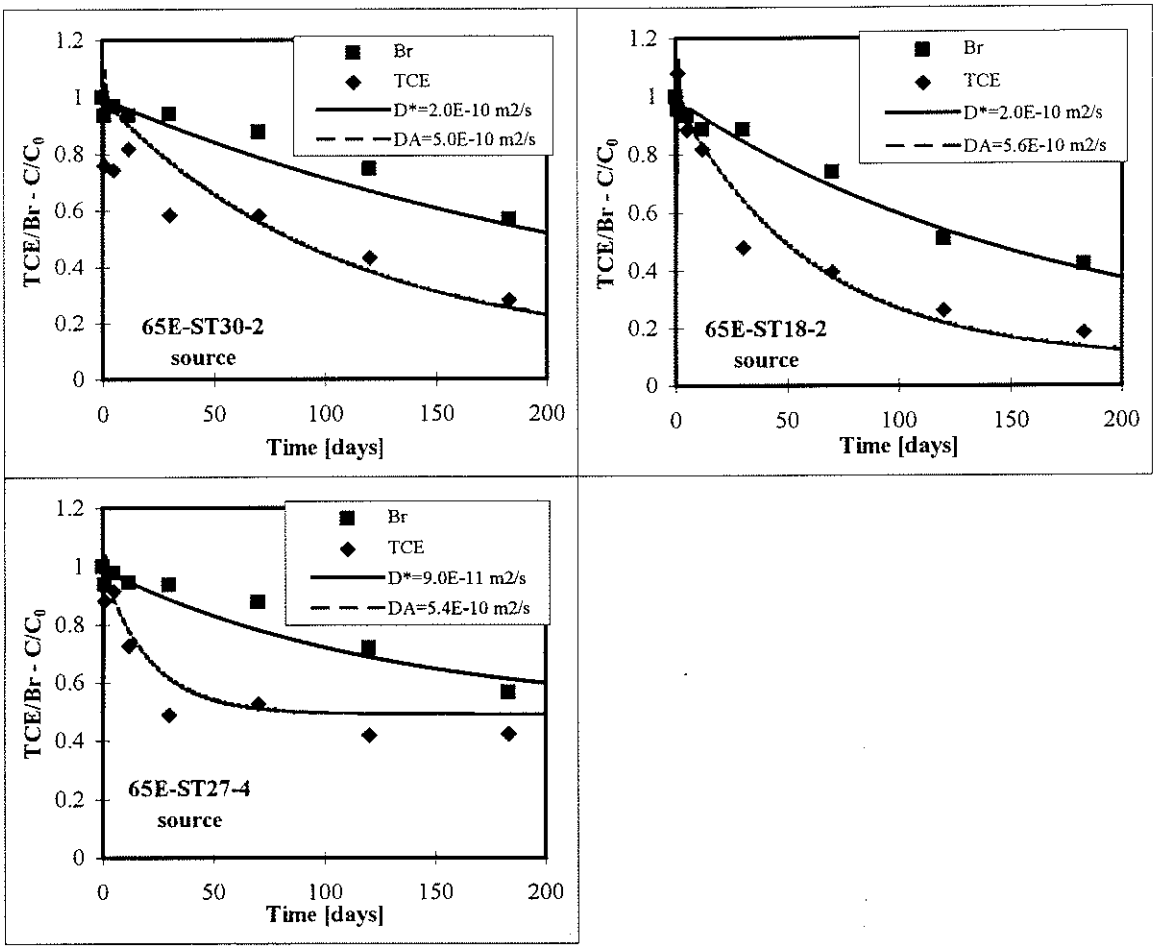

Figure 4.7, continued

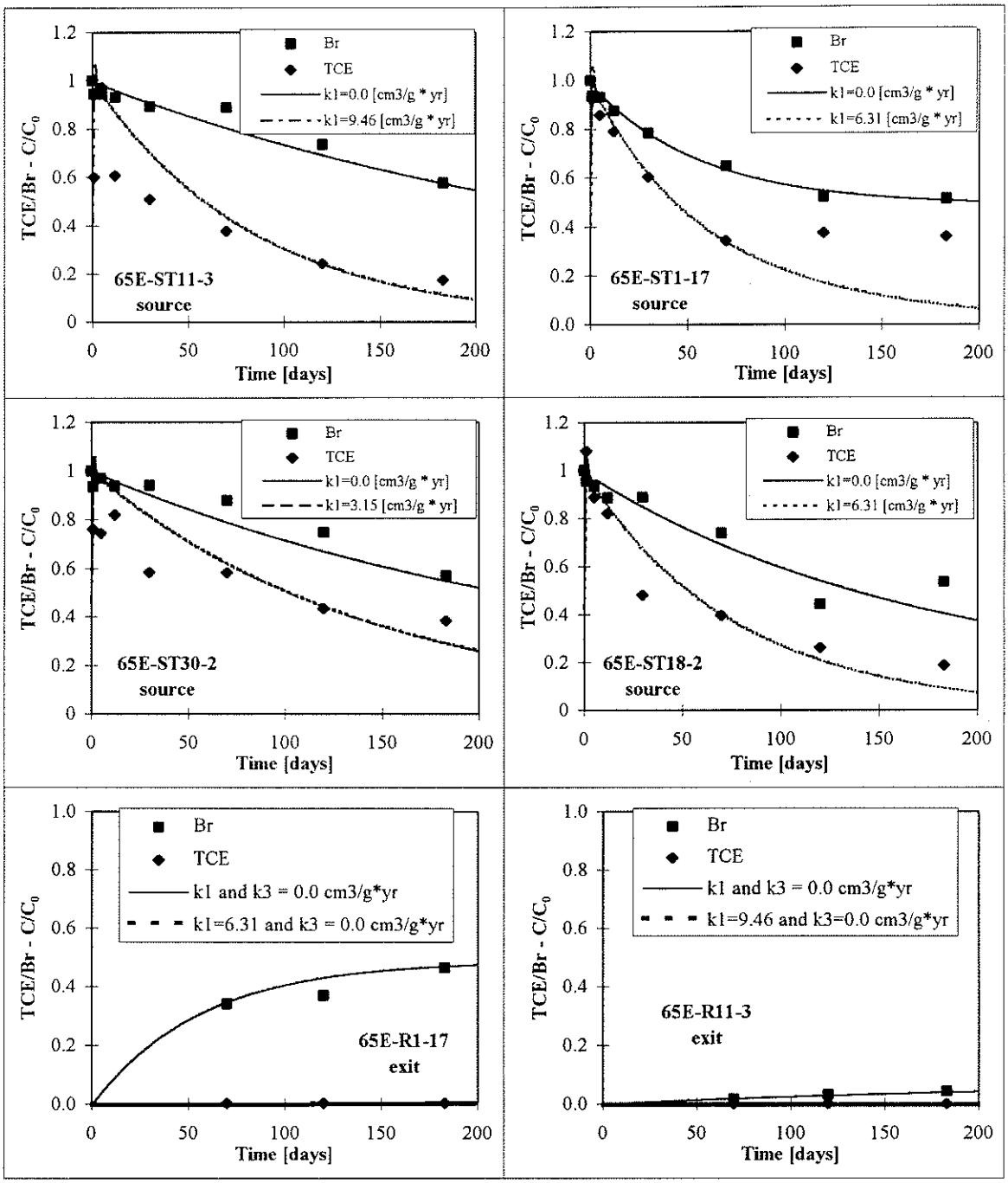

Figure 4.8: Experimental diffusion data and computed time - concentration profiles using the irreversible, first-order kinetic sorption model (III).

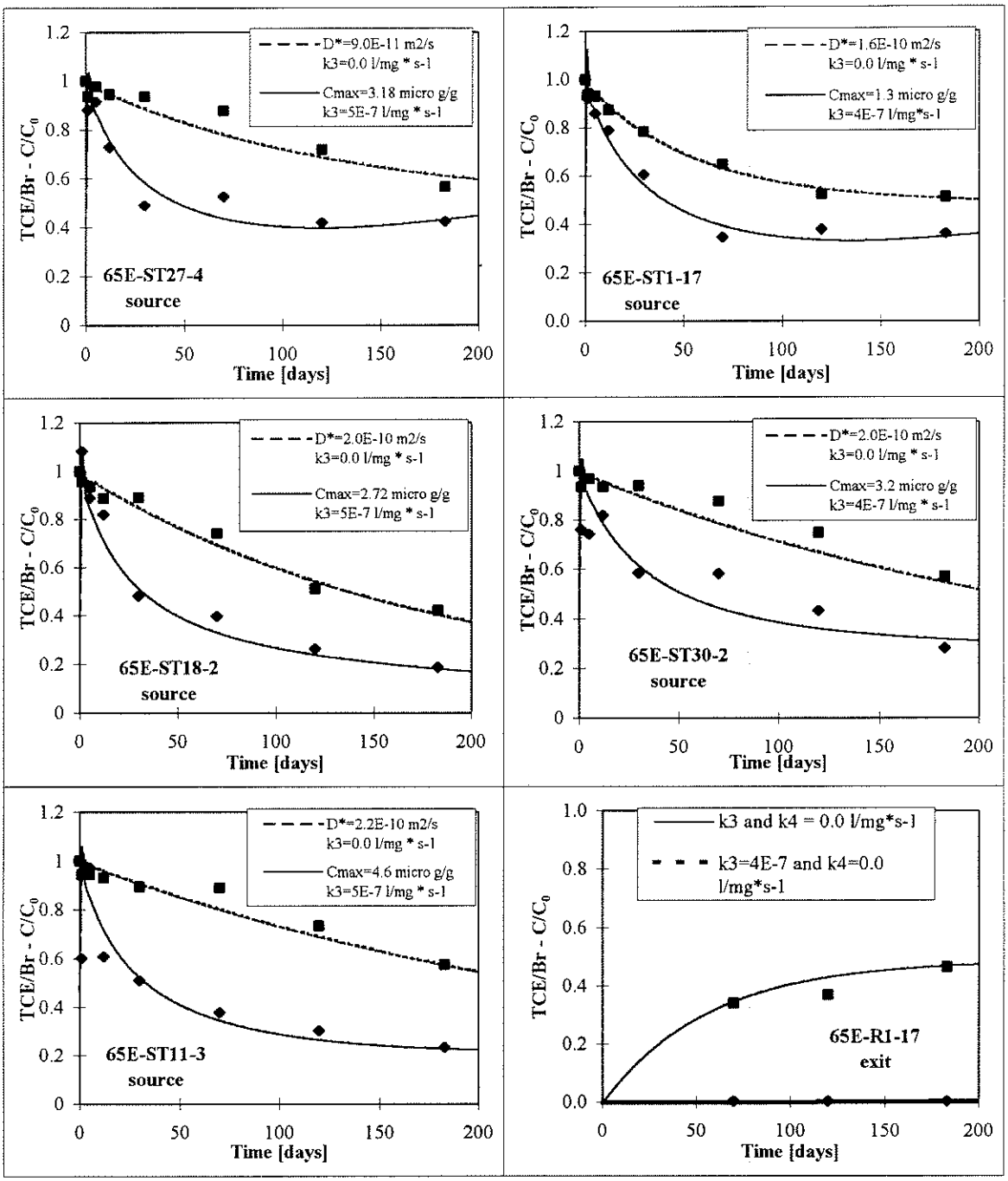

Figure 4.9: Experimental diffusion data and computed time - concentration profiles using the non-linear, kinetic Langmuir sorption model (IV).

Table 4.1
Organic Carbon Data from Stylolites and Argillaceous Bands

Unit	Leco CR12[3] Carbon Analyzer NWRI[2]	Leco RC412[3] Carbon Analyzer Leco Ltd.	Batch Tests[1] (TCE) NWRI
Eramosa			3.4 - 45.5% (11)
Vinemount Unit 2	4.00% (1)		
Vinemount Unit 1	0.00-3.62% (3)		
Goat Island	3.89 - 5.26% (4)	2.66 - 2.68% (1)	15.0% (1)
Gasport	0.01-0.05% (2)		0.01% (1)

Notes

Numbers in parentheses indicate the number of samples.

[1] Compilation of work by *Hilverda* (1997) and *Langer* (1997).
Carbon content determined from K_d assuming K_{oc}=120.226 cm^3/g.

[2] National Water Research Institute

[3] Compilation of work by *Hilverda* (1997) and *Langer* (1997).

Table 4.2
Organic Carbon Data from Dolostone Rock Matrix Samples

Unit	Leco CR12[3] Carbon Analyzer NWRI[2]	Leco RC412[3] Carbon Analyzer Leco Ltd.	Batch Tests[1] (TCE) NWRI
Eramosa	0.00 - 0.20% (7)	0.11% (1)	0.32 - 1.67% (11)
Vinemount Unit 2	0.00 - 0.12% (11)		
Vinemount Unit 1	0.02 - 0.10% (6)	0.27 - 0.29% (1)	
Goat Island	0.00 - 0.13% (6)	0.27 - 0.29% (1)	0.00% (1)
Gasport	0.00 - 0.04% (3)	0.15 - 0.16% (1)	0.00% (1)
Decew	0.00 - 0.04% (3)		
Rochester	0.00 - 0.07% (6)	0.24% (1)	

Notes

Numbers in parentheses indicate the number of samples.
[1] Compilation of work by *Hilverda* (1997) and *Langer* (1997).
Carbon content determined from K_d assuming K_{oc}=120.226 cm^3/g.
[2] National Water Research Institute
[3] Work by *Hilverda* (1997)

Table 4.3
Transport Equations for Conservative and Reactive Tracers

Model	Tracer	Transport Equation	Sorption Isotherm	Parameters Evaluated
conservative (model I)	Bromide	$\frac{\partial C}{\partial t} = D\frac{\partial^2 C}{\partial x^2}$ with $D = D_0\gamma$		D: effective diffusion coefficient γ: geometry factor
linear, reversible equilibrium Freundlich sorption (model II)	TCE	$\frac{\partial C}{\partial t} = D\frac{\partial^2 C}{\partial x^2} - \frac{\rho_b}{\theta}\frac{\partial (K_d C)}{\partial t}$ (3) or $\frac{\partial C}{\partial t} = \frac{D}{R}\frac{\partial^2 C}{\partial x^2}$ (4) with $R = 1 + \frac{\rho_b}{\theta}K_d$ and $D_A = \frac{D}{R}$	$C^* = CK_d$	D_A: apparent diffusion coefficient R: retardation coefficient K_d: distribution coefficient
irreversible and reversible, first-order kinetic sorption (model III)	TCE	$\frac{\partial C}{\partial t} = D\frac{\partial^2 C}{\partial x^2} - \frac{\rho_b}{\theta}\left(k_2 C - k_3 C^*\right)$ (6)	$\frac{\partial C^*}{\partial t} = k_2 C - k_3 C^*$ $k_3 \rightarrow 0$ irreversible	k_2, k_3: kinetic rate constants
non-linear, irreversible, kinetic Langmuir sorption (model IV)	TCE	$\frac{\partial C}{\partial t} = D\frac{\partial^2 C}{\partial x^2} - \frac{\rho_b}{\theta}k_4 C\left(C_{max} - C^*\right)$ (8)	$\frac{\partial C^*}{\partial t} = k_4 C\left(C_{max} - C^*\right)$	k_4: kinetic rate constant C_{max}: maximum sorption capacity

Table 4.4
TCE Distribution Coefficients for Pure Stylolite, Stylolitic Dolostone, and Dolostone Rock Samples

Type	Sample Mass [g]	TCE Distribution Coefficient K_d [cm^3/g]	Organic Carbon [%]
stylolite pure	11	17.61	15 (1)[1]
stylolitic dolostone	10.55-37.41	0.63-7.83	0.61-6.51 (11)
stylolite layer*	1.7-5.2	4.09-54.70	3.4-45.5 (11)
dolostone matrix	14.64-34.14	0.38-2.01	0.32-1.67 (11)

* K_d and f_{oc} are calculated, estimating the stylolite mass in each sample and assuming an organic carbon background value equal to the dolostine matrix value.

[1] Number in parentheses indicate the number of samples.

Table 4.5
Results from Diffusion Experiments using Model I and II

model I+II: source reservoirs

Sample	Tracer	Porosity [%]	Effective Diffusion Coefficient $D^*=D_0\,\gamma$ [m^2/s]	γ [ ]	Apparent Diffusion Coefficient $D_A=D^*/R$ [m^2/s]	Retardation Factor $R=D_0\,\gamma/D_A$
65E-ST27-4	**Br^-**	**5.1**	**$0.9x10^{-10}$**	**0.045**		
	TCE	**5.1**		**0.045**	**$5.4x10^{-10}$**	**0.17**
65E-ST18-2	**Br^-**	**3.9**	**$2.0x10^{-10}$**	**0.1**		
	TCE	**3.9**		**0.1**	**$5.6x10^{-10}$**	**0.36**
65E-ST30-2	**Br^-**	**2.0**	**$2.0x10^{-10}$**	**0.1**		
	TCE	**2.0**		**0.1**	**$5.0x10^{-10}$**	**0.4**
65E-ST11-3	**Br^-**	**2.0**	**$2.2x10^{-10}$**	**0.11**		
	TCE	**2.0**		**0.11**	**$12.1x10^{-10}$**	**0.18**
65E-ST1-17	**Br^-**	**7.0**	**$1.6x10^{-10}$**	**0.08**		
	TCE	**7.0**		**0.08**	**$5.0x10^{-10}$**	**0.32**
65E-ST18-1	**Br^-**	**8.0**	**$2.6x10^{-10}$**	**0.13**		
(control)	**TCE**	**8.0**		**0.13**	**$2.6x10^{-10}$**	**1**

model I+II: exit reservoirs

Sample	Tracer	Porosity [%]	Effective Diffusion Coefficient D*=D0 γ [m2/s]	γ [ ]	Apparent Diffusion Coefficient DA=D*/R [m2/s]	Retardation Factor R=D0 γ/DA
65E-R1-17	**Br^-**	**7.0**	**$1.6x10^{-10}$**	**0.08**		
	TCE	**7.0**		**0.08**	**$1.0x10^{-12}$**	**160**
65E-R11-3	**Br^-**	**2.0**	**$2.2x10^{-10}$**	**0.11**		
	TCE	**2.0**		**0.11**	**$2.0x10^{-12}$**	**110**
65E-R18-1	**Br^-**	**8.0**	**$2.6x10^{-10}$**	**0.13**		
(control)	**TCE**	**8.0**		**0.13**	**$2.6x10^{-10}$**	**1**

Table 4.6
Percent Error between Computed and Experimental Data

Tracer	Model	% Error
Br^-	model I	1.98 - 7.12
TCE	model III	16.14 - 26.37
TCE	model IV	6.00 - 14.99

Table 4.7
Results from Diffusion Experiments using Model IV

model IV: source reservoirs

Sample	Tracer	Porosity [%]	Effective Diffusion Coefficient[1] $D^*=D_0 \gamma$ [m^2/s]	γ [ ]	Maximum Adsorption Capacity C_{max} [µg/g]	Kinetic Rate Constant k_3 [$l/mg * s^{-1}$]
65E-ST27-4	**TCE**	**5.1**	**$0.9x10^{-10}$**	**0.045**	**3.18**	**$5x10^{-7}$**
65E-ST18-2	**TCE**	**3.9**	**$2.0x10^{-10}$**	**0.1**	**2.72**	**$5x10^{-7}$**
65E-ST30-2	**TCE**	**2.0**	**$2.0x10^{-10}$**	**0.1**	**3.2**	**$4x10^{-7}$**
65E-ST11-3	**TCE**	**2.0**	**$2.2x10^{-10}$**	**0.11**	**4.6**	**$5x10^{-7}$**
65E-ST1-17	**TCE**	**7.0**	**$1.6x10^{-10}$**	**0.08**	**1.3**	**$4x10^{-7}$**
65E-ST18-1 (control)	**TCE**	**8.0**	**$2.6x10^{-10}$**	**0.13**	**0**	**0**

[1] $D_{0\,TCE}=20.1*10^{-10}$ [m^2/s]

Chapter 5

Analytical and Numerical Simulations of Reactive Contaminant Transport in Fractured Porous Media

5.1 Introduction

Different conceptual models are used to simulate fluid flow and contaminant transport in the rock matrix and fracture network. In discrete fracture models each fracture might have individual parameters (e.g. fracture aperture and fracture wall retardation factor), whereas in dual porosity models fractures have the same average parameters and are distributed evenly throughout the domain. Both conceptual models have in common that fluid flow and contaminant transport dominates in the fractures. However, contaminant transport due to matrix diffusion from the fractures into the rock matrix has been recognized to be an important mechanism and causes significant contaminant retardation [Freeze and Cherry, 1979; McKay et al., 1993; Maloszewski and Zuber, 1993; Novakowski and Lapcevic, 1994]. When modeling reactive contaminant transport, the dissolved contaminant might interact with solids in the rock matrix by sorption and become retarded with respect to advective flow.

A basic understanding of contaminant migration processes occurring in a single fracture environment is required before attempting to simulate transport in larger, multiple fractured, two- or three-dimensional geological domains. Experimental investigations on contaminant transport through fractured porous media (single fracture environment) have been conducted in the laboratory [Grisak et al., 1980; Moreno et al., 1985; Schrauf and

Evans, 1986; Haldeman et al., 1991; Glass and Nicholl, 1995; Rasmussen, 1995; Tidwell et al., 1995; Vandergraaf, 1995] and field scale [Novakowski et al., 1985; Abelin, 1986; Raven et al., 1988; Rudolph et al., 1991; Novakowski et al., 1995]. These tests were primarily conducted to evaluate conservative and reactive tracer behavior, and confirmed that matrix diffusion and sorption are the dominant processes affecting solute migration.

A number of analytical solutions have been developed that idealize fluid flow and solute transport through fractures and porous matrix, by reducing the transport equation from a two-dimensional domain to two, coupled one-dimensional problems. In these models advection is assumed to be much more rapid in the fracture than it is within the matrix (where it can be neglected), and diffusion within the rock matrix occurs only perpendicular to the fracture flow. For a uniform flow field, Neretnieks [1980], Grisak and Pickens [1981], Tang et al. [1981], Rasmuson and Neretnieks [1981], Sudicky and Frind [1982], Maloszewski and Zuber [1984a,b], Rasmuson [1984], Neretnieks and Rasmuson [1984], Moreno and Rasmuson [1986], Rasmuson and Neretnieks [1986], Rowe and Brooker [1990], and Maleszewski and Zuber [1993] developed various analytical and semi-analytical solutions for different conditions. Baker [1982], Feenstra et al. [1984], and Chen [1985,1986] derived analytical solutions for radial flow. Moench [1989, 1995] extended this basic approach for a dual porosity aquifer.

For more complex geological domains with numerous fractures and a heterogeneous rock matrix, numerical modeling techniques have been employed. For examples, those of Grisak and Pickens [1980], Huyakorn et al. [1983], Baca et al. [1984], Smith and Schwartz [1984], Berkowitz et al. [1988], Germain and Frind [1989], Sudicky

and McLaren [1992], Gerke and van Genuchten [1993], Zimmerman et al. [1993], Ibaraki and Sudicky [1995], Tseng et al. [1995], and Hamm and Biaux [1996]. The two-dimensional groundwater flow and transport code, FRACTRAN, from Sudicky and McLaren [1992] uses the time-continuous Laplace transform Galerkin method [Sudicky, 1989], and accounts for saturated flow and transport, as well as for decay and linear sorption of reactive compounds in fractures and the matrix.

Unfortunately, none of the above codes accounts for non-linear sorption behavior. No doubt, this is due to the difficulty of keeping track of the sorption history at each location and updating it with time. Non-linear sorption of hydrophobic compounds can occur during migration through geological formations containing significant amounts of organic material. The impact on matrix penetration depths, and adsorption/desorption rates will depend on the amount of organic carbon present, its maximum sorption capacity for the chemical compound in question, and the chemical environment (i.e. pH, E_H, T, presence of multi-compounds). Non-linear sorption might cause significant changes in the actual contaminant transport velocity with time, and therefore influence the shape and downstream extension of a contaminant plume.

The main objective of the analytical and numerical research presented in this chapter is to evaluate the impact of stylolite layers on hydrophobic contaminant migration in a fractured, saturated aquifer. Stylolites are frequently found in calcareous rock formations and are thin, serrate, dark layers containing various amounts of organic material (see Chapter 1 and Chapter 4). Trichloroethene (TCE) is used as the representative hydrophobic contaminant in the analytical and numerical simulations

presented herein. Experimental matrix diffusion studies with TCE show that adsorption onto stylolitic dolostone samples can be best described with a Langmuir sorption isotherm, whereas the low observed desorption rates suggest either linear or non-linear behavior [Langer et al., 1998]. As a first approximation, contaminant transport and non-linear sorption in a single fracture environment is derived by incorporating Langmuir sorption processes within the rock matrix into the analytical solution of Tang et al. [1981]. The computer code CRAFLUSH [Sudicky, 1988] solves Tang's transport equations in Laplace space and yields solute concentrations after a numerical inversion. This code is modified to account for non-linear sorption within the rock matrix, and a comparison is made between the Freundlich and the Langmuir sorption models. In the analytical Langmuir sorption model stylolites are not modeled as discrete individual layers, but as part of a homogeneous matrix. This approach does not represent the physical reality accurately, but nevertheless gives valuable information on the significance of sorption onto organic matter in the rock matrix of carbonate aquifers. In a second approach the above mentioned numerical code FRACTRAN is employed to evaluate the significance of individual stylolite layers. The program allows the simulation of discrete stylolite layers and interaction between solute and stylolites through linear-Freundlich sorption. A sensitivity analyses with respect to stylolite thickness, closeness to fracture, length, and linear-Freundlich retardation factors is performed in a two-dimensional domain. From batch experiments and TCE desorption behavior in matrix diffusion experiments (Chapter 4) linear retardation factors are estimated. Although, as mentioned before, the TCE adsorption process onto stylolites is a kinetic non-linear process [Langer et al., 1998],

valuable information on the significance of individual stylolites and mass storage within the matrix can be retrieved from such simulations. As long as the pre-calculated maximum sorption capacity in the modeled domain is not reached, mass storage calculations for the rock matrix and mass adsorption calculations onto stylolites present a lower estimate. This means that a predicted contaminant plume would extend further than it actually would with kinetic sorption. For a special case study at Smithville (Ontario), the influence of numerous stylolites in a randomly fractured porous dolostone formation on TCE transport is investigated.

5.2 Semi-Analytical Solution For Single Fracture Model

5.2.1 Conceptual Model

The physical model consists of an infinite long, discrete fracture surrounded by a homogeneous, porous rock matrix. Advection and dispersion dominate fluid flow and contaminant transport in the fracture, whereas molecular diffusion perpendicular to the fracture is the only transport mechanism considered in the rock matrix (Fig. 5.1). A continuous source of constant concentration is specified at the fracture entrance. The two one-dimensional contaminant transport equations are coupled by the diffusive flux crossing the fracture-matrix interface. Retardation due to adsorption onto the fracture wall and decay are neglected, so that only the affects of matrix diffusion and sorption within the matrix can be studied. Langmuir sorption in the matrix accounts for the only contaminant/rock interaction. Contaminant migration within the matrix depends largely on

the rock matrix porosity and tortuosity, as well as on the kinetic rate of adsorption, the maximum sorption capacity and the molecular diffusion coefficient of the compound. Stylolites are not modeled as individual thin layers in this semi-analytical approach, but instead modeled as an integrated part of the rock matrix. The matrix is given non-linear, homogeneous sorption parameters. This conceptual model assumes that the organic material is evenly distributed within the matrix and not concentrated in individual stylolite layers. Note that this model does not represent the physical reality accurately, but can be used to evaluate the significance of sorption onto organic matter within the matrix.

5.2.2 Mass Transport Equations

The one-dimensional differential equation describing reactive contaminant transport in the rock matrix is (Tang et al., 1981):

$$-D\frac{\partial^2 c}{\partial x^2}+\frac{\partial c}{\partial t}+\frac{\rho_b}{\theta}\frac{\partial s}{\partial t}=0 \qquad b \le x \ge \infty \qquad (5.1)$$

with an effective diffusion coefficient $D=\tau D_0$, where x: coordinate into matrix, c: solute concentration in matrix, t: time, θ: porosity, ρ_b: bulk density, τ: tortuosity factor, D_0: molecular or free-water diffusion coefficient, and s: mass of solute adsorbed per unit mass of solid in the matrix. D_0 is assumed to be constant and not a function of temperature and concentration. The latter is only true for dilute solutions. Implementing the non-linear Langmuir sorption isotherm

$$\frac{\partial s}{\partial t} = kc\left(c_{\max} - s\right) \qquad \text{[Fetter, 1993]} \qquad (5.1a)$$

where c_{max}: maximum sorption capacity and k: kinetic rate constant, into equation (5.1) yields the final governing contaminant transport equation for the matrix

$$\frac{\partial c}{\partial t} - D\frac{\partial^2 c}{\partial x^2} + \frac{\rho_b}{\theta} kc\left(c_{\max} - s\right) = 0 \qquad (5.2)$$

The one-dimensional differential equation describing contaminant transport in a single fracture dominated by advection and dispersion without sorption or decay is

$$v_f \frac{\partial c'}{\partial z} - D^* \frac{\partial^2 c'}{\partial z^2} + \frac{q_n}{b} = 0 \qquad 0 \le z \ge \infty \qquad (5.3)$$

with $$D^* = \alpha_L v_f + D_0 \qquad \text{[Bear, 1972]}$$

where v_f: ground water velocity, c': solute concentration in fracture, q_n: diffusive flux, z: coordinate along the fracture axis, α_L: longitudinal dispersivity, D^*: dispersion, and b: half fracture width. Note that the two one-dimensional transport equations (5.2) and (5.3) are coupled by the diffusive mass flux of solute crossing the fracture-matrix interface, q_n. According to Flick's first law, the mass flux into the matrix along the interface (x=b) is defined by

$$q_n = -\theta D \left.\frac{\partial c}{\partial x}\right|_{x=b}$$

Substituting this diffusive flux term into equation (5.3) derives the final transport equation for the fracture

$$\frac{\partial c'}{\partial t} + v_f \frac{\partial c'}{\partial z} - D^* \frac{\partial^2 c'}{\partial z^2} - \frac{\theta D}{b} \frac{\partial c}{\partial x}\bigg|_{x=b} = 0 \qquad (5.4)$$

Using the Laplace transform method (Tang et al., 1981) and the following boundary and initial conditions solutions to equation (5.2) and (5.4) are found:

for (4):	$c'(0,t) = c_0$	for (2)	$c(b,z,t) = c'(z,t)$
	$c'(\infty,t) = 0$		$c(\infty,z,t) = 0$
	$c'(z,0) = 0$		$c(x,z,0) = 0$

A simplified mathematical approach is used to solve the mass transport problem, where the nonlinear Langmuir sorption term is treated as a linear expression. The sorbed-phase concentration (s) is assumed to be time-invariant during small time intervals. Solute concentrations are obtained by numerical inversion of the Laplace transformed solutions. A discrete time stepping approach is used to evaluate the solute concentration with time, where the amount sorbed (s) is calculated after each time step for each individual location, and summed up to calculate the sorption term for the next time step at that specific location.

$$\Delta s = \Delta t \, k \, c\left(c_{\max} - s\right)$$

$$s = \Delta s_{t1} + \Delta s_{t2} + \Delta s_{t3} \ldots..$$

A new sorption term for each location is obtained according to $\frac{\partial s}{\partial t} = kc\left(c_{\max} - s\right)$. During each time step (s) is independent of the aqueous tracer concentration.

5.2.3 Model Verification

Four different ways were used to verify contaminant concentrations obtained by the outlined semi-analytical model. First, the mathematical solutions are checked to verify that the defined boundary conditions are satisfied. All simulations, which are described later in the text (Fig. 5.5 to 5.9), confirm this by showing a concentration of C_0 at the fracture entrance at all times, a zero concentration at x or z equal infinity, and equal concentrations in the fracture and matrix at the interface. Secondly, the computed concentrations with a zero sorption rate constant were compared to published results by Tang et al. [1981] with a retardation factor of one. Results from contaminant transport simulations with no sorption are identical in both approaches. If the non-linear sorption parameters are set to zero, the transport model collapses into a simplified Tang solution. Thirdly, the one-dimensional, reactive diffusive mass transport in the porous media has been verified in paragraph 4.4.1 using a finite difference model derived by Fabritz [1995]. Performing sensitivity analyses with respect to the new input parameters such as the time

interval (Δt), kinetic constant (k), and maximum sorption capacity (C_{max}) provide further valuable insight into whether the model performs as expected. At steady state the maximum sorption capacity of C_{max} should be reached.

5.2.4 Sensitivity Analyses and Model Performance

A set of base-case input parameters was chosen to represent a fractured stylolitic dolostone environment, where the maximum sorption capacity of the rock matrix is one hundredth of pure stylolite material (see Table 5.1). This value is estimated to represent the sorption capacity of stylolitic dolostone when the organic carbon content of all individual stylolites in the Lockport Formation is evenly distributed throughout the matrix. The other input parameters are chosen for easy comparison with published results from Tang et al. (1981).

As the outer plume boundary and "penetration distance" downstream in the fracture and within the matrix, a concentration of 1 % C_0 is chosen. The penetration distance in the fracture for the base case is 8.55 m and without sorption increases to 13.86 m. Sensitivity analyses with respect to the kinetic constant (k) and maximum sorption capacity (C_{max}) show that the penetration distance ($d_{0.01}$) approaches 13.86 m when k and C_{max} decreases to zero (Fig. 5.2). When the matrix porosity approaches zero matrix diffusion becomes negligible, and $d_{0.01}$ after 100 days reaches 86.4 m. This is expected at zero longitudinal dispersion and an advective fracture flow velocity of 0.864 m/d (Fig.

5.2). The influence of the time step (Δt) on $d_{0.01}$ was less than 2% (<2 cm) for the base case and decreased with increasing total time. The negligible effect of various time increments (0.01 to 40 days) can be best seen by the almost identical total amounts sorbed at the interface (x=b) after 10, 100 and 1000 days (Fig. 5.3). The sorption behavior at the fracture wall after 20 day time increments is shown in Figure 5.4. The largest amount is sorbed during the first interval with decreasing amounts during each successive interval, while the maximum sorption capacity is reached. This kinetic sorption behavior is expected when modeling non-linear, irreversible Langmuir sorption. After 100 days, the maximum sorption capacity at x=b has been achieved at locations as far as about 2 m into the fracture. A decreasing maximum sorption capacity from $2.0x10^{-7}$ mg/mg to $8.0x10^{-9}$ mg/mg causes an increase in the outer plume extension in the fracture from 4.25 m to 12.55 m, whereas the penetration distance ($d_{0.01}$) into the matrix increases only from 4 cm to 13.5 cm (Fig. 5.5). The two-dimensional plots (Fig. 5.5, 5.6, 5.9 and 5.10) are graphed from solute concentrations calculated at about 500 locations. While studying the contaminant migration with time (Fig. 5.6), the most unexpected observation is that $d_{0.01}$ increases only very slightly from 8.5 cm to 10.0 cm when increasing the time period from 100 to 1000 days. As expected, lowering the maximum sorption capacity increases the observed differences in penetration distance for fracture and matrix. Note, the unnatural, stepwise contaminant concentrations outlining the plume in the matrix are due to the assumption that matrix diffusion takes place only in one dimension perpendicular to the fracture. The mathematical model does not allow for horizontal concentration gradients in the matrix to be equilibrated by two-dimensional molecular diffusion. The maximum

sorption capacity causes a vertical pulse-like migration of the contaminant front in the rock matrix.

5.2.5 Comparison between the Freundlich and Langmuir Sorption Model

The plume extensions in the fracture and the rock matrix are simulated after 10, 100 and 1000 days using a non-linear, Langmuir sorption isotherm (model L). They are compared to simulations using a linear Freundlich sorption isotherm with retardation factor 100 (model F100), and to a no sorption case with retardation factor 1 (model F1). After 10 days travel time, contaminant concentrations in the fracture from model L are close to the non-sorption model F1, and penetration distances of 3.54 m and 3.64 m, respectively, are almost identical (Table 5.2 and Fig. 5.7). With increasing time, the Langmuir model develops a sharper front compared to the Freundlich models F1 and F100. The penetration distance ($d_{0.01}$) increases to 9.83 m for model L, to 46.5 m for model F1, and to 4.75 m for model F100 after 1000 days. Travel velocities for the plume front were calculated using 10 day intervals. In the first interval (0 to 10 days), the plume front migrates through the fracture with a velocity of 3.54 m/d for model L, 3.64 m/d for model F1, and 0.47 m/d for model F100. Due to the kinetic sorption behavior in model L, the plume decelerates more rapidly compared to model F1 and F100. After 90 days the transport velocity of the plume front for model L decreases to 0.005 m/d, and drops below the transport velocity simulated for model F100.

In this section, transport models L and F, which have the same fracture penetration distance ($d_{0.01}$), are compared. This scenario is of interest when an outer plume boundary with 1 % of the source concentration say, reaches an observation well and no detailed information about the solute/rock matrix sorption behavior is available. A matrix retardation factor of 2.8 (model F2.8) is required to calibrate the same penetration distance as model L after 100 days, and a factor of 23.4 (model F23.4) after 1000 days (Fig. 5.8). At T=100 days, both models (L and F2.8) have similar contaminant distributions in fracture and rock matrix (Fig. 5.8). Note, that no distinction between the two models and their sorption behavior can be made from their observed solute distribution. At long travel times a sharp contaminant front develops in model L simulations. Therefore, it was expected that rock matrix concentrations and plume extension into the matrix would be quite different for model L and model F simulations. However, after 1000 days, computed concentrations for model L produce only a slightly larger plume extension into the matrix compared to a retardation factor of 23.4 (model F23.4), even though the observed matrix concentrations are quite different (Fig. 5.9). Note that solute concentrations within the rock matrix are significantly higher for model L and a sharp concentration gradient at the plume edge developed not only in the fracture but also within the matrix. In conclusion, the observed plume boundaries in fracture and matrix can be calibrated easily with either a Langmuir or Freundlich sorption isotherm. A distinction between the two models can be made when knowing exact solute distributions

and concentration gradients at the plume boundary, or when observing solute concentrations over longer periods of time.

5.3 Numerical Simulations

In order to investigate the impact of discrete stylolite layers on reactive contaminant transport in a larger two-dimensional fractured domain, numerical simulations are performed. The objectives of this numerical study are (i) to perform stylolite sensitivity analyses in a single fracture environment, and (ii) to make a lower estimate of the amount of mass stored in the rock matrix and the amount of mass adsorbed onto stylolites in a geological setting similar to Smithville. The computer program FRACTRAN (Sudicky and McLaren, 1992) is utilized to simulate discrete fractures and individual stylolite layers. For validation and accuracy of the computer code the reader is referred to Sudicky (1989), and to Sudicky and McLaren (1992). Program parameters are chosen after following the suggestions by Sudicky and McLaren (1992). These yield solute concentrations that are accurate to four significant figures. A linear-Freundlich sorption isotherm is employed to account for solute/rock interaction in the matrix. Therefore, it can be assumed that mass calculations represent a lower estimate as long as the potential sorption capacity of stylolites, embraced by the contaminant plume, is not reached.

5.3.1 Conceptual Model

A physical domain similar to the upper Lockport Formation in Southern Ontario is simulated. The conceptual model (Fig. 5.10) incorporates the following assumptions:

i) Fluid flow and transport in the fracture is one-dimensional and controlled by advection, dispersion and retardation.

ii) Fluid flow in the fracture ranges between $10x10^{-2}$ to $10x10^{-8}$ m/d.

iii) Fluid flow in the matrix is assumed to be negligible (K_y=$10x10^{-12}$ to $10x10^{-14}$ m/s; K_x=$10x10^{-10}$ to $10x10^{-12}$ m/s). Diffusion and sorption therefore dominate mass transport in the rock matrix.

iv) Stylolites are represented by thin (0.5 cm), horizontal layers.

v) Hydrophobic sorption is modeled, where the contaminant sorbs solely onto organic matter in stylolites.

vi) Stylolite layers in the rock matrix are acting as contaminant sinks and sorption is described with a linear-Freundlich sorption isotherm. Instantaneous equilibrium is assumed.

vii) At the matrix/fracture interface, instantaneous contaminant equilibrium is reached by diffusion.

5.3.2 Stylolite Sensitivity Analyses in Single Fracture

5.3.2.1 Boundary Conditions and Domain Discretization

The impact of a stylolite layer on reactive solute transport is first studied in a single fracture environment. A model is set up with the following boundary and initial conditions (Fig. 5.11). At all times a constant hydraulic gradient is applied to the porous matrix and the fracture. The top and bottom of the domain are no flow boundaries, and the fracture aperture yields the fluid flux in the fracture. On the upstream boundary, Dirichlet conditions were imposed with $c_0 = 1$ at $z = 1.0$ m and $c = 0$ along the boundary sections $1 < z \leq 2$ m and $0 \geq z < 1$ m. On all other boundaries zero flux conditions are imposed. The initial condition utilized is $c(x, z, t = 0) = 0$.

The problem domain is rectangular with length, $L_x = 8$ m and width, $L_z = 2$ m. The single fracture is located at $z = 1$m from $x = 0$ to 8 m. Most parts of the domain are discretized by a finite element grid with $\Delta x = 0.1$ m and $\Delta z = 0.02$ m, with refinements near stylolite layers and the outer plume boundary according to each simulation. In this way penetration distances were determined within an accuracy of 0.01 m. A very fine vertical discetization was required in order to implement stylolites at specific locations. Near stylolite layers the grid was refined in the vertical direction with $\Delta z = 0.005$ m. The described discretization produced a total of 8,000 to 10,000 rectangular elements. Note that a further horizontal refinement at the stylolite interface resulted in no significant

changes of solute concentrations. This is due to negligible advective flow in the matrix and slow diffusive mass transport.

5.3.2.2 Fracture and Rock Matrix Input Parameters

Typical base case input parameters (Table 5.3) for a fractured stylolitic dolostone domain are estimated from field and laboratory experiments conducted for the Lockport Formation at Smithville (Ontario). A representative fracture aperture (2b) of 200 μm is taken from pump test and tracer experiment data, which are published by Novakowski et al. [1995], Lapcevic et al. [1995], and Radcliffe [1995]. Values for a velocity (v_f) of 0.1 m/d and longitudinal dispersivity (α_L) 0.1 m are assumed. Using Karickhoff's linear sorption theory for chlorinated hydrocarbons, and organic carbon estimates from batch experiments for stylolite layers (Chapter 4), linear-Freundlich retardation factors ranging between 100 to 1000 are estimated. For the upper Lockport Formation (Eramosa Member) the rock matrix effective diffusion coefficient (D_{TCE}), hydraulic conductivity (K_x, K_z), tortuosity factor (τ), and porosity (θ) are determined in laboratory sorption, diffusion and permeability experiments. These are $17.37x10^{-5}$ m^2/d, $8.64x10^{-6}$ m/d, 0.1, and 5.68 % respectively (Chapter 4). Dispersion in the matrix is assumed to be dominated by diffusion with the longitudinal and transverse dispersivities equal to zero. Stratigraphic observations of the Lockport Formation from an open pit mine near Smithville and drill cores confirm that stylolites run mostly parallel to the horizontal bedding plane orientation,

extend laterally for several meters, and range in thickness from about 0.1 to 0.5 mm. A stylolite thickness of 5 mm and an infinite stylolite extension are taken as base case input parameters. In the following paragraph results of the performed simulations are discussed.

5.3.2.3 Results from Stylolite Sensitivity Simulations

In all stylolite sensitivity simulations solute concentrations are generated for time t_1 = 1000 days. The penetration distance ($d_{0.01}$) in the fracture for base case input parameters with a stylolite layer positioned 5 cm away from the fracture and a retardation factor of 100 is 4.3 m (Fig. 5.12 and Table 5.4). The plume extension is strongly affected by the distance between the stylolite layer and fracture. Increasing the distance to 20 cm result in a 23 % increase in fracture penetration length (Fig. 5.12). Closing the gap between the stylolite and the fracture to 1 cm causes a higher retardation of the contaminant plume migration with a decrease in fracture penetration distance to 2.50 m. Increasing the retardation factor to 1000, causes the fracture penetration distance ($d_{0.10}$) for the base case to decrease only from 4.30 m to 3.92 m , a decrease of 8 % (Table 5.5). Further sensitivity analyses were performed with respect to stylolite extension. Stylolite extension has a great impact on contaminant penetration into the matrix (Fig. 5.13), which is approximately 45 cm near the contaminant source without the stylolite and below 20 cm with a stylolite layer in the adjacent rock matrix. The mass stored within the matrix after 1000 days increased marginally (0.63 %) due to linear Freundlich sorption onto stylolites. Varying the stylolite thickness (Table 5.6) from 1 to 5 mm has negligible effect on plume extension

in fracture and matrix. This was found in simulations with retardation factors 100 and 1000.

In summary, stylolite length and its distance from fractures are the parameters having the largest impact on mass transport and plume extension.

5.3.3 Simulation of TCE Transport in the Upper Lockport Formation

5.3.3.1 Physical Model and Domain Discretization

The Upper Lockport Formation (Eramosa Member) is composed of fractured, stylolitic dolostone. Bedding planes and stylolite layers are simulated to be horizontal. The heterogeneous matrix is divided into segments of contaminant sorbing stylolites and non-sorbing dolostone. Stylolite layers of 0.005 m thickness with a frequency of one stylolite per meter are implemented into the dolostone matrix. Matrix properties are the same as described in the above single fracture model (paragraph 5.3.2.2), causing contaminant transport in the matrix to be dominated by diffusion and sorption. The model domain is rectangular with length, L_x = 100 m and width, L_z = 13 m. A random, discrete fracture network, with a minimum horizontal fracture spacing of 2 m and a minimum vertical fracture spacing of 5 m, is generated. The total number of fractures is determined by the size of the domain and a fracture density factor (De). De_{horiz} and De_{vert} are arbitrary set to be 0.01. In addition, an individual vertical fracture located at x = 20 m and $5 \leq z \geq 13$ m is implemented in the domain. It is assumed here that chlorinated hydrocarbons migrated as dense non-aqueous phase liquid (DNAPL), driven by gravity, vertically down into the

discrete fracture at x = 20 m. The fracture then serves as continuous source segment from which a dissolved chlorinated hydrocarbon plume is generated. A source concentration of 1 kg/m^3 is assumed, which is just slightly below the maximum TCE solubility. All fractures have the same aperture (2b) and longitudinal dispersivity (α_L) of $2.0x10^{-4}$ m and 0.1 m, respectively. A constant hydraulic gradient of 0.00035 is applied to the domain resulting in steady state fluid flow and a fracture flow velocity (v_f) of 1 m/d, where

$$v_f = \frac{\rho g(2b)^2}{12\mu}\frac{\partial h}{\partial l}$$

The problem domain was first discretized by a finite element grid with $\Delta x = 1$ m and $\Delta z = 0.5$ m. Subsequently the grid was refined near stylolite layers and adjacent to fractures yielding a total of 17000 to 50000 rectangular elements. Program and computer capacity limitations required the number of grid elements to be kept reasonably low.

5.3.3.2 Results from TCE Transport Simulations

The top and bottom of the domain are set to no-flow boundaries. For mass transport, on the upstream boundary Dirichlet conditions were imposed with $c = 0$ for $0 \leq z \geq 13$ m. On the top boundary between $0 \leq x > 20$ m and $20 < x \geq 100$ m, and on the entire bottom and downstream boundaries zero flux conditions are imposed. The initial condition utilized is $c(x, z, t=0) = 0$. For $t > 0$, a constant source concentration with $c = c_0 = 1$ at $x = 0$ and $0 \leq z \geq 13$ m is implemented. Solute concentrations in the domain are calculated after $t_1 = 1000$ days and $t_2 = 10{,}000$ days for the sorption models with stylolite

retardation factors 100 (model 2) and 1000 (model 3). The resulting plumes from model 2 and model 3 after t_1 are graphed in Figure 5.14 and Figure 5.15, respectively. The outer plume boundary represents a solute concentration of 1 % of the source concentration. Note that the lateral plume extension will depend on the fracture network. Due to the chosen fracture network realization, contaminant transport downstream starts at 6 m depth from the surface (Fig. 5.14 to 5.19). After t_1 the plume extends about 6 m downstream in model 3 and 19 m in model 2. A solute concentration of 50 ppb, the maximum acceptable drinking water concentration for TCE [Guidelines for Canadian Drinking Water Quality, 1993], can be found 46 m downstream from the source fracture in model 2. Mass transport into the matrix results in a maximum plume width of about 1 m near the source fracture. A higher stylolite retardation factor results in an increase of total mass stored in the system from 0.53 kg TCE to 0.81 kg TCE, and an increase in the percentage of mass sorbed to stylolites from 54.2 % to 81.2 % (Table 5.7). The total mass stored in the matrix is larger than 98 %; this is also found in the non-sorbing simulations with a homogeneous rock matrix (model 1).

After t_2, the contaminant plume in model 2 extends vertically and horizontally over several fractures that are connected with each other (Fig 5.16). The outer plume boundary reaches 73 m downstream from the source. In model 3, mass transport is still limited to one horizontal fracture with a lateral plume extension of 22 m (Fig. 5.17). The total mass stored in the domain after t_2 increased to 3.9 kg TCE for model 2, and to 4.3 kg TCE for model 3. Of the 98 % total mass stored in the matrix, 40.7 % and 85.0 % are sorbed onto stylolites in model 2 and model 3, respectively.

Without TCE sorption in the matrix, mass transport extends significantly in the downstream direction. After t_1, the plume also spreads over several meters vertically due to the two-dimensional fracture network (Fig. 5.18). The fracture penetration distance for the outer plume boundary is 59 m from the source, compared to 6 m and 19 m with model 2 and 3. In the non-sorbing model the total mass stored in the matrix drops to 0.48 kg TCE. After 3000 days, the plume extends beyond the domain boundary on the downstream side to about 110 m, and reaches the surface at x = 71 m (Fig. 5.19).

5.4 Discussion and Conclusions

Stylolites are found to have a significant impact on mass transport in a fractured porous media like the Upper Lockport Formation. Stylolites enhance the amount of mass stored in the matrix and cause significant retardation of the reactive contaminant plume. This conclusion is true when modeling stylolites as part of a homogeneous sorbing matrix, as well as when modeled as discrete, horizontal layers. In the former case, solute concentrations and plume migration were examined using semi-analytical mass transport models with both the linear sorption isotherm derived by Tang et al. [1981] and a modified Langmuir sorption model. Solute concentrations calculated with the non-linear, Langmuir model depended largely on the kinetic constant (k) and the maximum sorption capacity (C_{max}). The most significant observation was that simulated contaminant plumes develop a sharp concentration gradient along the outer edge in the fracture, as well as within the matrix. This is in contrast to solute simulations using the linear sorption model. Comparing

two contaminant plumes with the same fracture penetration distance ($d_{0.01}$), one generated with a Freundlich sorption model the other with a Langmuir sorption model, it is import to notice the large differences in matrix solute concentrations, whereas the matrix penetration distance is almost identical. Due to the non-linear sorption behavior contaminant transport velocities in the fracture decrease rapidly compared to the velocities simulated with a Freundlich sorption model. This is independent of the retardation factor.

The semi-analytical solutions in a single fracture environment are useful tools to study parameter sensitivity, and to produce first approximations on plume penetration distances in fracture and within rock matrix. The newly derived semi-analytical solution might be useful to validate future numerical codes, which are able to simulate non-linear Langmuir sorption.

Sensitivity analyses in a single fracture environment demonstrate clearly that lateral extension and closeness to the fracture are the most important stylolite factors in a discrete model. Note that a single stylolite layer caused a considerable amount of retardation and increased the amount of mass stored within the matrix. After 1000 days, the fracture penetration distance ($d_{0.01}$) decreased from 5.3 m (no stylolite present) to 4.3 m (single stylolite present) for the base case parameters with a fracture flow velocity of 0.1 m/d.

Simulations of the Upper Lockport Formation with a random fracture network and a stylolite frequency of one stylolite per meter revealed that 41 to 54 % of the solute mass are sorbed onto stylolites with a Freundlich retardation factor of 100, and 82 to 85 % when modeling stylolites with a retardation factor of 1000. This means that after 1000 days of continuous dissolution of TCE from the source fracture, a total mass of 0.53 to

0.81 kg TCE (values are for R = 100 and R = 1000, respectively) leached into the domain and 0.29 to 0.66 kg TCE are adsorbed by stylolites. The maximum sorption capacity of the stylolitic dolostone matrix covered by the plume is estimated to range between 1.7 and 6.1 kg. Therefore, the presented mass calculations from numerical simulations represent a lower estimate of TCE sorbed onto stylolites. Results from mass calculations after 10,000 days can be found in Table 5.7. TCE release from organic material in stylolites is extremely slow, and this makes stylolites act as long term contaminant sources once the original source has been depleted. Those who try to remove or neutralize pollutants in the subsurface, have to acknowledge that over 98 % of the solute mass in fractured porous media may be stored in the matrix. Cleaning up the fracture network with a pump and treat method generally leaves large amounts of solute and adsorbed contaminant mass within the matrix. It can be speculated that, when dealing with organic pollutants in dual porosity aquifers that in situ remediation methods might be more applicable and less expensive than pump and treat methods. However, this evaluation is beyond the scope of this research.

References

Abelin, H., Migration in a single fracture: An in situ experiment in a natural fracture, Ph.D. thesis, Dep. of Chem. Eng., R. Inst. of Technol., Stockholm, 1986.

Baca, R. G., R. C. Arnett, and D.W. Langford, Modelling fluid flow in fractured-porous rock masses by finite-element techniques, Int. J. for Num. Methods in Fluids, 4, 337-348, 1984.

Baker, J. A., Laplace transform solutions for solute transport in fissured aquifers, Adv. Water Resour., 5, 98-104, 1982.

Bear, J., Dynamics of Fluids in Porous Media, American Elsevier Environmental Series, 1972.

Berkowitz, B., J. Bear, and C. Braester, Continuum models for contaminant transport in fractured porous formations, Water Resour. Res., 24(8), 1225-1236, 1988.

Chen, C.-S. Analytical and approximate solutions to radial dispersion from an injection well into a hydrogeologic unit with simultaneous diffusion into adjacent strata, Water Resour. Res., 21(8), 1069-1076, 1985.

Chen, C.-S., Solutions for radionuclide transport from an injection well into a single fracture in a porous formation, Water Resour. Res., 22(4), 508-518, 1986.

Feenstra, S., J. A. Cherry, E. A. Sudicky, and Z. Haq, Matrix diffusion effects on contaminant migration from an injection well in fractured sandstone, Groundwater, 22(3), 307-316, 1984.

Fetter, C. W., Contaminant Hydrogeology, Macmillan Publishing Company, New York, 1993.

Freeze, R. A., and J. A. Cherry, Groundwater, Prentice-Hall, Englewood Cliffs, New Jersey, 1979.

Gerke, H.H., and M. T. van Genuchten, A dual-porosity model for simulating the preferential movement of water and solutes in structured porous media, Water Resour. Res., 29 (2), 309-319, 1993.

Germain, D., and E. O. Frind, Modelling contaminant migration in fracture networks: Effects of matrix diffusion, in Contaminant Transport in Groundwater, edited by H. E. Kobus and W. Kinzelbach, pp. 267-274, A. A. Balkema, Rotterdam, Netherlands, 1989.

Glass, R. J., and M. J. Nicholl, Quantitative visualization of entrapped phase dissolution within a horizontal flowing fracture, Geophys. Res. Letters, 22(11), 1413-1416, 1995.

Grisak, G. E., and J. F. Pickens, Solute transport through fractured media, 1. The effect of matrix diffusion, Water Resour. Res., 16 (4), 719-730, 1980a.

Grisak, G. E., J. F. Pickens, and J. A. Cherry, Solute transport through fractured media, 2, Column study of fractured till, Water Resour. Res., 16(4), 731-739, 1980b.

Grisak, G. E., and J. F. Pickens, An analytical solution for solute transport through fractured media with matrix diffusion, J. of Hydrology, 52, 47-57, 1981.

Haldeman, W. R., Y. Chuang, T. C. Rasmussen, and D. D. Evans, Laboratory analysis of fluid flow and solute transport through a fracture embedded in porous tuff, Water Resour. Res., 27(1), 53-65, 1991.

Hamm, S.-Y., and P. Bidaux, Dual-porosity fractal models for transient flow analysis in fissured rocks, Water Resour. Res., 32 (9), 2733-2745, 1996.

Huyakorn, P. S., B. H. Lester, and J. M. Mercer, An efficient finite element technique for modeling transport in fractured porous media, 2, Nuclide decay chain transport, Water Resour. Res., 19 (5), 1286-1296, 1983.

Ibaraki, M., and E. A. Sudicky, Colloid-facilitated contaminant transport in discretely fractured porous media, 1. Numerical formulation and sensitivity analysis, Water Resour. Res., 31(12), 2945-2960, 1995.

Langer, V. W., K. Novakowski, and A. Woodbury, Sorption of trichloroethene onto stylolites, in submission to J. Contam. Hydrol., February, 1999.

Lapcevic, P., K. Novakowski, G. Bickerton, and J. Voralek, Preliminary results of the fall 1995 drilling and hydraulic testing program at the Smithville phase IV bedrock remediation site, NWRI Contribution, 96-50, 1996.

McKay, L. D., R. W. Gillham, and J. A. Cherry, Field experiments in fractured clay till, 2, Solute and colloid transport, Water Resour. Res., 29(12), 3879-3890, 1993b.

Maloszewski, P., and A. Zuber, Interpretation of artificial and environmental tracer in fissured rocks with porous matrix, in Isotope Hydrology 1983, Proceedings of an International Symposium on Isotope Hydrology in Water Resources Development, International Atomic Energy Agency, Vienna, 1984a.

Maloszewski, P., and A. Zuber, On the theory of tracer experiments in fissured rocks with a porous matrix, Rep. 1244 AP, Inst. of Nucl. Phy., Cracow, Poland, 1984b.

Maloszewski, P., and A. Zuber, Tracer experiments in fractured rocks: Matrix diffusion and the validity of models, Water Resour. Res., 29(8), 2723-2735, 1993.

Moench, A. F., Convergent radial dispersion: A Laplace transform solution for aquifer tracer testing, Water Resour. Res., 25(3), 439-447, 1989.

Moench, A. F., Convergent radial dispersion in a double-porosity aquifer with fracture skin: Analytical solution and application to a field experiment in fractured chalk, Water Resour. Res., 31(8), 1823-1835, 1995.

Moreno, L., I. Nerentnieks, and T. Eriksen, Analysis of some laboratory tracer runs in natural fissures, Water Resour. Res., 21(7), 951-958, 1985.

Neretnieks, I., Diffusion in the rock matrix: An important factor in radionuclide retardation?, J. Geophys. Res., 85(B8), 4379-4397, 1980.

Neretnieks, I., and A. Rasmuson, An approach to modeling radionuclide migration in a medium with strongly varying velocity and block sizes along the flow path, Water Resour. Res., 20(12), 1823-1836, 1984.

Novakowski, K. S., G. V. Evans, D. A. Lever, and K. Raven, A field example of measuring hydrodynamic dispersion in a single fracture, Water Resour. Res., 21(8), 1165-1174, 1985.

Novakowski, K. S., and P. A. Lapcevic, Field measurement of radial solute transport in fractured rock, Water Resour. Res., 30(1), 37-44, 1994.

Novakowski, K. S., P. A. Lapcevic, J. Voralek, and G. Bickerton, Preliminary interpretation of tracer experiments conducted in a discrete rock fracture under conditions of natural flow, Geophys. Res. Letters, 22(11), 1417-1420, 1995.

Radcliffee, A. J., Analysis of stylolitization and fracturing in the rock core from the Smithville phase IV site, unpublished thesis, University of Waterloo, 1995.

Rasmuson, A., Migration of radionuclides in fissured rock: Analytical solutions for the case of constant source strength, Water Resour. Res., 20(10), 1435-1442, 1984.

Rasmuson, A., and I. Neretnieks, Radionuclide transport in fast channels in crystalline rock, Water Resour. Res., 22(8), 1247-1256, 1986.

Rasmuson, A., and I. Neretnieks, Migration of radionuclides in fissured rock: The influence of micropore diffusion and longitudinal dispersion, J. Geophys. Res., 86(B5), 3749-3758, 1981.

Rasmussen, T. C., Laboratory characterization of fluid flow parameters in porous rock containing a discrete fracture, Geophys. Res. Letters, 22(11), 1401-1404, 1995.

Raven, K. G., K. S. Novakowski, and P. A. Lapcevic, Interpretation of field tracer tests of a single fracture using a transient solute storage model, Water Resour. Res., 24(12), 2019-2032, 1988.

Rowe, R. K., and J. R. Booker, Contaminant migration through fractured till into an underlying aquifer, Can. Geotech. J., 27(4), 484-495, 1990.

Rudolph, D. L., J. A. Cherry, and R. N. Farvolden, Groundwater flow and solute transport in fractured lacustrine clay near Mexico City, Water Resour. Res., 27(9), 2187-2201, 1991.

Schauf, T. W., and D. D. Evans, Laboratory studies of gas flow through a single natural fracture, Water Resour. Res., 22(7), 1038-1050, 1986.

Smith, L., and F. W. Schwartz, An analysis of the influence of fracture geometry on mass transport in fractured porous media, Water Resour. Res., 20(9), 1241-1252, 1984.

Sudicky, E. A., CRAFLUSH, unpublished Fortran computer code, 1988.

Sudicky, E. A., The Laplace transform Galerkin technique: A time continuous finite element theory and application to mass transport in groundwater, Water Resour. Res., 25(8), 1833-1846, 1989.

Sudicky, E. A., and E. O. Frind, Contaminant transport in fractured porous media: Analytical solutions for a system of parallel fractures, Water Resour. Res., 18(6), 16-34-1642, 1982.

Sudicky, E. A., and R. G. McLaren, The Laplace transform Galerkin technique for large scale simulation of mass transport in discretely fractured porous formations, Water Resour. Res., 28 (2), 499-514, 1992.

Tang, D H., E. O. Frind, and E. A. Sudicky, Contaminant transport in fractured porous media: Analytical solution for a single fracture, Water Resour. Res., 17(3), 555-564, 1981.

Tidwell, V. C., R. J. Glass, and W. Peplinski, Laboratory investigation of matrix imbibition from a flowing fracture, Geophys. Res. Letters, 22(11), 1405-14-8, 1995.

Tseng, P.-H., A. Sciortino, and T. Th. van Genuchten, A partitioned solution procedure for simulating water flow in a variably saturated dual-porosity medium, Adv. in Water Res., 18 (6), 335-343, 1995.

Vandergraaf, T. T., Radionuclide migration experiments under laboratory conditions, Geophys. Res. Letters, 22(11), 1409-1412, 1995.

Zimmerman, R. W., G. Chen, T. Hadgu, and G. S. Bodvarsson, A numerical dual-porosity model with semianalytical treatment of fracture/matrix flow, Water Resour. Res., 29 (7), 2127-2137, 1993.

Guidelines for Canadian Drinking Water Quality, 1993.

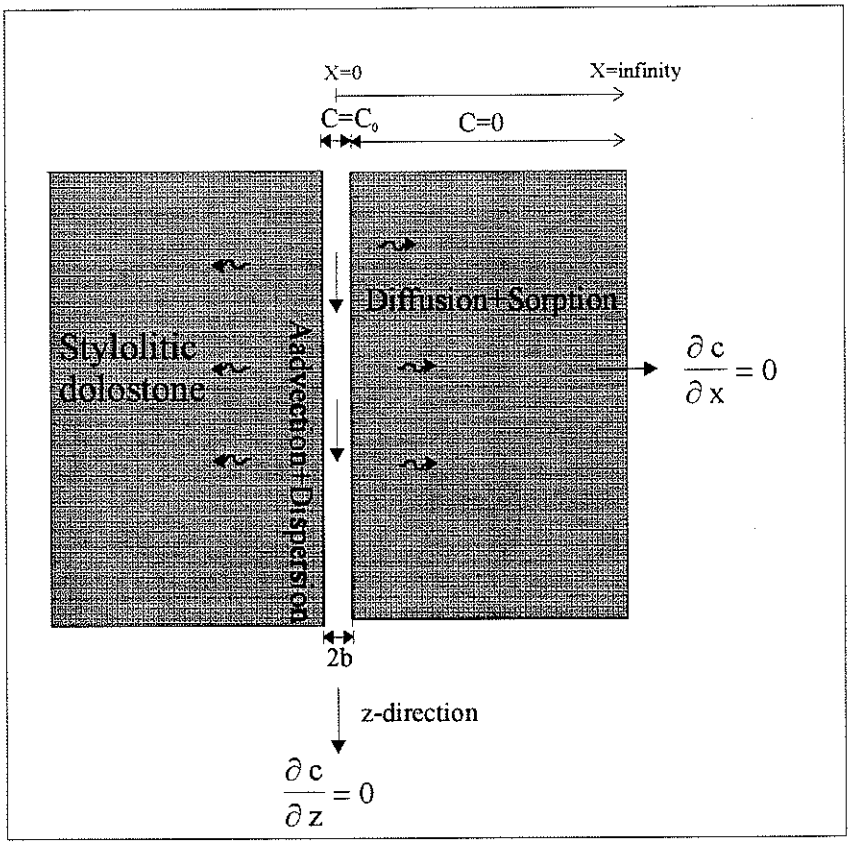

Figure 5.1: Conceptual model for solute transport simulations in a single fracture environment.

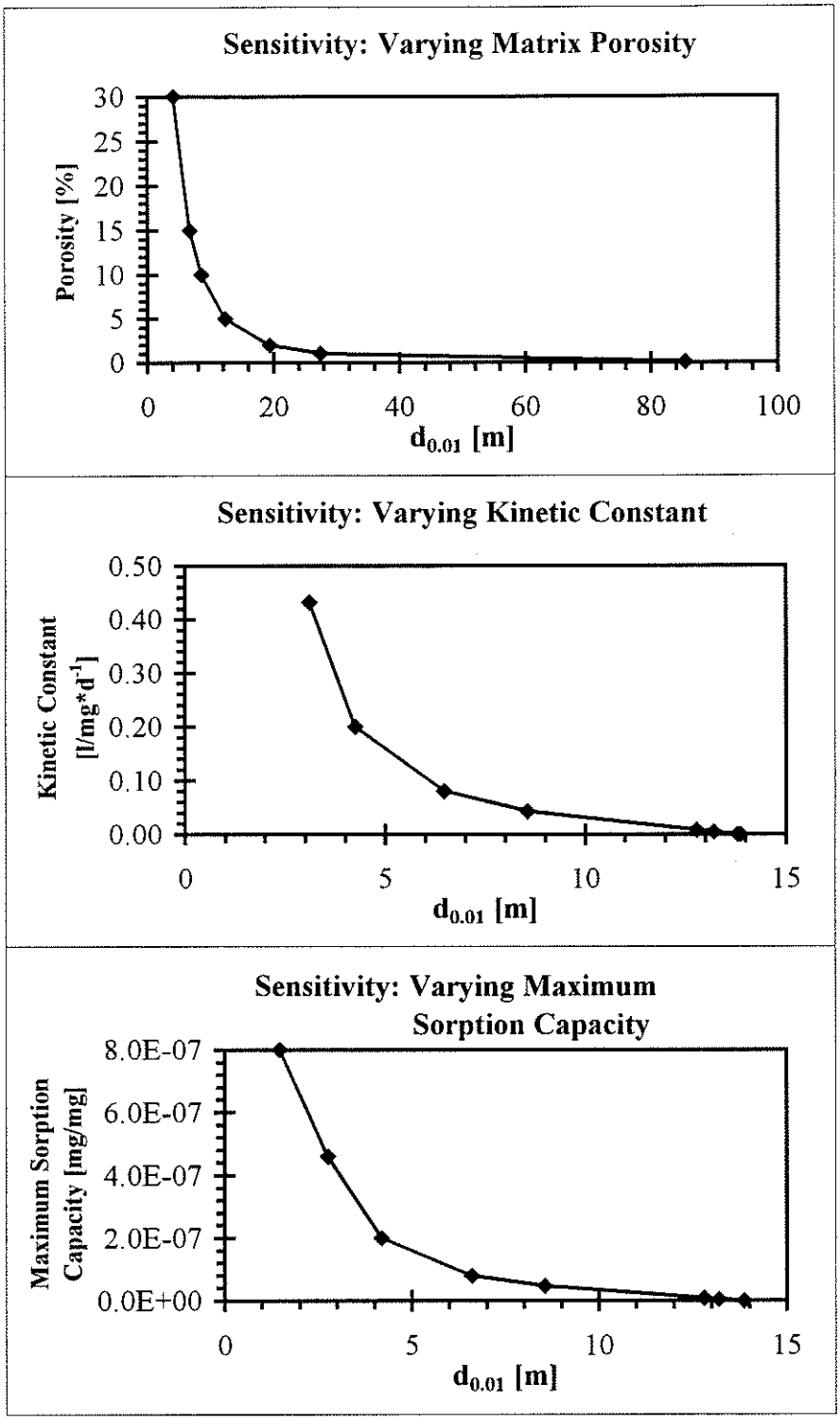

Figure 5.2 Mass transport sensitivity analyses for single fracture model. The penetration distance ($d_{0.01}$) along the fracture is defined as 1% of the source concentration C_0.

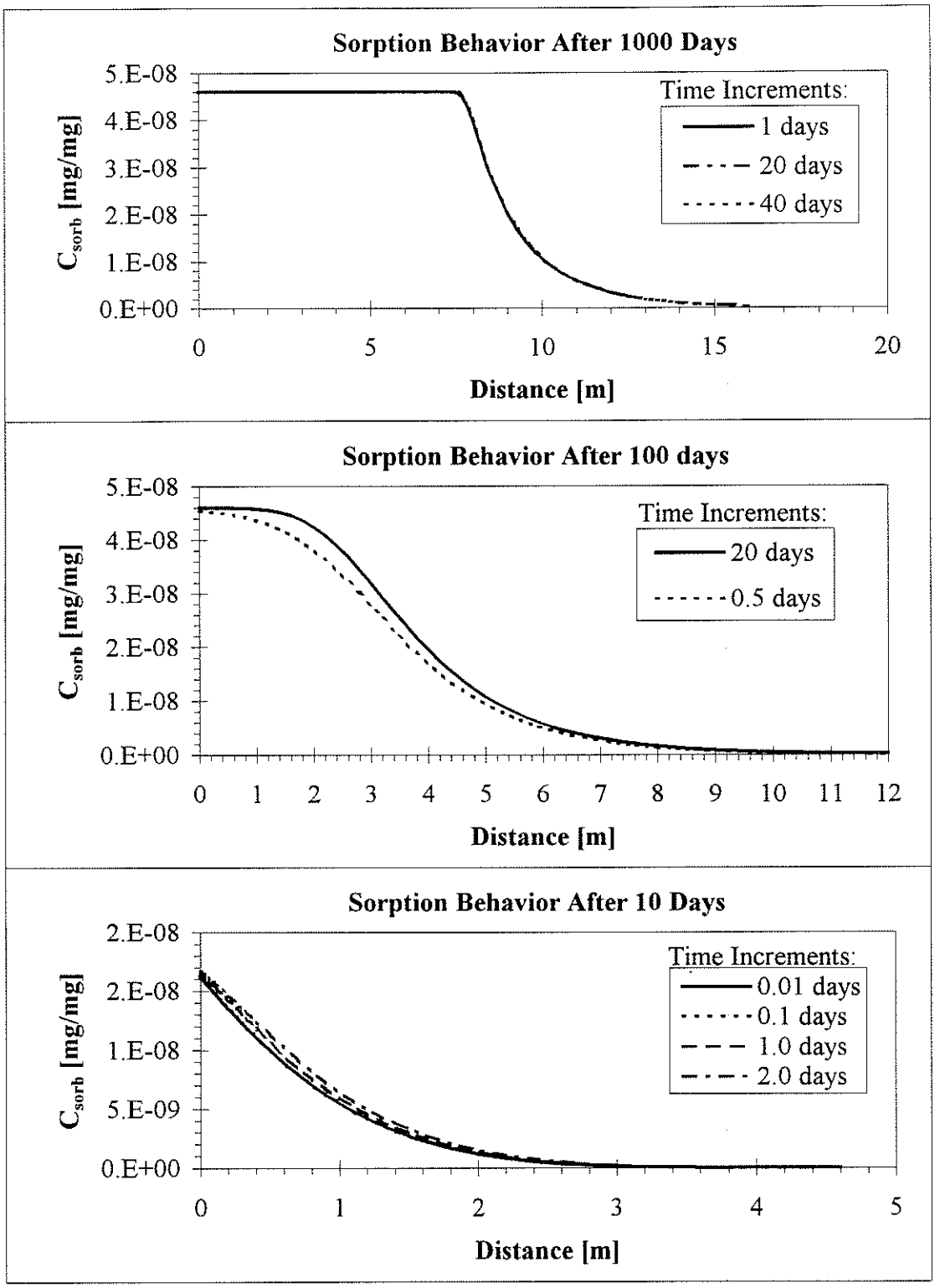

Figure 5.3: Sorption behavior at the fracture/rock matrix interface after different time periods using different time increments.

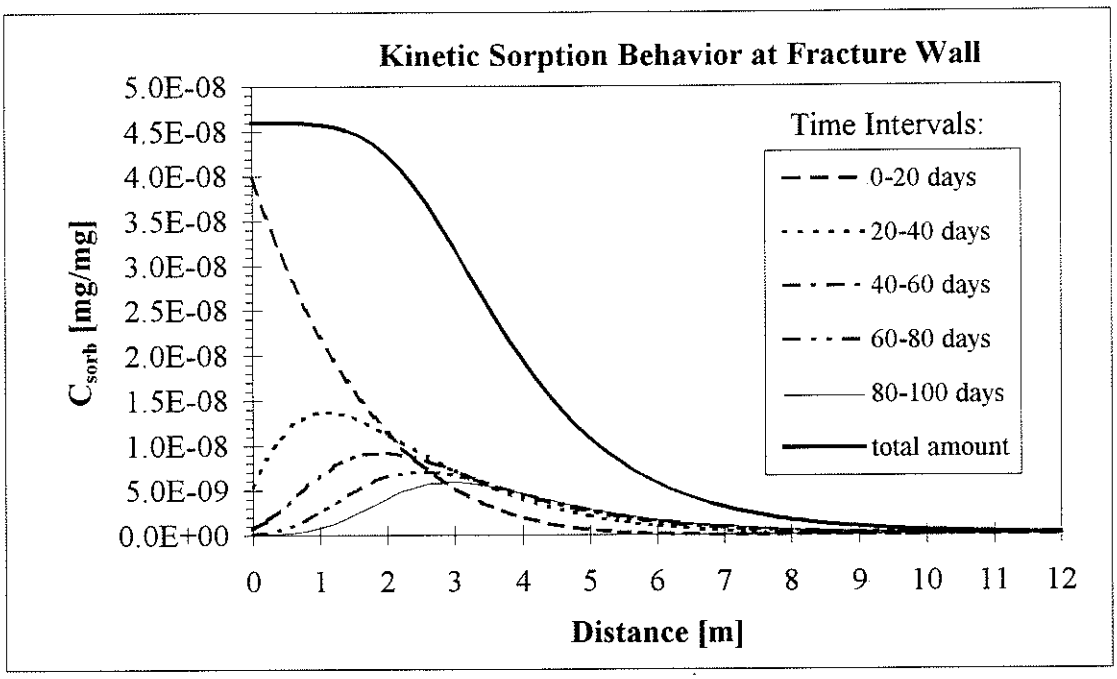

Figure 5.4: Sorption behavior at the fracture/rock matrix interface during different time intervals.

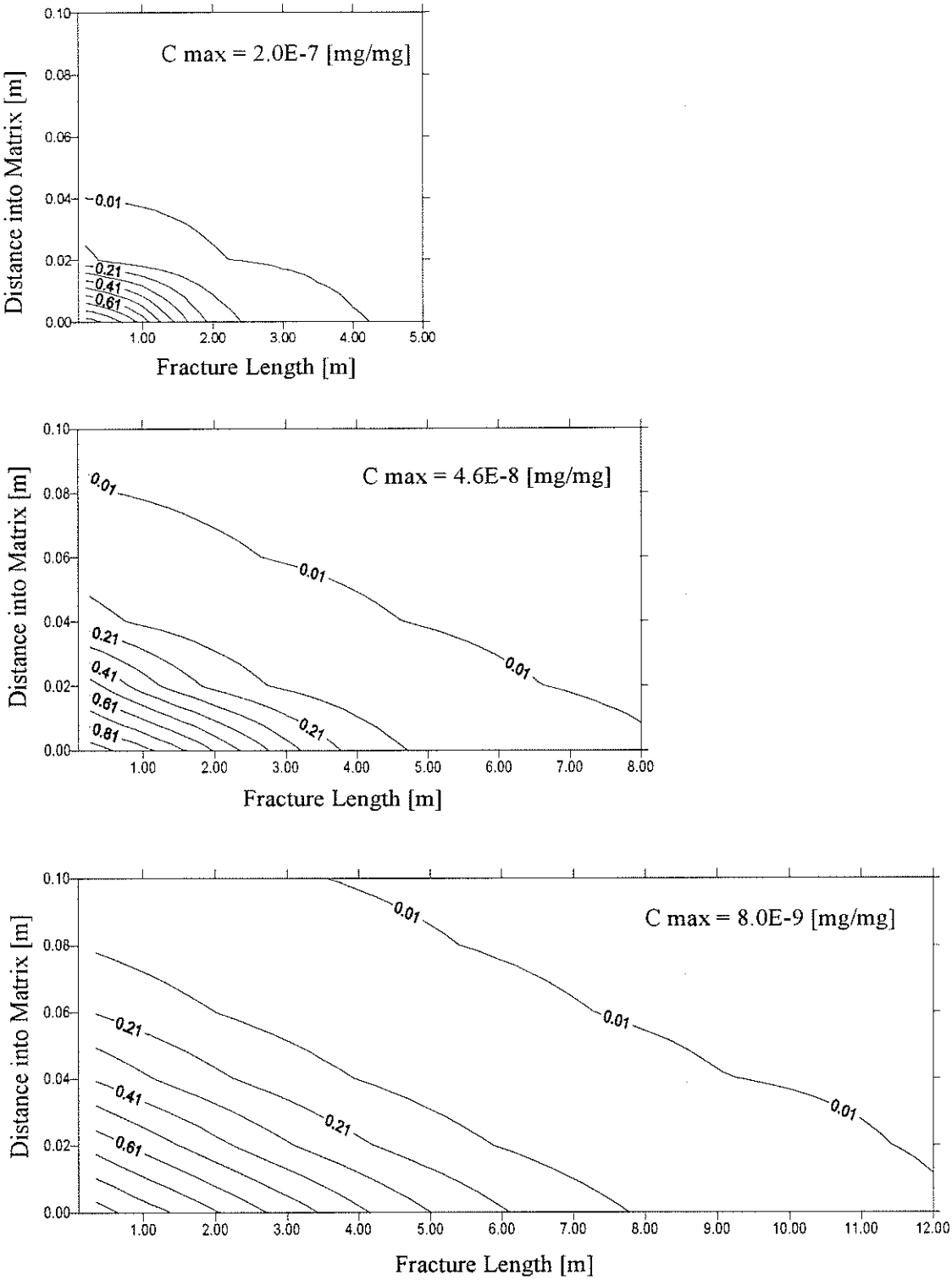

Figure 5.5: Solute concentrations are modeled using Langmuir sorption isotherms with different maximum sorption capacity. All concentrations are calculated after 100 days.

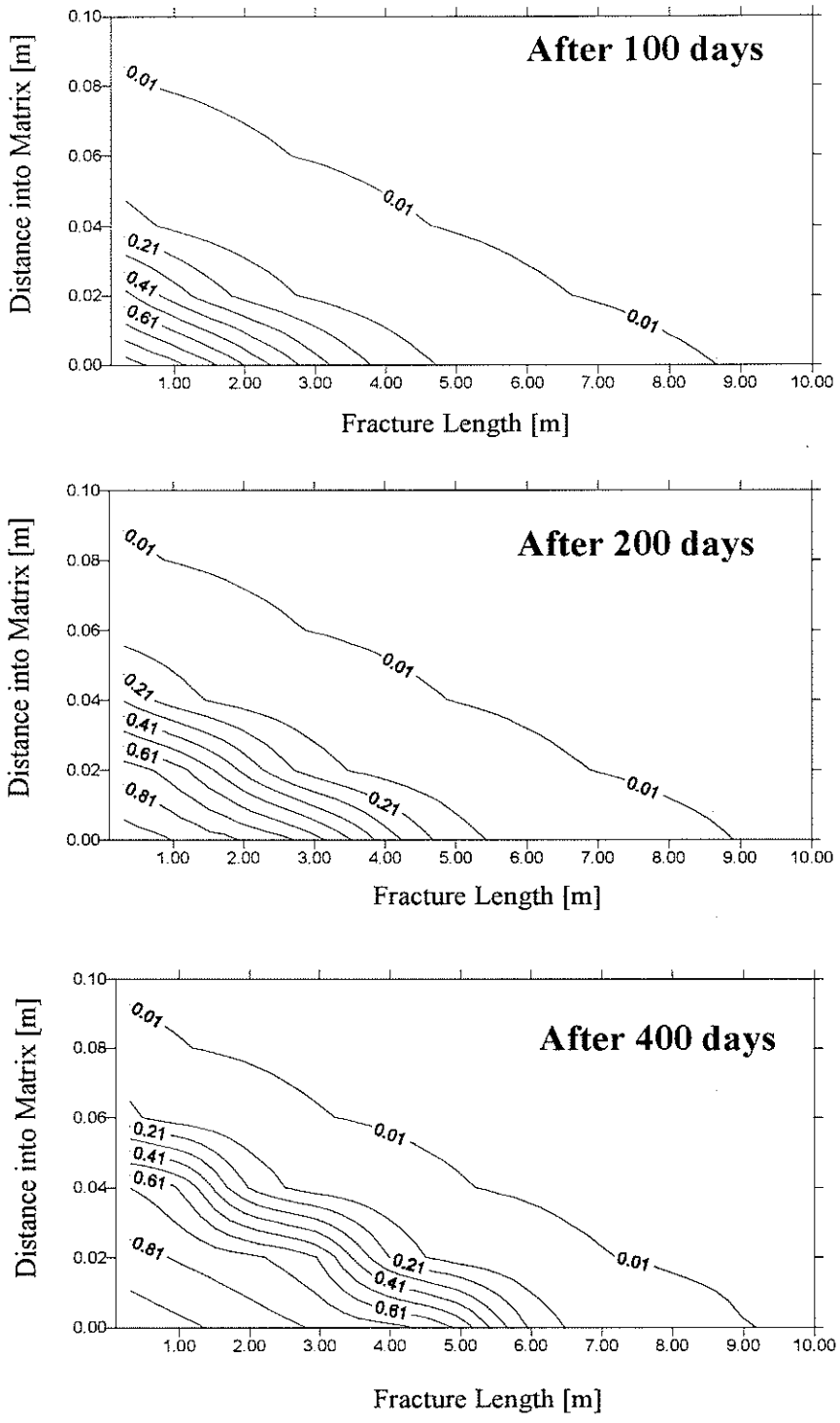

Figure 5.6: Solute concentrations are modeled using a Langmuir sorption isotherm, and are shown after different time intervals (after 100, 200, 400, 600, 800 and 1000 days). Figure 5.6 continues on the next page.

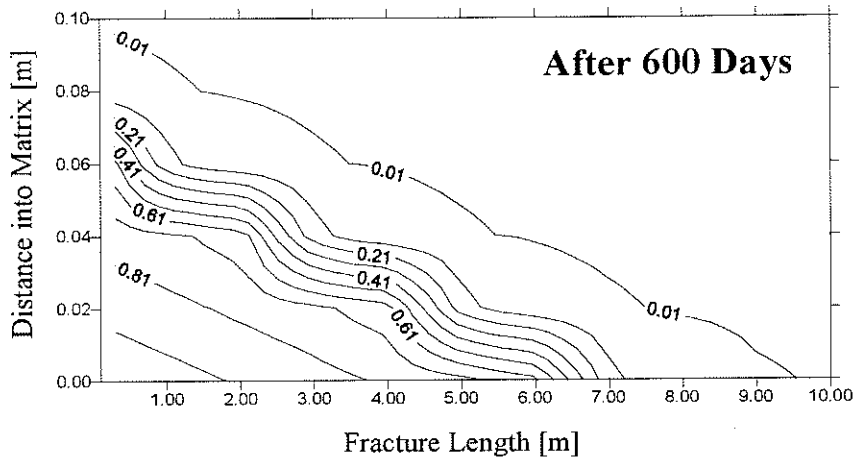

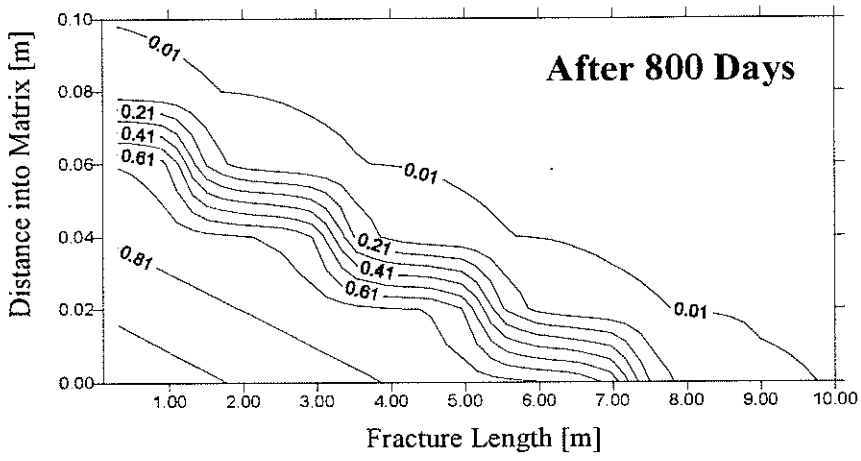

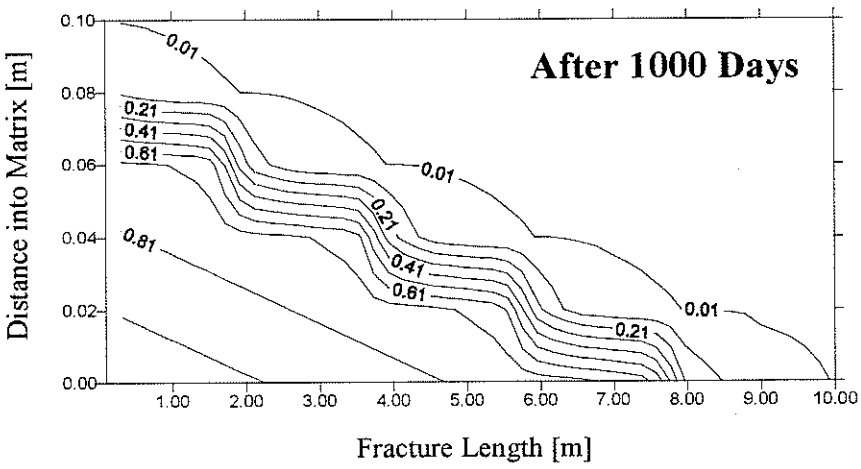

Figure 5.6, continued

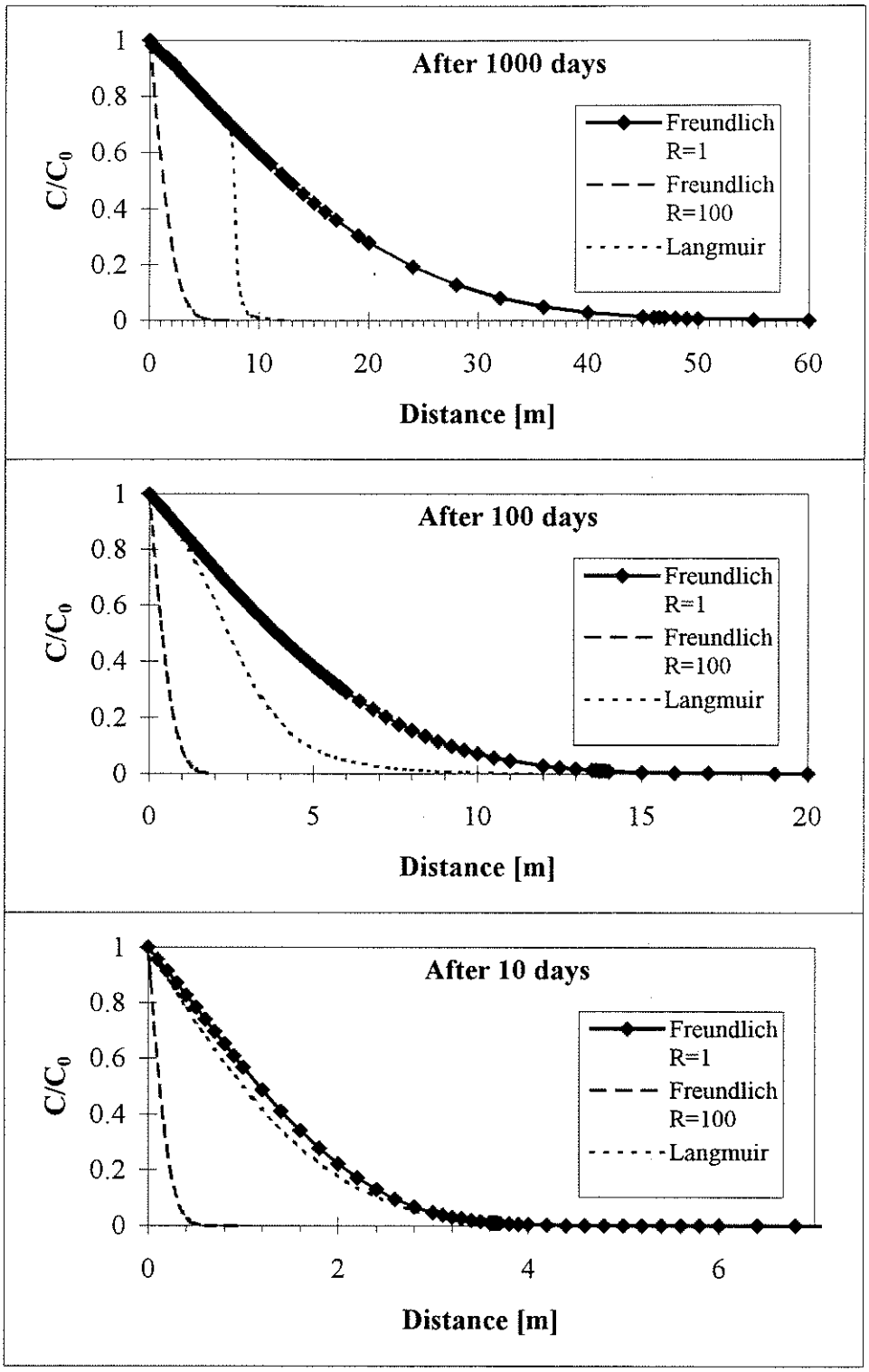

Figure 5.7 Comparison of solute concentrations in the fracture, which are calculated using Freundlich sorption models with R=1 and R=100 (models F1 and F100, and a Langmuir sorption model (model L).

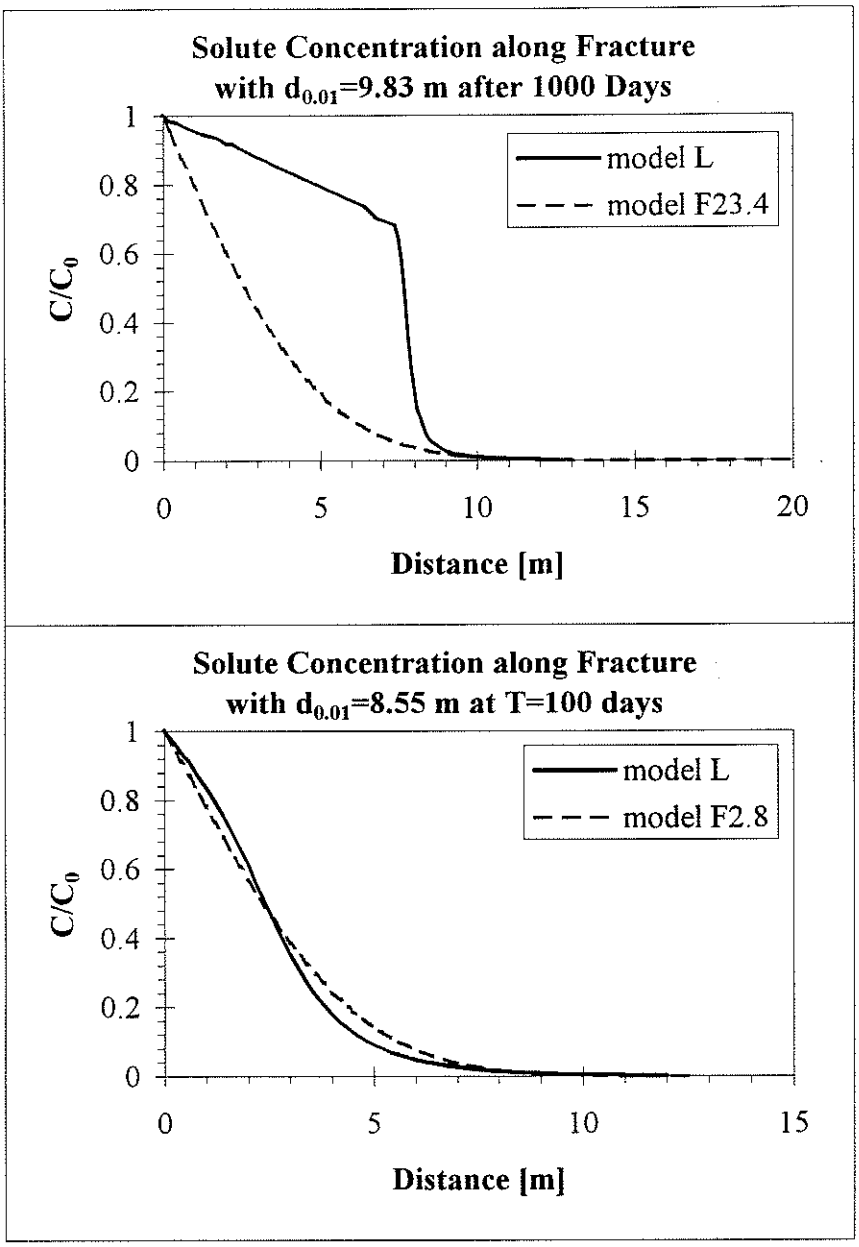

Figure 5.8: Comparison of solute concentrations in the fracture between a Langmuir sorption model (model L) and Freundlich sorption models with R=23.4 and R=2.8 (model F23.4 and F2.8). Simulations after 1000 days (model L and model F23.4) and after 100 days (model L and model F2.8) have the same fracture penetration distance with $d_{0.01}$=9.83 m and $d_{0.01}$= 8.55 m, respectively.

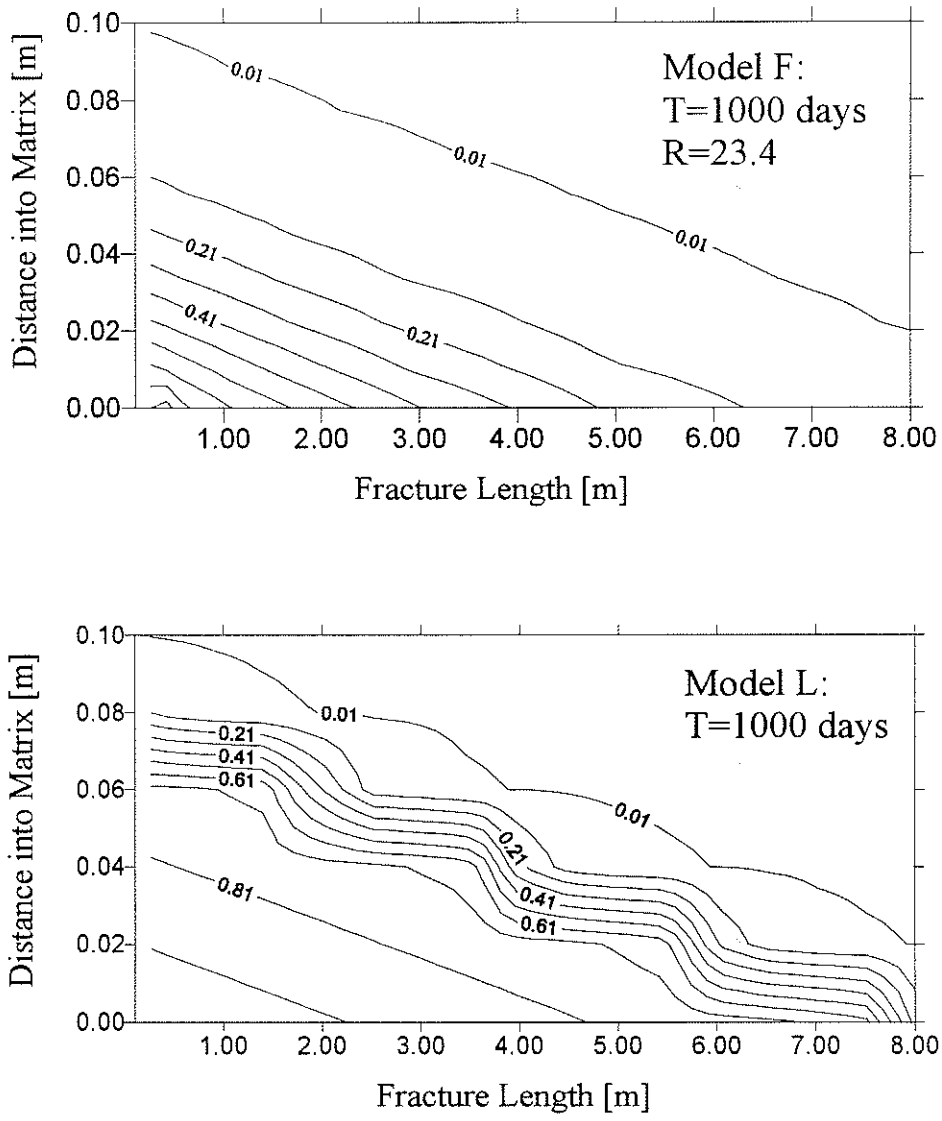

Figure 5.9: Simulated solute concentrations using a Freundlich sorption model with R=23.4 (model F23.4) and a Langmuir sorption model (model L). Concentrations are calculated after 1000 days.

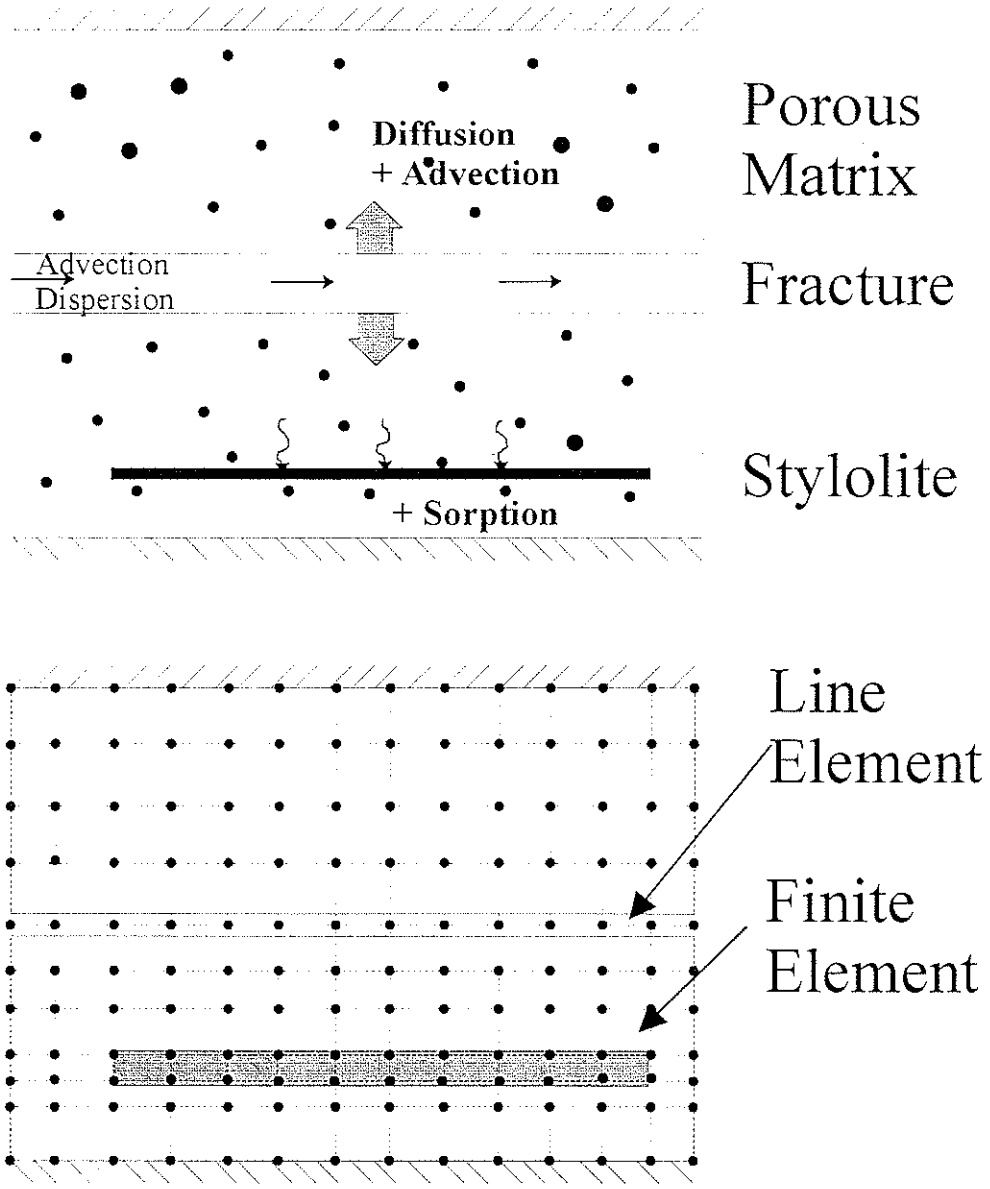

Figure 5.10: Conceptual model for numerical mass transport simulations, and discrete finite element representation.

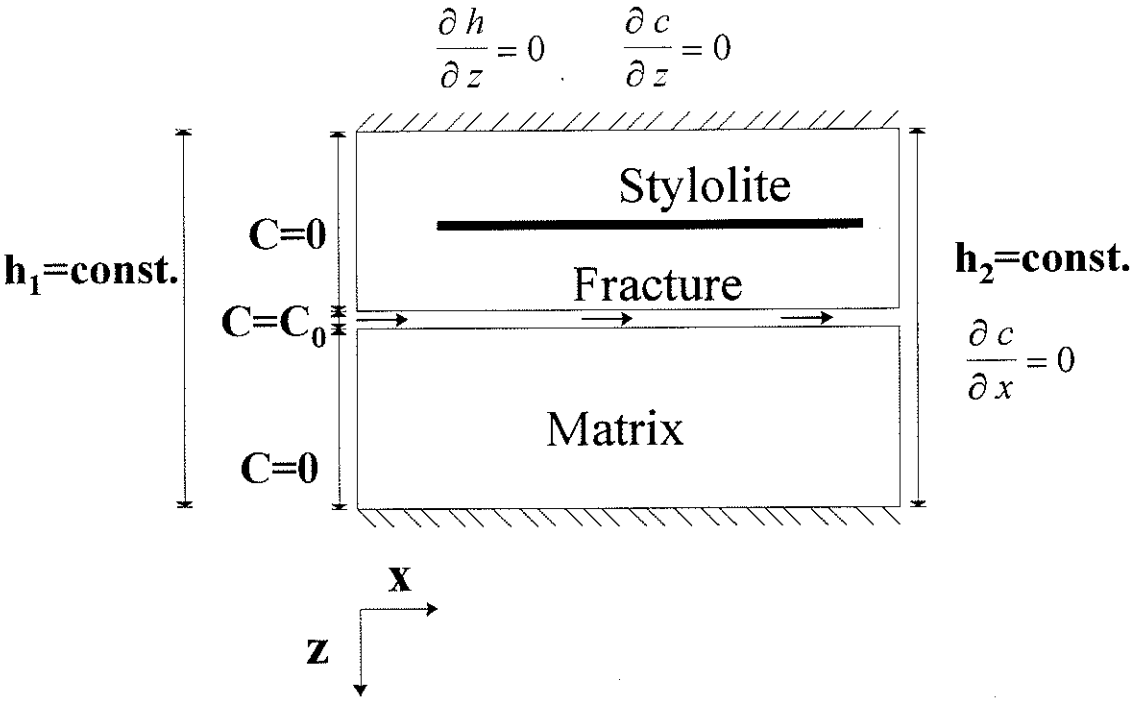

Figure 5.11: Boundary conditions for numerical simulations.

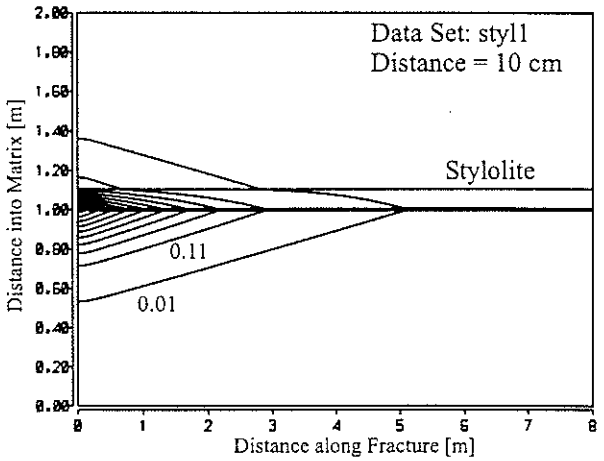

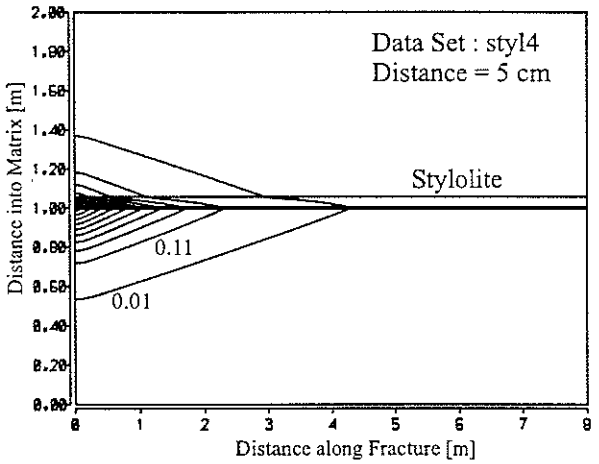

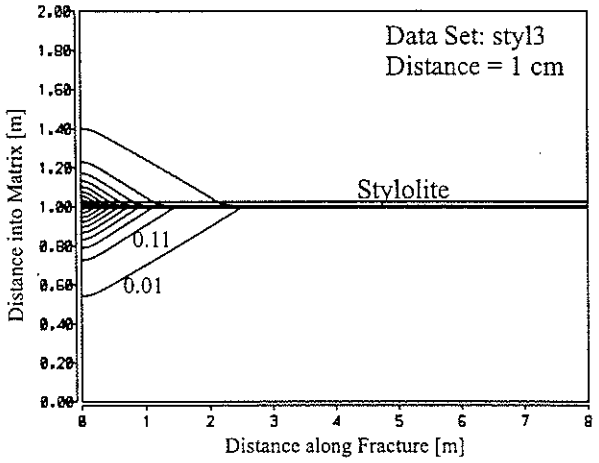

Figure 5.12: Solute concentrations in a single fracture model containing an individual stylolite layer. Sensitivity analysis with respect to stylolite - fracture distance.

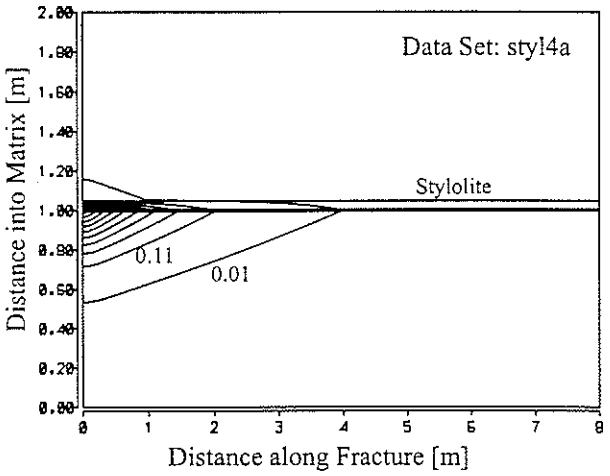

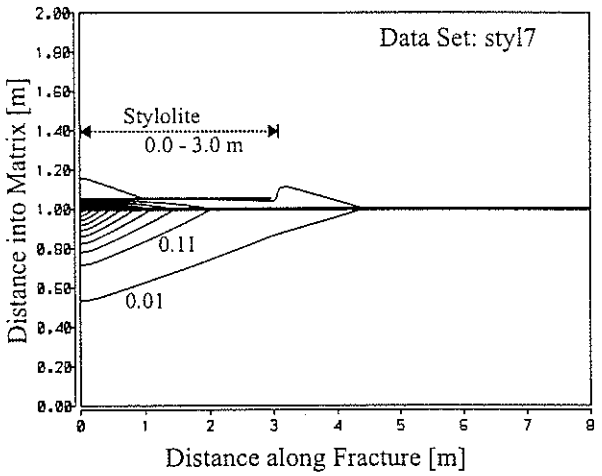

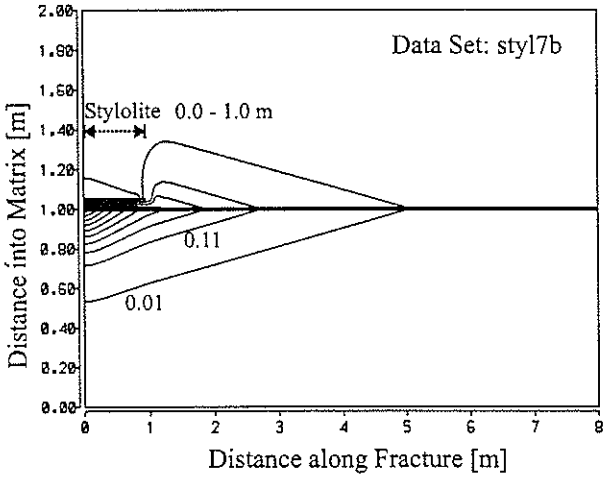

Figure 5.13: Solute concentrations in a single fracture model containing an individual stylolite layer. Sensitivity analysis with respect to stylolite extension.

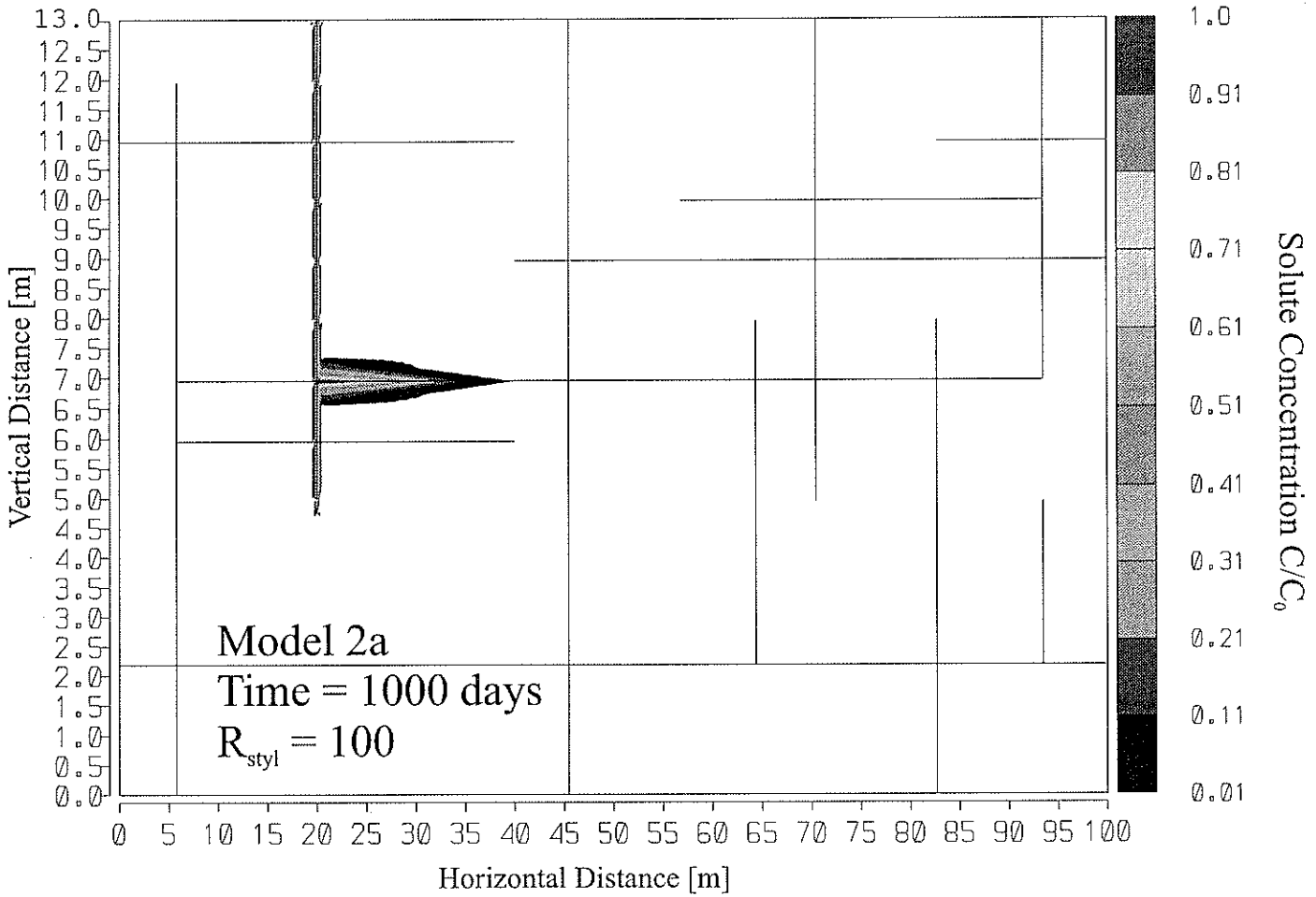

Figure 5.14: Simulation of plume migration in the randomly fractured Upper Lockport Formation with a heterogeneous rock matrix, after 1000 days. Stylolites are implemented in the rock matrix with a frequency of one stylolite layer per meter and a retardation factor of 100.

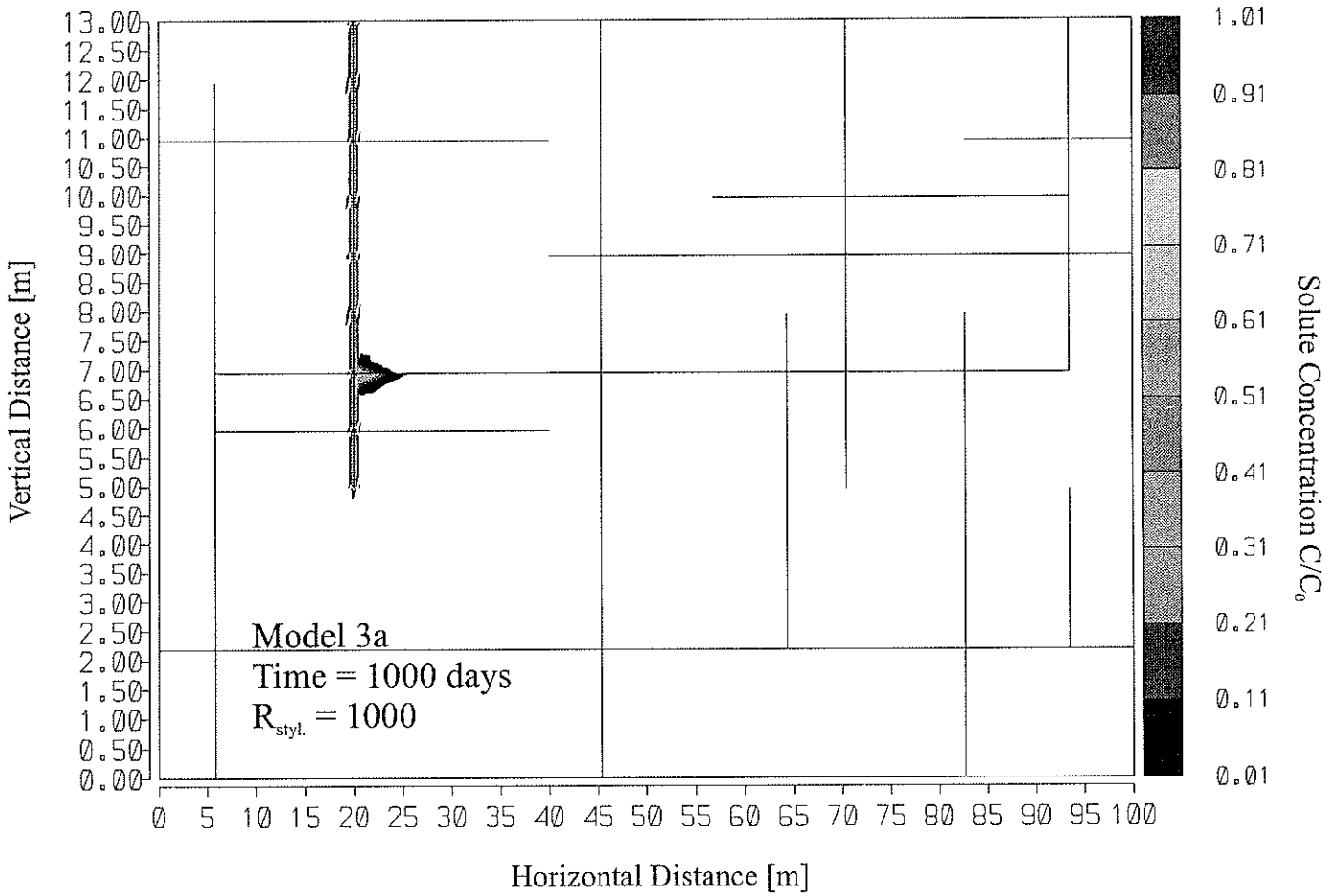

Figure 5.15: Simulation of plume migration in the randomly fractured Upper Lockport Formation with a heterogeneous rock matrix, after 1000 days. Stylolites are implemented in the rock matrix with a frequency of one stylolite layer per meter and a retardation factor of 1000.

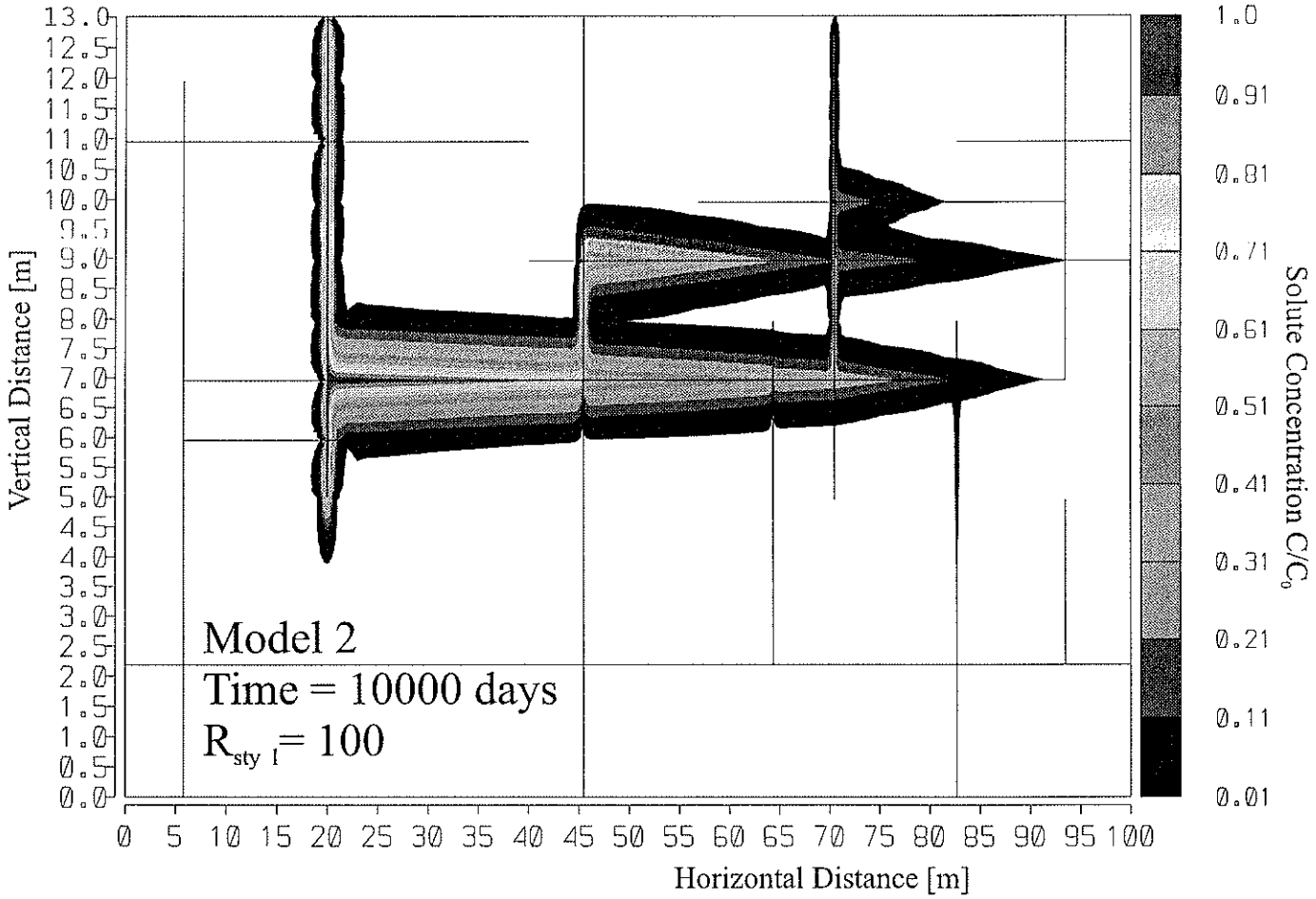

Figure 5.16: Simulation of plume migration in the randomly fratured Upper Lockport Formation with a heterogeneous rock matrix, after 10000 days. Stylolites are implemented in the rock matrix with frequeny of one stylolite layer per m,eter and a retardation factor of 100.

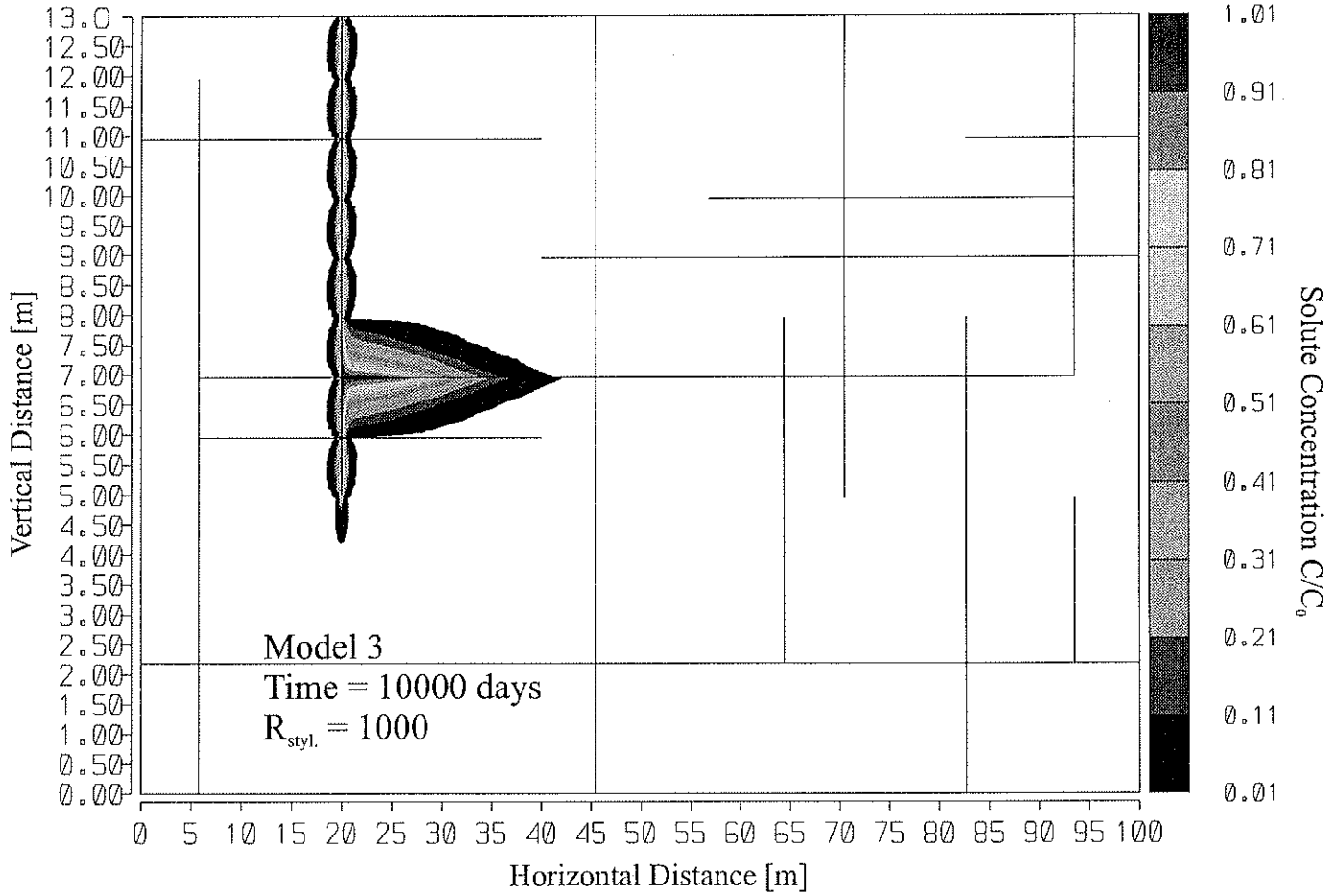

Figure 5.17: Simulation of plume migration in the randomly fractured Upper Lockport Formation with a heterogeneous rock matrix, after 10000 days. Stylolites are implemented in the rock matrix with a frequency of one stylolite layer per meter and a retardation factor of 1000.

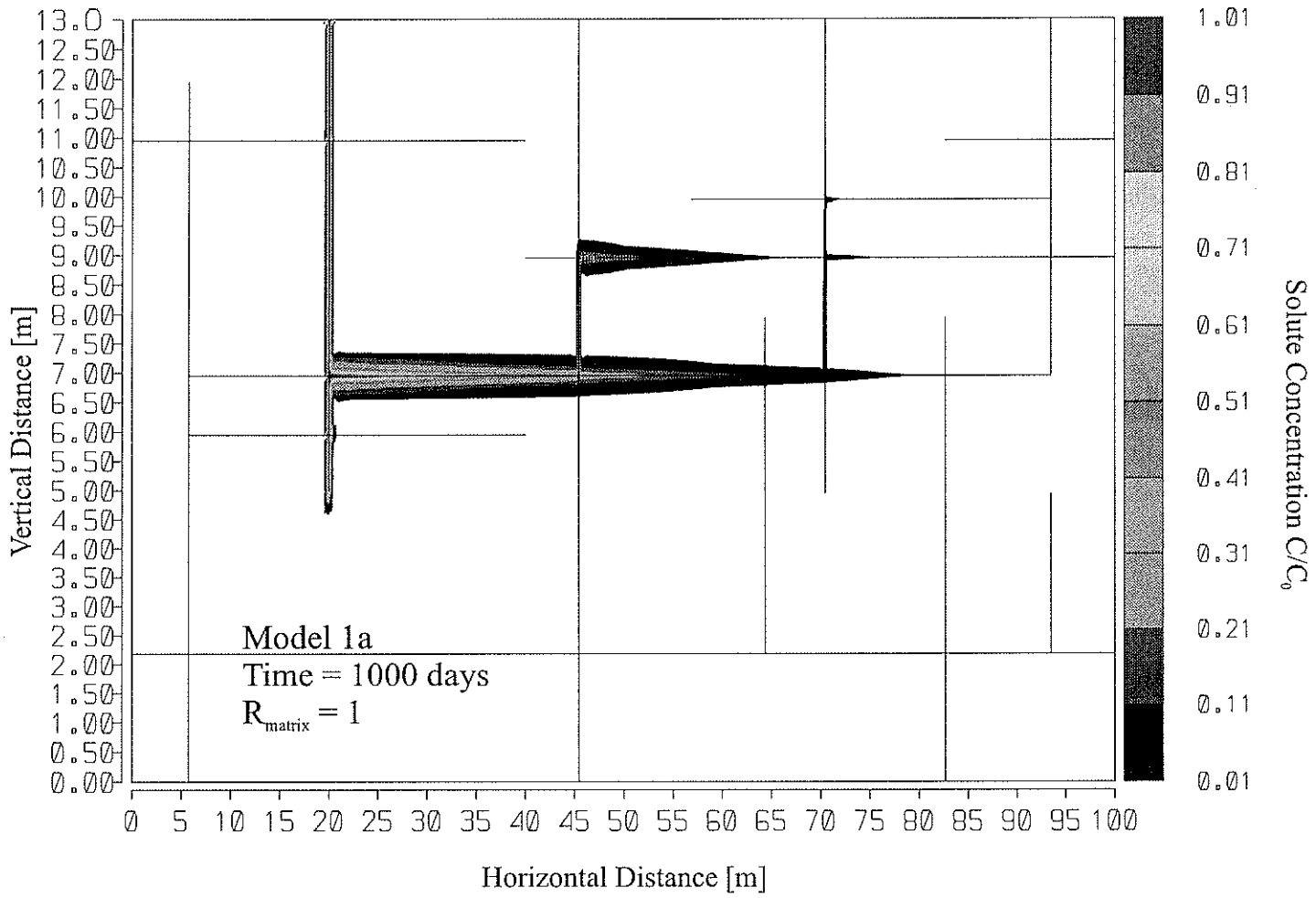

Figure 5.18: Simulation of plume migration in the randomly fractured Upper Lockport Formation with a homogeneous rock matrix, after 1000 days.

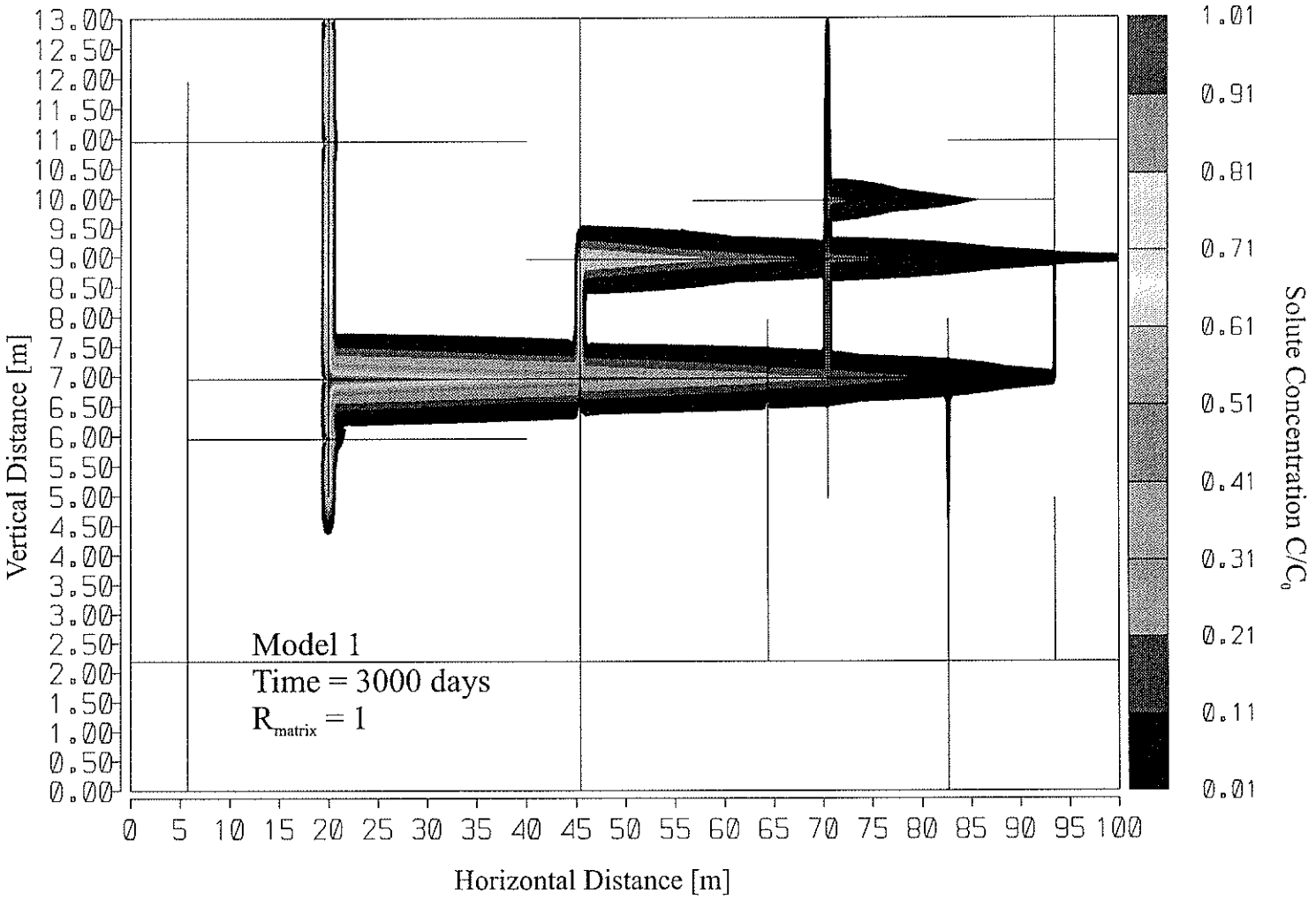

Figure 5.19: Simulation of plume migration in the randomly fractured Upper Lockport Formation with a homogeneous rock matrix, after 3000 days.

Table 5.1
Base-Case Input Parameters for Semi-Analytical Single Fracture Model

Molecular diffusion coefficient:	$1.73x10^{-4}$ [m^2/d]
Fracture width:	$4x10^{-4}$ [m]
Longitudinal dispersion:	0.0 [m]
Porosity:	0.1 [%]
Tortuosity factor:	0.1
Fracture velocity:	0.864 [m/d]
Kinetic constant:	$4.32x10^{-2}$ [l/mg d^{-1}]
Maximum sorption capacity:	$4.6x10^{-8}$ [mg/mg]
Constant point source:	1.0 [mg/l]
Rock matrix density:	$2.5x10^{6}$ [mg/l]
Time:	100 [d]

Table 5.2
Comparison of Fracture Penetration Distances Simulated with Transport Models F and L

Time [days]	Model F[1] ($R_m = 1$) $d_{0.01}$ [m]	Model F[1] ($R_m = 100$) $d_{0.01}$ [m]	Model L[2] ($C_{max} = 4.6x10^{-8}$ mg/mg) $d_{0.01}$ [m]
1000	46.50	4.75	9.83
100	13.86	1.50	8.55
10	3.64	0.47	3.54

[1] Model F: A linear-Freundlich sorption isotherm is employed.
[2] Model L: A kinetic Langmuir sorption isotherm is employed.

Table 5.3
Base Case Parameters for Stylolite Sensitivity Analyses in Two-Dimensional Finite Element Simulations.

Stylolite Parameters	
Number of Stylolites	single
Thickness	0.5 [cm]
Distance to Fracture	5.0 [cm]
Retardation Factor (R)	100, 1000
Fracture Parameters	
Aperture (2b)	$2.0x10^{-4}$ [m]
Fracture Flow Velocity (v_f)	0.1 [m/d]
Longitudinal Dispersivity (α_L)	0.1 [m]
Matrix Parameters	
Hydraulic Conductivity(K_x, K_z)	$8.64x10^{-6}$ [m/d]
Dispersivity (α_L, α_T)	0.0 [m]
Porosity (θ)	5.68 [%]
Retardation Factor (R)	0
Tortuosity Factor (γ)	0.1
Effective Diffusion Coefficient (D)	$1.737x10^{-5}$ [m^2/d]

Table 5.4
Stylolite Sensitivity Analyses with Respect to Fracture Distance for R_{styl} = 100 and 1000 after 1000 days. Fracture Penetration Distance ($d_{0.01}$) is defined at 1 % Solute Source Concentration.

Model	$d_{0.01}$ in Fracture [m]	Stylolite Position [m]	Distance [cm]	$R_{styl.}$
styl2a	5.30	1.2 to 1.205	20	1000
styl1a	5.05	1.1 to 1.105	10	1000
styl4a	3.92	1.05 to 1.055	5	1000
styl5a	2.30	1.02 to 1.025	2	1000
styl3a	1.51	1.01 to 1.015	1	1000

Model	$d_{0.01}$ in Fracture [m]	Stylolite Position [m]	Distance [cm]	$R_{styl.}$
styl2	5.30	1.2 to 1.205	20	100
styl1	5.10	1.1 to 1.105	10	100
styl4	4.30	1.05 to 1.055	5	100
styl5	3.10	1.02 to 1.025	2	100
styl3	2.50	1.01 to 1.015	1	100

Table 5.5
Stylolite Sensitivity Analyses with Respect to Extension for R_{styl} = 1000 after 1000 days. Fracture Penetration Distance ($d_{0.01}$) is defined at 1 % Solute Source Concentration.

Model	$d_{0.01}$ in Fracture [m]	Stylolite Extension [m]	Distance [cm]	$R_{styl.}$
styl4a	3.92	8.0	5	1000
styl7a	4.40	3.0	5	1000
styl7a	4.70	2.0	5	1000
styl7b	5.00	1.0	5	1000
styl7c	5.15	0.5	5	1000

Table 5.6
Stylolite Sensitivity Analyses with Respect to Stylolite Thickness for R_{styl} = 100 and 1000 after 1000 days. Fracture Penetration Distance ($d_{0.01}$) is defined at 1 % Solute Source Concentration.

Model	$d_{0.01}$ in Fracture [m]	Stylolite Position [m]	Thickness [mm]	Distance [cm]	$R_{styl.}$
styl4a	4.30	1.05 to 1.055	5	5	100
styl6	4.32	1.05 to 1.054	4	5	100
styl6a	4.40	1.05 to 1.053	3	5	100
styl6b	4.52	1.05 to 1.052	2	5	100
styl6c	4.75	1.05 to 1.051	1	5	100

Model	$d_{0.01}$ in Fracture [m]	Stylolite Position [m]	Thickness [mm]	Distance [cm]	$R_{styl.}$
styl4a	3.92	1.05 to 1.055	5	5	1000
styl6d	3.96	1.05 to 1.054	4	5	1000
styl6e	4.00	1.05 to 1.053	3	5	1000
styl6f	4.04	1.05 to 1.052	2	5	1000
styl6g	4.10	1.05 to 1.051	1	5	1000

Table 5.7
Mass Calculations for TCE Simulations in the Upper Lockport Formation (Eramosa Member)

Model	$R_{stylolite}$	Time [days]	M_{SM} [kg]	M_{TM} [kg]	M_{sorbed} [kg]	$\%M_{sored}$	$M_{SVF}=M_{TVF}$ [kg]	$M_{SHF}=M_{THF}$ [kg]	M_{TSS} [kg]	$d_{0.01}$ [m]
model 1a	1	1000	0.486	0.486	0	0	$1.77x10^{-3}$	$6.56x10^{-3}$	0.494	59
model 1	1	3000	1.249	1.249	0	0	$2.07x10^{-3}$	$12.2x10^{-3}$	1.263	90
model 2a	100	1000	0.241	0.526	0.285	54.19	$1.60x10^{-3}$	$9.49x10^{-3}$	0.530	19
model 2	100	10000	2.304	3.890	1.586	40.77	$2.24x10^{-3}$	$14.9x10^{-3}$	3.907	73
model 3a	1000	1000	0.147	0.810	0.663	81.80	$1.60x10^{-3}$	$0.46x10^{-3}$	0.812	6
model 3	1000	10000	0.649	4.318	3.670	84.98	$1.60x10^{-3}$	$2.44x10^{-3}$	4.322	22

$R_{stylolite}$: Retardation factor of stylolite layers.
M_{SM}: Mass in solution stored in the matrix.
M_{TM}: Total mass stored in the matrix.
M_{sorbed}: Mass sorbed onto stylolites.
$\%M_{sorbed}$: Percent mass sorbed onto stylolites from total mass stored in the matrix.
M_{SVF}: Mass in solution stored in vertical fractures.
M_{TVF}: Total mass stored in vertical fractures.
M_{SHF}: Mass in solution stored in horizontal fractures.
M_{THF}: Total mass stored in horizontal fractures.
$d_{0.01}$: Penetration distance of the 1% C_0 concentration contour.
M_{TSS}: Total mass stored in the system.

Chapter 6

Discussion and Conclusions

6.1 Introduction

To avoid unnecessary repetition the reader is referred to each chapter for an in-depth discussion on the methodology and results of the experimental, analytical, and numerical investigations. Due to the length of the study a brief summary with emphasis on the major issues is presented in this chapter. Subsequently, an outlook toward future research is given. At the end of the chapter this work is put into final perspective.

6.2 Summary

In this section the major findings of the presented research are condensed on a chapter by chapter basis. In Chapter 2 the major objective was to resaturate dry, dense dolostone slices in a back-pressured triaxial cell for the purpose of subsequent use in diffusion experiments. It was shown that, despite using ASTM Standard D5084-90 [1990] recommended back-pressures, the degree of sample resaturation was inadequate. Under the conditions described in Chapter 2, the highest degree of resaturation was 84.2 %. Increasing the back-pressure further required higher confining pressures in the triaxial cell in order to avoid fluid flow surpassing the specimen, and resulted subsequently in specimen volume reduction and crack initiation. Singh [1997] used triaxial cell

experiments to study these changes in pore volume and crack initiation in detail. In the present study it was interesting to find that two geologically similar specimens with the same total pore volume but different water content (one resaturated to 72.2 % and subsequently to 84.2 %, the other saturated at all times) had the same measured hydraulic conductivity. In order to explain this phenomenon, it is conjectured that the remaining pore space represents 'dead end pores', which do not contribute towards hydraulic conductivity.

Chapter 3 explored the heterogeneous porosity in the fractured, horizontally - stratified dolostone sequence of the Lockport Formation. The primary objectives were to obtain detailed vertical porosity profiles, and to evaluate the impact of heterogeneous porosity in the vicinity of fractures on mass transport. In the hydrogeological literature it is well established that mass transport in fractured, porous media is significantly affected by mass diffusion from fractures into the surrounding rock matrix. The main physical parameter influencing this diffusion process, and determining the amount of mass transfer that takes place per unit surface area, is the rock matrix porosity [Novakowski and Lapcevic, 1994]. Therefore, the conducted porosity study in the Lockport Formation is of significant importance when evaluating the fate of dissolved pollutants. This study showed that porosity data varied greatly, from 0.43 to 20.63 %. Thin layers with high biomoltic porosity (10 to 20 %) were found in the uppermost part of the Lockport Formation. The most important finding was that porosity adjacent to fractures is enhanced up to 17 % from the background value in the Eramosa Member and up to 8 % in the Vinemount and

Gasport Members. These enhanced porosity values penetrate 2 to 3 cm deep into the rock matrix. A leaching process due to chemical disequilibrium is thought to be the cause [Giles and De Boer, 1989 and 1990]. The impact of porosity variations adjacent to fractures was studied with mass transport simulations. Heterogeneous porosity data were implemented into a single fracture model. The study showed that pollutant penetration depth into the rock matrix, travel distance along the fracture, and peak concentrations were affected by the heterogeneous porosity profiles. It is important to note that by not accounting for enhanced porosity near the fracture a significant overestimate of the bulk porosity of the medium or fracture aperture will be obtained when calibrating transport data from tracer experiments. Another important finding was that when simulating the rock matrix with decreasing porosity away from the fracture, an increased amount of mass will be stored in the rock matrix under a high fracture flow velocity compared to a low fracture flow velocity. From the present study it can be concluded that heterogeneous porosity represents an additional challenge to those who try to evaluate rock properties and hydrogeological parameters for mass transport simulations from tracer experiments.

The work in Chapter 4 is considered to represent the major scientific achievement of this thesis since it marks the first time that TCE - diffusion and sorption studies with stylolitic dolostone samples have been conducted. The primary aim was to prove the hypothesis that stylolites adsorb significant amounts of organic pollutants. This was conclusively shown in batch and double reservoir diffusion experiments with stylolite containing dolostone samples from the Lockport Formation. Employing the hydrophobic

sorption theory [Karickhoff et al., 1979; Schwarzenbach and Westall, 1981; Hassett and Banwart, 1989] and a log-normalized octanol - water partition coefficient for TCE of 2.29 [Giger et al., 1983], the fraction of organic carbon in dolostone and stylolitic dolostone samples were estimated from batch experiments. The organic carbon content in stylolites was determined to range between 3.4 % and 45.5 %. Here, TCE is conjectured to sorb only onto the organic carbon and clay fractions in dolostone samples. A diffusion experiment with a presumably clay and organic carbon free dolostone sample confirmed this hypothesis.

For the first time TCE, a volatile chlorinated hydrocarbon, was used in long term (6 month) diffusion experiments. This is an experimental challenge due to expected volatile TCE loss during the experiment. With the design of a special double reservoir diffusion cell built out of stainless steel and Teflon, the volatile TCE loss could be minimized to about 10 % from the initial mass input. Concentrations in a blank (without rock sample) diffusion cell were monitored to account for the loss, and concentrations from all diffusion cells were normalized with respect to the concentrations in the blank, assuming similar volatile TCE loss for all diffusion cells. Looking at the source and exit reservoir equilibrium concentrations with rock sample 65E-ST1-17 (presumably clay and organic carbon free), this standard procedure proved to work well. The major findings from the diffusion experiments were that (a) the TCE adsorption process onto stylolites could best be described with a kinetic Langmuir sorption isotherm, and that (b) the desorption process could be modeled with either a linear or non-linear sorption isotherm due to its slow kinetic behavior. The maximum sorption capacity for TCE sorption onto

stylolites is estimated to range between 1.3 and 4.6 μg/g. This represents a significant amount. For example, the upper Lockport Formation (Eramosa Member) contains an average of 55 horizontal stylolite layers with an average thickness of 0.5 mm per stylolite and is predicted to be able to adsorb 78.7 to 278.3 g TCE per square meter surface area. A dissolved TCE plume that extends over 5000 m^2 could lead to TCE attenuation in stylolites of 393.3 to 1391.5 kg (270 to 955 l pure TCE), assuming that all stylolites are reached by the TCE plume and the maximum possible amount of TCE is absorbed. Bedrock remediation plans for carbonate aquifers that are contaminated with dissolved organic pollutants need to take sorption onto stylolites and its kinetic behavior into account.

The primary aim of Chapter 5 was to simulate the impact of stylolites in a fractured carbonate aquifer (like the Lockport Formation) on TCE mass transport. Stylolites were implemented into the matrix by two different approaches. In analytical simulations stylolites were part of a homogeneous sorbing matrix, whereas in numerical finite element simulations each individual stylolite was modeled as discrete, horizontal layer. In the first approach sorption was simulated with a kinetic Langmuir sorption isotherm, while in the latter a linear, equilibrium sorption isotherm was employed. Both approaches showed that stylolites cause significant retardation. The two-dimensional finite element code FRACTRAN [Sudicky and McLaren, 1992] was utilized. A stylolite sensitivity analysis in a single fracture model was conducted and revealed that lateral extension and closeness to the fracture are the most important stylolite properties in a

discrete model. Simulations of the upper Lockport Formation (Eramosa Member) with a random fracture network, a continuous line source, and a stylolite frequency of one stylolite per meter revealed that after 1000 days, a total mass of 0.53 to 0.81 kg TCE (values are for R = 100 and R = 1000, respectively) leached into the domain and 0.29 to 0.66 kg TCE are adsorbed by stylolites. Remediation programs have to acknowledge that over 98 % of the solute mass in fractured porous media might be stored in the matrix due to diffusion from fractures into the surrounding matrix and due to sorption.

6.3 Future Research

As work on this thesis progressed, it became apparent that a number of issues related to the presented research warrant further investigations. These topics are summarized in point form.

- Separating the effective porosity from the total porosity of rock matrix is an important issue for all mass transport problems in fractured porous media. Depending on the pollutant size and pore diameters, a certain amount of the total pore space might not be available for mass storage. In the present matrix porosity study (Chapter 3) effective porosity could not be evaluated. One recent approach that researchers have taken to estimate the effective porosity and determine porosity heterogenities in porous media is by visualization of solutes with x-rays [Tidwell et al., 1995]. Investigating the effective porosity

on dolostone slices with visualization methods might allow for even more accurate mass transport simulation models in the Lockport Formation.

- In Chapter 3 it was recognized that heterogeneous porosity of the rock matrix adjacent to fractures has a potential significant impact on mass transport in a fractured dolostone aquifer. It can be assumed that heterogeneous matrix porosity in general, not just in the vicinity of fractures, is an important issue. Further geostatistical investigations that lead to the implementation of porosity variations into a numerical model might improve the prediction of contaminant plume migration.

- It was postulated in Chapter 4 and Chapter 5 that the organic carbon content in stylolites cause adsorption of significant amounts of organic pollutants. The number of stylolite samples analyzed directly for organic carbon was small. Note that the organic carbon estimates from batch sorption experiments indicated much higher values. This conflict might be due to a significant clay fraction in the stylolites, which also adsorbs organic pollutants, or due to a non-representative selection of stylolite samples. Further organic carbon analyses on stylolites, as well as clay fraction measurements and studies on the clay mineral composition, are needed.

- Evaluation of time - solute concentration data from the source reservoir of double diffusion cells (chapter 4) suggest that stylolites have a maximum sorption capacity for adsorbing organic pollutants. This conjecture requires further experimental proof. From batch experiments with repeated TCE input a maximum sorption capacity could be found experimentally and compared to the computed values. Given appropriate equilibration time after each TCE input, accurate mass calculations should be possible.

- The desorption behavior of TCE could not be studied accurately with the diffusion experiments described in Chapter 4. In recent studies it was postulated that TCE desorption from organic carbon in porous media is a slow kinetic process and depends on advective fluid flow [Pavlostathis and Jaglal, 1991] and on sorption history (i.e. TCE exposure time) [Grathwohl and Reinhard, 1993; Cluver et al., 1997]. Batch desorption experiments with stylolite samples, which had been exposed to the same amount of TCE but for different periods of time, might provide further information on this issue.

- The actual small scale, chemical and mass transport processes that are taking place in the rock matrix are difficult to study. Visualizing dissolved and adsorbed organic pollutants during different stages of their migration through stylolitic dolostone slices might help to provide further insight. Tidvell et al.

[1995] have shown that tracers with high atomic mass can be easily imaged with x-ray adsorption. One suggestion would be to use iodine benzenes in diffusion studies with stylolitic dolostone and investigate its travel path through the porous rock sample.

- In Chapter 5 it has been demonstrated that stylolites have a large impact on TCE transport through the discretely fractured porous dolostone sequence at Smithville. However, the sorption process was modeled with a linear, reversible, equilibrium Freundlich isotherm. Whether the amount of adsorbed TCE changes significantly in a large scale model when employing a non-linear, irreversible, kinetic Langmuir sorption isotherm requires investigation. This could be achieved with further computer simulations using a discrete fracture model that allows for kinetic sorption within the matrix.

6.4 Final Perspective

The thesis should be viewed in respect to its contributions towards the protection of groundwater resources in fractured aquifers. As fractured carbonates contain large drinking water resources in Europe and North America, a detailed knowledge of fluid flow and mass transport mechanisms are a necessity in order to prevent and predict pollution of these resources. Recognizing the immense capability of temporary mass storage in the rock matrix of dual porosity aquifers, this research focused on matrix diffusion and

sorption processes. The different aspects of this thesis contribute towards a better understanding of rock matrix - solute interactions that take place in fractured carbonate aquifers. As has been pointed out earlier, a common feature in carbonate formations is the presence of stylolites. Their significant role in organic pollutant transport has been studied in this research for the first time. Further in-depth research is needed to fully understand temporal mass storage processes in dual porosity aquifers.

References

ASTM Standard D 5084-90, Standard test method of measurement of hydraulic conductivity of saturated porous materials using a flexible wall permeameter, ASTM, 151-158, 1990.

Culver, T. B., Hallisey, S. P., Sahoo, D., Deitsch, J. J., and J. A. Smith, Modeling the desorption of organic contaminants from long-term contaminated soil using destributed mass transport rates. Environmental Science and Technology, 31 (6), 1581-1587, 1997.

Giger, W., R.P. Schwarzenbach, E. Hoehn, K. Schellenberg, J.K. Schneider, H.R. Wasmer, J. Westall, and J. Zobrist, Das Verhalten organischer Wasserinhaltsstoffe bei der Grundwasserbildung und im Grundwasser. Gas - Wasser - Abwasser, 63, (9), 517-531, Zürich, 1983.

Giles, M. R. and R. B. de Boer, Secondary porosity: creation of enhanced porosities in the subsurface from the dissolution of carbonate cements as a result of cooling formation waters, Marine and Petroleum Geology, v.6, 261-269, 1989.

Giles, M. R. and R. B. de Boer, Origin and significance of redistributional secondary porosity, Marine and Petroleum Geology, v.7, 378-397, 1990.

Grathwohl, P., and M. Reinhard, Desorption of trichloroethylene in aquifer material. Rate limitation at the grain scale. Environmental Science and Technology, 36(1), 89-108, 1993.

Hassett, J. J., W. L. Banwart, and R. A. Griffin, Correlation of compound properties with sorption characteristics of nonpolar compounds by soils and sediments: concepts and limitations. in: Environment and solid wastes, ed., C. W. Francis and S. I. Auerbach, Butterworths, Boston, 1983.

Karickhoff, S.W., D.S. Brown, and T.A. Scott, Sorption of hydrophobic pollutants on natural sediments. Water Research, 13 (3), 241-248, Oxford (Pergamon Press), 1979.

Novakowski, K. S., and P. A. Lapcevic, Field measurement of radial solute transport in fractured rock, Water Resour. Res., 30(1), 37-44, 1994.

Pavlostathis, S. G., and K. Jaglal, Desorption behavior of trichloroethylene in contaminated soil. Environmental Science and Technology, 25 (2), 274-279, 1991.

Schwarzenbach, R.P., and J. Westall, Transport of nonpolar organic compounds from surface water to groundwater. Laboratory sorption studies. Environ. Sci. Technol., 15 (11), 1360-1367, Washington, 1981.

Singh, A. B., Study of rock fracture by permeability method, J. of Geotech. and Geoenviromental Eng., 7, 601-608, 1997.

Sudicky, E.A., and R.G. MaLaren, The Laplace transform Galerkin technique for large scale simulation of mass transport in discretely fractured porous formations. Water Resour. Res., 28 (2), 499-514, 1992.

Tidwell, V. C., and R. J. Glass, Laboratory investigation of matrix imbibition from a flowing fracture, Geophysical Research Letters, v.22, no.11, 1405-1408, 1995.